AD-A035 175 KAMAN AEROSPACE CORP BLOOMFIELD CONN F/G 1/3
ELASTIC PITCH BEAM TAIL ROTOR.(U)
DEC 76 P F MALONEY, J D PORTERFIELD DAAJ02-72-C-0006
UNCLASSIFIED R-1399 USAAMRDL-TR-76-35 NL

1 OF 3
AD A035175

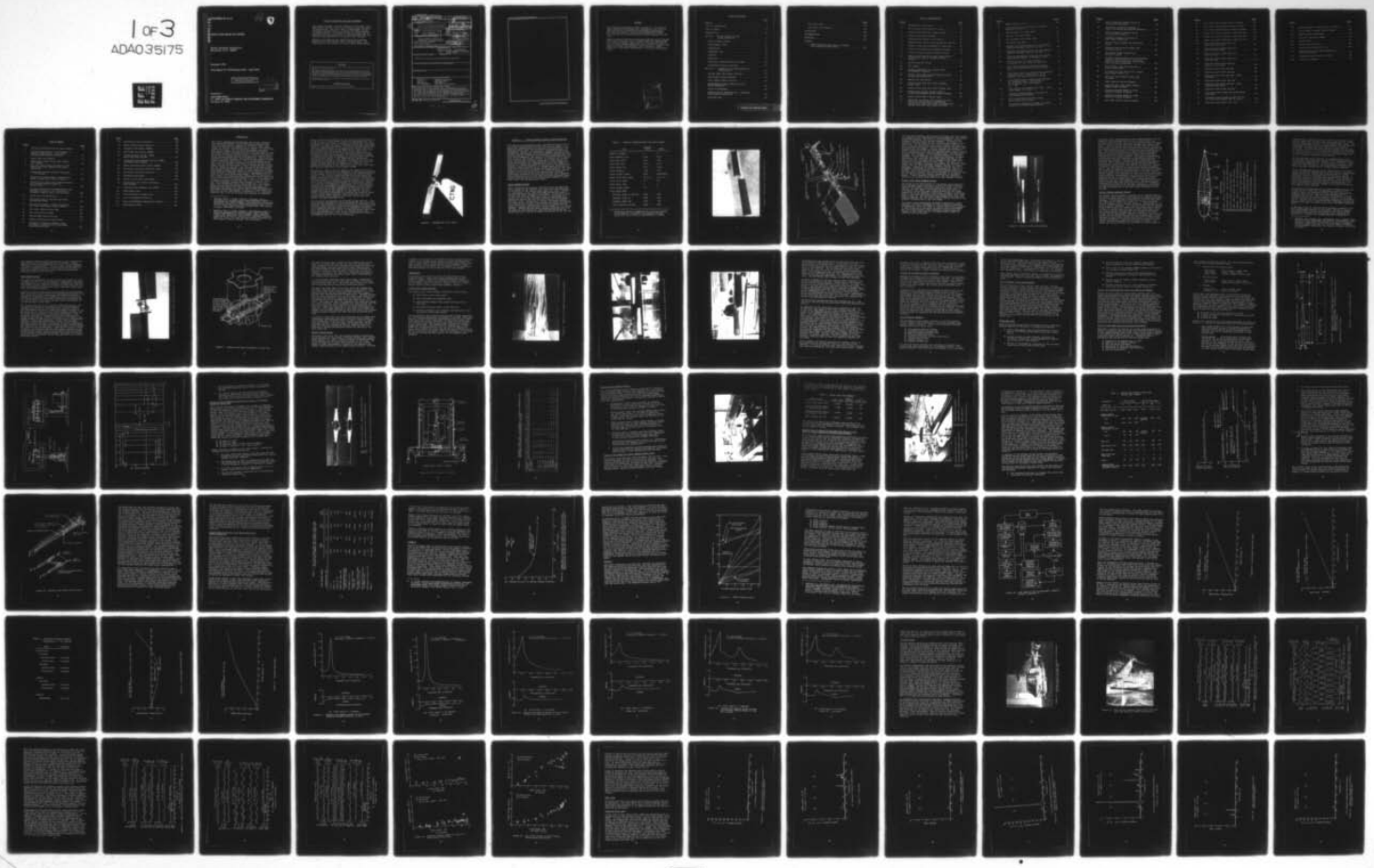

USAAMRDL-TR-76-35

ELASTIC PITCH BEAM TAIL ROTOR

Kaman Aerospace Corporation
Bloomfield, Conn. 06002

December 1976

Final Report for Period August 1971 - April 1976

Prepared for

EUSTIS DIRECTORATE
U. S. ARMY AIR MOBILITY RESEARCH AND DEVELOPMENT LABORATORY
Fort Eustis, Va. 23604

EUSTIS DIRECTORATE POSITION STATEMENT

This report presents a design concept for helicopter tail rotors which use the elastic pitch beam concept for obtaining blade pitch. The tail rotor, as fabricated, has an instability problem due to a coupling of inplane bending and teeter motion. A redesign of the tail rotor spar to eliminate this coupling effect is required before the concept can find application in teetering rotor systems.

Results of the program have demonstrated the potential gains in tail rotor weight, cost, and simplicity. The feasibility of the concept has been clearly demonstrated.

UNCLASSIFIED

SECURITY CLASSIFICATION OF THIS PAGE (When Data Entered)

REPORT DOCUMENTATION PAGE	READ INSTRUCTIONS BEFORE COMPLETING FORM
1. REPORT NUMBER: USAAMRDL TR-76-35	2. GOVT ACCESSION NO.
	3. RECIPIENT'S CATALOG NUMBER
4. TITLE (and Subtitle): ELASTIC PITCH BEAM TAIL ROTOR,	5. TYPE OF REPORT & PERIOD COVERED: FINAL REPORT, August 1971 — April 1976
	6. PERFORMING ORG. REPORT NUMBER: R-1399
7. AUTHOR(s): Paul F. Maloney, John D. Porterfield	8. CONTRACT OR GRANT NUMBER(s): DAAJ02-72-C-0006
9. PERFORMING ORGANIZATION NAME AND ADDRESS: Kaman Aerospace Corporation, Bloomfield, Connecticut 06002	10. PROGRAM ELEMENT, PROJECT, TASK AREA & WORK UNIT NUMBERS: 63211A 1F263211DB41
11. CONTROLLING OFFICE NAME AND ADDRESS: Eustis Directorate, U.S. Army Air Mobility R&D Laboratory, Fort Eustis, Virginia 23604	12. REPORT DATE: December 1976
	13. NUMBER OF PAGES: 214
14. MONITORING AGENCY NAME & ADDRESS (if different from Controlling Office) 214 p.	15. SECURITY CLASS. (of this report): UNCLASSIFIED
	15a. DECLASSIFICATION/DOWNGRADING SCHEDULE

16. DISTRIBUTION STATEMENT (of this Report)

Approved for public release; distribution unlimited.

17. DISTRIBUTION STATEMENT (of the abstract entered in Block 20, if different from Report)

18. SUPPLEMENTARY NOTES

19. KEY WORDS (Continue on reverse side if necessary and identify by block number)

Helicopter	Composite Structures
Rotors	Hingeless Rotor
Tail Rotors	Flex Rotor
UH-1 Helicopter	Soft Out-of-Plane Rotor

20. ABSTRACT (Continue on reverse side if necessary and identify by block number)

The objectives of this program were to demonstrate the flight worthiness and to evaluate the reliability and maintainability of the Elastic Pitch Beam tail rotor designed for the UH-1H helicopter. This was accomplished by an engineering program which included design, analyses, static testing, fatigue testing, whirl testing, and ground and flight testing of the Elastic Pitch Beam tail rotor on a UH-1H helicopter.

DD FORM 1 JAN 73 1473 EDITION OF 1 NOV 65 IS OBSOLETE

UNCLASSIFIED

SECURITY CLASSIFICATION OF THIS PAGE (When Data Entered)

404 362

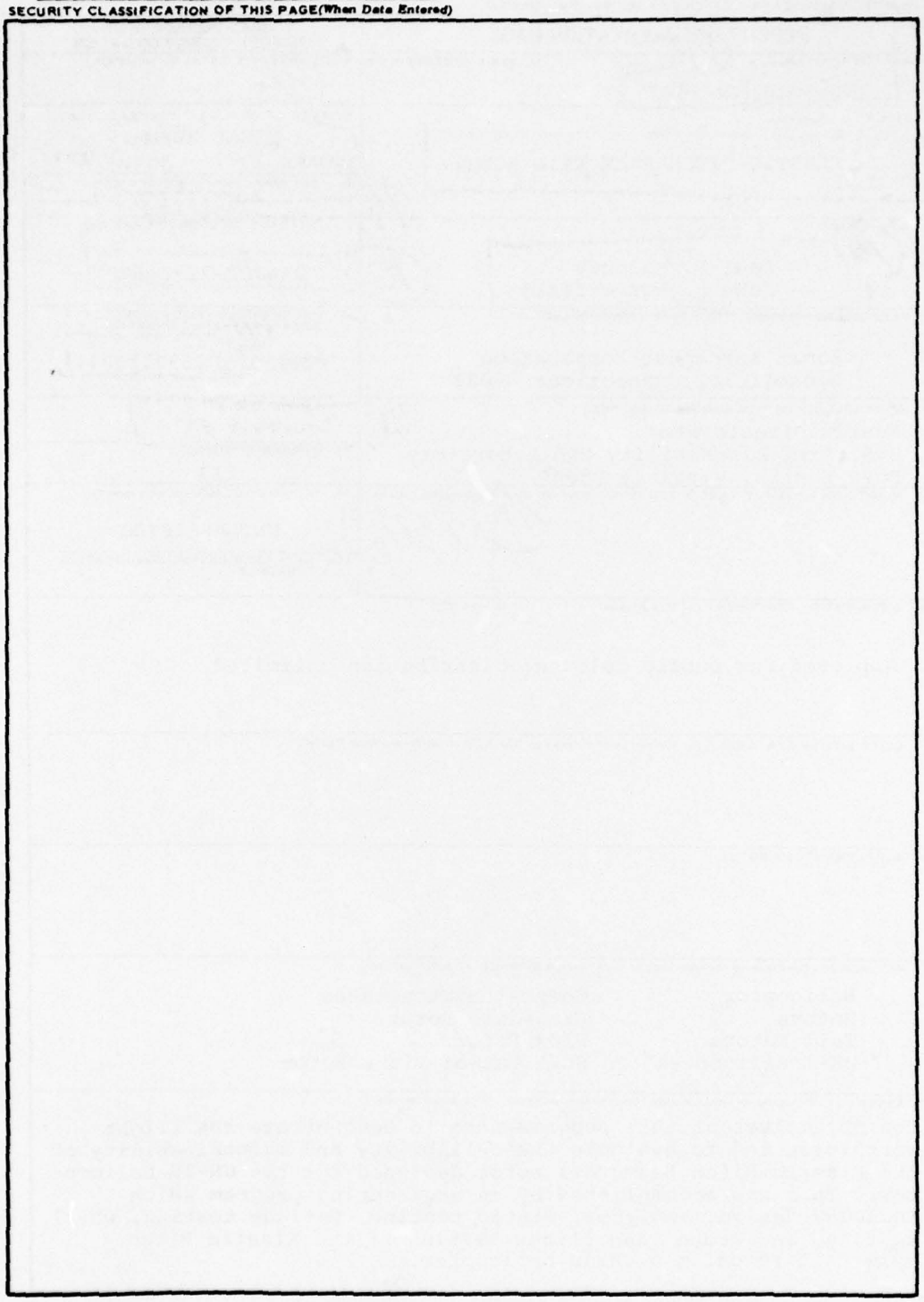

PREFACE

This report was prepared by Kaman Aerospace, a division of Kaman Corporation of Bloomfield, Connecticut, for the U.S. Army Air Mobility Research and Development Laboratories, Fort Eustis, Virginia, under Contract DAAJ02-72-C-0006. Mr. James Waller was the technical contract monitor for the Army.

Kaman Aerospace Corporation personnel engaged in this program were Paul F. Maloney, John D. Porterfield, and James Miller of the Dynamic Stress Group; Robert E. Collins and Frank K. Dunn of the Aerodynamic/Dynamics Group; Frank B. Clark of the Materials Group; and Anthony D. Rita, William F. Spurr, Frank Bill, and Robert Hintermister of the Test Engineering Group.

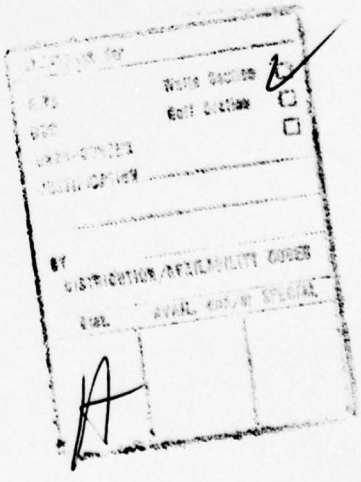

TABLE OF CONTENTS

LIST OF ILLUSTRATIONS

LIST OF TABLES

INTRODUCTION

The service experience of helicopter tail rotors is marked with recurring problems and high maintenance requirements. High rotational speeds, complex and variable inflow, high vibratory loading, a susceptibility to failure from inherent causes, as well as from foreign object damage, and erosion are some of the reasons for tail rotor maintenance problems. Preliminary studies investigating the use of the Elastic Pitch Beam (EPB) concept, References 1 and 2, indicate that many of the potential trouble sources affecting a tail rotor's reliability and maintainability may be eliminated. The EPB design requires no pitch bearings, and minimizes the number of highly loaded structural connections. This is accomplished by the use of a directed fiber structure, called the Elastic Pitch Beam, that is continuous from blade to blade, passing uninterrupted through the hub region so that centrifugal force loads are not reacted by the hub. The portions of the EPB between the hub and the attachment points on each blade must transmit blade bending moments and shears to the hub while still permitting sufficient torsional flexibility to accommodate the full range of tail rotor blade pitch change. The feasibility of this concept has previously been demonstrated by the bench and whirl testing reported in References 1 and 2. This testing of an EPB tail rotor, developed for use on the UH-1 helicopter, included overspeeds to 110% RPM, full pitch range of -6^{o} to $+19^{o}$, and simulated forward flight speeds up to 105 knots. Thus, this preliminary elastic pitch beam tail rotor (EPBTR) design has met many of the more rigorous requirements of production helicopter tail rotors, and further development of the elastic pitch beam concept to obtain a flight-worthy tail rotor for the UH-1 helicopter is considered to be a desirable objective and is the one to which this program is addressed.

---

1. Maloney, Paul F., Clark, Frank B., McIntyre, Hugh H., APPLICATION OF DIRECTED GLASS FIBER REINFORCED PLASTIC TO HELICOPTER TAIL ROTOR ASSEMBLY, Kaman Aerospace Corporation, Bloomfield, Connecticut; USAAVLABS Technical Report TR 68-29, U.S. Army Aviation Materiel Laboratories, Fort Eustis, Virginia, June 1968, AD 674252.

2. Maloney, Paul F., Clark, Frank B., and McIntyre, Hugh H., STUDY AND EVALUATION OF DIRECTED GLASS FIBER REINFORCED PLASTIC HELICOPTER TAIL ROTOR ASSEMBLY, Kaman Aerospace Corporation, Bloomfield, Connecticut; USAAVLABS Technical Report TR 69-43, U.S. Army Aviation Materiel Laboratories, Fort Eustis, Virginia, October 1969, AD 863062.

Design guidelines established at the onset of this program were to use the basic requirements previously established for the standard UH-1H tail rotor to develop an EPBTR design that would eliminate the need for highly loaded pitch bearings; that would result in improved performance, reliability and maintainability; and that would preserve the flapping/pitch characteristics of the standard tail rotor at the EPBTR to tail rotor shaft juncture by retaining the 35-degree delta-three teeter axis. During whirl testing of the rotor and during ground tie-down testing with the rotor mounted on a UH-1H helicopter, however, it became evident that an instability problem existed with the teetering rotor system. This condition was subsequently eliminated by locking out the teeter freedom of the rotor and permitted the program to continue to its completion with some flight envelope restrictions caused by an increase in hub moments being applied to the tail rotor shaft, tail rotor gearbox, and tail pylon due to the teeter lockout.

The program, reported herein, explores the capabilities of an elastic pitch beam tail rotor developed to the same requirements as the current UH-1H tail rotor blade and hub assembly shown in Figure 1. This effort progressed from the design/analytical phase through bench and whirl testing to the final phases of ground and flight testing on a UH-1H helicopter. Also reported are the results of a reliability and maintainability investigation, which included the development of field service repair kits and repair procedures, a controlled "mock" field service evaluation of the repair kits and procedures, whirl testing of repaired tail rotor blade assemblies to determine the limits of repairability, flight testing of two repaired tail rotor assemblies to verify the adequacy of the repairs, and the results of analyses performed to determine the potential impact of the elastic pitch beam tail rotor on the UH-1 tail rotor subsystem and control system reliability, maintainability, safety, and cost characteristics.

The results of the program are presented in two sections. The first section includes the design/analysis/test phase up to and including the engineering flight evaluation of the elastic pitch beam tail rotor, and the second section presents the results of the reliability and maintainability investigation including whirl testing and flight testing of repaired elastic pitch beam tail rotor assemblies as well as the results of the cost effectiveness analysis, which measures the potential impact of the EPBTR on the UH-1 tail rotor subsystem.

Figure 1. Standard UH-1 tail rotor.

SECTION I - DESIGN THROUGH INITIAL FLIGHT EVALUATION

This section of the program covers the detailed design of the tail rotor system giving specific attention to weight, cost, durability, producibility, reliability, maintainability, and improved service life; the results of analyses defining the aerodynamic, dynamic, and structural capabilities and characteristics of the system; fabrication methods, procedures, and tooling required to produce the individual components and final tail rotor assemblies; the results of structural bench testing such as static and fatigue testing; the results of a 50-hour whirl test program covering a spectrum of rotor speeds and pitch settings that are representative of actual flight; the results of a ground test program during which the EPBTR was mounted on a UH-1H helicopter to determine the functional and stability characteristics of all systems affected by the tail rotor so as to insure the safety and acceptability of the rotor system, as well as the aircraft, for flight testing; and the results of a 20-hour flight test program that included a qualitative evaluation of directional control and a quantitative evaluation of tail rotor loads and power required during flights covering the level flight envelope sidewards flight, hover turns, and maximum power climbs.

ROTOR ASSEMBLY DESIGN

Table 1 presents the physical characteristics and operating rotor speeds for the standard UH-1 tail rotor and those used in the design of the elastic pitch beam tail rotor. Figure 2 is a photograph of the completed EPBTR system, and Figure 3 presents the basic features of the EPBTR. It should be noted at this time that the EPBTR shown here is configured as a teetering rotor having the same 35-degree delta-three angle between the teeter axis and the pitch axis as the standard UH-1 tail rotor. During whirl testing, and ground testing of the EPBTR on the aircraft, test results indicated the presence of an instability involving teeter motion coupled with the symmetric inplane bending mode at pitch angles of 12 to 12-3/4 degrees. Locking out the teeter freedom eliminated this mode of vibration and allowed full spectrum testing during the ground runs up to the drive system limitations of the aircraft.

TABLE 1. PHYSICAL CHARACTERISTICS AND ROTOR SPEEDS

Item	Standard Rotor	EPBTR
Number of Blades	2	2
Rotor Diameter (Ft)	8.50	8.50
Blade Area (Ft^2)	5.95	7.08
Disk Area (Ft^2)	56.75	56.75
Blade Chord (In.)	8.41	10.00
Rotor Solidity	.105	.125
Blade Airfoil (NACA)	0015	0022-0009.5
Blade Pitch Range (Deg)	19 to -6	19 to -6
Delta Three (Deg)	35	35*
Blade Twist (Deg)	0	0
Blade Precone (Deg)	1.5	0
Rotor Speed (RPM)		
Minimum, Power On and Off	1454	1454
Maximum, Power On	1654	1654
Maximum, Power Off	1732	1732
Limit Power On and Off	1819	1902

*Delta-three angle for EPBTR having teetering freedom is 35 degrees. For EPBTR with teetering freedom locked out, delta three is approximately 0 degree.

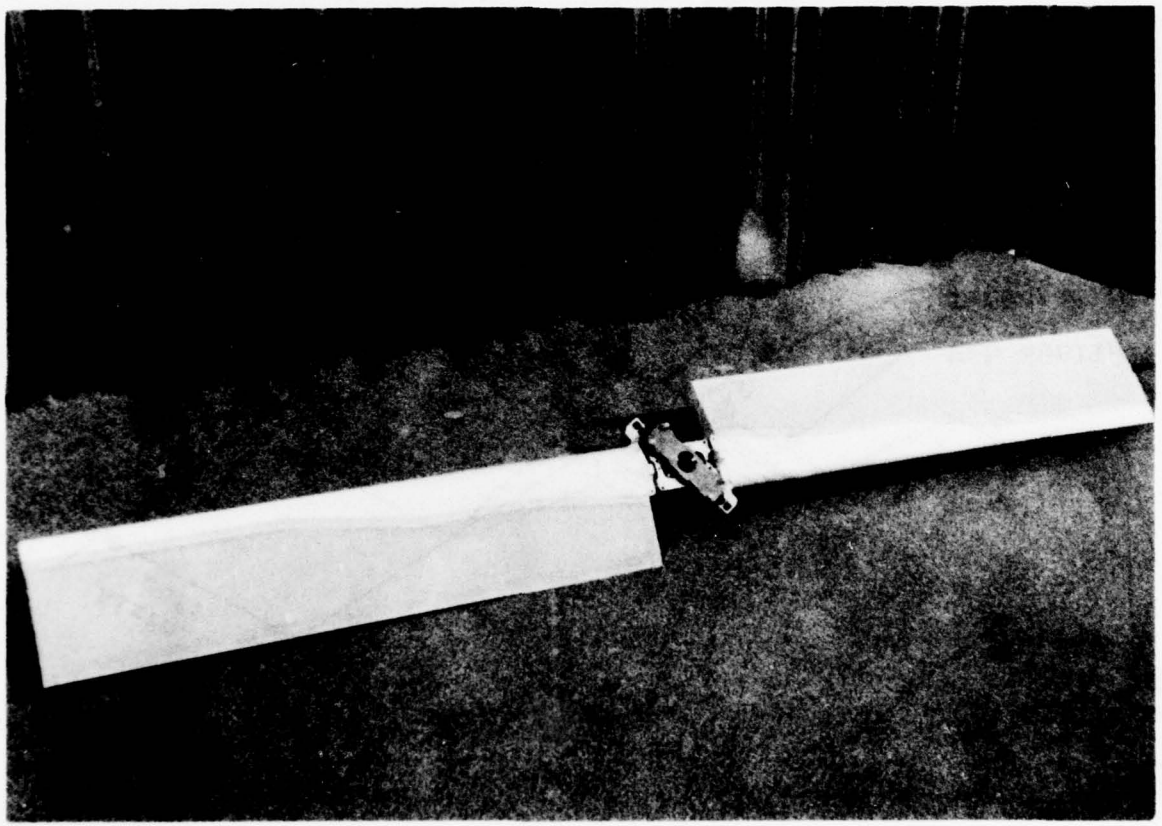

Figure 2. UH-1 elastic pitch beam tail rotor.

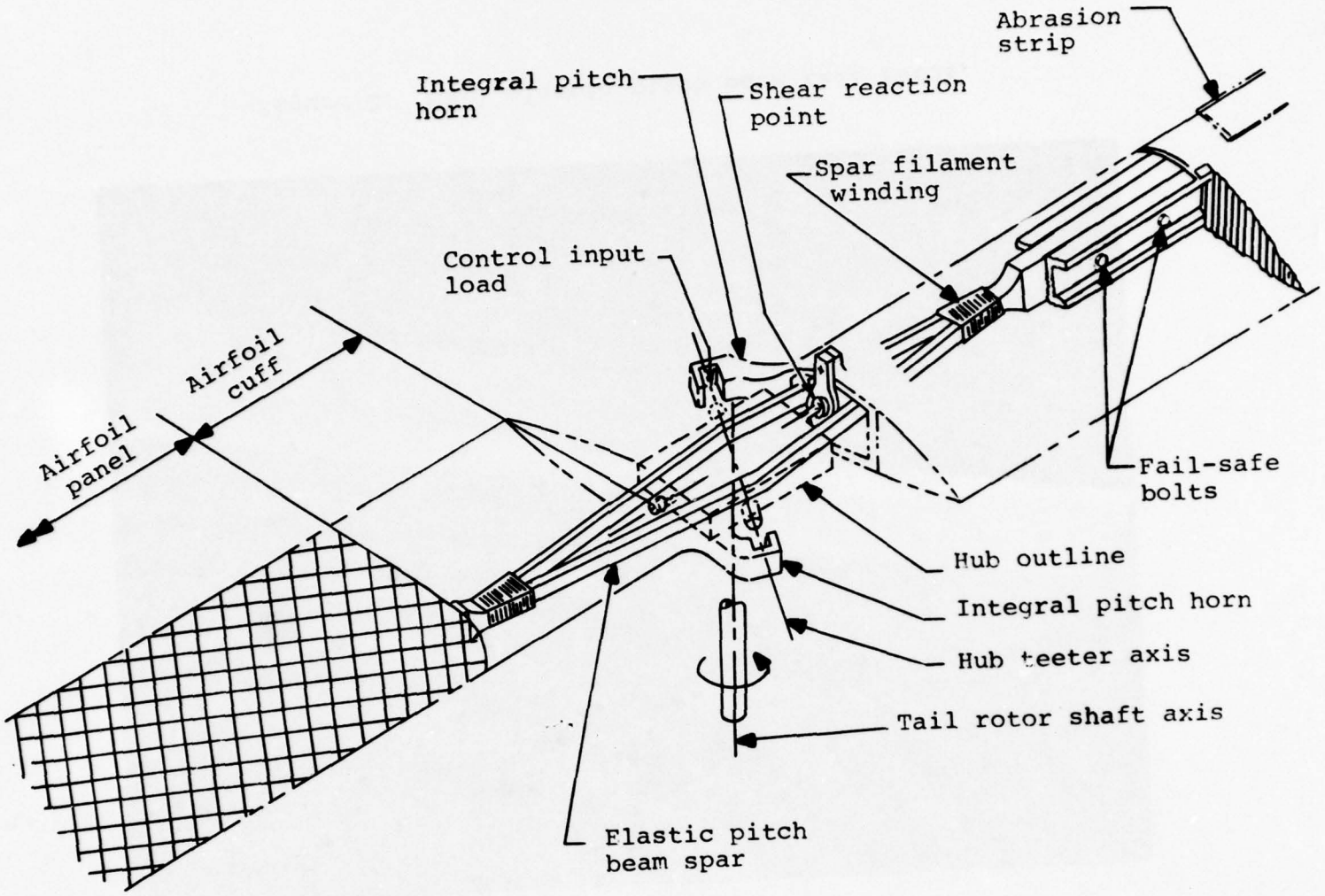

Figure 3. Elastic pitch beam tail rotor concept.

For ease of discussion, the elastic pitch beam tail rotor system is considered to be comprised of four subassemblies: the elastic pitch beam assembly, the airfoil section assembly, the hub assembly, and the control system assembly. In general, the elastic pitch beam forms the main load-carrying system of the structure. The centrifugal force of the airfoil section as well as inplane and out-of-plane bending moments and shear must be carried by this member. Airfoil sections are bonded to the outboard ends of the EPB and extend inboard over the EPB to form a torsionally stiff cuff for applying pitch control moments to the airfoil section - EPB attachment area. The EPB passes through, and is bonded to, the inner hub portion of the hub assembly. Teeter bearings are mounted on trunnions, integral portions of the inner hub, and within bores provided in the split outer hub, to permit teeter freedom of the EPBTR with respect to the outer hub-tail rotor shaft. The outer hub is splined and clamped to the tail rotor shaft and transmits shaft torque into the inner hub-EPBTR assembly through the teeter bearings. Changes to the present control system required to accommodate the EPBTR on the UH-1H helicopter are kept to a minimum. Only the 204-011-711 crosshead assembly mounted on the 204-010-742 control tube need be revised to reflect the use of the larger pitch horn offset incorporated in the EPBTR design. A more complete discussion of the four assemblies making up the elastic pitch beam tail rotor assembly follows.

Elastic Pitch Beam Assembly Design

The elastic pitch beam portion of the elastic pitch beam tail rotor assembly shown in Figure 4 is built up from two unidirectional "Scotchply" Type 1002-1014S glass straps .380 inch wide by .600 inch deep, interconnecting I-section webs of $\pm$ 45-degree 1002-1014S glass located between the two straps symmetrical to the assembly's centerline, outboard reinforcing webs of .040-inch-thick 301-¼ hard stainless steel, four outer spacer blocks per end fabricated from chopped glass fiber and molding compound, and "S" glass filament winding located at the outboard intersections of the two straps.

The elastic pitch beam design selected is basically a glass composite structure configured to form a tapered I-beam that is symmetrical about its center at the hub and tapers outboard to form verticies at the point of airfoil section attachment with the unidirectional glass composite straps forming the flanges of the I-beam and the $\pm$ 45-degree glass composite structure forming the web.

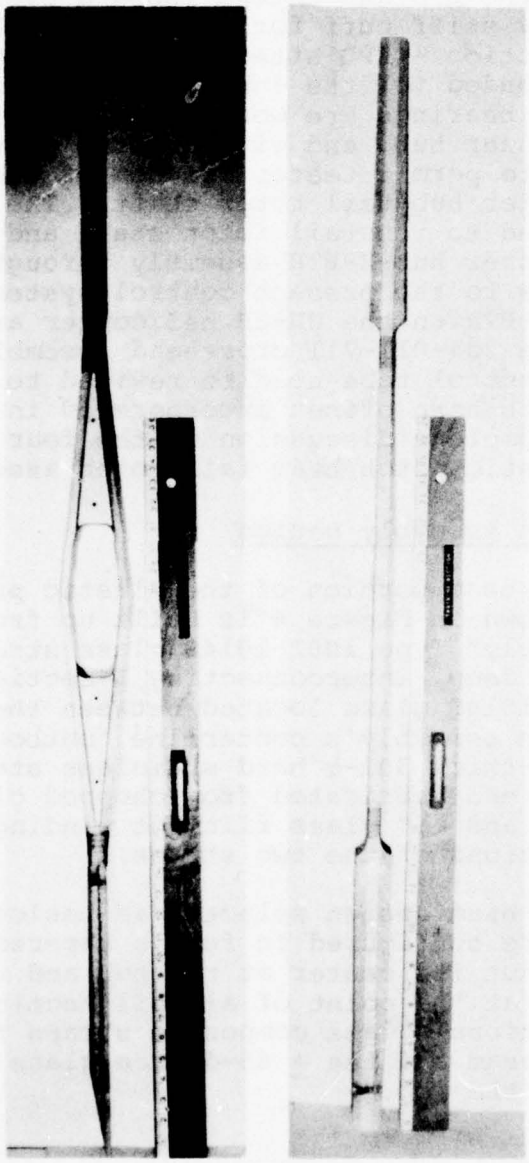

Figure 4. Elastic pitch beam assembly.

Stainless steel reinforcing webs were inserted between the two straps at their outboard ends to aid in distributing the concentrated strap loads into the four spacer blocks and thence into the airfoil section structure through their bonded interfaces. These stainless steel webs are also used to increase the bearing area for the two fail-safe bolts passing through the two aluminum airfoil section channels and the two straps of the EPB. The tapered portions of the elastic pitch beam located between the hub and the inboard airfoil section attachment areas provide the torsional freedom about the pitch axis required for pitch change control. The tapered configuration was selected over other possible configurations because it is a torsionally flexible structure having a relatively low torsional spring rate, a relatively low out-of-plane bending stiffness and a relatively high inplane bending stiffness. Low torsional spring rates are required to limit the increase in control loads required to obtain the desired blade pitch angle. Low out-of-plane and high inplane bending stiffnesses are dictated by stability considerations. In order to minimize the total weight and to reduce the duty of the tail rotor's control system, it is desirable to limit the use of centrifugal twisting moment counterweights for overcoming excessive centrifugal restoring, or feathering, moments that are, in part, dependent on the configuration of the elastic pitch beam portion of the tail rotor assembly. The tapered beam configuration accomplishes this objective due to the small compact cross section of the EPB at its outer verticies. Reductions in inplane stiffness of the EPB with increasing pitch angles are also minimized due to the small cross-sectional area of the EPB.

Airfoil Section Assembly Design

The airfoil section assembly attached to the outboard ends of the elastic pitch beam is an aluminum-glass composite structure having a constant planform chord width of 10 inches and tapers uniformly in thickness from a NACA 0022 airfoil at Station 3.5 to a NACA 0009.5 airfoil at Station 51. A .050-inch-thick 6061-T6 aluminum alloy C-section forms the leading-edge of the airfoil section assembly. Two .063-inch-thick 6061-T6 aluminum alloy channels form the closure for the leading edge C-section to form a D-section spar and also provides the primary structure for attaching the outer ends of the elastic pitch beam The forward channel extends from just inboard of the EPB-airfoil section attachment outboard to the blade tip at Station 51, and the aft channel extends from the inboard pitch fitting outboard to just beyond the outer portion of the EPB-airfoil section attachment. A typical cross section through the EPB-airfoil section attachment area is shown in Figure 5. As noted, the airfoil section is orientated at a pitch angle of

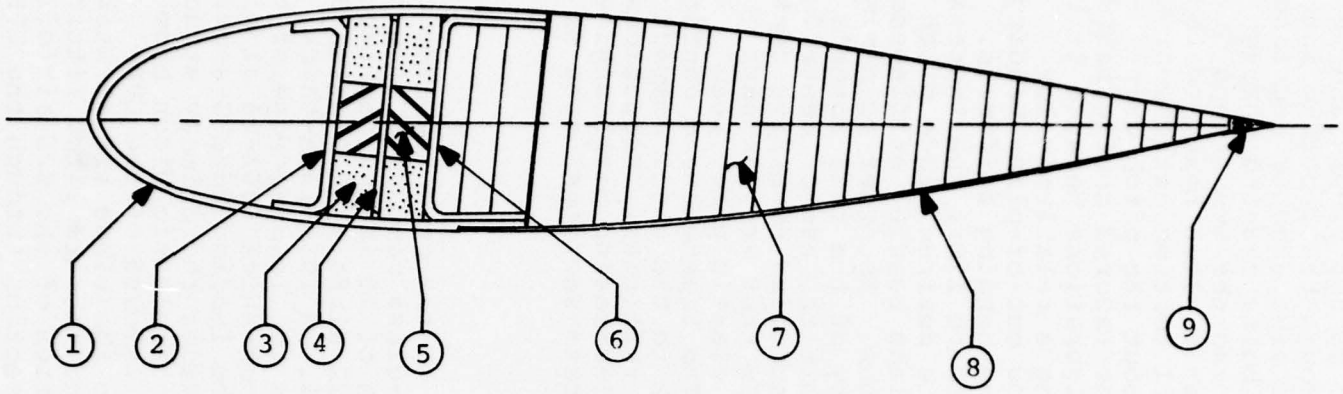

NOMENCLATURE

(1) Spar, .050-in.-thick 6061-T6 Al Alloy.

(2) Forward channel, .063-in.-thick 6061-T6 Al Alloy.

(3) Blocks, molded chopped glass fiber.

(4) Web, .040-in.-thick 301 CRES 1/4 hard.

(5) Straps, .600-in. x .380-in. 1002-1014S glass.

(6) Aft channel, .063-in.-thick 6061-T6 Al Alloy.

(7) Core, 1/8 - 1.8 polyamide honeycomb.

(8) Skins, .020-in.-thick BP-919/7581 fiberglass.

(9) Spline, BP-919/7581 fiberglass.

Figure 5. Cross section details at station 13.

5 degrees with respect to the X-Z plane of the elastic pitch beam to lessen the torsional duty of the EPB when the airfoil section experiences its full -6 to 19 degree pitch range. The elastic pitch beam assembly is bonded between the two channels and between the upper and lower portions of the leading C-section. Two fail-safe bolts passing through the fore and aft channels and the elastic pitch beam assembly are provided, as shown in Figure 3, to increase the clamp-up between the EPB and the channels as well as to provide a secondary load path in case of partial attachment bond failure.

The aft structure of the airfoil is constructed from 2-ply BP 919/7581 fiberglass upper and lower skins supported by 1/8 - 1.8 polyamide honeycomb core (Nomex), and a BP 919/7581 fiberglass trailing-edge spline. This structure is bonded to the upper and lower surfaces of the leading-edge C-section and to the aft channel inboard and the forward channel outboard.

At the leading-edge portion of the inboard end of the airfoil section, a 6061-T6 aluminum alloy pitch fitting is inserted and bonded between the leading-edge C-section and aft channel. A pitch link clevis, an integral part of the pitch fitting, provides a means for attaching the standard UH-1H 204-011-762 pitch link assembly used for pitch control. Also located on the pitch fitting are two lugs used for attaching the centrifugal counterweight arm/shear reaction bearing housing. A 2-ply BP 919/7581 fiberglass inboard rib is used to close the aft inboard airfoil section.

Provisions are incorporated at the forward outboard end of the airfoil section within the leading-edge C-section and the forward channel for attaching weights used for balancing the complete elastic pitch beam tail rotor assembly and for retaining the tip cap. Fine tuning of the assembly is accomplished by adding or removing washers located in the tip cap cavity. The aft portion of the airfoil section at the outboard tip is closed off by a 3-ply BP 919/7581 fiberglass closure rib bonded to the upper and lower skins and to the Nomex honeycomb core.

An abrasion strip of .060-inch-thick urethane is bonded to the outer leading-edge portion of the airfoil section to protect the leading-edge C-section from abrasion and erosion damage. Urethane was selected for this purpose after reviewing the results of an erosion test program reported in Reference 3.

---

3. Falcone, A.S., Clark, F.B., and Maloney, P.F., ELASTIC PITCH BEAM TAIL ROTOR OPERATIONAL SUITABILITY INVESTIGATION, Kaman Aerospace Corporation, Bloomfield, Connecticut; USAAMRDL Technical Report TR-74-60, U.S. Army Air Mobility Research and Development Laboratory, Fort Eustis, Virginia, July 1974, AD 784595.

Test results indicated that urethane had a high resistance to sand erosion but was susceptible to rain erosion. Harder materials that had acceptable erosion rates in rain had poor resistance to sand erosion. The use of the urethane material was thus a compromise and was chosen because of the ease in which the urethane abrasion strips could be replaced when required and due to its low cost.

HUB ASSEMBLY DESIGN

The teetering hub design for the elastic pitch beam tail rotor is shown in Figure 6. This assembly is comprised of two basic subassemblies: the inner hub assembly including the inner hub, cover plate, bearing sleeves, and shear raction pins; and the outer hub assembly including the split outer hub, teeter bearings, and bearing housings.

Physical features incorporated in the design of the stainless steel inner hub are two rectangular-shaped grooves through which the elastic pitch beam straps pass, two integral trunnions located at 35 degrees to the chordwise axis of the rotor and used to establish the delta-three teeter axis, provisions for the installation of two shear reaction pins, and surfaces to be used as teeter limit stops.

The configuration of the two elastic pitch beam grooves, and the physical dimensions and properties of the polyurethane elastomer separating the EPB straps from the hub, Figure 7, were selected to relieve the high local bending stresses in the EPB strap at the location of the strap emergence from the hub by controlling the bending curvature of the straps. This elastomer also aids in protecting the straps from fretting. Strips of polyurethane, having a durometer of 95 Shore A, were bonded between the EPB straps and the hub using a polyurethane adhesive. Tests were performed to insure that the shear strength of the polyurethane strips and the shear strengths of the bonds between the hub, polyurethane strips, and EPB straps were adequate for transferring the applied shear forces between the inner hub and the EPB strap. Shear forces acting at these interfaces are primarily due to shaft torque, inplane and out-of-plane shear forces originating outboard on the rotor blade, and differential axial strains between the straps and the hub resulting from centrifugal forces being applied to the elastic pitch beam straps.

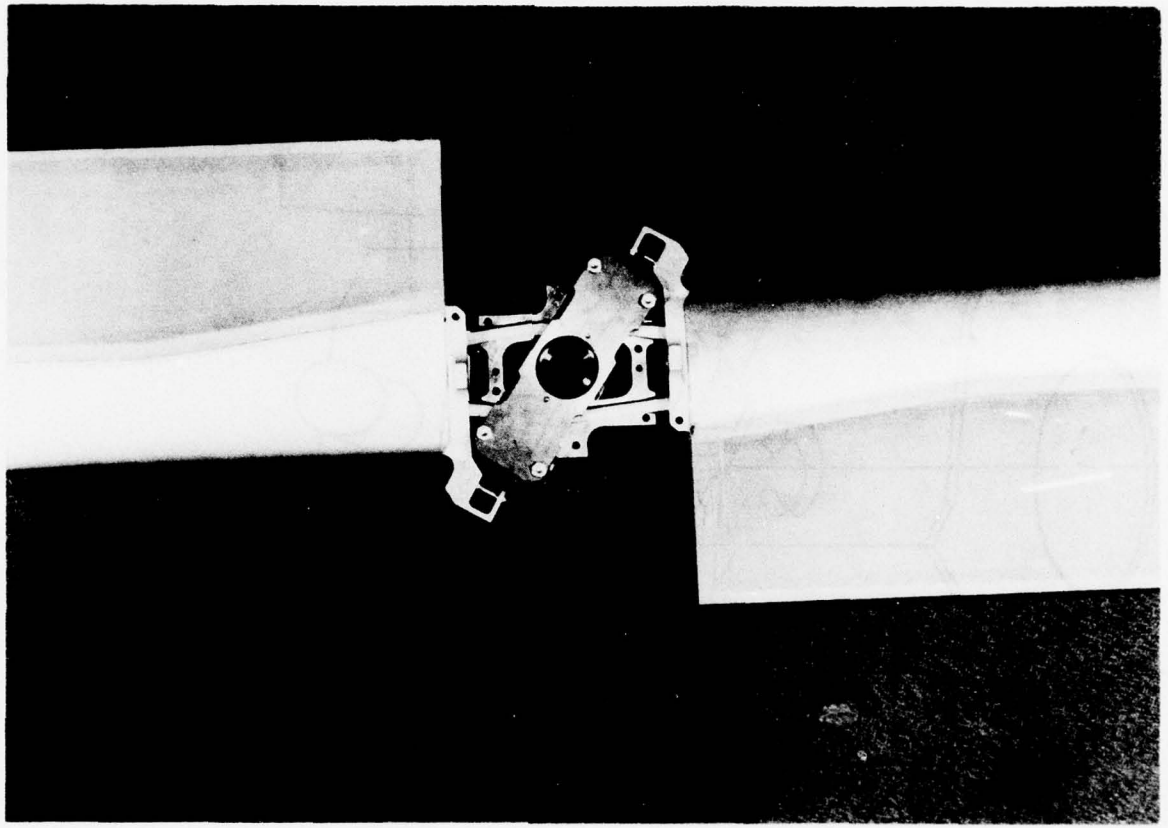

Figure 6. Teetering hub (cover plate removed for clarity).

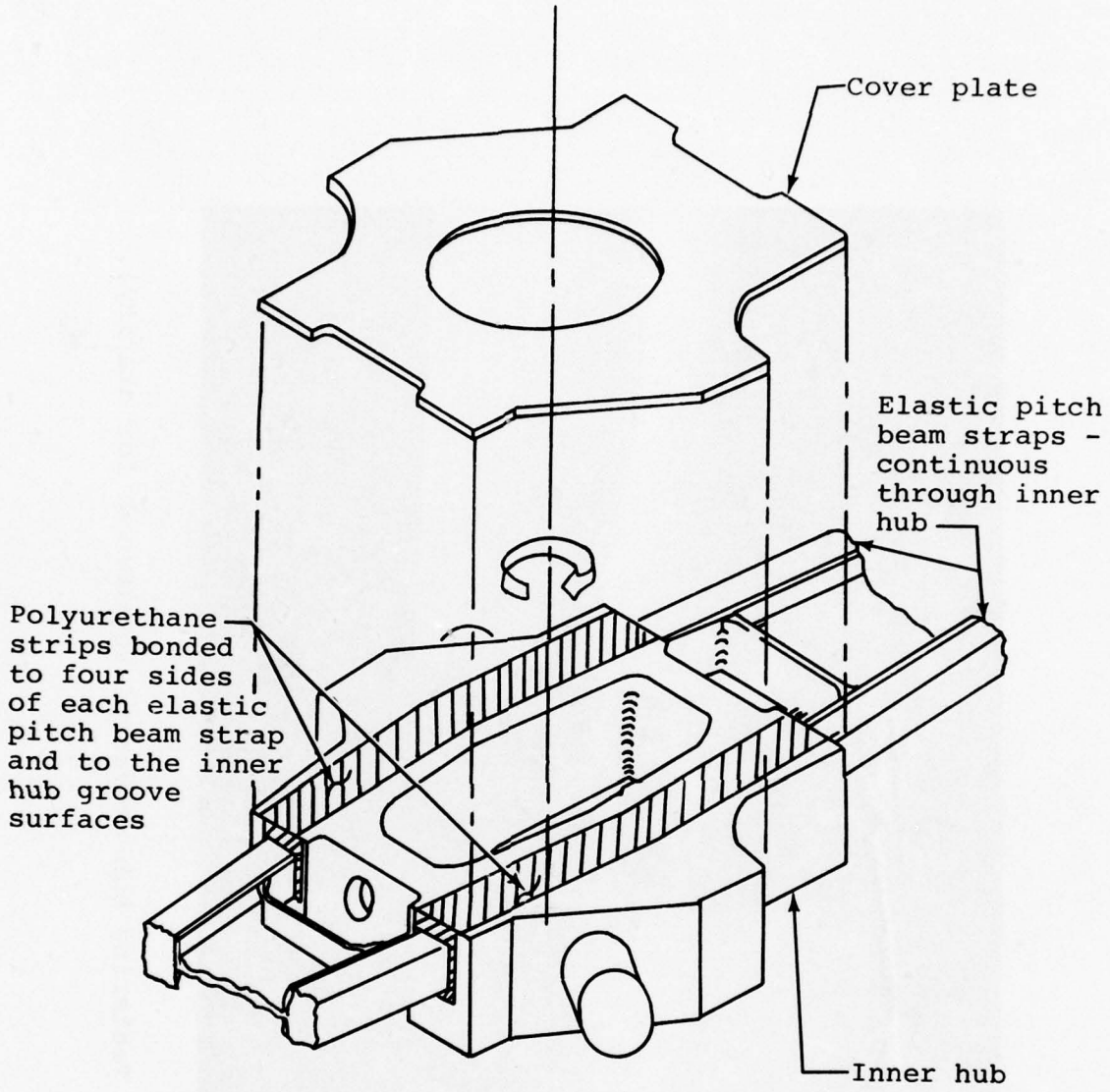

Figure 7. Elastic pitch beam attachment to inner hub.

Two shear reaction pins, located on the spanwise axis of the rotor at the outer ends of the inner hub, are pressed into holes provided in the inner hub and are retained by dowel pins passing through the inner hub and the shear reaction pins. The inboard ends of the shear reaction pins are drilled and tapped to facilitate their removal. These pins are used to transfer a portion of the shear loads originating outboard on the blades inboard to the hub and also aids in establishing the flapping axis location.

A .125-inch-thick stainless steel cover plate, conforming to the planform outline of the inner hub is bolted to the outer surface of the inner hub. This cover plate aids in the retention and protection of the elastic pitch beam straps.

The upper and lower hubs of the split outer hub assembly are provided as matched sets and are mounted on the present UH-1 tail rotor shaft using current attachment hardware, i.e., the matched cone set and the attachment nut (Bell Part Numbers 204-010-724-5 and 204-010-719-1 respectively). Matched splines, that are also compatible with the tail rotor shaft spline, are provided at the centers of the upper and lower hub to insure interchangeability of the EPBTR with the present UH-1 tail rotor. The inner and outer hub assemblies are connected through the teeter bearings. Teeter bearings are first pressed into the bearing housings and then installed on the trunnions of the inner hub. Upper and lower hubs of the outer hub assembly are placed in their proper position on each side of the inner hub assembly and are then connected by four bolts which also provide clamping pressure between the outer hub and the bearing housings.

It should be noted that with the elimination of the teeter axis requirements resulting from locking out the teeter freedom of this system, the hub design shown in Figure 3 could be simplified considerably. The outer hub, teeter bearings, bearing housings, and the trunnions forming an integral part of the inner hub could be eliminated, and the inner hub could be modified to include the hub-shaft spline now located in the split outer hub.

Control System Design

Revisions to the UH-1 tail rotor control system involved only the replacement of the present crosshead assembly (Bell Drawing Number 204-011-711) with a longer, stronger crosshead assembly to accommodate the larger pitch horn offset of the EPBTR. The resulting reduction in pitch angle sensititity for a given amount of pedal displacement is offset by the improved aerodynamic characteristics of the EPBTR airfoil section. As noted

in Table 1, the chord of the EPBTR has been increased from 8.41 inches to 10.0 inches or an increase in rotor solidity from .105 to .125, and the EPBTR airfoil section tapers from a NACA 0022 airfoil at the inboard portion of the blade to a NACA 0009.5 airfoil at the blade tip as compared to the nontapered NACA 0015 airfoil of the present UH-1 tail rotor blade.

FABRICATION

The elastic pitch beam tail rotor was fabricated in four distinct steps: elastic pitch beam assembly fabrication, Figure 4; elastic pitch beam to channel bondment, Figure 8; final assembly, at which time the airfoil panels are bonded to the elastic pitch beam/channel assembly, Figures 9 and 10; and the hub to elastic pitch beam bondment, Figure 6.

Elastic Pitch Beam Assembly

The elastic pitch beam assembly consists of the following:

- Two elastic pitch beam straps.
- Two interconnecting composite webs.
- Eight molded chopped fiber spacer blocks, four at each end.
- Two stainless steel webs, one at each end.
- Filament winding at the outboard intersections of the two elastic pitch beam straps.

The two straps of the elastic pitch beam were molded separately in a cavity mold machined to the contour of the EPB. Forty-two plies of .600-inch-wide epoxy impregnated unidirectional 1002-1014S glass were laid in the mold. A closure bar having the same contour as the EPB and the cavity mold was then inserted in the cavity mold. The complete mold assembly was vacuum-bagged and the EPB strap was cured at a temperature of 330°-350°F and a pressure of 45 psi for 1½ hours at temperature. Stops, built within the mold, limited the travel of the closure bar to insure that the desired .380 inch thickness of the strap as well as the desired resin content of the composite were obtained.

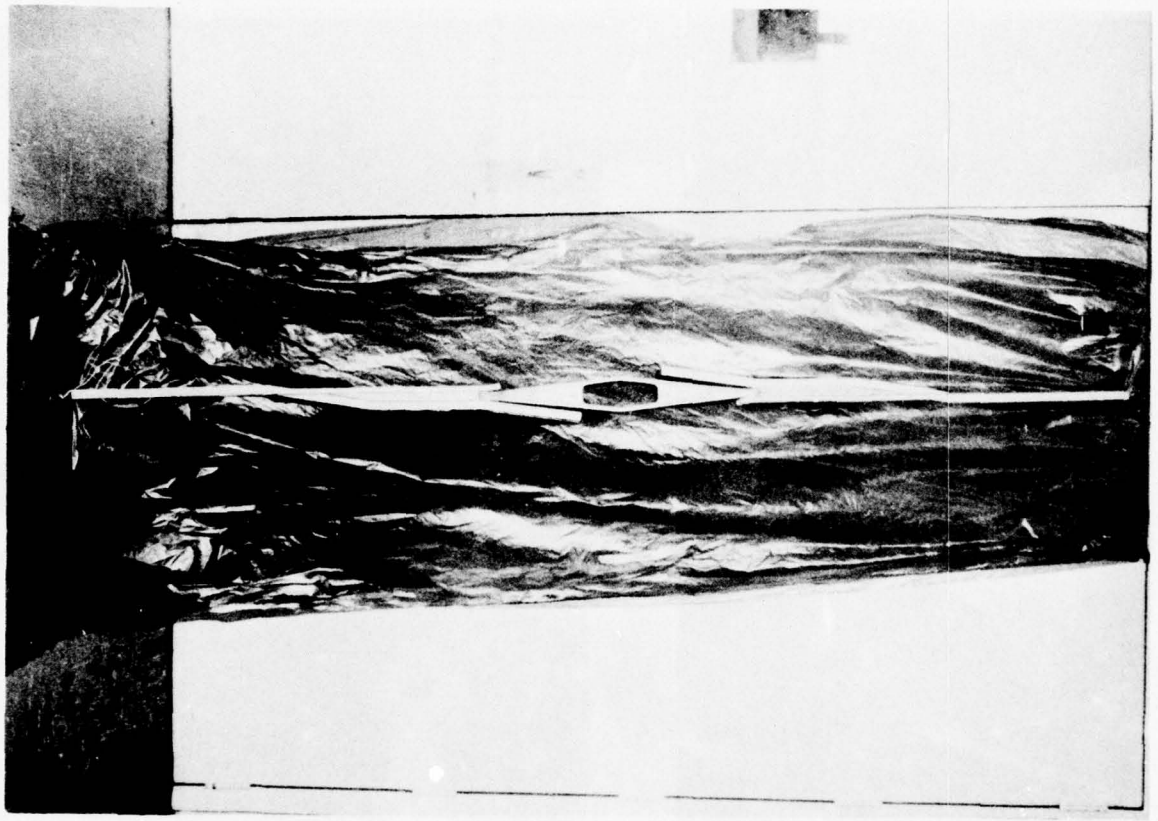

Figure 8. Elastic pitch beam with channels attached.

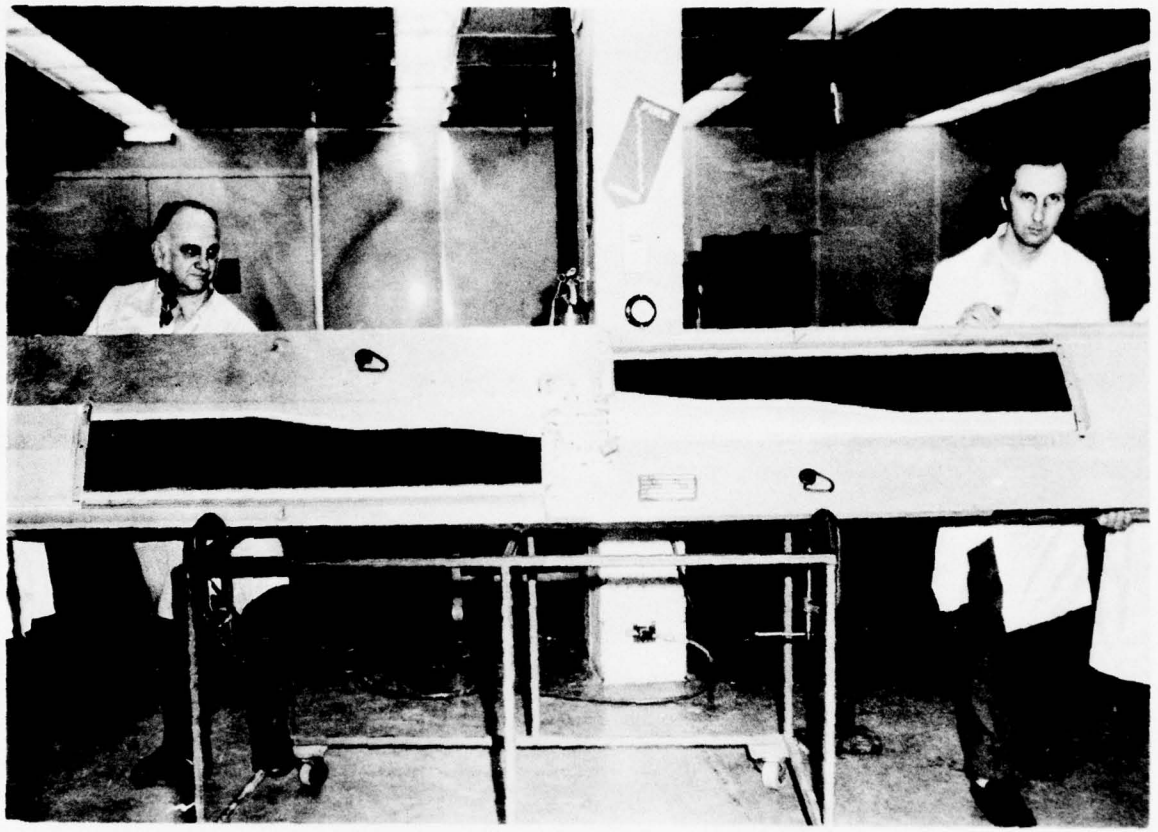

Figure 9. Airfoil section assembly bonding fixture.

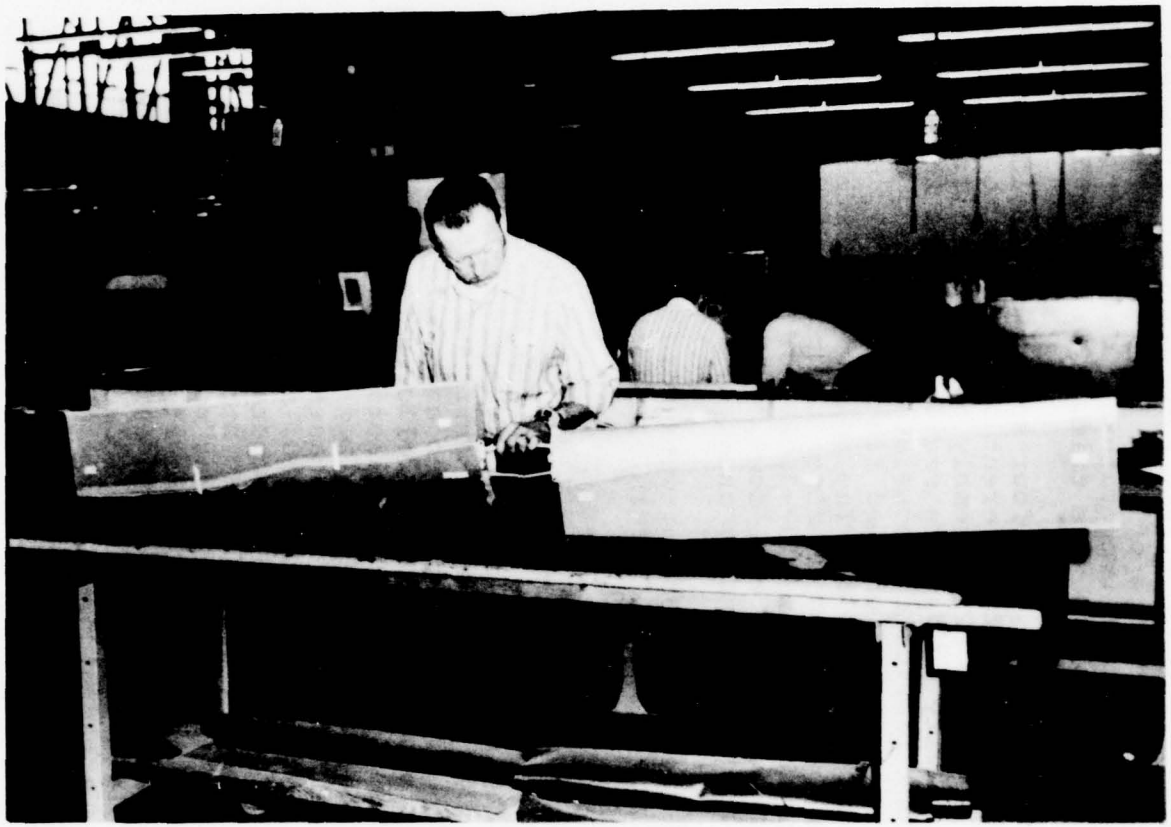

Figure 10. Elastic pitch beam tail rotor after removal from airfoil section assembly bonding fixture.

Interconnecting web assemblies were fabricated from six plies of ± 45-degree 1002-1014S glass. Three plies each were positioned on two forming and curing mandrels, and the flanges of the interconnecting web were hand-formed around the perimeter of the mandrels. The two mandrels were positioned together with the six plies of "S" glass sandwiched between them. This assembly was then vacuum-bagged and cured in an autoclave at a pressure of 45 psi and a temperature of 330°-350°F for 1½ hours at temperature. On completion of the cure cycle, the web flanges were trimmed to size and inspected.

As shown in Figure 5, the four spacer blocks located at each end of the EPB are of different contour due to the 5-degree orientation of the EPB assembly to the airfoil. As such, four different cavity molds were required to form these blocks. Spacer block fabrication consisted of placing a weighed charge of epoxy impregnated chopped fibers, 3M-1157, uniformly into a cavity compression mold. The mold was vibrated and then heated and pressurized to close the mold. A cure temperature was maintained between 340°-360°F for 1½ hours. Upon completion of the cure cycle and cool down, the spacer was removed from the mold and dimensionally checked.

Stainless steel reinforcing webs were blanked out of a .040-inch-thick 1/4 hard 301 stainless steel sheet and dimensionally checked.

On completion of the fabrication and inspection of the subassemblies, a dry layup of the strap assembly was made. All of the strap subassemblies were vapor-blasted, water break tested on all adhesive faying surfaces, and oven dried at 130°-150°F. The stainless steel web assemblies went through an additional pickle of HNO_3-HF followed by priming with Plastilock 718-2 primer. One layer of Plastilock 717, .030-lb/sq ft nonsupported adhesive was applied to the faying surfaces of all the subassemblies. The strap assembly was then placed on an assembly fixture, vacuum-bagged, and autoclave-cured at 35 psi, 250°-270°F for 1½ hours at temperature. On completion of cure and cool down the assembly was stripped from the assembly fixture, the adhesive flash was removed, and the strap assembly was visually inspected for adhesive integrity. The strap assembly was trimmed to length using a trimming fixture and an abrasive blade (Mfg: Norton, Blue Safety Blade, M.R.-822) mounted on a radial arbor saw. During trimming of the strap assembly, water was used to cool the composite assembly and the blade.

After trimming, the EPB was prepared for filament winding at the outboard strap intersection areas at both ends of the assembly. The faying surfaces were wiped with solvent, abraded with 180-grit sand paper, and wiped with solvent again. These

prepared areas were filament wound with eight consecutive layers of SCG 150 ¼-inch 3.8_S HTS 901 glass fiber. During the winding operation, an epoxy resin, Epon 820, was impregnated into the glass wraps and was subsequently cured at 150°-170°F for a minimum of 1½ hours. Figure 4 shows the completed EPB assembly.

Elastic Pitch Beam To Channel Bondment

Bonding of the fore and aft channels to the elastic pitch beam assembly was accomplished in an assembly fixture. On completion of a dry fit-up within the fixture, the channels were cleaned, etched, and primed with Plastilock 718-2 primer. Faying surfaces of the EPB assembly were vapor blasted, alkaline cleaned, checked for water break, and oven dried at 130°-150°F for 1 hour, minimum.

Plastilock 717, .060-lb/sq ft nonsupported adhesive was placed between all channel/EPB assembly faying surfaces with the exception of the trimmed outboard surfaces of the EPB assembly. The trimmed surfaces were covered with one ply of .025-inch-thick FM-37 manufactured by American Cyanamid Company. After placing the channels and the EPB assembly in the assembly fixture, the adhesive was cured in an air circulating oven at 250°-270°F for 1½ hours, while windjammers applied a pressure of 35 psi to the channels. After completion of the cure cycle, excessive adhesive flash was removed and the assembly was sonic tested for bond quality and was dimensionally checked. At this time, the two fail-safe bolts were installed in bolt holes drilled through the two channels and through the EPB assembly. Figure 8 shows the completed EPB assembly with the two channels attached.

Final Assembly Bondment

The attachment of the airfoil sections to the EPB assembly/channel bondment was accomplished in the final assembly bond fixture shown in Figure 9. Details and subassemblies bonded together during this phase were:

- EPB assembly/channel bondment
- C-shaped aluminum leading edge
- Nomex contoured honeycomb core
- Precured fiberglass skins
- Precured fiberglass trailing-edge spline
- Inboard pitch fitting
- Inboard closure rib
- Outboard closure rib

All aluminum faying surfaces were cleaned, acid etched, and primed after being dry-fitted in the assembly fixture. FM-37 foaming adhesive, .056-inch-thick, was placed on all four edges

of the nomex honeycomb core. Plastilock 717 adhesive, .030 lb/sq ft, was used to bond the skins to the nomex core, and Plastilock 717, .060-inch-thick, supported adhesive was used on all other faying surfaces. The assembly was vacuum-bagged and autoclave-cured at 250°-270°F at a pressure of 17 psi for 1½ hours at temperature. On completion of the cure, the assembly was allowed to cool to 150°F prior to releasing the pressure.

Upon removal from the bonding fixture, the EPBTR was cleaned of excessive adhesive flash, X-rayed, sonic tested, and dimensionally checked. Figure 10 shows the EPBTR at this fabrication stage.

Hub to Elastic Pitch Beam Bondment

The stainless steel inner hub was vapor blasted, alkaline cleaned, checked for water breaks, and oven dried at 130°-150°F for 30-60 minutes. Faying surfaces of the EPB were wet sanded, checked for water breaks, and oven dried at 130°-150°F for 30-60 minutes. Strips of .125-inch-thick and .015-inch-thick H-Tuff thermoset polyurethane, used between the inner hub grooves, cover plate, and EPB straps for stress control and fretting protection as shown in Figure 7, were trimmed to the proper sizes. The .125-inch-thick polyurethane strips are used between the EPB straps, the bottoms of the inner hub grooves, and the cover plate, whereas the .015-inch-thick polyurethane strips are used between the EPB straps and the sides of the inner hub grooves. The polyurethane strips were hand sanded, solvent wiped three times, and were then bonded to the EPB straps and the inner hub using Furane 8615 A/Bx, a two-part room temperature curing adhesive. Curing time for this adhesive was 24 hours at 70°F. Figure 6 shows the inner hub bonded to the EPB and also the outer hub attached to the inner hub at the teeter axis.

STRUCTURAL TEST

Bench testing conducted under this program and the concurrent program reported in Reference 3 included the following:

- Static development tests for perfecting the attachment of the elastic pitch beam to the outer airfoil panels.
- Fatigue testing of small flexural specimens for selecting a protective coating system to be used on the elastic pitch beam assembly.
- Effects of environmental conditions on the torsional spring rate of the elastic pitch beam.

- Sand and erosion testing to develop leading-edge erosion protection for the outer airfoil panels.

- Static test of the complete EPBTR assembly to determine its ultimate strength capability.

- Fatigue testing of elastic pitch beams exposed to various environmental conditions and having teeter freedom.

- Fatigue tests of complete EPBTR assemblies having teeter freedom.

- Fatigue tests of UH-1 tail rotor shafts and EPBTR's having the teeter degree of freedom locked out.

Elastic Pitch Beam/Airfoil Panel Attachment Development

During the early stage of this program, several full size elastic pitch beam/airfoil panel attachment designs were fabricated and evaluated to optimize the static strength capabilities of this critical area. Various schemes were investigated to transfer the centrifugal forces from the airfoil panels into the elastic pitch beam before the final configuration shown in Figure 4 was selected. Testing of the final design consisted of low-speed tension cycling from 500 to 15,000 pounds for a total of 1741 cycles. Stress-strain curves were recorded after every 200-cycle interval. No changes in the stress-strain curves were noted during the cyclic load portion of the testing. Sonic testing of retention channels to elastic pitch beam bonds indicated the possible presence of some voids in this bonded attachment. The specimen was then loaded in tension up to the ultimate failure load of the attachment area. An ultimate load level of 44,550 pounds was attained during this test, which is 1.82 times the ultimate centrifugal force load of 24,450 pounds acting on the elastic pitch beam at this location.

Elastic Pitch Beam Protective Coating Evaluation

Reference 3 reports the results of a study program designed to select a protective coating system that could be readily applied to the inboard exposed area of the elastic pitch beam to protect it from mechanical damage as well as from environmental conditions that might tend to degrade it. Parameters used in determining the suitability of coating systems were:

- Flexibility at temperatures of $-65^{o}F$
- Adhesion to fiberglass surfaces
- Tear and gouge resistance
- Resistance to aging and weathering
- Resistance to synthetic oils and fuels
- Ease of application.

As a result of a material survey, the three coating systems selected for further evaluation were:

1. Acrylic Nitro-Cellulose System

MIL-C-8514	Wash Primer (.0004-.0007)
MIL-C-7962	Primer (.0003-.0006)
MIL-L-19538	Acrylic Lacquer (.0005-.0008)

2. Urethane System

MIL-P-23377	Epoxy Primer (.0006-.0009)
MIL-C-81773	Aliphatic Urethane (.001-.0015)

3. Urethane

MIL-P-23377	Primer (.0006-.0009)
Adiprene L-167	Moca (.010-.015)

The fatigue test specimens used in the coating evaluation, Figure 11, were designed to be installed in a Krause-type reverse bending fatigue test machine. In order to reduce the duration of this test program, a special machine was designed to test five specimens simultaneously and was sized to fit inside an American Research Corporation Environmental Chamber Model No. SH027 as shown in Figure 12. This chamber is capable of temperature cycling, humidity control and solar simulation. The environmental cycle which was continually repeated after every 72 hours of testing consisted of:

- 48 hours at 95% relative humidity at 120°F
- 8 hours under solar simulation at approximately 105°F
- 8 hours at -65°F
- 8 hours at 130°F

Fatigue test results of bare and coated specimens are shown in Figure 13. Conclusions reached during this test program were:

1. The fatigue property of unidirectional S-Glass Type 1002-1014S under flexure is severely degraded by humidity when tested at 96,000 psi maximum stress. Coatings provide no significant protection at this stress level.

2. Fatigue properties of unidirectional S-Glass Type 1002-1014S are adversely affected by environmental cycling at the 85 ksi maximum stress level. The increase in the cycles to failure at the 85 ksi maximum stress level compared to the cycles to failure at the 96 ksi maximum stress level indicates that greater resistance to environmental factors could be expected at lower stress levels typical of normal design usage.

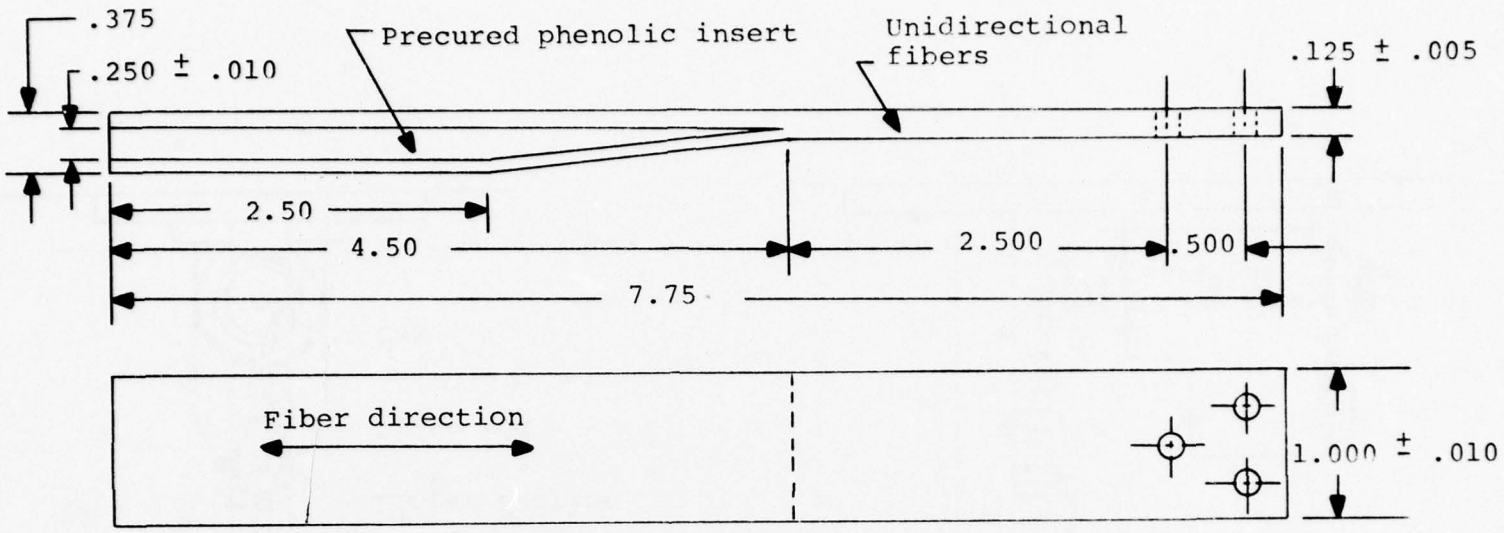

Materials: Phenolic insert - Machined from laminate of style 128 Fabric and Palmer No. 1000 resin
Unidirectional fibers - 1014S glass in epoxy matrix (3M-1002 system)

Dimensions are in inches.

Figure 11. Fatigue specimen design.

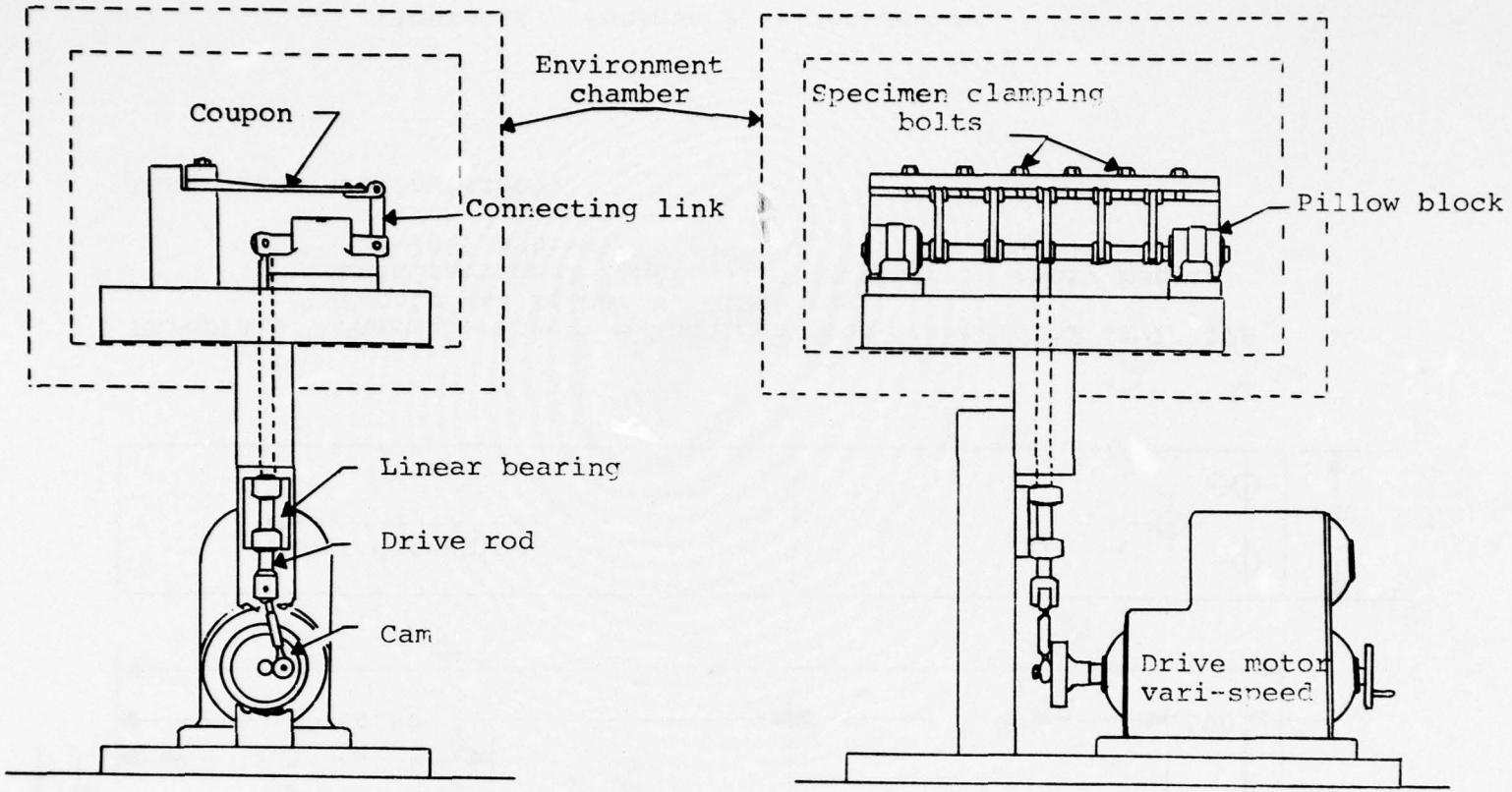

Figure 12. Test setup.

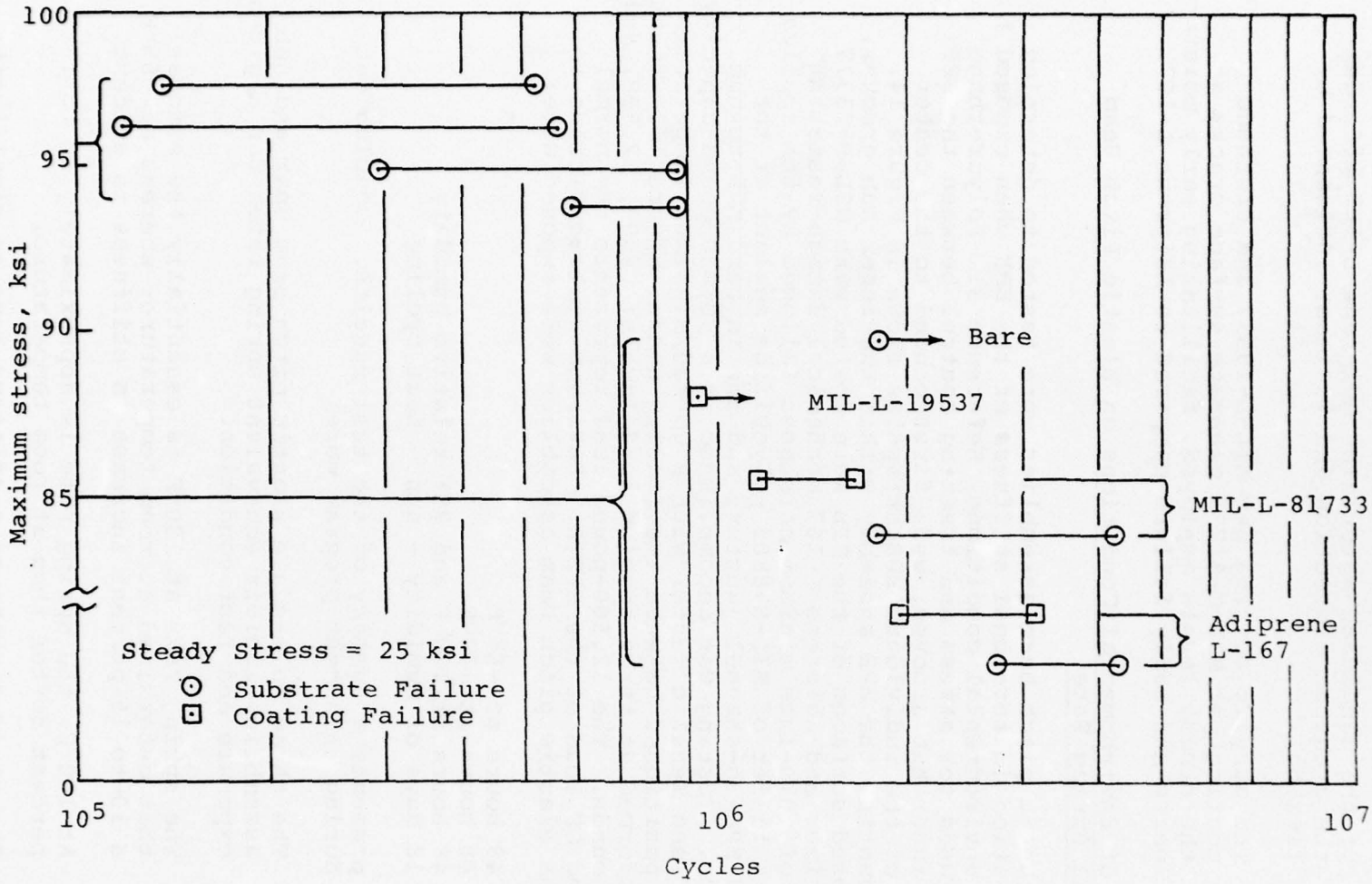

Figure 13. Fatigue performance of coatings under environmental exposure.

3. Of the candidate materials, Adiprene L-167 affords the greatest protection and is least influenced by flexing.

4. The acrylic coating per MIL-L-19537 and urethane coating per MIL-C-81773 generate surface cracks at the stress levels employed, facilitating early moisture entry and early failure compared to Adiprene L-167.

Effects of Environmental Conditions on Elastic Pitch Beam Torsional Spring Rate

Three elastic pitch beam assemblies were tested to determine the variation in torsional stiffness of the EPB when exposed to various environmental conditions, Reference 3. Polyurethane strips, used for stress and fretting control between the EPB and the inner hub grooves, were first bonded to the center portion of the individual EPB straps as shown in Figure 14. After mounting the EPB assembly within the inner hub grooves, the exposed surfaces of the EPB were coated with MIL-P-23377 epoxy primer and Adiprene L-167 mechanical-damage-resistant coating of .010-inch minimum thickness followed by the application of a fillet of MIL-S-8802 polysulfide sealant at the outboard EPB-to-channel juncture and the inboard EPB-to-hub interface. Testing was accomplished in a 60,000-pound-capacity Tinius Olsen Tensile Tester with a Conrad/Missimer Temperature Cabinet positioned between the loading heads, Figure 15. Tests were performed at three tension load levels: 6000, 12,500, and 15,000 pounds. The 12,500-pound load represents the normal operating CF load of the EPBTR. Environmental conditions to which the elastic pitch beam assemblies were exposed were:

- 48 hours at -65°F
- 48 hours at 130°F
- 48 hours at 120°F and 95% relative humidity
- 18 days of humidity - sun - heat cycling

Table 2 presents a summary of the test results. Conclusions reached during this test program were:

1. The three full-scale elastic pitch beam spar and hub assemblies exhibit equivalent spring rates for a given exposure and test condition.

2. The spring rate at 130°F is essentially the same as that determined at room temperature; whereas at -65°F, a 10- to 15-percent increase in stiffness is evident.

3. At 160°F, the spring rate is approximately 10 to 15 percent softer than at room temperature.

4. The various exposure conditions have no significant effect on spring rate.

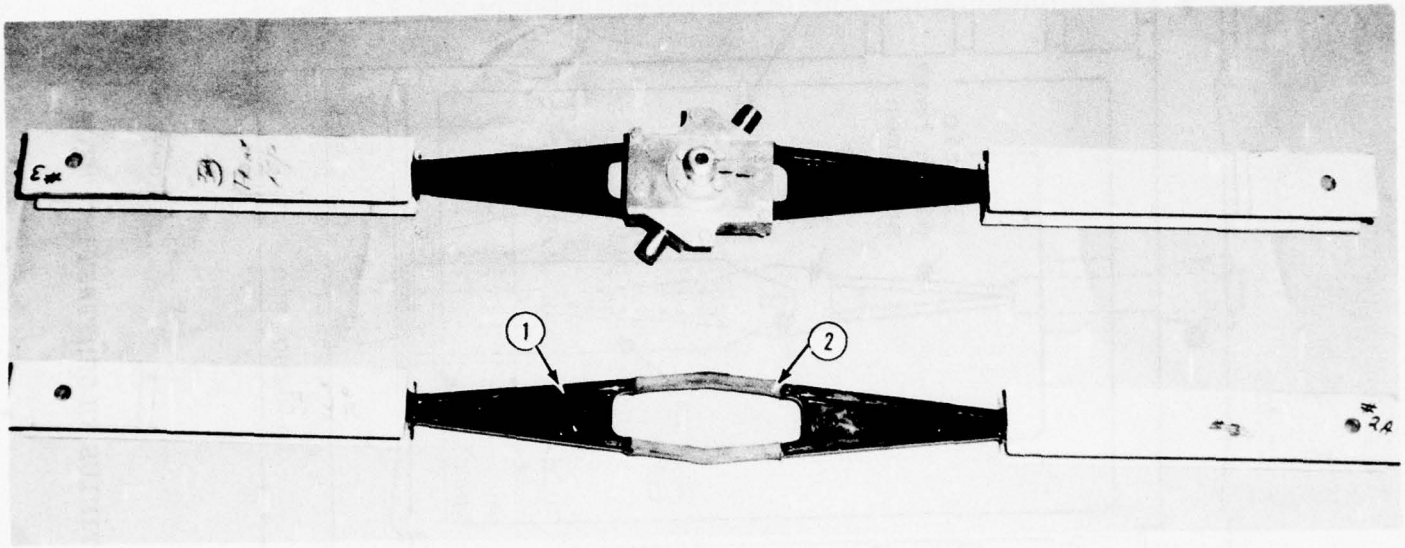

(1) Adiprene L-167 coating - elastic pitch beam region

(2) Urethane filler hub to spar attachment area

Figure 14. Elastic pitch beam test specimens with and without hub installation.

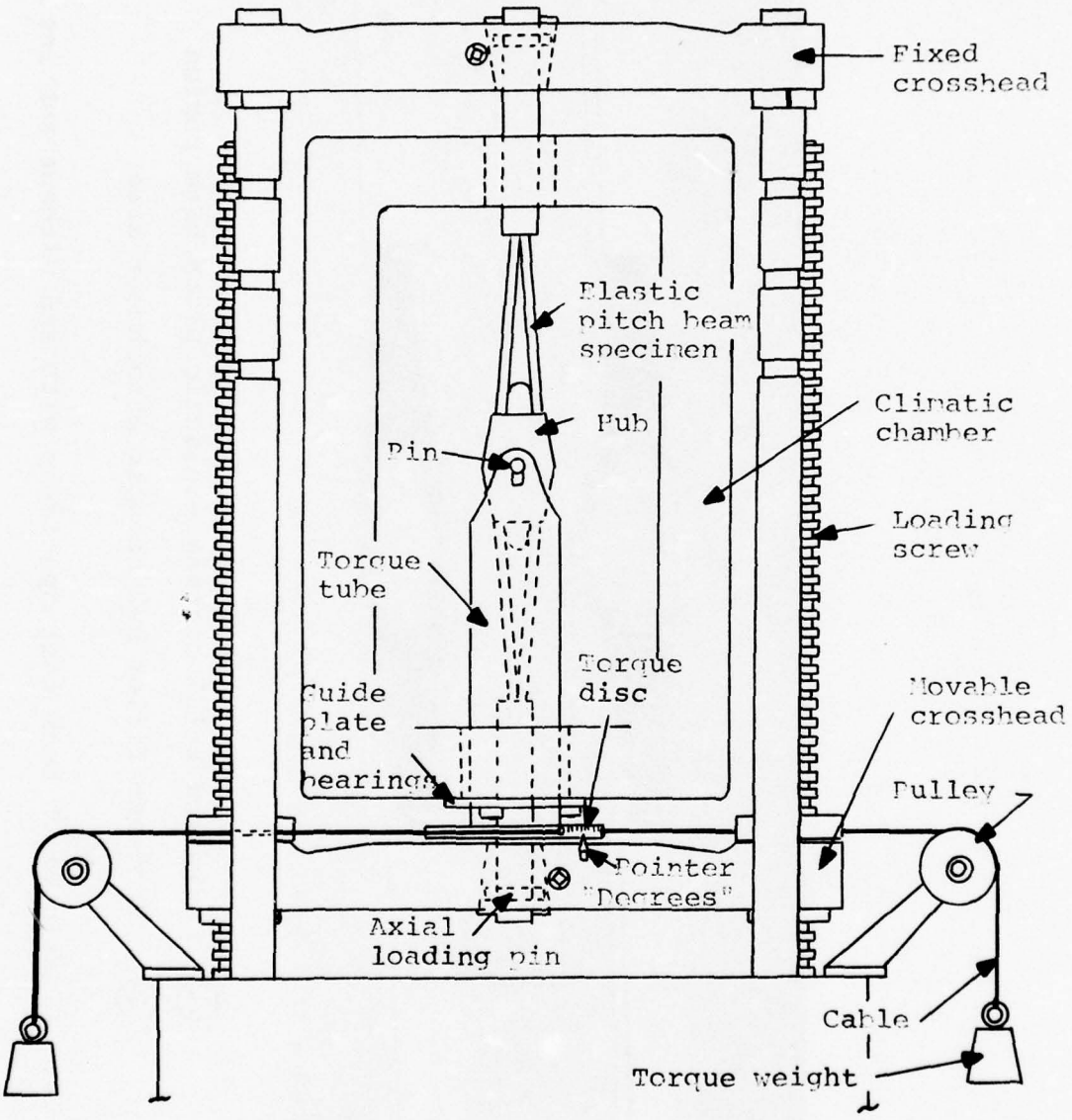

Figure 15. Spring rate test setup.

TABLE 2. TORSIONAL SPRING RATE, IN.-LB/DEGREE, AT VARIOUS TEMPERATURE AND LOAD LEVELS FOLLOWING ENVIRONMENTAL EXPOSURE

Test Temperature		-65°F			Room Temp			130°F			140°F			150°F			160°F		
C.F. Load (lb)		6,000	12,500	15,000	6,000	12,500	15,000	6,000	12,500	15,000	6,000	12,500	15,000	6,000	12,500	15,000	6,000	12,500	15,000
Spar No.	Environmental Exposure																		
2A	-	35.7	42.2	-	32.2	37.6	-	30.8	35.7	-	-	-	-	-	-	-	-	-	-
2B	-	37.6	39.9	-	30.2	33.0	-	32.2	35.7	-	-	-	-	-	-	-	-	-	-
3	-	37.6	42.2	-	32.2	35.7	-	30.8	35.7	-	-	-	-	-	-	-	-	-	-
2A	48 Hr @ -65°F	37.6	42.2	-	30.8	34.1	-	30.4	33.9	-	-	-	-	-	-	-	-	-	-
3	48 Hr @ -65°F	35.7	39.9	-	30.8	34.6	-	29.5	32.2	-	-	-	-	-	-	-	-	-	-
2A	48 Hr @ 130°F	36.5	40.8	-	32.2	35.4	-	30.8	34.6	-	-	-	-	-	-	-	-	-	-
3	48 Hr @ 130°F	36.5	40.8	-	32.2	35.4	-	30.8	35.7	-	-	-	-	-	-	-	-	-	-
2A	48 Hr @ 120°F and 95% R.H.	33.9	37.6	-	28.1	31.4	-	27.0	30.8	-	-	-	-	-	-	-	-	-	-
3	48 Hr @ 120°F and 95% R.H.	38.1	45.0	-	31.4	35.7	-	29.5	33.0	-	-	-	-	-	-	-	-	-	-
2A	18-Day Humidity-Sun-Heat Cycling	35.7	39.9	39.9	30.8	35.7	37.6	29.5	33.0	35.7	28.1	32.2	33.9	28.1	32.2	33.9	27.0	30.8	32.2
3	18-Day Humidity-Sun-Heat Cycling	37.6	40.8	42.2	30.4	35.7	35.4	31.4	33.0	35.7	30.8	34.6	35.7	30.4	33.0	35.7	28.8	32.2	33.0
2B	Control No Exposure	37.6	42.2	43.8	30.2	35.7	35.4	30.8	33.0	35.7	29.8	33.9	34.6	29.5	32.2	33.9	29.1	31.4	32.2

Sand and Rain Erosion Testing

The erosion protection task reported in Reference 3 evaluated various leading-edge materials for possible use on the elastic pitch beam tail rotor. Tests were conducted on a whirling arm rig at velocities approaching tail rotor tip speeds under controlled rates of sand and rainfall to simulate operational service in the Army environment. Conclusions arrived at during this test program were:

1. Polyurethane erosion guard provides the greatest resistance to sand abrasion by a factor of 10 over the best metallic material tested at a sand fall rate of 144 grams per minute at 530 mph (777 fps).

2. Electroformed nickel and titanium leading edge exhibit the lowest wear rates of the metallic materials tested. Although the wear rate in grams per minute is equivalent, the relative wear for titanium is 2.5 times that for nickel.

3. Electroformed nickel leading edges exhibit a failure mode characterized as wear, whereas stainless steel, Stellite and titanium after some wear exhibit a buckling type of failure mode at a thickness range of .004-.008 inch.

4. Stainless steel, titanium, and electroformed nickel leading edges can endure whirl test in a combination of sand and rainfall without damage from rain at 1-inch-per-hour rainfall at 500 mph (733 fps).

5. Polyurethane material cannot survive in a combination sand and rain environment, but merit for the thicker erosion guard was demonstrated.

6. Polyurethane material provides maximum cost effectiveness on the basis of maximum sand abrasion resistance, lowest weight, field repairability and low cost.

Elastic Pitch Beam Tail Rotor Assembly Static Test

The Elastic Pitch Beam Tail Rotor Assembly, K27-101 S/N 2, was tested statically as shown in Figure 16 to determine its ultimate strength and the critical failure location. Limit loads used for comparison are based on the 120-knot high-speed yaw condition at a tail rotor speed of 1902 rpm. Loadings applied during the test were centrifugal force, flatwise bending moment, edgewise bending moment, and shaft torque.

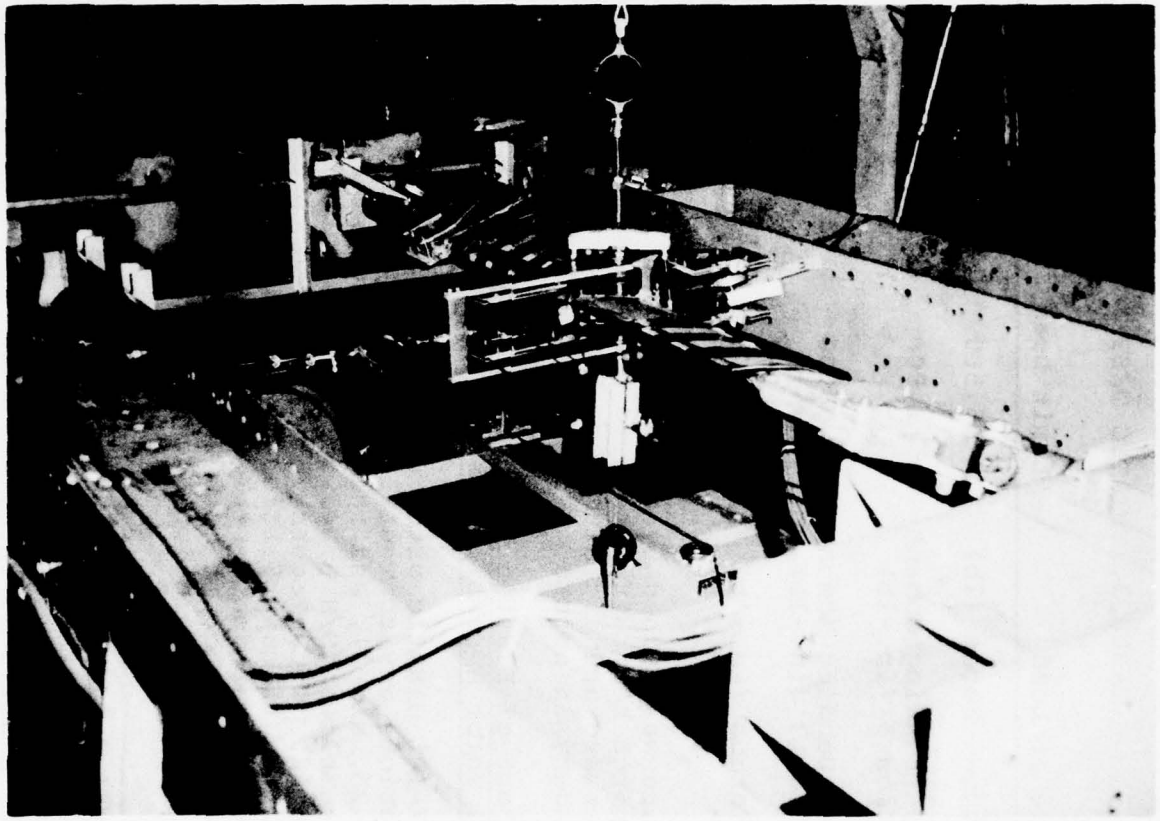

Figure 16. Elastic pitch beam tail rotor assembly static test.

Torsional stresses in the EPB and the cuff were also applied by locking in the maximum blade pitch angles of 19 degrees. Table 3 presents a comparison of the loads at failure to the limit loads.

TABLE 3. STATIC TEST LOAD SUMMARY

Type of Load	Limit Load	Load at Failure	% of Limit Load
Centrifugal Force (lb)	16,500	40,446	245
Flatwise Bending Moment at Station 3 (in.-lb)	1,800	5,040	280
Edgewise Bending Moment at Station 3 (in.-lb)	5,000	10,000	290
Shaft Torque (in.-lb)	12,000	24,000	200

The failure was caused by an adhesive bond failure of the elastic pitch beam attachment to the stainless steel web and to the forward and aft aluminum channels. Other damage noted was secondary in nature.

Fatigue Test of Elastic Pitch Beams and Elastic Pitch Beam Tail Rotor Assemblies Having Teeter Freedom

Three K27-105 elastic pitch beam assemblies previously subjected to the various environmental conditions reported in Reference 3 (S/N 2A, 2B, and 3), and three K27-101 elastic pitch beam tail rotor assemblies (S/N 3, 4, and 7) were fatigue tested as shown in Figure 17. These tests were performed to determine the fatigue strength capabilities of the EPB and EPBTR and also to determine to what degree the fatigue strength of the elastic pitch beam would be affected when exposed to a spectrum of humidity, solar simulation, low temperatures, and high temperatures.

Loads applied during these tests were centrifugal force, steady and vibratory flatwise bending moment, steady and vibratory edgewise bending moments, steady shaft torque, steady thrust, and steady elastic pitch beam twist. Centrifugal force was applied by hydraulic cylinders, and the magnitude of the force was monitored by a calibrated strain gage link. Steady shaft torque was applied at the hub using a deadweight-cable-pulley system attached to a torque arm. Fixed blade pitch of 10 degrees (5-degree twist of the elastic pitch beam) was

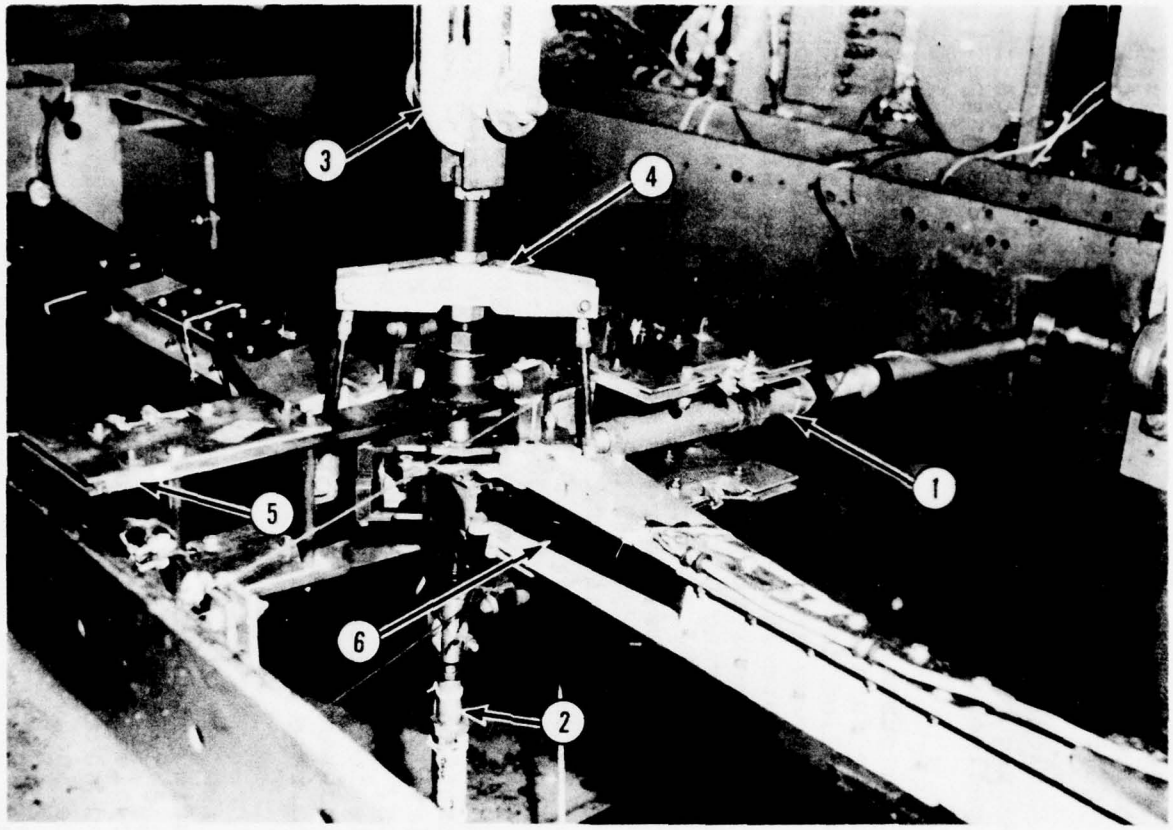

(1) Inplane bending input rod

(2) Out-of-plane bending input rod

(3) Steady blade thrust load

(4) Fixed pitch adjustment

(5) Steady shaft torque input lever

(6) Test specimen

Figure 17. Elastic pitch beam tail rotor fatigue test.

introduced and locked in by the blade pitch links attached to an adjustable cross beam. A steady thrust load was applied at the hub via a bungee and cable system and was monitored by a calibrated link. Flatwise and edgewise bending moments were applied simultaneously to the specimen at the hub centerline by cam actuated pushrods driven by an electric motor at a frequency of 565 rpm. Phasing was adjusted by indexing the timing belts so that both moments peaked together.

Instrumentation on the fatigue specimens consisted of flatwise and edgewise bending bridges located at Station 3 on both the EPB and EPBTR specimens and at Station 17 on the EPBTR specimens.

Table 4 presents a summary of the loads applied during each test as well as the duration of each test. Axial loads and bending moments applied to the elastic pitch beam at Station 3 were converted to steady and vibratory stresses and are shown as an S-N plot in Figure 18. Loads applied to the six fatigue test specimens were conservatively selected to cover the flight loadings anticipated during high-speed level flight and were also selected to cover the majority of maneuvers that were anticipated during the subsequent flight test program when the EPBTR would be mounted on a UH-1H helicopter. The steady mean stress due to the centrifugal force applied to all specimens was 27,400 psi. Blades S/N 4 and S/N 7, and elastic pitch beam S/N 2B were fatigue tested at a vibratory stress level of 39,100 psi for 10^6 cycles to simulate the high level maneuver condition while Blade S/N 3 and elastic pitch beam S/N 3 were tested at a vibratory stress level of 28,000 psi for 10^7 cycles to simulate a level somewhat higher than the high-speed level flight condition. Elastic pitch beam S/N 2A was step-tested in 2×10^6 cycle increments to 10^7 cycles in an effort to establish the endurance limit and to determine the onset of torsional spring rate decay as noted in the upper portion of Figure 18.

In addition to the bending stress cycles, all specimens (excluding elastic pitch beam S/N 2A) were subjected to 2000 ground-air-ground cycles wherein the axially applied centrifugal force was cycled between 1250 and 12,500 pounds to simulate rotor runups and shut downs so that the effects of low cycle fatigue would be included in these tests.

Observations made during the test program and examination of the specimens following completion of these tests indicated the following:

1. All specimens continued to transmit full centrifugal force when testing was terminated.

TABLE 4. TEETER-FREE ELASTIC PITCH BEAM FATIGUE TEST SUMMARY

Drawing No. →	K27-101 Rotor			K27-105 Pitch Beam		
Serial No. →	3	4	7	2A	2B	3
Centrifugal Force (lb)	12,500	12,500	12,500	12,500	12,500	12,500
Vibratory Edgewise Bending Moment (in.-lb)						
Sta 3	3,500	4,800	4,800	2,500 max (step test)	4,800	3,500
Sta 17	1,400	2,200	2,200	--	--	--
Vibratory Flatwise Bending Moment (in.-lb)						
Sta 3	540	940	940	310 max (step test)	940	540
Sta 17	750	974	974	--	--	--
Thrust (lb)	600	600	600	600	600	600
Shaft Torque (in.-lb)	1,700	1,700	1,700	1,700	1,700	1,700
Pitch Angle (deg)	10	10	10	10	10	10
Angle of Pitch Beam Twist (deg)	5	5	5	5	5	5
Cycles	10^7	10^6	10^6	10^7	10^6	10^7
Ground-Air-Ground Centrifugal Force Cycles (1,250-12,500-1,250 lb)	2,000	2,000	2,000	None	2,000	2,000

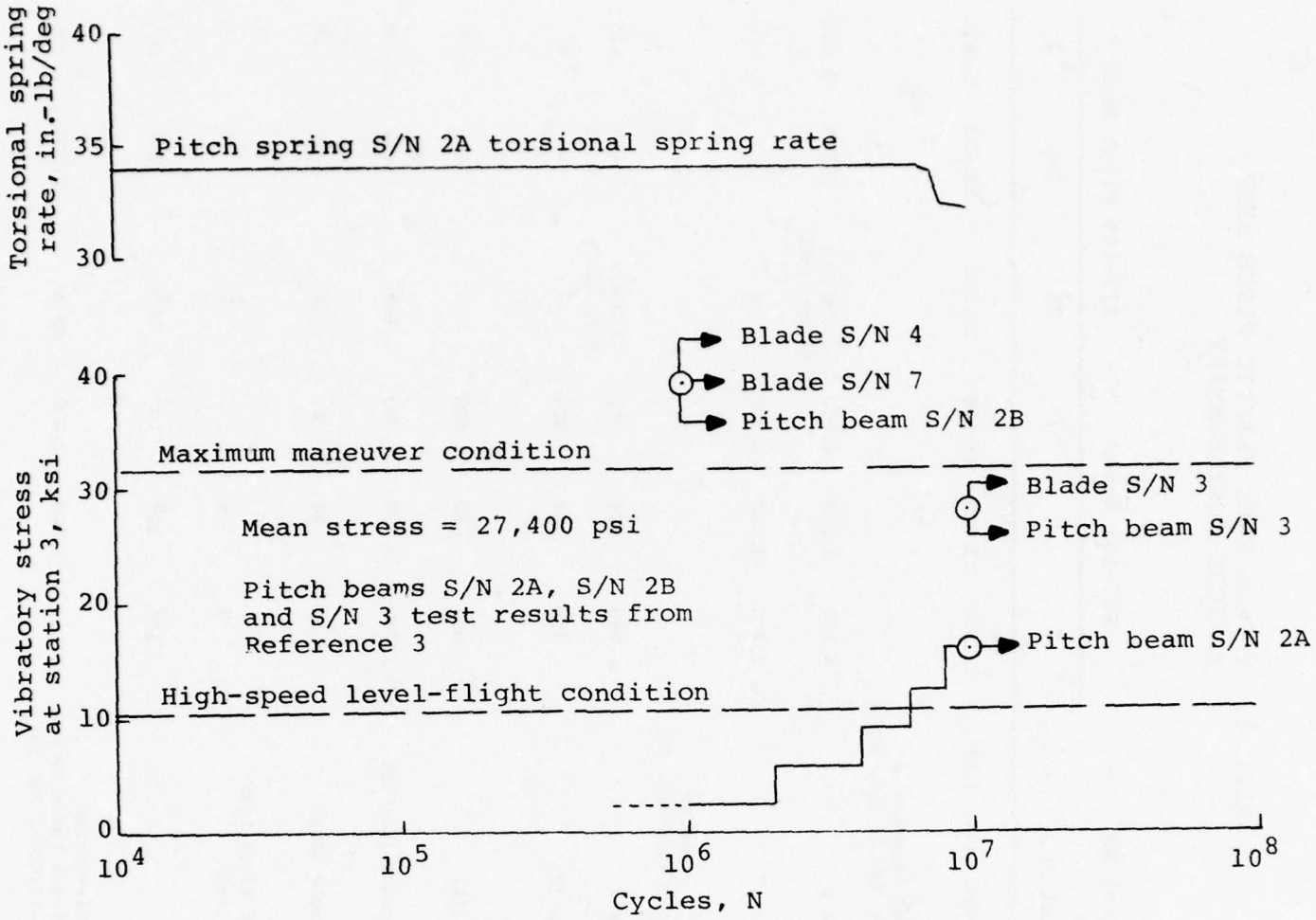

Figure 18. Fatigue test results of UH-1 elastic pitch beam specimens having teeter freedom.

2. No elastic pitch beam strap failures were noted.

3. Some delamination of the bond between the elastic pitch beam straps and the flanges of the interconnecting web was evidenced on all six specimens. These separations were the result of high shear stresses caused principally by both edgewise and flatwise bending moments, in part by tensile stresses in the bond in the vicinity of the strap apex as a result of centrifugal force induced splitting forces, and in part by shear stresses in the bond caused by twisting of the elastic pitch beam strap to attain a +10-degree pitch angle.

4. Failure of the filament winding at the outboard juncture of the two elastic pitch beam straps was noted on all fatigue specimens. These failures were primarily due to excessive tensile stresses imposed on the filaments by the splitting loads associated with the applied centrifugal force as shown in Figure 19. Secondary stresses associated with the delamination of the interconnecting web to elastic pitch beam strap, deformations caused by twisting the straps to obtain the desired pitch angle, as well as the failure of the aluminum channels to properly contain the geometry of the straps at their interfaces may have also contributed to failure of the filament winding.

5. Fatigue cracks occurred in the aluminum channels at their inboard bonded juncture with the elastic pitch beam straps. These cracks are associated with flexing of the channel webs by the elastic pitch beam straps as a result of the loss of filament winding continuity.

6. As shown in Figure 18, the onset of torsional stiffness degradation of elastic pitch beam specimen 2A occurred at approximately 7×10^6 cycles and a vibratory stress level of 4800 psi. At 10^7 cycles and vibratory stress level of approximately 6200 psi, a 5-percent reduction in torsional stiffness had occurred. It is conjectured that this loss of torsional stiffness is related to the separation of the interconnecting web and the elastic pitch beam straps.

The critical areas of the unidirectional 1002-1014S glass elastic pitch beam straps that were closely monitored for signs of wear or filament fracture are as illustrated in Figure 19. These critical points are the point of strap

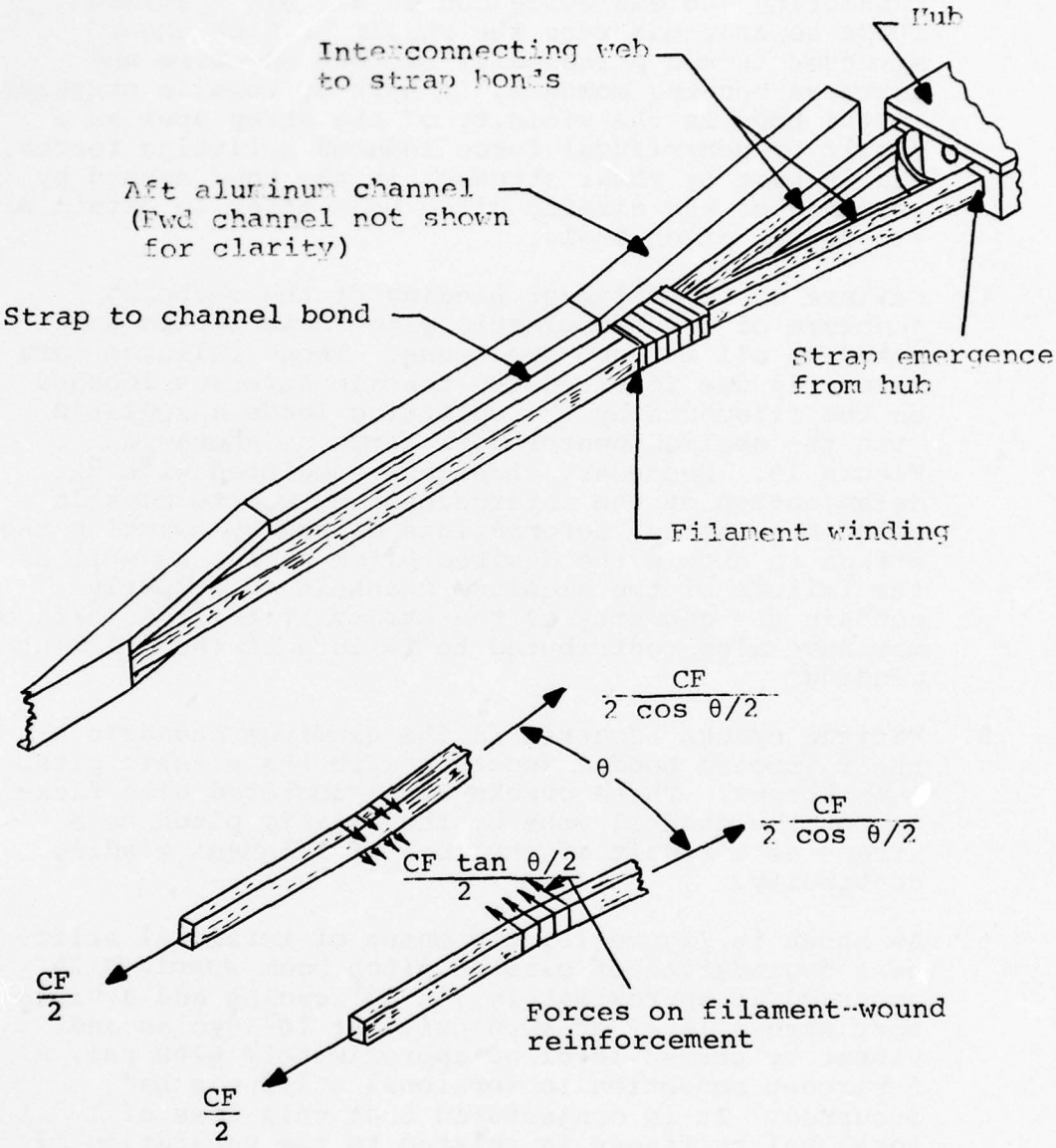

Figure 19. Elastic pitch beam critical areas.

emergence from the hub, the interface between the straps and the interconnecting web, the area of the straps directly under the filament winding, and the interface between the straps and the aluminum channels. The point of strap emergence from the hub is considered to be a prime suspect area for strap failure due to the presence of high vibratory flatwise and edgewise bending stresses, axial stresses due to centrifugal force, torsional shear stresses due to twisting of the straps through the required pitch angles, as well as transverse shear stresses caused by rotor torque and thrust--all of which are conducive to producing high filament stresses, fretting damage at the hub-strap interface, interlaminar, shear stresses in the straps, and bond shear stresses between the straps and the elastomer-lined hub interfaces. The straps, along their interfaces and the interconnecting web, are considered to be critical because they are subjected to high shear stresses as well as secondary lateral tensile forces required to maintain the structural continuity between the straps and the web through their bonded juncture, creating interlaminar shear stresses in the outer plies of the strap structure. The area of the straps lying directly beneath the filament winding is also critical because it is subjected to localized lateral shear and bearing forces, tending to cut or fret the filaments of the straps which are in contact with the filament winding. The filament windings are critical themselves because they are subjected to centrifugal induced splitting forces within the laminate caused by a change in strap planform configuration in this localized area. The bonded juncture of the elastic pitch beam strap with the two aluminum channels is also considered to be an area where strap damage might occur. Examination of these critical areas revealed no indication of filament breakage, interlaminar shear failure, or fretting damage associated with the strap design. The conclusion that can be drawn from this evidence is that the strength of the strap and the adequacy of its attachment to the hub and aluminum channels have been clearly demonstrated.

The separation of the interconnecting webs from the elastic pitch beam strap resulted in a degradation of the elastic pitch beam's torsional stiffness of approximately 5 percent at the load levels tested, as noted in Figure 18 for elastic pitch beam specimen S/N 2A. Similar loss of torsional stiffness for specimens 2B and 3 was evidenced; however, precise measurements were not available. Modest redesign of the strap-web connection could substantially improve the fatigue performance of this joint. An improved elastic pitch beam strap-web connection would also be instrumental in eliminating filament winding failures and fatigue cracking of the aluminum channels by redistributing the stresses in these localized areas.

The fatigue test results for the elastic pitch beam specimens S/N 2A, S/N 2B and S/N 3 previously exposed to adverse environmental conditions and protected by a coating of Adiprene L-167 show no failures or degradations that could be attributed to either the exposure or the coating when they were compared to the results obtained from fatigue tests of unexposed, unprotected specimens (Figure 18). Coating failures were noted only in those areas where a separation between the elastic pitch beam and the interconnecting web occurred. It is therefore anticipated that the service life of the elastic pitch beams will not be affected substantially by adverse environmental conditions experienced and that the protective Adiprene L-167 coating will perform its function satisfactorily provided there is no degradation of the underlying elastic pitch beam structure.

Fatigue Test of the UH-1 Tail Rotor Shaft With Teeter Locked Out

Previous fatigue test results of the UH-1 elastic pitch beam tail rotor and elastic pitch beams shown in Figure 18 were obtained with the inner rotor hub free to teeter with respect to the outer rotor hub and the tail rotor shaft. With the decision made to lock out the teeter freedom, it was necessary to substantiate the fatigue strength of both the elastic pitch beam and UH-1 tail rotor shaft for flight in the teeter locked mode. This was accomplished by fatigue testing three UH-1 tail rotor shafts with three EPBTR/EPB specimens in the fatigue test fixture shown in Figure 17. Minor modifications to the test fixture and to the rotor hub assembly were required to facilitate locking out the teeter freedom between the inner and outer hub assemblies and for applying a vibratory hub moment between the tail rotor shaft and the rotor hub. Teeter freedom was locked out by using a shim-clamp arrangement between the inner and outer hub assemblies, and application of the hub moment was accomplished by a motor drive cam actuated pushrod connected to the inboard end of the tail rotor shaft. Vibratory shears induced at this location produced vibratory bending moments throughout the length of the shaft. Two strain gage bridges were mounted on the shaft so that the hub moment/flapping angle relationship could be monitored during the fatigue test as well as during the subsequent flight test program.

Steady loads applied to the three specimens tested were centrifugal force, thrust, torque, and EPB twist loads applied by locking in the desired rotor blade pitch angle. Vibratory hub moments for a given flapping angle were applied by adjusting the offset of the motor-driven cam. Table 5 presents a summary of the loads applied, the nominal vibratory bending stress at the critical location of the tail rotor shaft, and the duration

TABLE 5. UH-1 TAIL ROTOR SHAFT AND ELASTIC PITCH BEAM FATIGUE TEST SUMMARY WITH TEETER LOCKED OUT

TEST SPECIMEN NUMBER →	EPBTR S/N 7		EPB S/N 3	EPB S/N 2A
Flapping Angle, Deg →	±3.5	±5.0	±4.5	±5.0
CF, lb	12,500	12,500	12,500	12,500
Thrust, lb	600	600	600	600
Torque, in.-lb	1650	1650	1650	1650
Blade Pitch Angle, deg	10	10	10	10
Hub Moment/Flapping Angle Spring Rate, in.-lb/deg	1814	1814	1805	1800
Hub Moment, in.-lb	±6349	±9070	±8118	±9000
Critical Shaft Bending Stress, psi	±45,872	±65,531	±58,652	±65,025
EPB Flatwise Bending Moment at Station 3, in.-lb	±881	±1254	±1108	±1219
EPB Flatwise Bending Stress at Station 3, psi	±19,318	±27,504	±24,292	±26,736
Test Duration, Cycles x 10^{-6}	5.0	1.0	1.04	.21
Remarks	No failure	No failure	No failure	No failure

of the test in the terms of cycles for each of the specimens tested. Also included are the vibratory flatwise bending moments and stresses acting at Station 3 of the elastic pitch beam. No failure occurred during this test program.

Fatigue test results obtained for the UH-1 tail rotor shaft/EPBTR assembly with the teeter freedom locked out are compared to the previously established (Reference 4) S-N curve for the current UH-1 tail rotor shaft, Figure 20. Test results indicated that the current UH-1 tail rotor shaft S-N curve would be very conservative if used for monitoring the EPBTR flight test program.

Vibratory flatwise bending moments or stresses imposed on the elastic pitch beam at Station 3 during this test program, for flapping angles of up to $\pm$ 5 degrees, exceeded those anticipated during the subsequent flight test program. As such, it was concluded that locking out the teeter freedom would have no adverse effects on the fatigue life of the EPB.

DYNAMICS

During the design stage of this program, the natural frequencies of the EPBTR were calculated for various modes of interest as a function of operating speed. As the overlapping beam configuration of the EPBTR is relatively unique when compared to conventional rotor systems, special computer programs were required to properly treat the boundary conditions for the elastic pitch beam and its overlapping cuff. The analytical complexity of this system, the determination of the lead-lag and flapping spring rates of the root-end restraint, the effective length of the elastic pitch beam, and the difficulty in predicting stiffness properties of composite structures early in the design stage, led to high estimates of the inplane natural frequencies. This condition first became evident during the EPBTR whirl test program where a review of the test records revealed that at a pitch angle of approximately 18 degrees and a rotor speed of 1650 rpm, the vibratory flatwise and edgewise bending moment amplitudes increase unexpectedly to several times their steady-state magnitudes and the frequency changed

---

4. J. Childs, FATIGUE LIFE SUBSTANTIATION OF DYNAMIC COMPONENTS OF UH-1B & UH-1E HELICOPTERS INCORPORATING THE MODEL 540 DOOR-HINGE ROTOR, Bell Report Number 204-099-297, Bell Helicopter Company, Fort Worth, Texas, June 1, 1966.

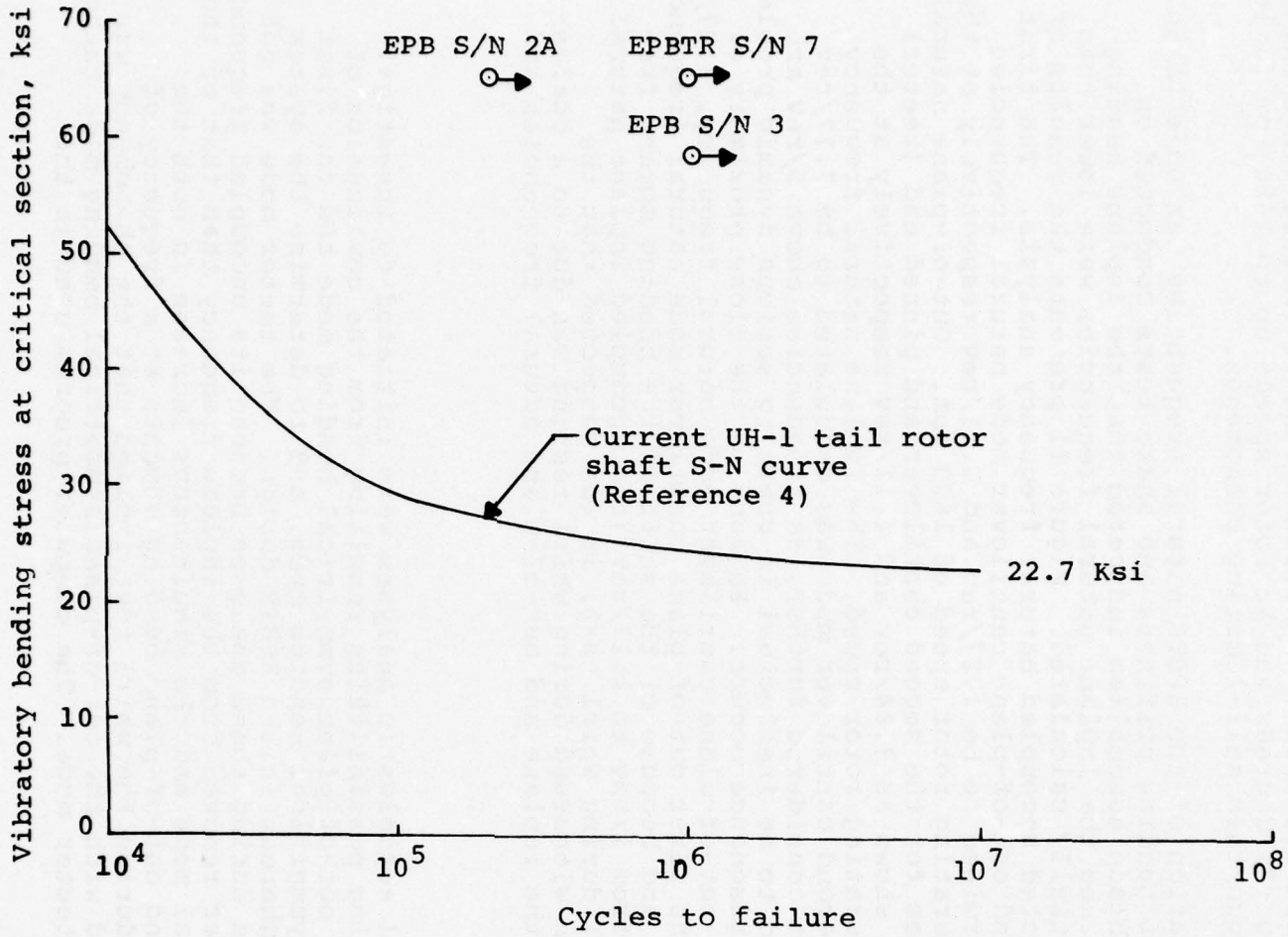

Figure 20. Comparison of fatigue test results for UH-1 tail rotor shafts having nonteetering elastic pitch beam tail rotors installed with current UH-1 tail rotor shaft S-N curve.

from 1/rev to 1.27/rev. This condition was self-limiting and decayed without action by the test operator. As only one blade was being recorded at the time, full definition of the vibration mode was not available. Additional runs at various pitch angles from -6 to +21 degrees and at rotor speeds up to 1650 rpm failed to reproduce this self-limiting phenomenon.

A reevaluation of the EPBTR natural frequencies was undertaken. Results of bending stiffness and shake tests conducted on complete blade assemblies indicated that the inplane bending stiffness and the inplane natural frequencies were lower than those initially calculated. Figure 21 presents the results of the corrected uncoupled natural frequency analysis. The first inplane and out-of-plane cantilever mode natural frequencies were determined to be 1.27/rev and 1.11/rev respectively at the normal operating rotor speed of 1650 rpm. Out-of-plane natural frequencies for the second cantilever and pinned end (teeter) modes are shown as 3.84/rev and 4.11/rev respectively at the normal operating rotor speed. The inplane natural frequency for the second cantilever mode was calculated to be 7.77/rev and is not considered further, as frequencies above 5/rev are considered to be ineffectual in creating serious dynamic problems unless a resonance occurs. Because of the close proximity of the first out-of-plane cantilever mode natural frequency, 1.27/rev, to the first out-of-plane cantilever mode natural frequency, 1.11/rev, and because of the shift of the bending moment frequencies from 1/rev to 1.27/rev (the uncoupled inplane natural frequency) during whirl test, it was suspected that the phenomenon witnessed during whirl testing was due to a coalescence of the inplane and out-of-plane natural frequencies and modes.

Analysis

Additional aeroelastic analyses were initiated to investigate the coupling possibilities resulting from the combination of the first out-of-plane symmetrical bending mode and the first inplane symmetrical bending mode, and to determine the system damping inherent in the EPBTR design. The teeter mode was not considered during these analyses because its uncoupled frequency was further removed from the inplane frequency than that of the symmetrical mode and the simultaneous increase in both the inplane and out-of-plane bending moments at a frequency of 1.27/rev during the whirl test implied that the phenomenon was associated with the out-of-plane symmetrical bending mode rather than the teeter mode. The computer program used in the

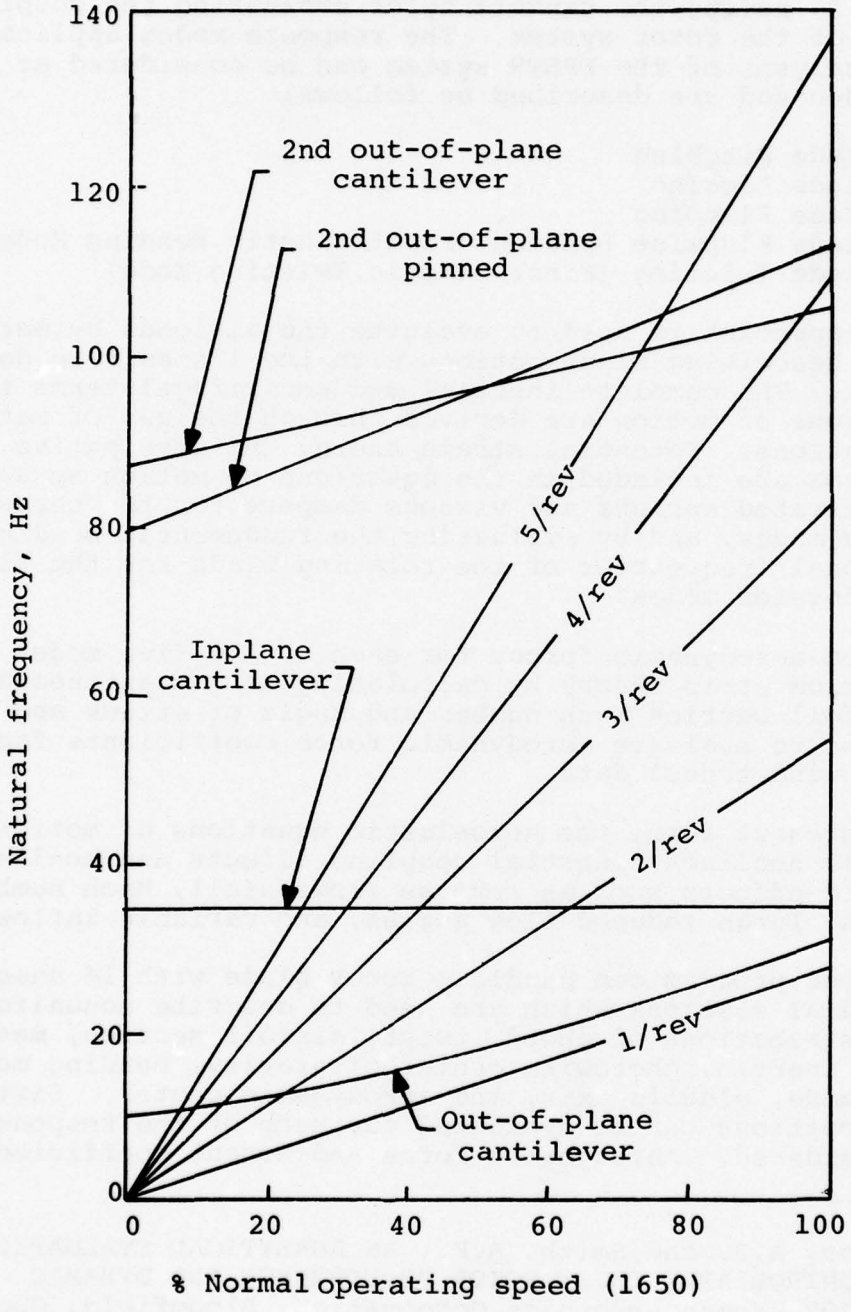

Figure 21. EPBTR frequency plot.

investigation was the 6F coupled aeroelastic analysis program, Reference 5, having the capability of evaluating the coupled responses of the rotor system. The response modes applicable to this analysis of the EPBTR system can be considered as normal modes and are described as follows:

- Blade Pitching
- Blade Lagging
- Blade Flapping
- Blade Flapwise Bending (First Elastic Bending Mode)
- Blade Twisting (First Elastic Twisting Mode)

The model approach is used to evaluate the airloads by mathematically describing blade motions with the listed five degrees of freedom. The complete inertial and centrifugal terms for the equations of motion are derived through the use of matrix transformations. Potential strain energy and dissipative energy terms are included in the equations of motion by assuming concentrated springs and viscous dampers for the three rigid body modes, and by evaluating the fundamental bending and torsional frequencies of the rotating blade for the flapwise and torsion modes.

Generalized aerodynamic forces for each of the five modes are obtained from strip theory by calculating an instantaneous local airfoil section Mach number and angle of attack and using these to evaluate aerodynamic force coefficients from available wind tunnel data.

In their present form, the aeroelastic equations of motion include all nonlinear inertial coupling effects and nonlinear aerodynamic effects such as reverse flow, stall, Mach number variations, large induced flow angles, and variable inflow.

The computer program can handle a rotor blade with 16 unequally spaced radial stations which are used to describe nonuniform radial distributions of chord, twist, airfoil section, mass, moment of inertia, chordwise center of gravity, bending mode, twisting mode, elastic axis, and aerodynamic center. Sixty azimuth positions can be evaluated for each of the response modes considered. Aerodynamic force and moment coefficient

---

5. Lemnios, A.Z. and Smith. A.F., AN ANALYTICAL EVALUATION OF THE CONTROLLABLE TWIST ROTOR PERFORMANCE AND DYNAMIC BEHAVIOR, Kaman Aerospace Corporation, Bloomfield, Connecticut; USAAMRDL Technical Report 72-16, U.S. Army Air Mobility Research and Development Laboratory, Eustis Directorate, Fort Eustis, Virginia, May 1972, AD 747808.

data are tabulated up to 3 airfoil sections at 5 Mach numbers and 49 angles of attack. Unsteady airfoil characteristics are estimated by force and moment derivatives based on Theodorsen theory.

Figure 22 illustrates schematically the basic program logic for computation of the rotor airloads and responses. Data for the specific rotor are input, and rotor inertias and linear aerodynamic terms are calculated. Pertinent information is stored on the disk for intermediate storage. The coefficients of the linearized equations are calculated and integrated to form the |A| matrix. This matrix is inverted to form the periodic response matrix that is stored on the disk for use in all subsequent solutions. The initial value matrix is determined, and the transient responses are obtained. Boundary conditions for steady-state solutions are generated and also stored on the disk.

The above described portion of the computer program is designated as the Part I solution. It is run for each operating condition represented by the independent variables such as rotor speed, airspeed, and the physical characteristics of the rotor system. It is independent of the trim thrust or blade pitch control requirements. Blade pitch control for a rotor trim condition as defined by specific values of thrust, propulsive force and side force is determined in the Part II solution of the 6F program. This solution defines the steady-state responses of the fully coupled nonlinear equations of blade motion. It must, therefore, be solved for each trim condition represented by either rotor force equilibrium or by specified control inputs. The program will iterate, as necessary, by varying the control setting to obtain the desired force equilibrium.

Using the data stored on the disk and the input for the controls, the linear forcing functions are now calculated, and the linear steady-state responses are determined. The local angles of attack are computed from these linear responses, and the local airloads are determined from blade element theory. The nonlinear forcing functions are obtained using these airloads, and new blade responses are computed. The iterative process of computing nonlinear airloads and nonlinear responses is cycled until convergence is reached between successive iterations. Rotor performance is calculated from the converged airloads by integrating the various airloads distributions radially and azimuthally over the disk.

The 6F program analyzes the steady-state dynamic oscillation of a single rotor blade with specified root end boundary conditions. When the blades of a multi-bladed rotor are identical, all blades have precisely the same motions versus azimuth position

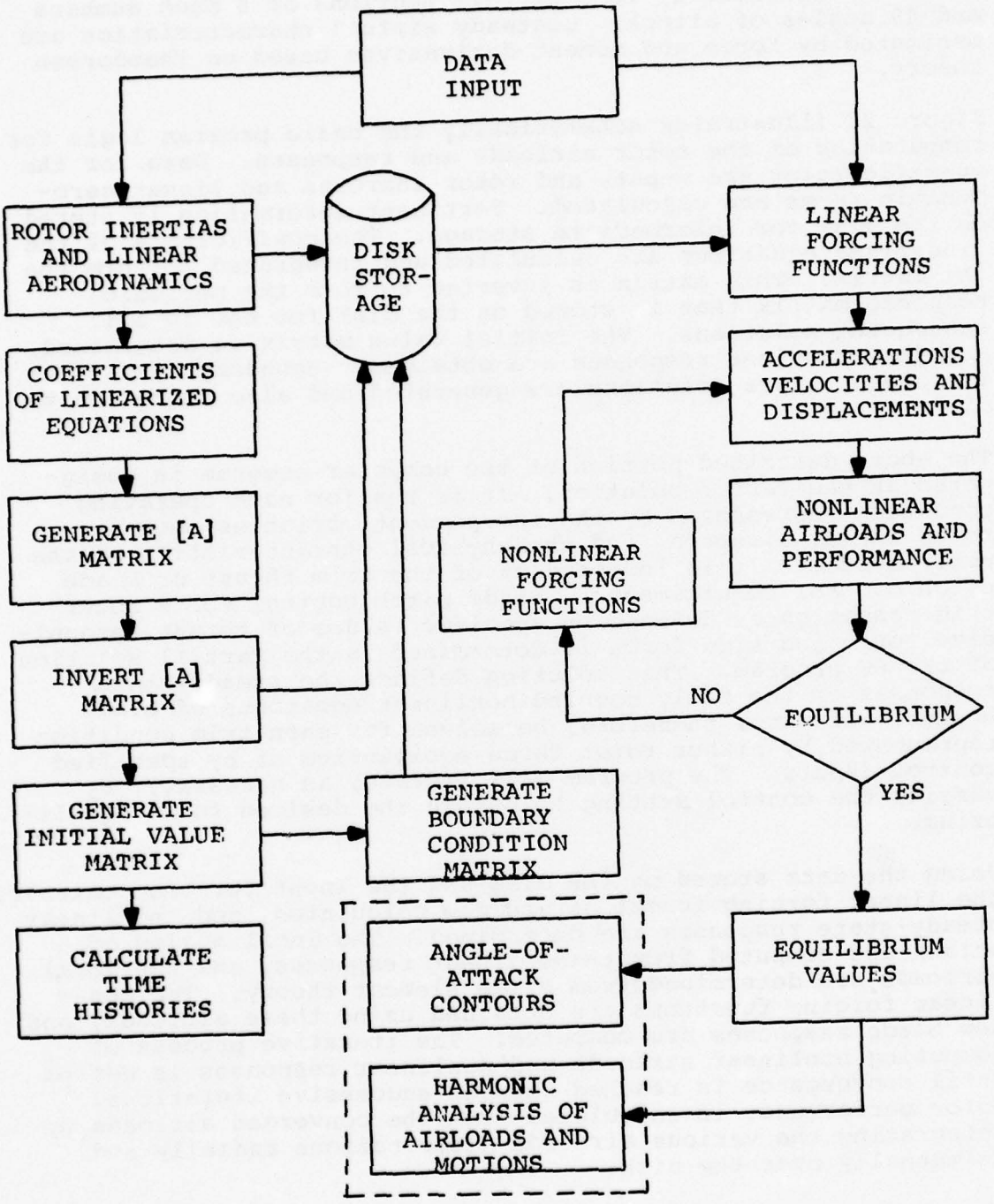

Figure 22. Flow chart of the 6F aeroelastic computer program (Reference 5).

for the steady-state condition. For blade stability analyses with identical blades and infinite impedence hub, all the modes are exactly representable as pinned or cantilevered modes of a single blade.

Blade responses are printed in the form of radial and azimuthal distributions of angles of attack, airloads normal to the shaft plane, airloads in the shaft plane, feathering moments, torques, Mach numbers, and critical Mach number ratios. Time histories of the coupled blade responses and the pitch horn control loads are also output. Standard harmonic analysis techniques automatically resolve the waveforms of angles of attack, airloads, moments, and blade responses to yield the harmonic content of each parameter. Angle-of-attack distributions are also interpolated automatically to locate radial stations corresponding to integer values in angle of attack.

In order to use the 6F aeroelastic computer program, it was necessary to obtain a mathematical model of the EPBTR assembly to simulate the first modes of bending with virtual hinge offset and root springs in and out-of-plane. The selected model represents a flexible rotor with virtual flapping and lag hinges located at the 8.2 percent offset ratio (rotor station 4.2 inches). Because of the redundancy of the blade structure in the inboard cuff area, a specialized computer program was developed to obtain the first and second inplane and out-of-plane uncoupled frequencies and mode shapes. The validity of this program was demonstrated by shake testing of the EPBTR assembly to experimentally obtain the desired in and out-of-plane natural frequencies.

With the frequencies and mode shapes obtained, a mathematical model of the EPBTR was constructed with out-of-plane and inplane hinges and root springs that matched the mode shapes shown in Figures 23 and 24 and the first mode natural frequencies of inplane and out-of-plane bending presented in Table 6. The mode shape of the second mode of out-of-plane bending given in Figure 25 and the second mode out-of-plane natural frequency presented in Table 6 were used as inputs to the 6F program. A Holzer analysis of the blade model was used to obtain the torsional mode shape, Figure 26, which was also used as input to the 6F program.

Results of the harmonic analysis of the time histories from the 6F Part I solution at 100 percent RPM in hover are presented in Figures 27 through 29. Blade response and damping are shown for the first two out-of-plane and the first inplane modes at blade pitch angles of 0 to 19 degrees. For the first inplane and first out-of-plane bending modes, Figures 27 and 28, the system response is at a frequency slightly greater than 1/rev, which is the expected fundamental frequency placement for these

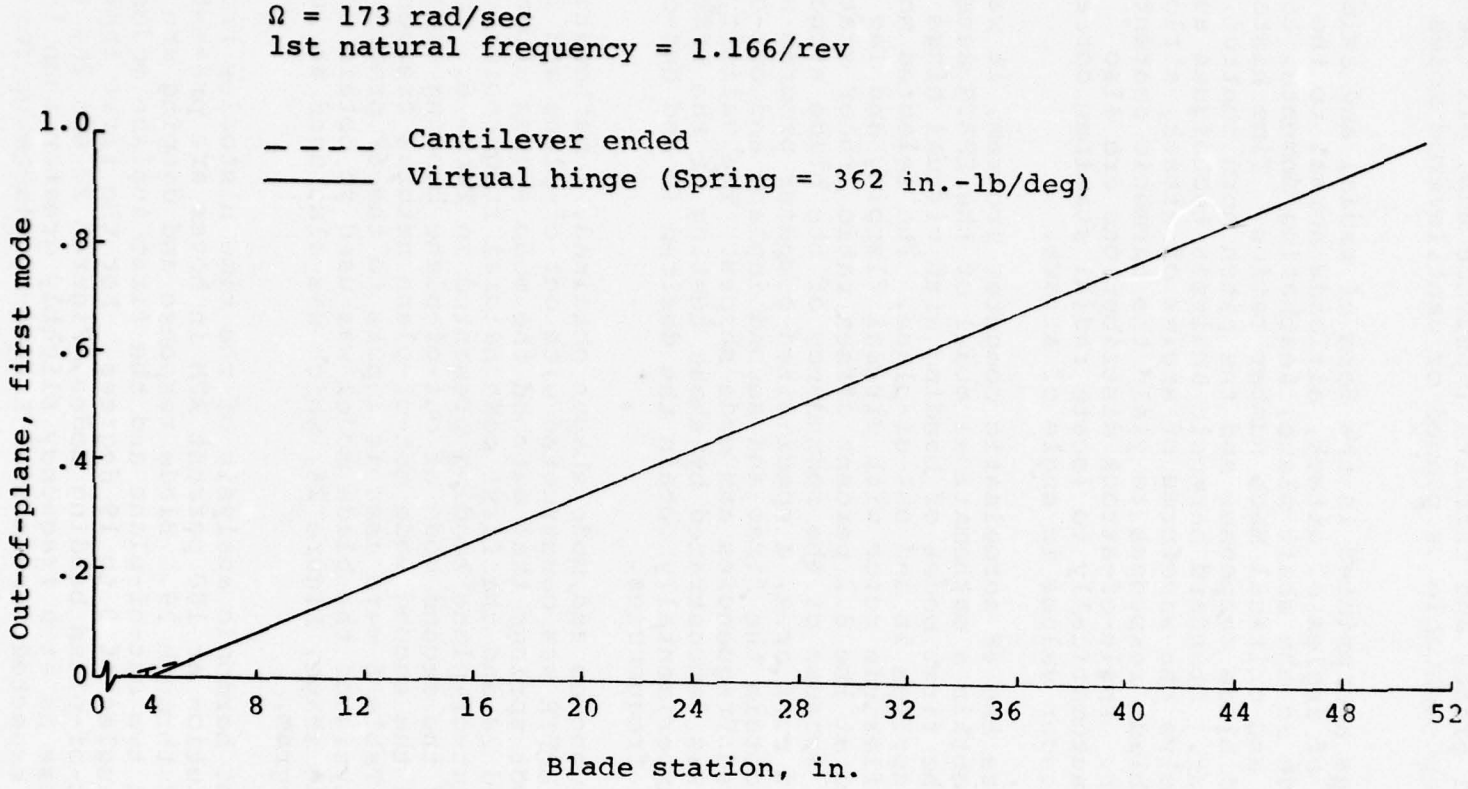

Figure 23. Out-of-plane first mode shape.

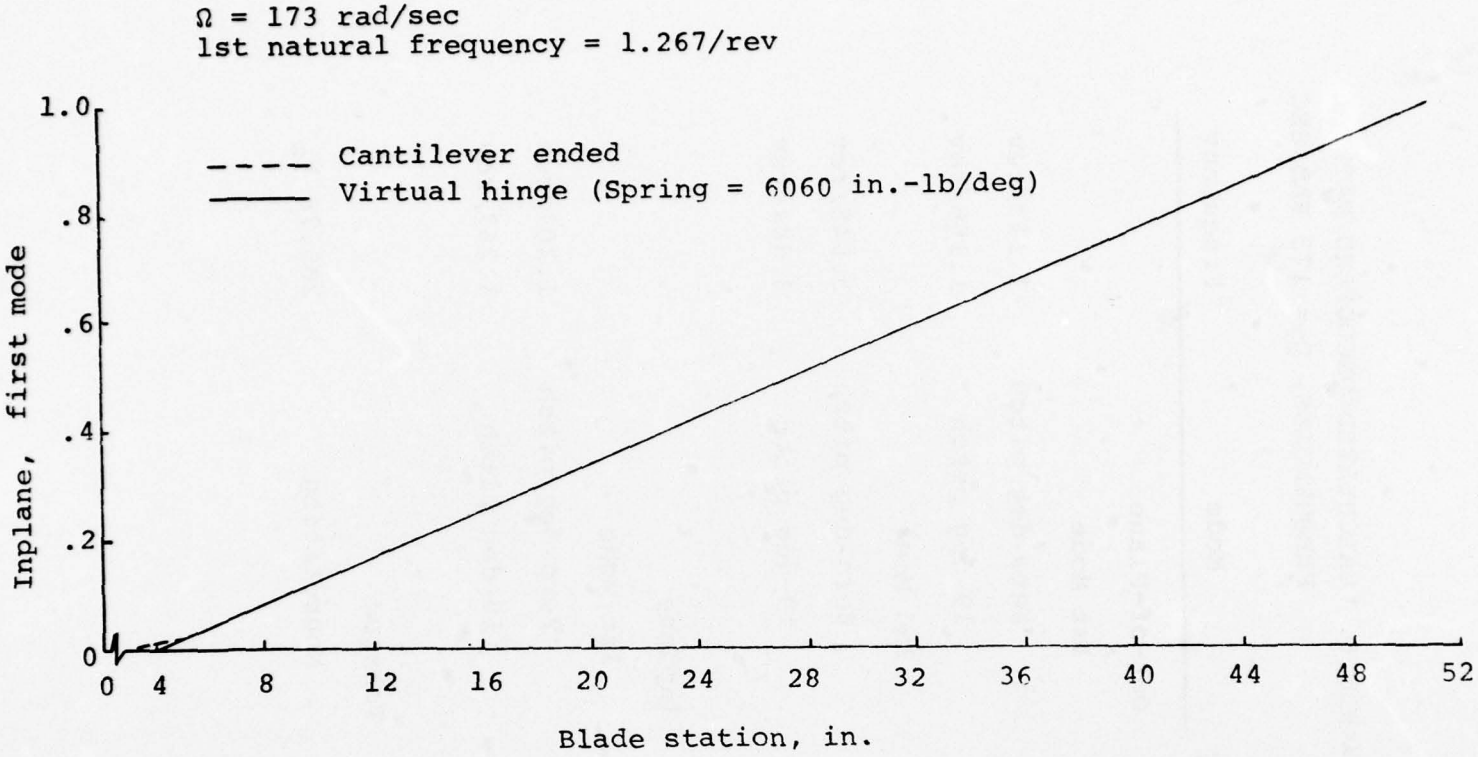

Figure 24. Inplane first mode shape.

TABLE 6. CALCULATED UNCOUPLED NATURAL FREQUENCIES, Ω = 173 RAD/SEC

Mode	Frequency
Out-of-Plane	
1st Mode	
Zero-deg pitch	1.113/rev
19-deg pitch	1.166/rev
2nd Mode	
Zero-deg pitch	3.845/rev
19-deg pitch	3.884/rev
Inplane	
1st Mode	
Zero-deg pitch	1.307/rev
19-deg pitch	1.267/rev
Torsion	
Nonrotating	205.78 H_z

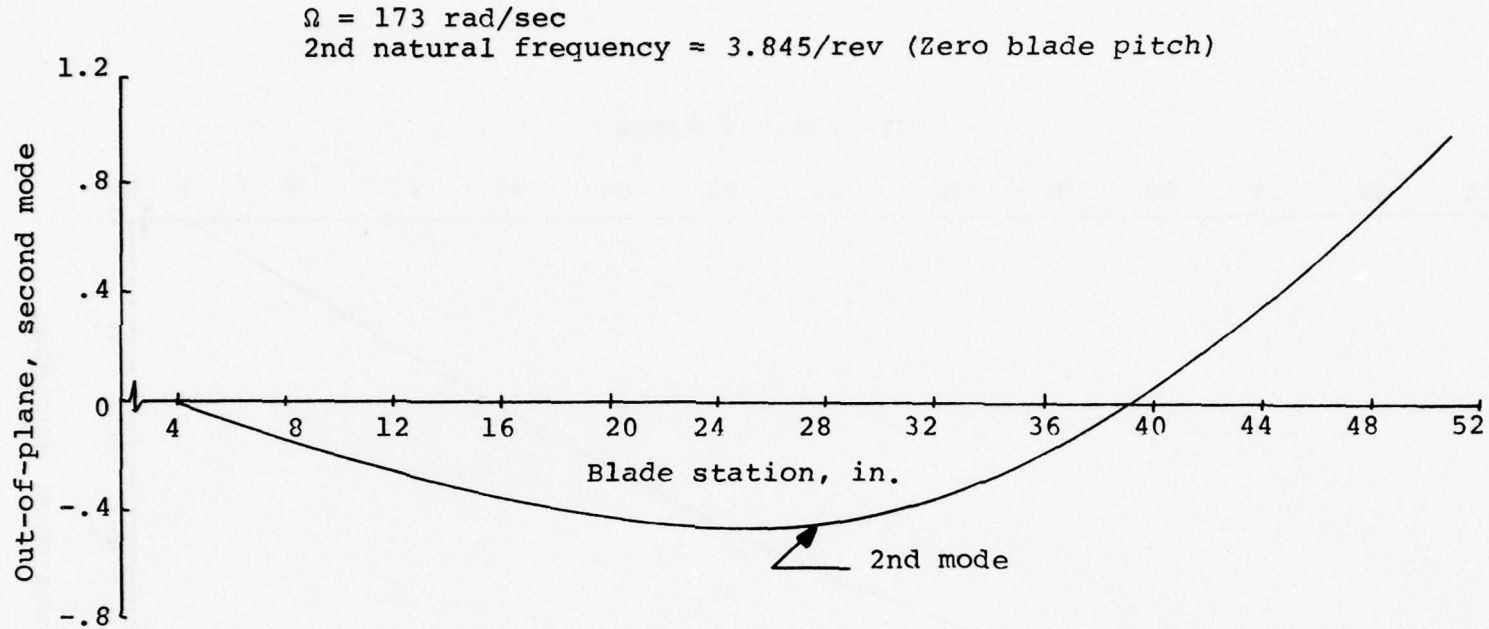

Figure 25. Out-of-plane second mode shape.

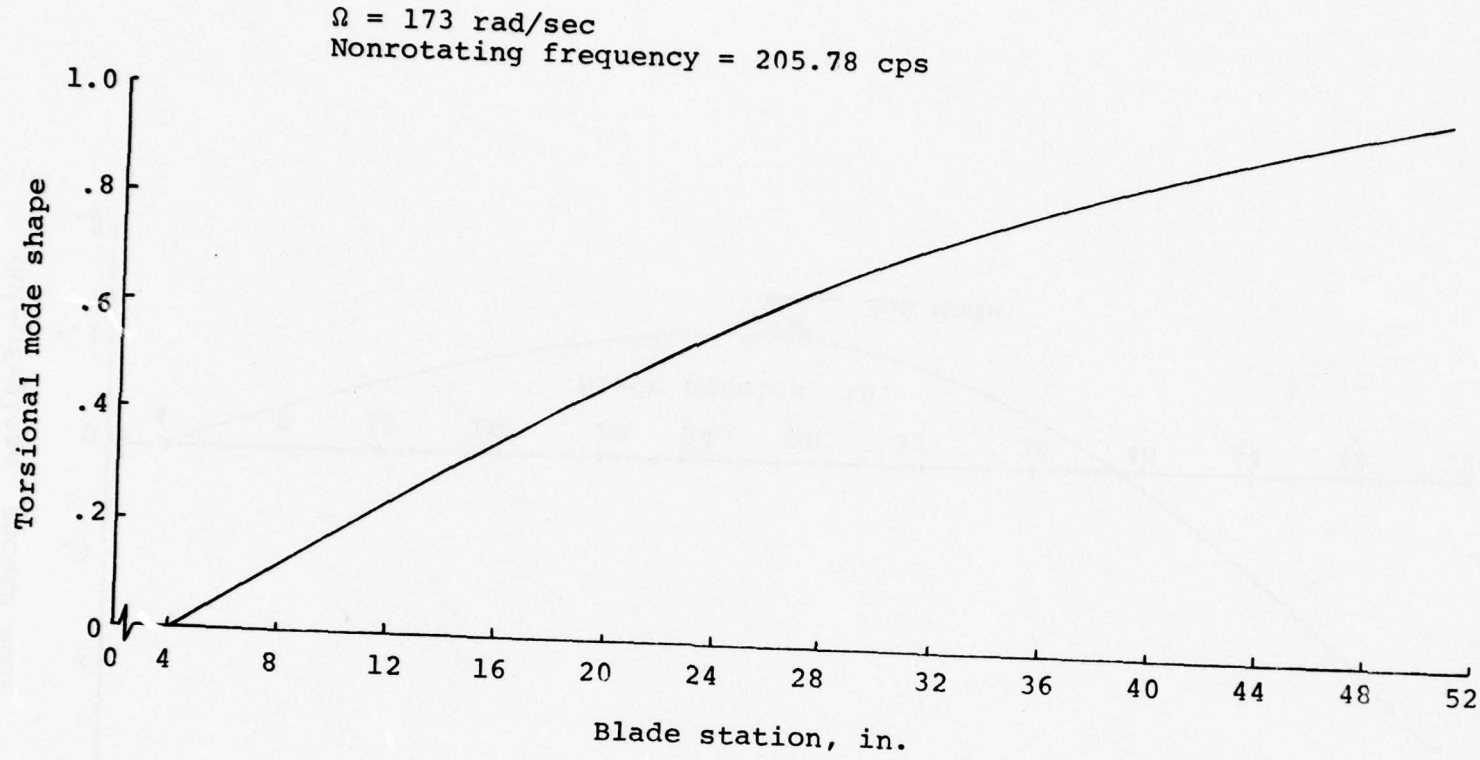

Figure 26. Torsional mode shape.

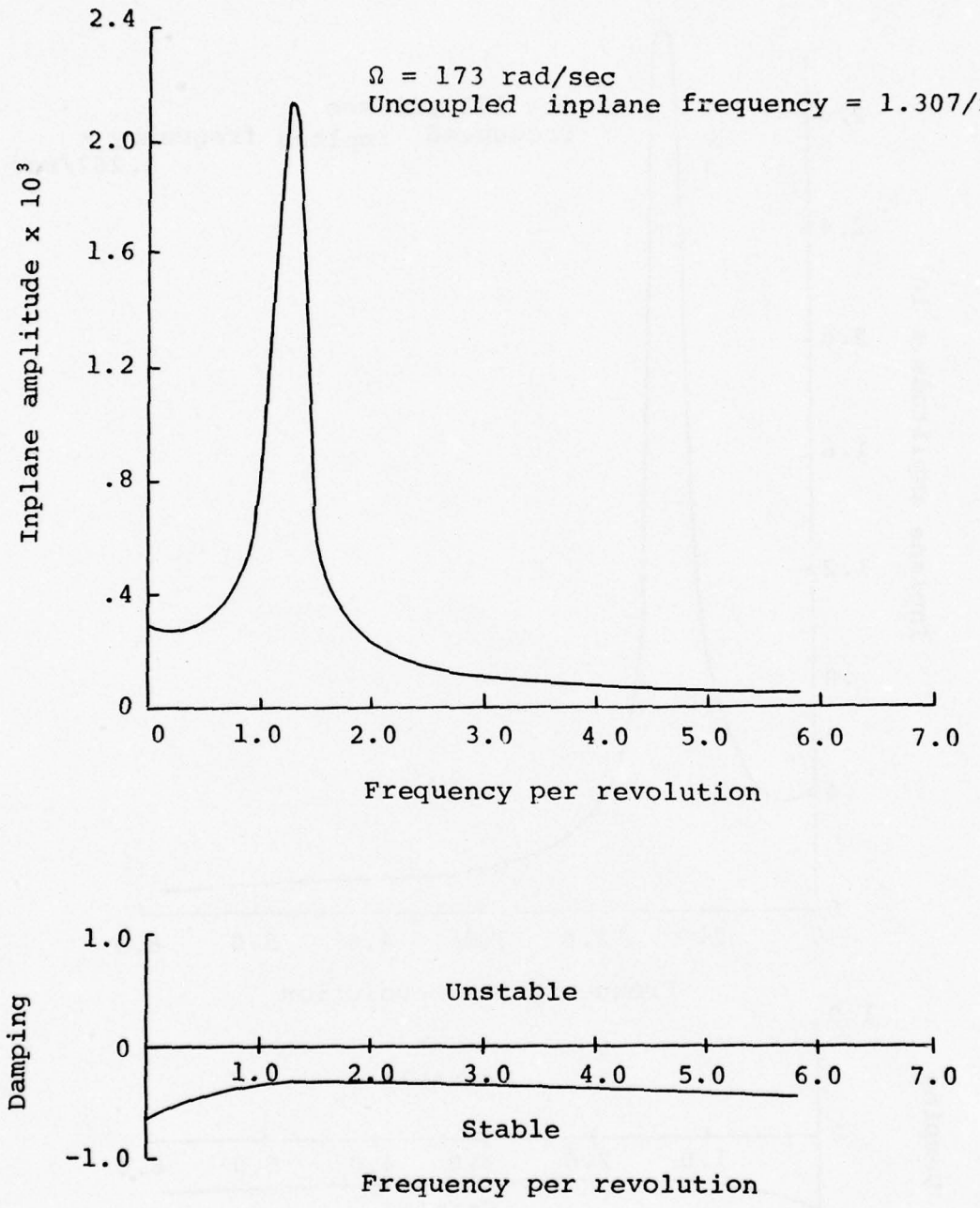

(a) Pitch angle θ = 0 degrees.

Figure 27. Response and damping curves for the inplane degree-of-freedom condition in hover.

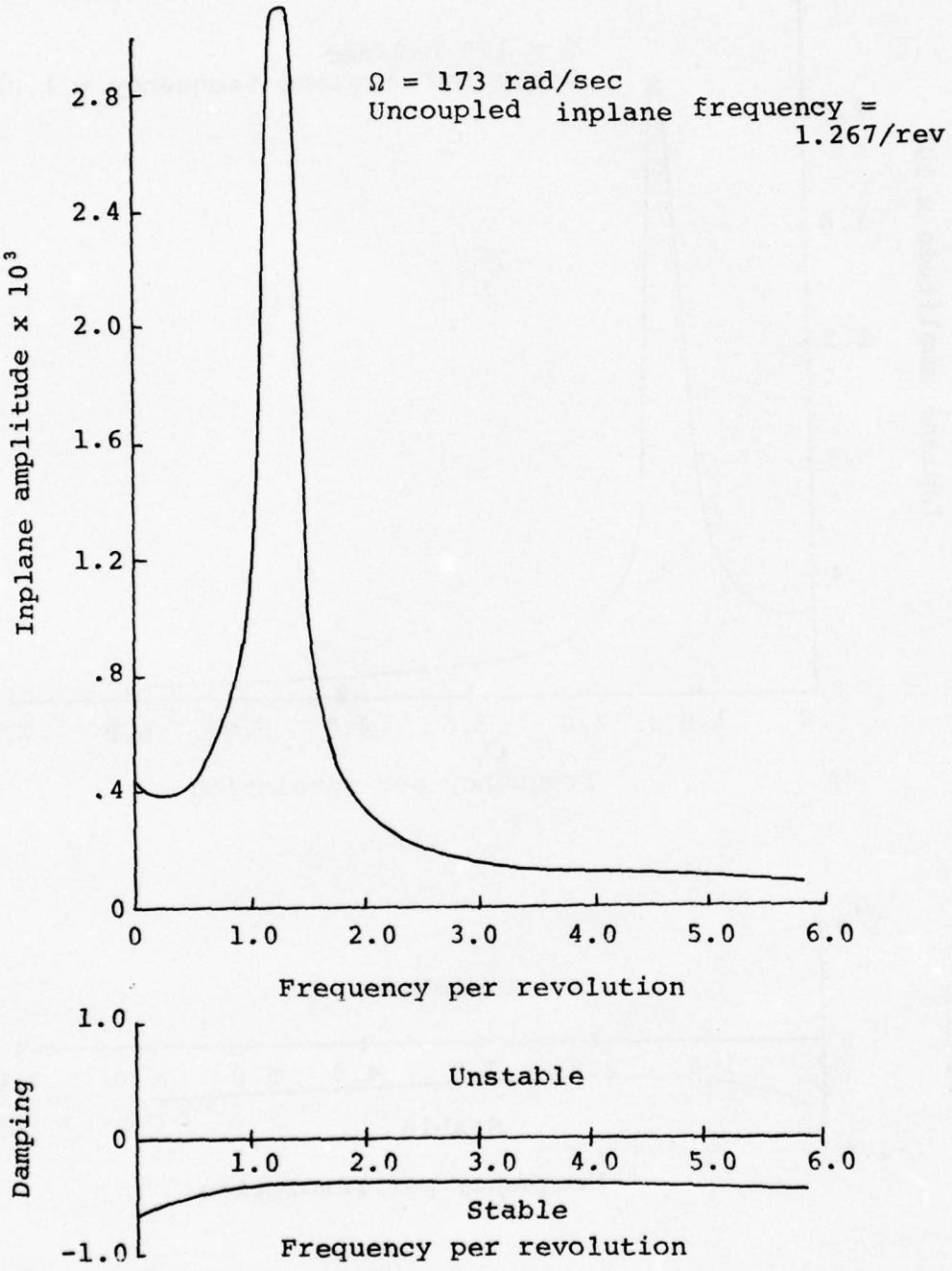

(b) Pitch angle θ = 19 degrees.

Figure 27. Continued.

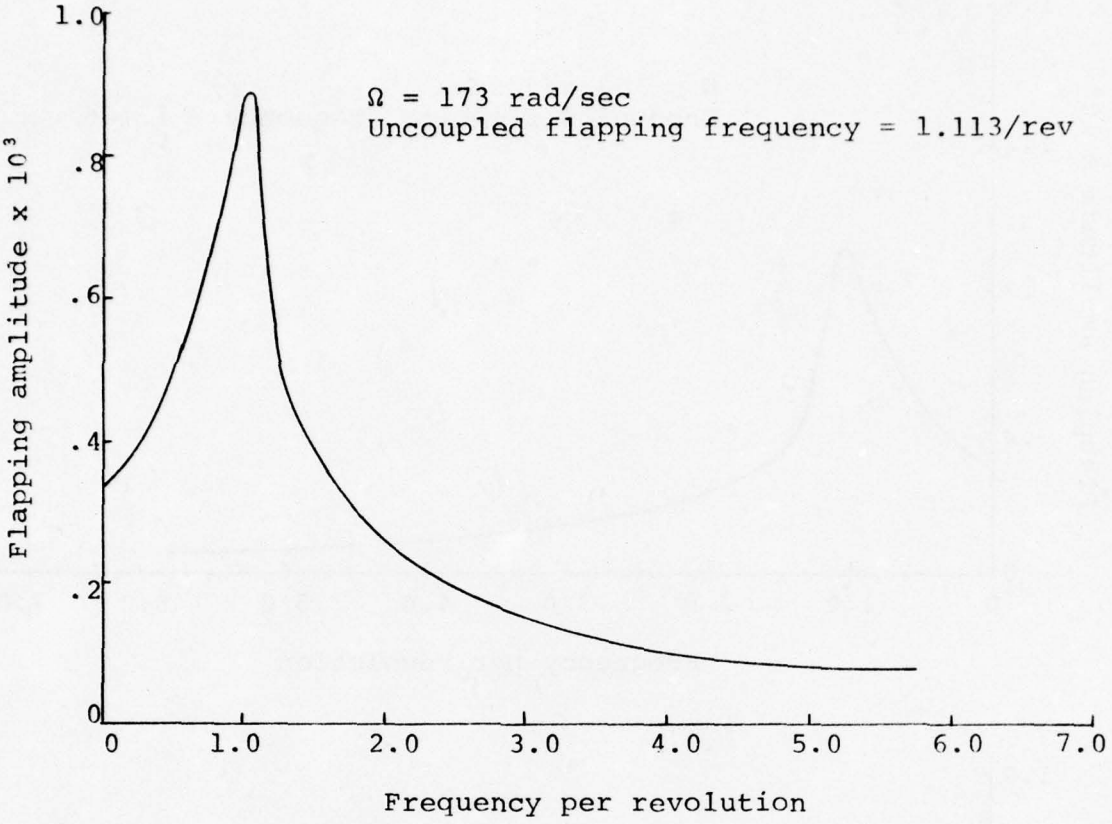

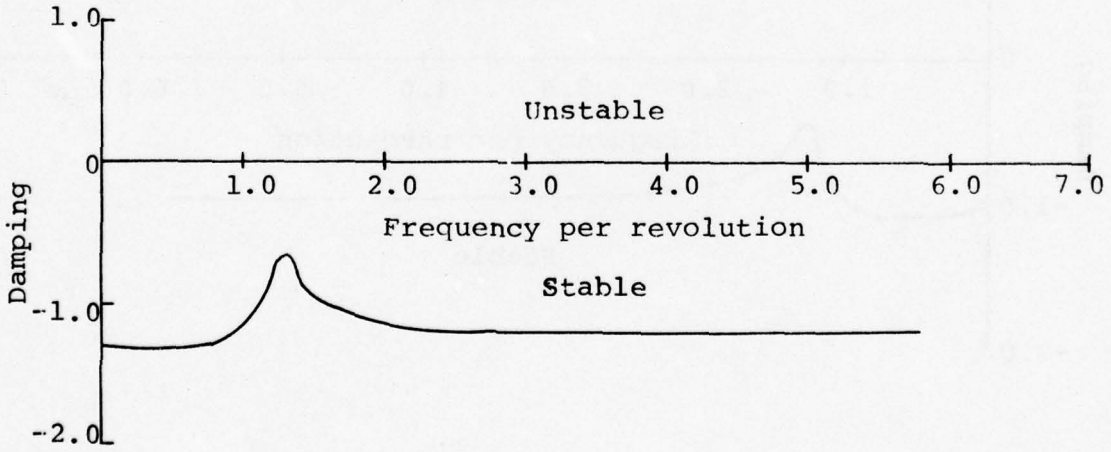

(a) Pitch angle θ = 0 degrees.

Figure 28. Response and damping curves for the flapping degree-of-freedom condition in hover.

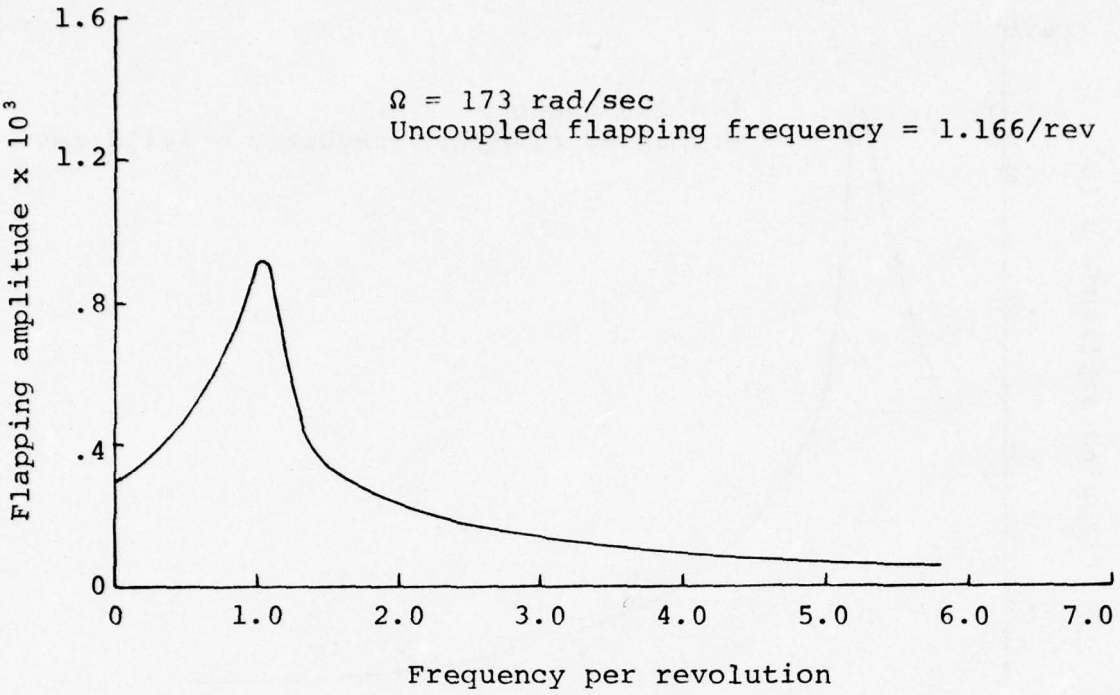

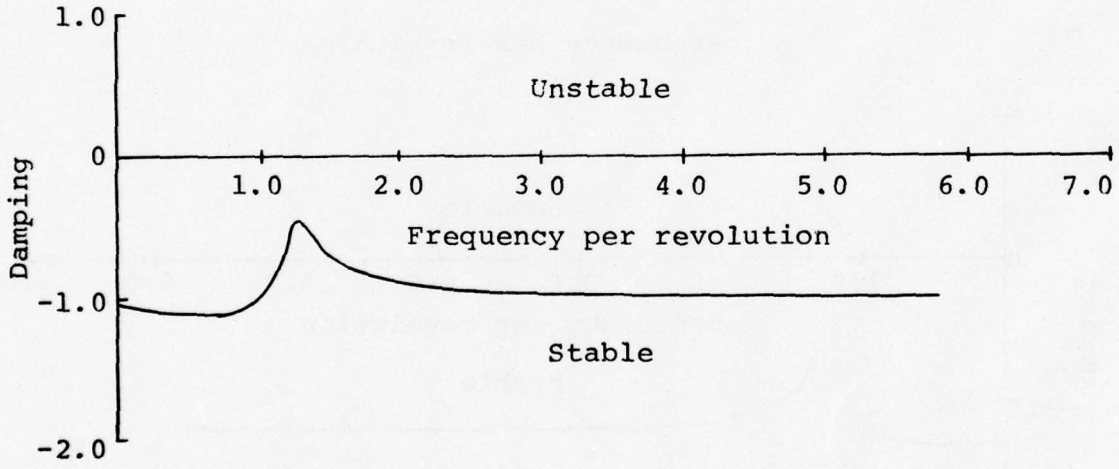

(b) Pitch angle θ = 19 degrees.

Figure 28. Continued.

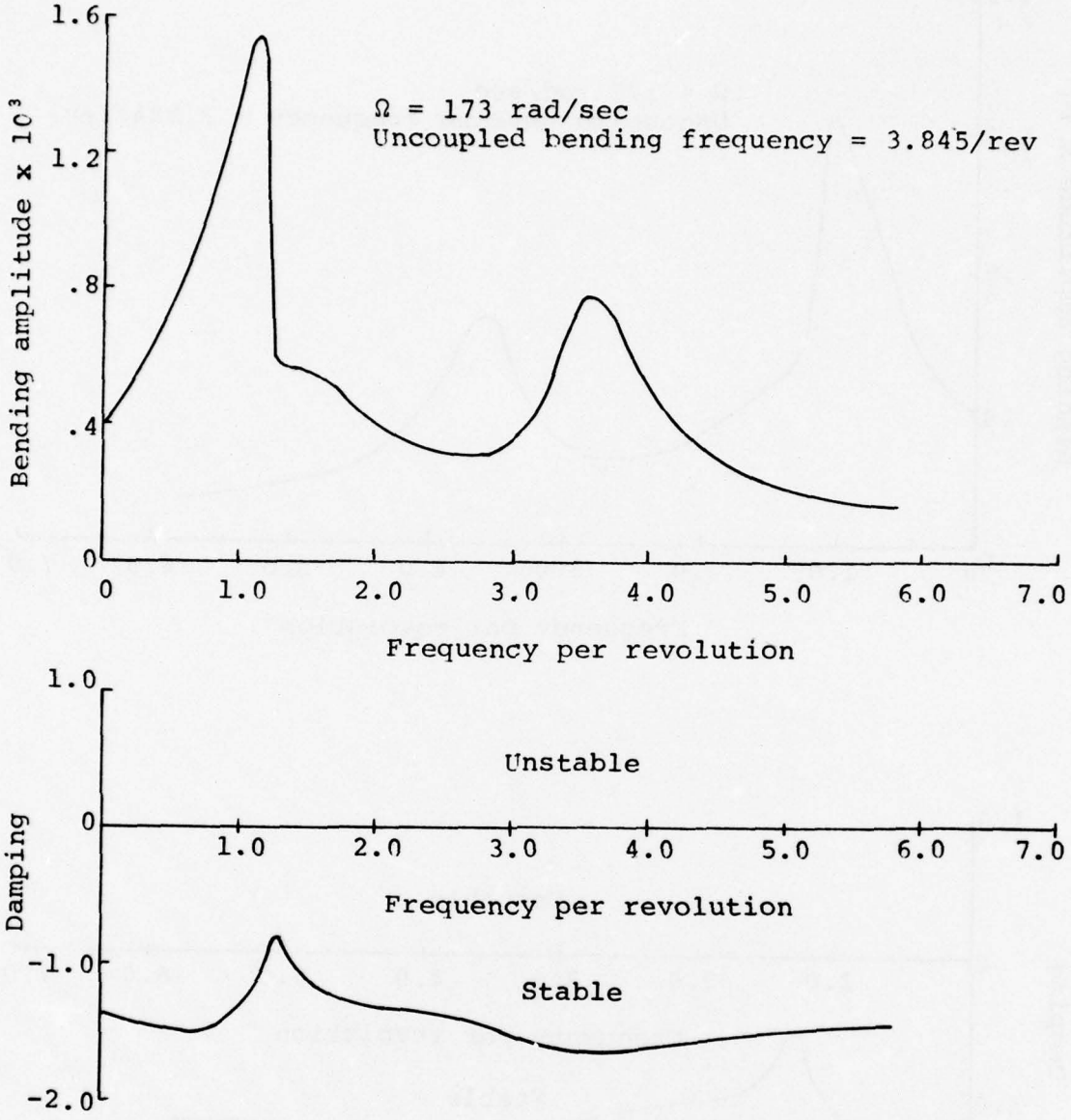

(a) Pitch angle θ = 0 degrees.

Figure 29. Response and damping curves for the out-of-plane bending degree of freedom in hover.

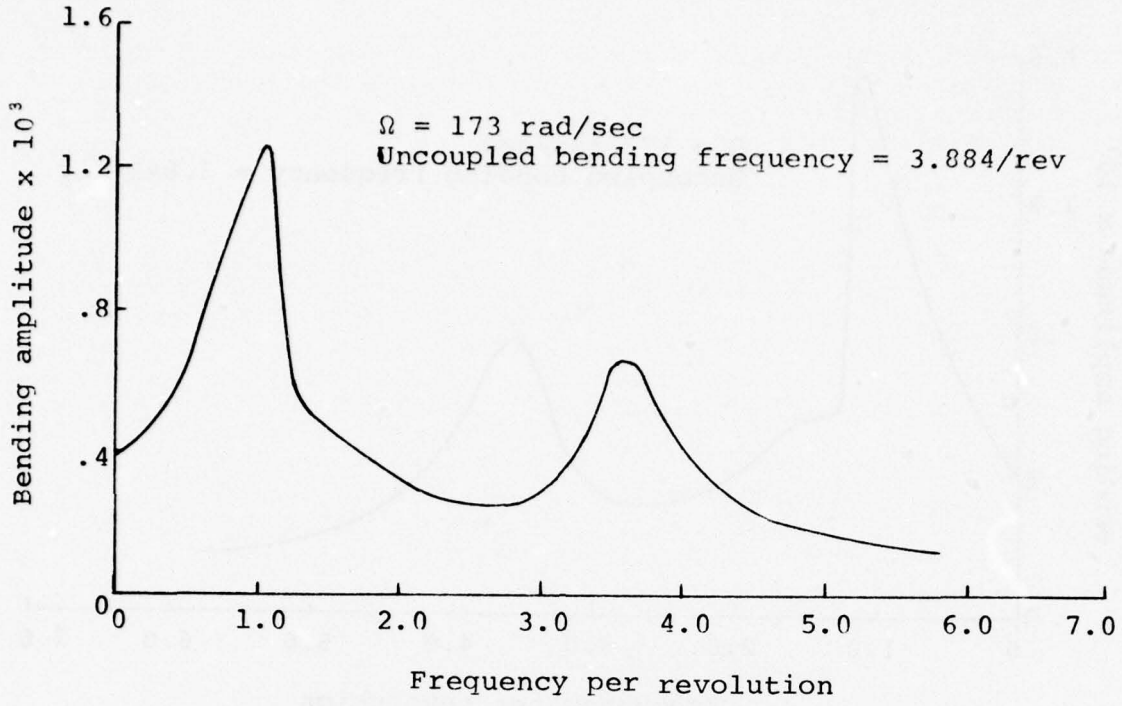

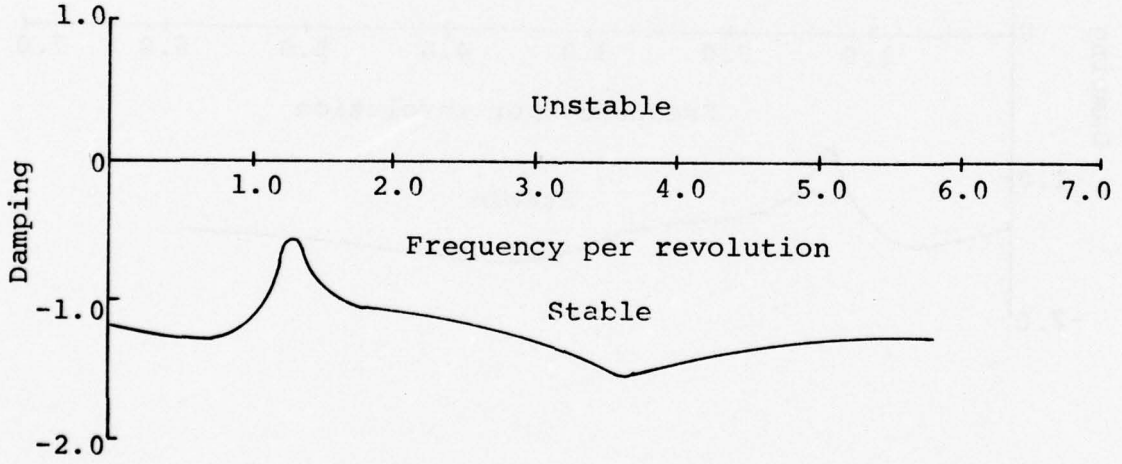

(b) Pitch angle θ = 19 degrees.
Figure 29. Continued.

cantilever modes. No evidence of rotor instability is noted in these results, and the magnitude of the damping coefficients are such that adequate damping margin would be present in the system to insure blade stability.

Tie-down Tests

Further dynamic testing was conducted with the teetering EPBTR mounted on a UH-1H helicopter during the ground tie-down test program. The primary emphasis of this program was directed towards identifying the modes of vibration for the EPBTR installation and to identify the cause of the vibratory load excursion witnessed during the previous whirl test program. This was accomplished by providing adequate instrumentation to study the phenomenon once it occurred and by providing a hydraulic shaker that could be used as a means for producing an external vibratory excitation to the tail pylon. Views of the UH-1H helicopter configured for the ground tie-down testing of the EPBTR are shown in Figures 30 and 31.

Preliminary independent test operations of the hydraulic shaker and of the aircraft with the tail rotor installed were performed to verify proper operation of each before beginning the combined test of running the tail rotor with shaker excitation of the fuselage. During these preliminary tests, with the tail rotor operating at 100% speed (1650 rpm) and the shaker not attached, a self-excited vibration was found to occur at a blade pitch angle 12.75 degrees. At lower pitch settings it did not occur. Figures 32 and 33 show the time history recorded for pertinent rotor parameters before and during the self-excited limit vibration respectively. It will be noted that both the amplitude and frequency of blade bending and teeter motion changed. During the vibration all amplitudes increased and the predominant frequency became 1.4/rev (40 h_z). The principal mode involved teeter motion coupled with symmetric inplane bending, though out-of-plane bending increased as well. Reducing pitch setting after the vibration occurred reduced the amplitude but did not eliminate the 1.4 frequency. Subsequent runs to the same setting produced the same results.

In accordance with the original test plan, numerous attempts were made to excite this mode of vibration at lower pitch angles by exciting the tail pylon at frequencies from 10 to 80 Hertz. These attempts were unsuccessful even when operating the rotor at 12 degrees of pitch, the edge of the self-excited range, and shaking at various frequencies including 68 Hertz, the predominant frequency in the nonrotating system when the vibration occurred. Other experiments, such as suddenly disconnecting the shaker from the fuselage, producing the equivalent of a step input to the tail pylon, were also not able to excite the vibration.

Figure 30. On-site view of the test vehicle as configured for the ground tie-down test.

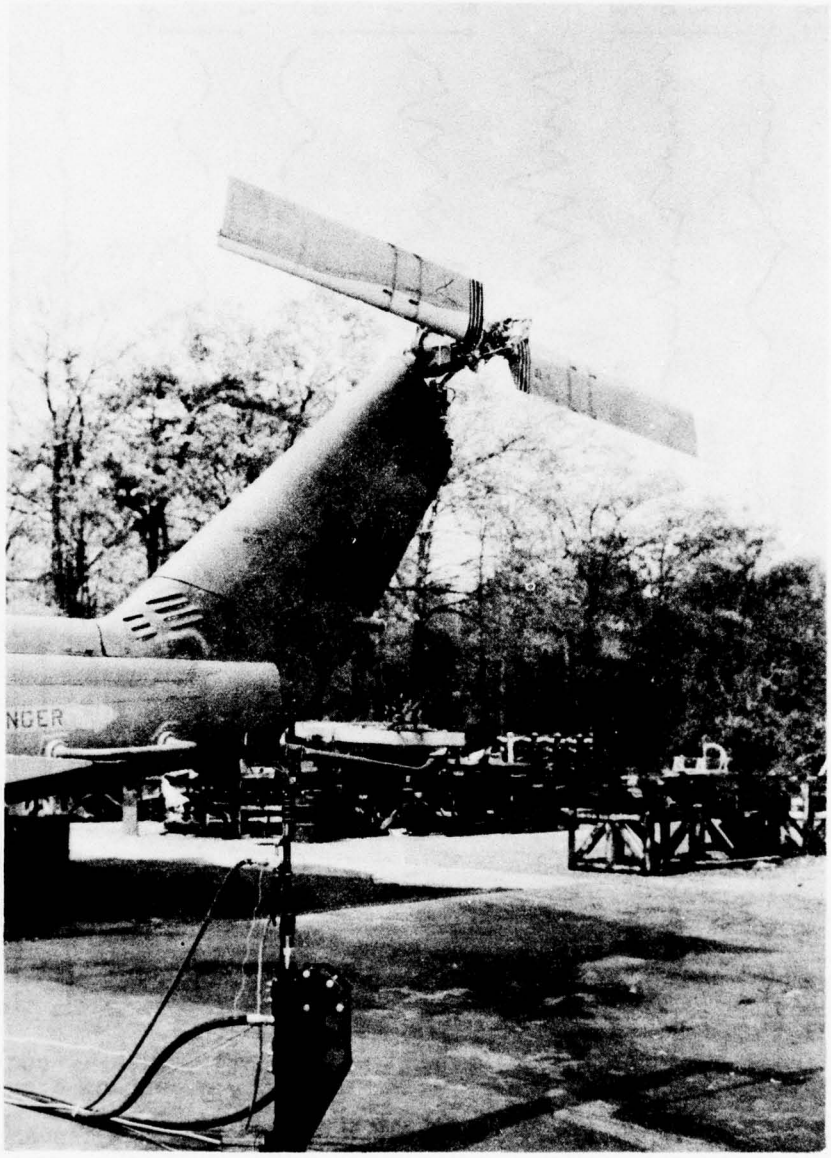

Figure 31. Test vehicle showing elastic pitch beam tail rotor and hydraulic shaker installation.

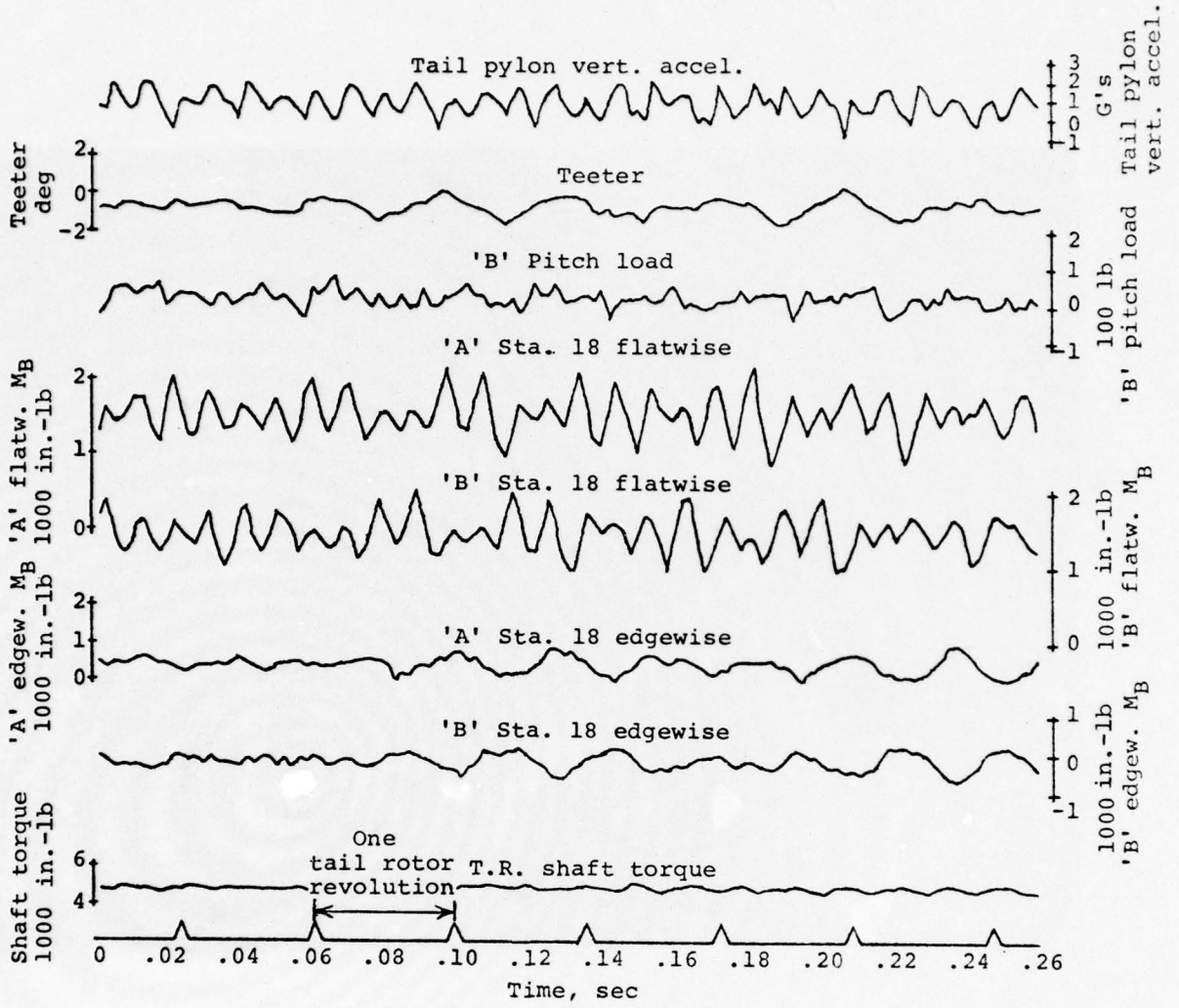

Figure 32. Time history prior to self-excited vibration for teetering rotor. Blade pitch = 12.75 degrees, tail rotor speed = 27.35 cps.

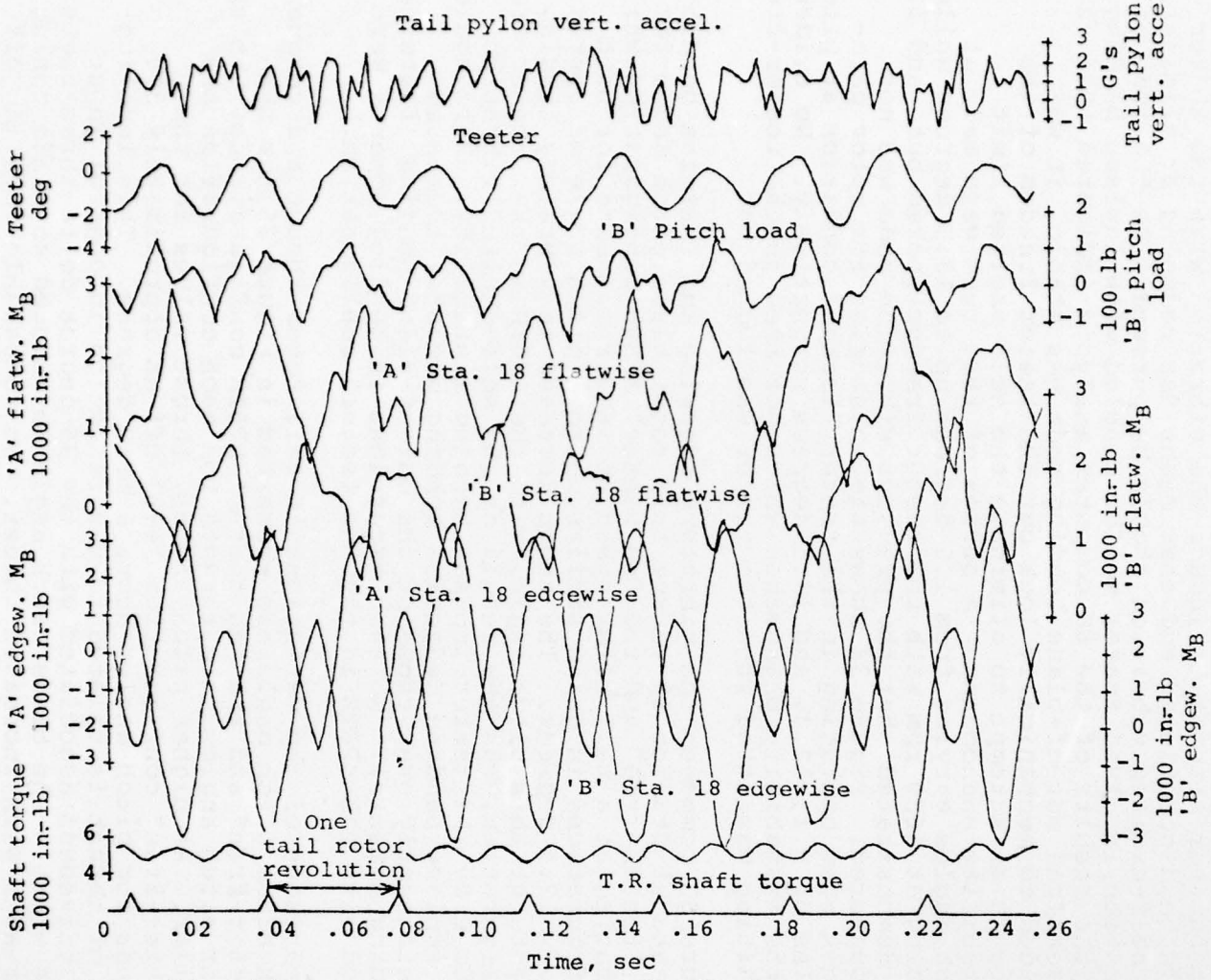

Figure 33. Time history during self-excited vibration for teetering rotor. Blade pitch = 12.75 degrees, tail rotor speed = 27.35 cps.

Since the primary purpose of the test was to induce the vibratory load excursion exhibited during the whirl rig tests with adequate instrumentation to study it, this basic goal was achieved during this test program. It was therefore decided that further attempt to induce the vibration with the shaker would be discontinued and that means for reducing or eliminating the self-excited vibration should be pursued. As the mode of vibration involved teeter motion coupled with inplane bending, and the results of the 6F computer analysis indicated that the symmetrical out-of-plane bending mode was stable, it was decided to mechanically lock out the teeter freedom of the rotor in an attempt to eliminate the self-excited limit instability phenomenon. A series of test runs were made at pitch angles varying from 1.5 degrees up to 13.5 degrees while running at 1650 rpm with the teeter freedom locked out, and it was demonstrated that the previous vibration mode was not encountered. Figure 34 shows time histories for rotor parameters when operating in the teeter "locked" condition at pitch angles of 9.1, 12.3, and 13.5 degrees respectively. No evidence of the instability phenomenon which occurred in the teeter-free condition was noted when the teeter was locked out.

Figure 35 compares the vibratory edgewise and flatwise bending moments at Station 18 versus tail rotor blade pitch angle for the "teeter-free" and the "no teeter" EPBTR configuration while operating at a tail rotor speed of 1650 rpm. Data for both configurations is quite similar up to a pitch angle of approximately 12.5 degrees. The sharp increase in vibratory bending moments at this pitch angle, with the EPBTR in the "teeter-free" configuration, was the result of the self-excited vibration induced by the teeter-inplane bending instability. Here again, the inplane bending (edgewise bending moments) increased significantly over those of the out-of-plane bending (flatwise bending moments). No such excursions in bending moments were noted with the EPBTR in the "no teeter" configuration.

Comparisons of the variations in tail rotor thrust and torque with blade pitch angle are presented in Figure 36 for the "teeter-free" and the "no teeter" EPBTR configurations. At the lower pitch angles, the thrusts for each configuration are similar. At higher pitch angles, thrust values for the "teeter-free" configuration level off at approximately 500 pounds for pitch angles above 8 or 9 degrees. This leveling-off of thrust is related to the reduction in control input effectiveness associated with the 35-degree delta-three teeter axis wherein the blade pitch angle is reduced as blade coning increases with increased thrust. No comparable leveling off of thrust is noted when the EPBTR is in the "no teeter" configuration as the delta-three angle is essentially reduced to zero when the teeter freedom is locked out. Tail rotor shaft torques for each EPBTR configuration are essentially the same for the range of pitch angles tested.

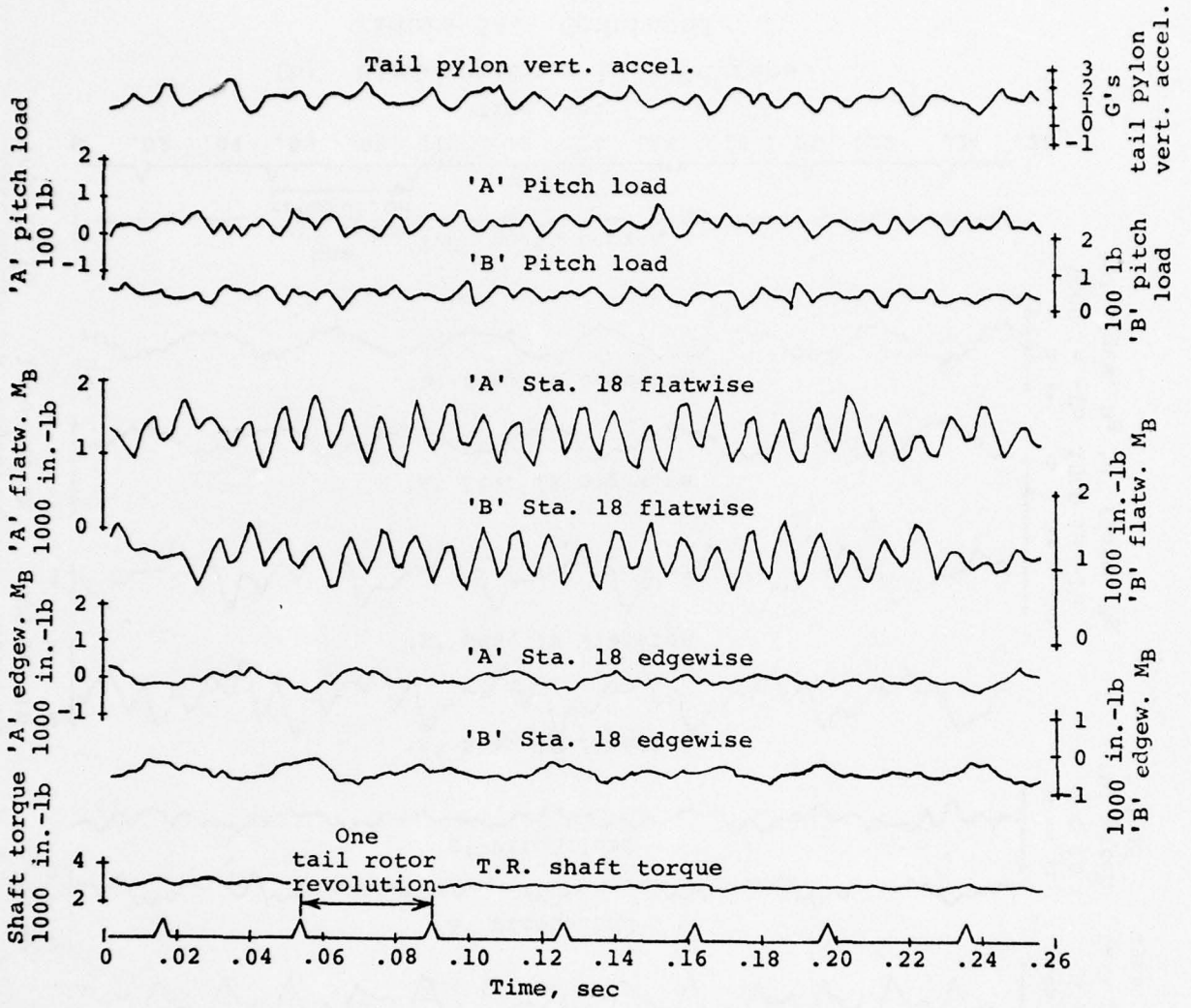

(a) Blade pitch = 9.1 degrees.

Figure 34. Time history for nonteetering rotor. Tail rotor speed = 27.35 cps.

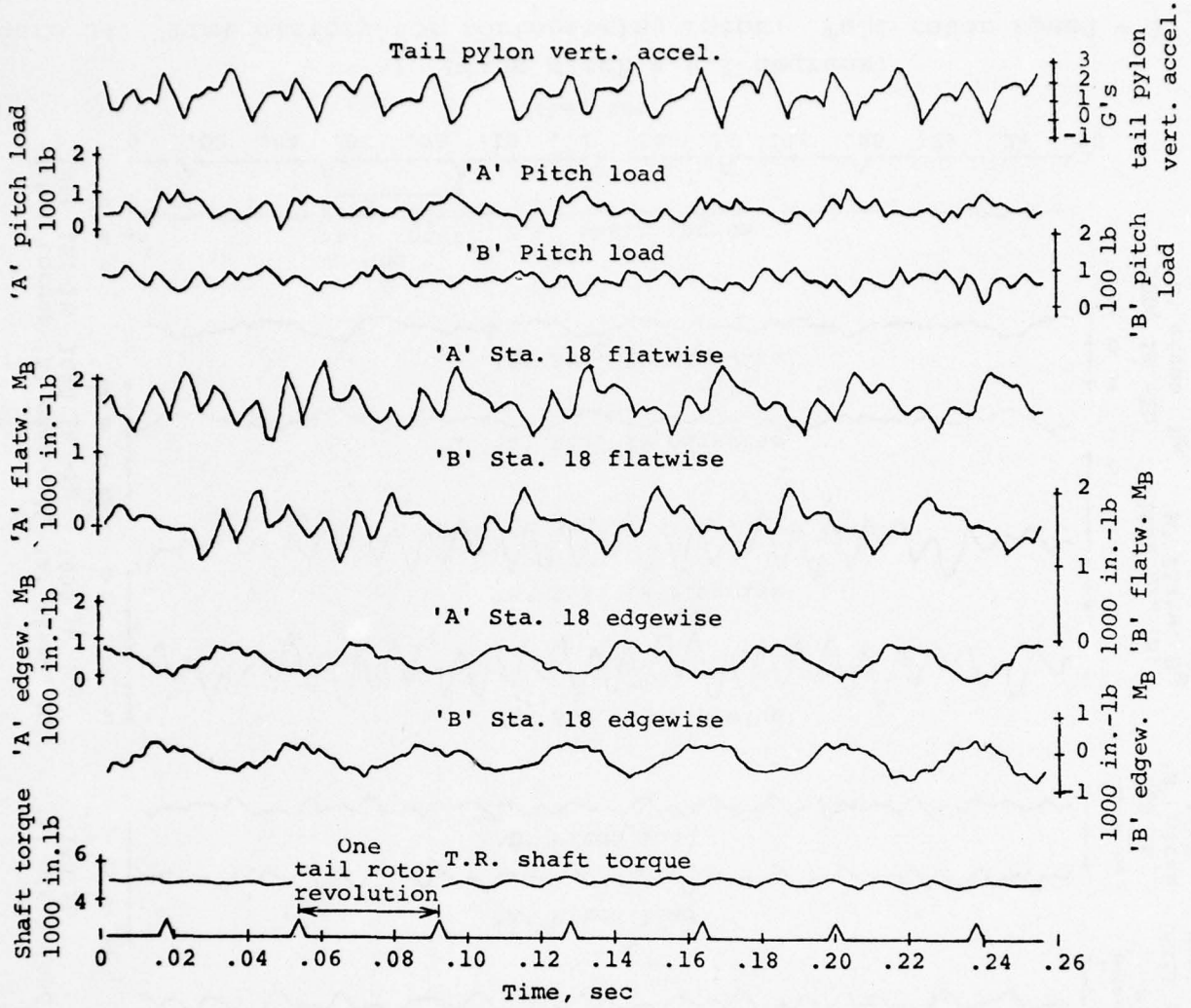

(b) Blade pitch = 12.3 degrees.

Figure 34. Continued.

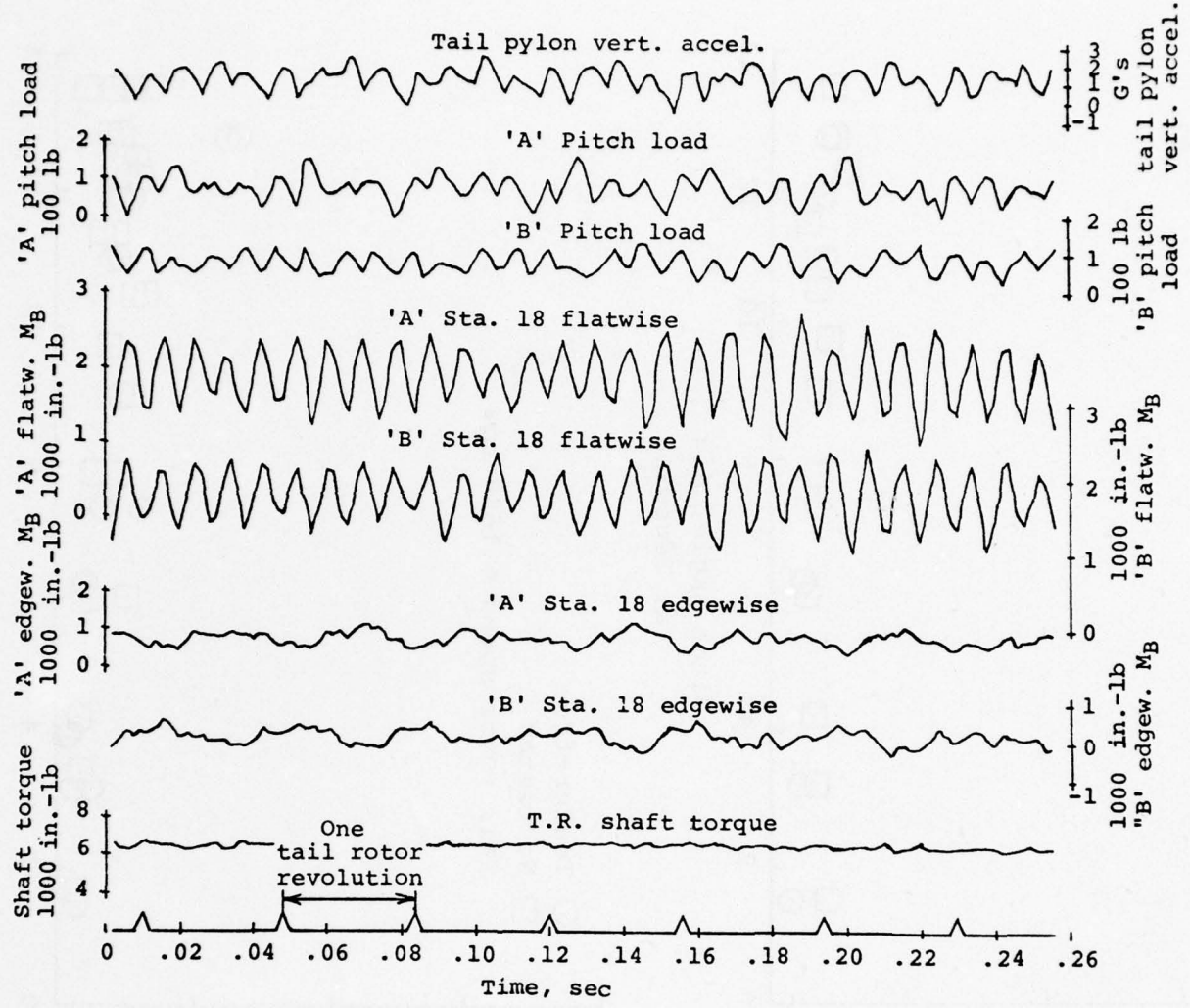

(c) Blade pitch = 13.5 degrees.

Figure 34. Continued.

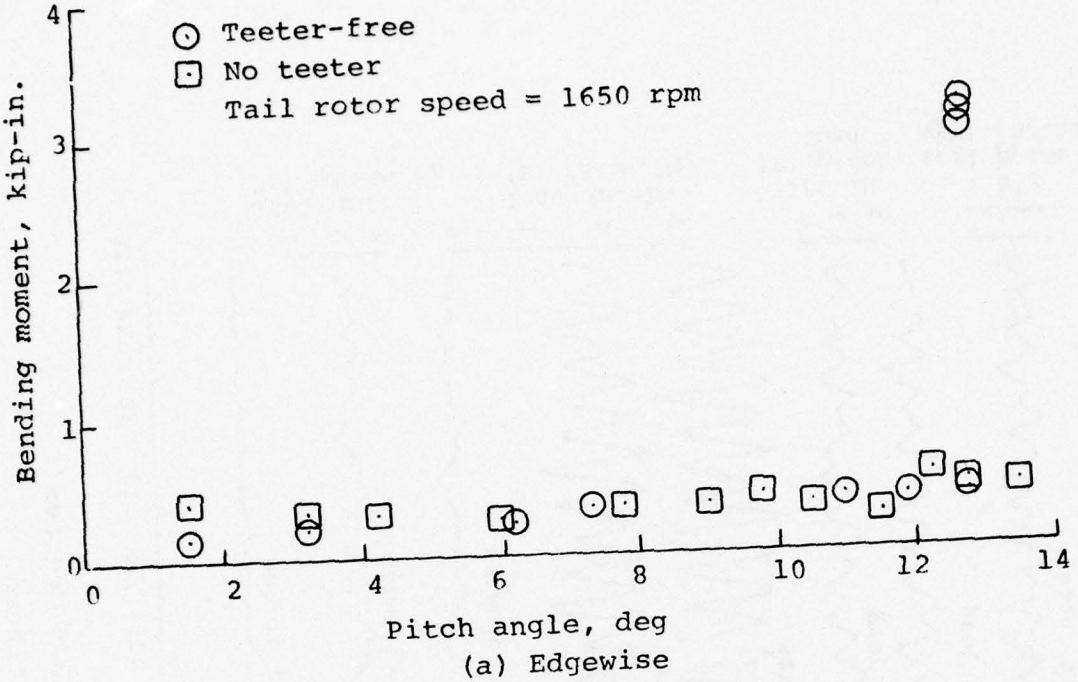

(a) Edgewise

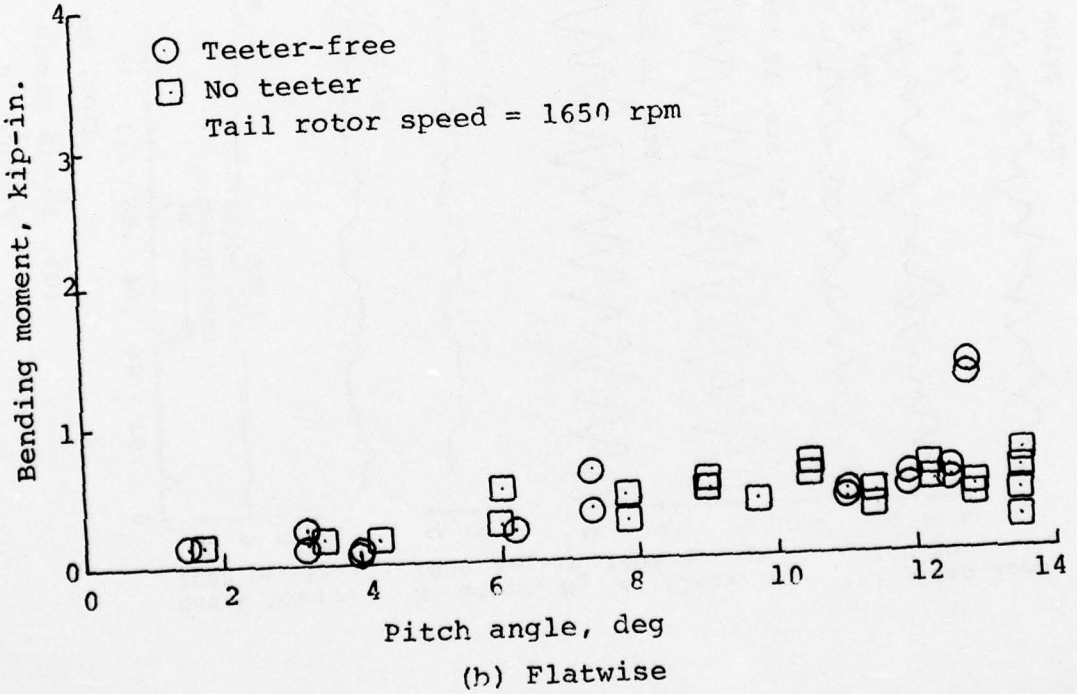

(b) Flatwise

Figure 35. Vibratory bending moment at station 18 versus blade pitch angle.

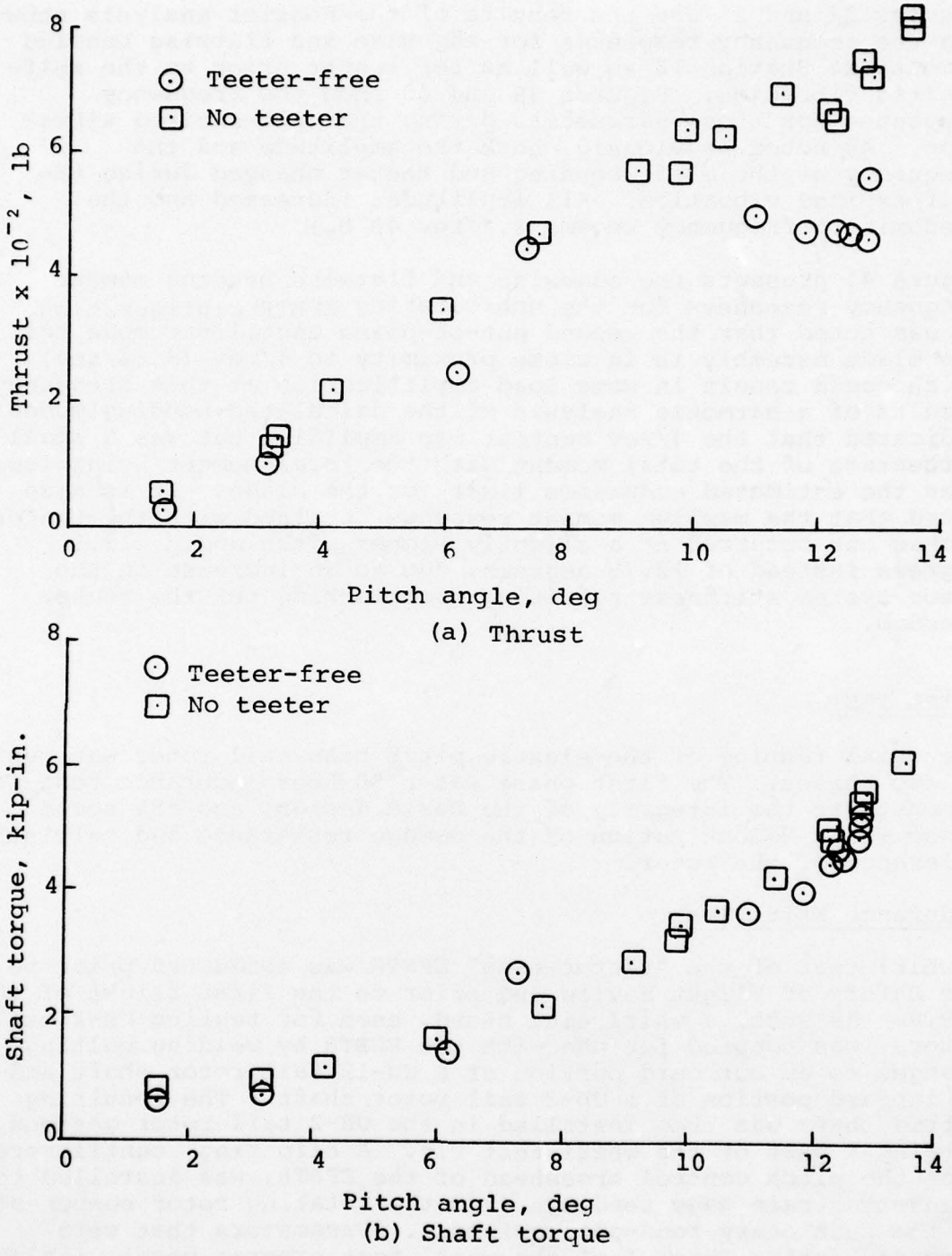

Figure 36. Tail rotor thrust and shaft torque versus blade pitch angle.

Figures 37 and 38 are the results of the Fourier analysis showing the frequency responses for edgewise and flatwise bending moments at Station 18 as well as for teeter prior to the self-excited vibration. Figures 39 and 40 show the frequency responses for these parameters during the self-excited vibration. As noted previously, both the amplitude and the frequency of the blade bending and teeter changed during the self-excited vibration. All amplitudes increased and the predominate frequency became 1.4/rev 40 h_z).

Figure 41 presents the edgewise and flatwise bending moment frequency responses for the nonteetering EPBTR configuration. It was noted that the second out-of-plane cantilever mode for the blade assembly is in close proximity to 4/rev (3.84/rev), which could result in some load amplification at this frequency. Results of a harmonic analysis of the calculated bending moments indicated that the 4/rev content was amplified but was a small percentage of the total moment, with the total moment being lower than the estimated endurance limit for the blade. It is also noted that the maximum moment response obtained with the teeter locked out occurred at a slightly higher pitch angle, 13.5 degrees instead of 12.75 degrees, due to an increase in the rotor system stiffness resulting from locking out the teeter freedom.

WHIRL TEST

The whirl testing of the elastic pitch beam tail rotor was run in two phases. The first phase was a 50-hour endurance test to demonstrate the integrity of the basic design, and the second phase was a demonstration of the damage resistance and ballistic tolerance of the rotor.

Endurance Whirl Test

A whirl test of the "teeter-free" EPBTR was conducted prior to the Safety of Flight Review and prior to the first flight of the EPBTR. As such, a whirl test stand, used for testing UH-2 tail rotors, was adapted for use with the EPBTR by welding bolting flanges to an outboard portion of a UH-1H tail rotor shaft and an inboard portion of a UH-2 tail rotor shaft. The resulting hybrid shaft was then installed in the UH-2 tail rotor gearbox, forming a part of the whirl test rig. A slip ring, cantilevered from the pitch control crosshead of the EPBTR, was installed to transmit strain gage readings from the rotating rotor components to the stationary read-out equipment. Parameters that were recorded during Phase I of the whirl test program were: Inplane and out-of-plane bending moments at Stations 3 and 18, pitch link load, and pitch angle on the "B" blade; tail rotor shaft torque; fore and aft and vertical accelerations of the tail rotor gearbox; and rotor rpm.

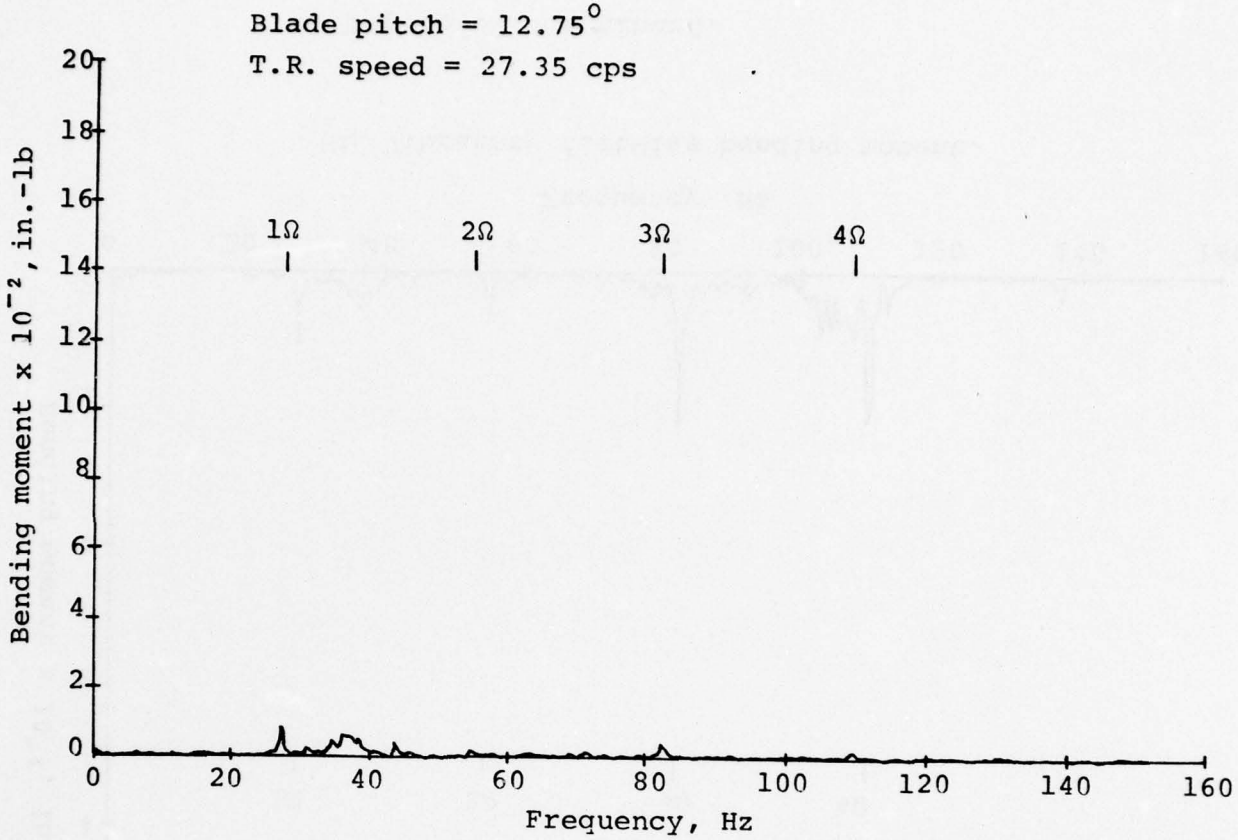

(a) Vibratory edgewise bending moment.

Figure 37. Teeter-free frequency response at station 18 prior to self-excited vibration.

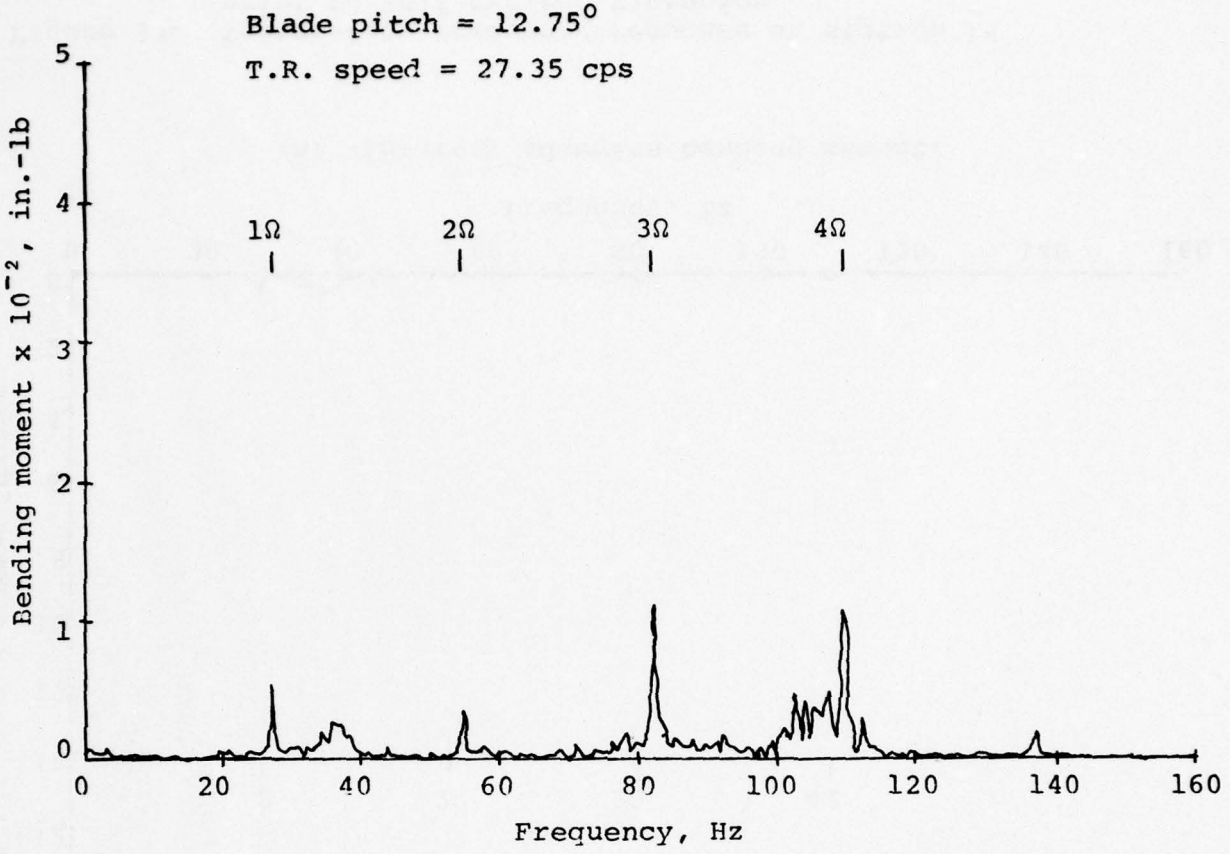

(b) Vibratory flatwise bending moment.

Figure 37. Continued.

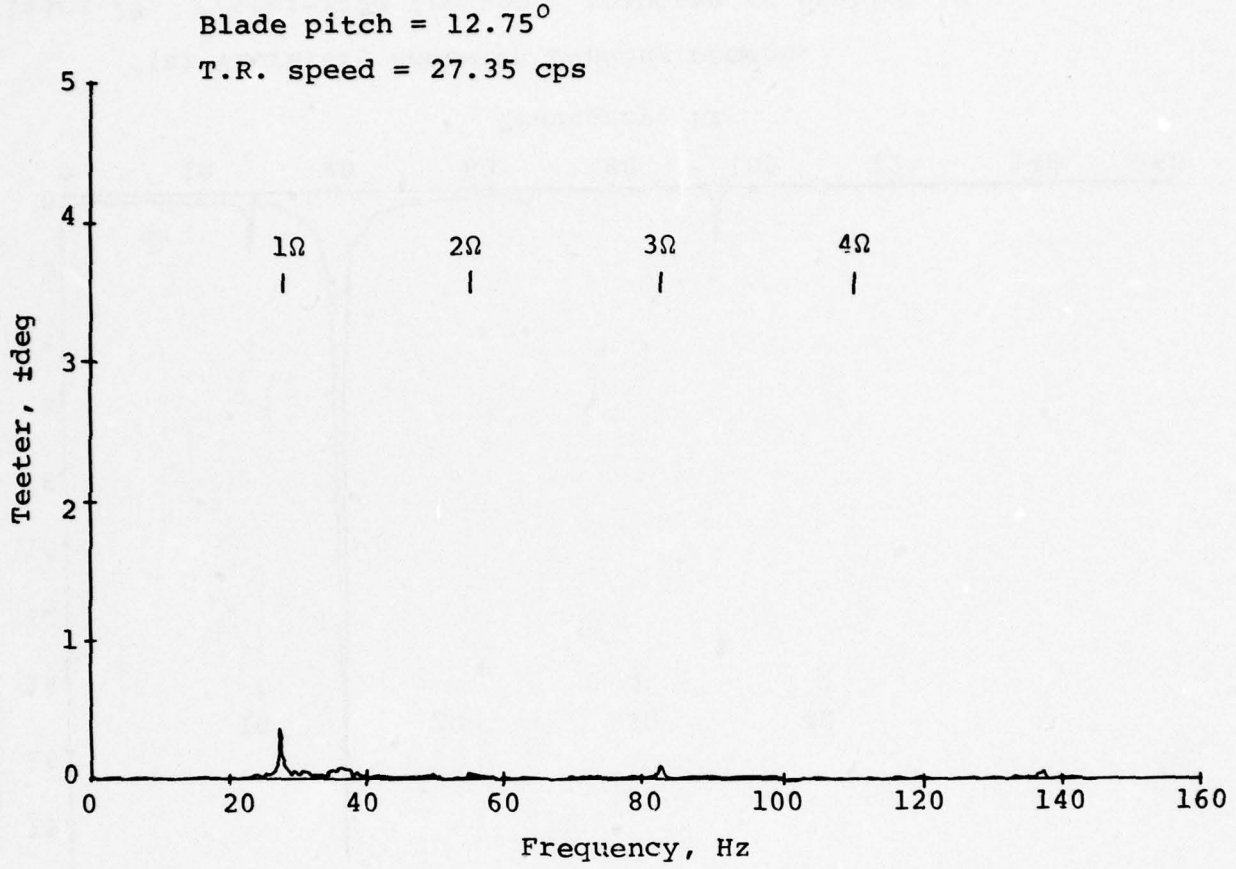

Figure 38. Teeter frequency response prior to self-excited vibration.

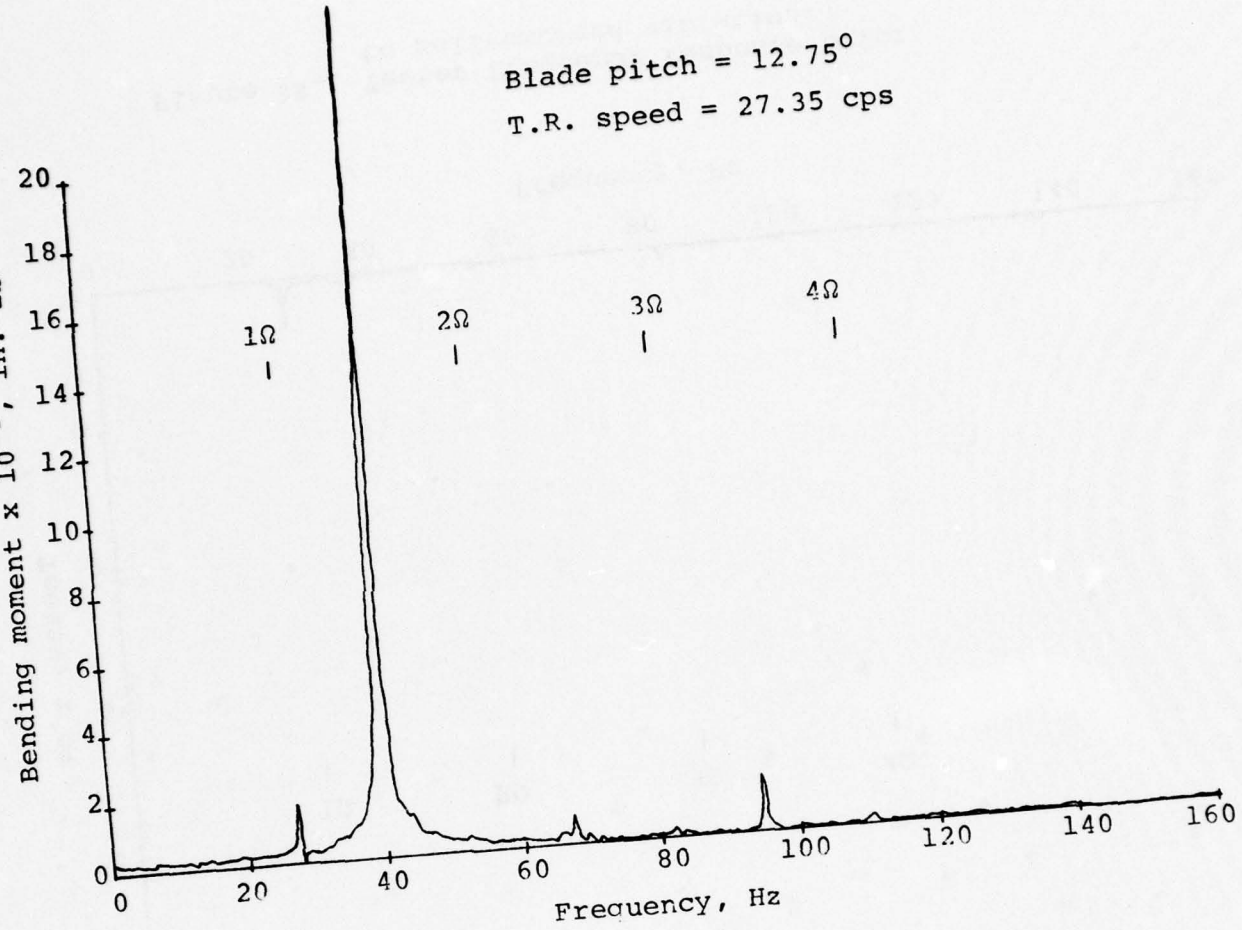

(a) Vibratory edgewise bending moment.

Figure 39. Teeter-free frequency response at station 18 during self-excited vibration.

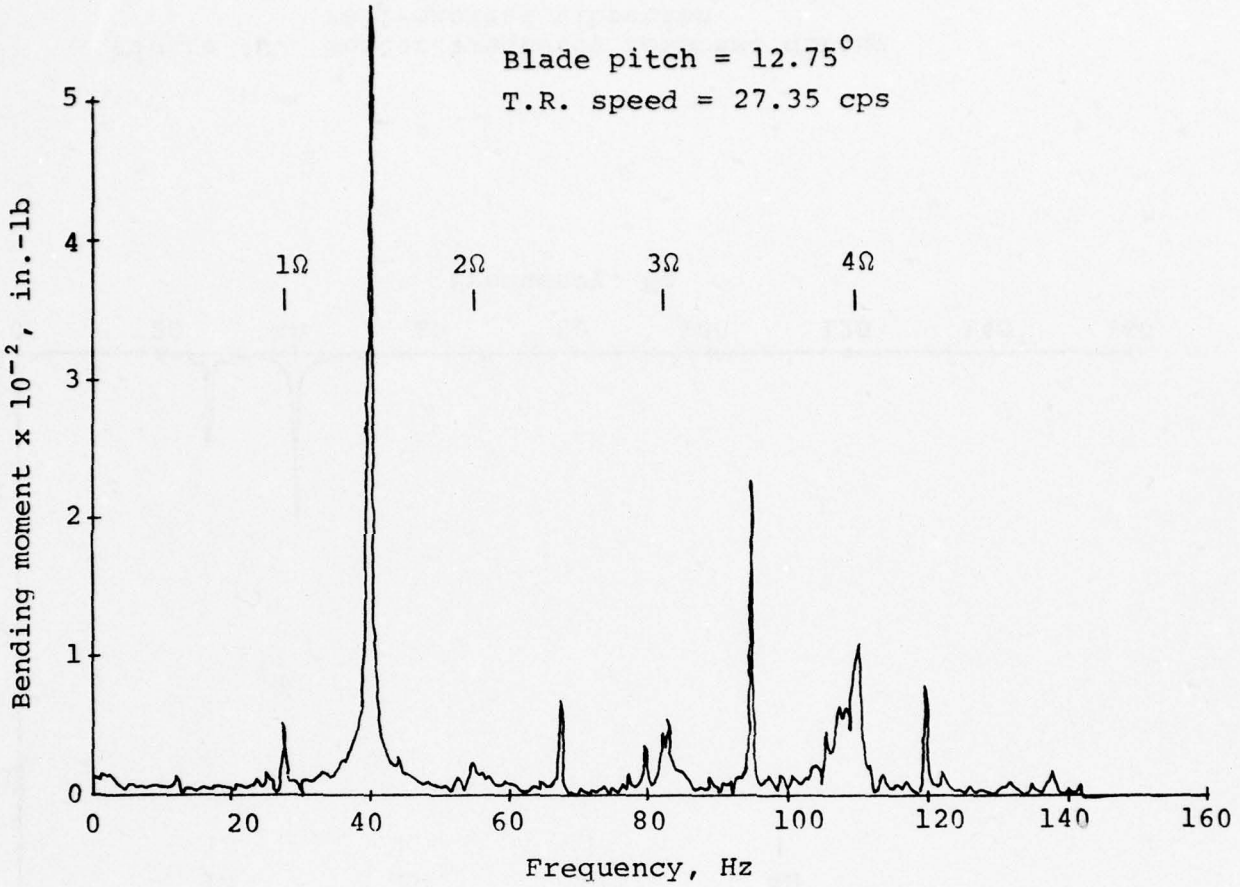

(b) Vibratory flatwise bending moment.

Figure 39. Continued.

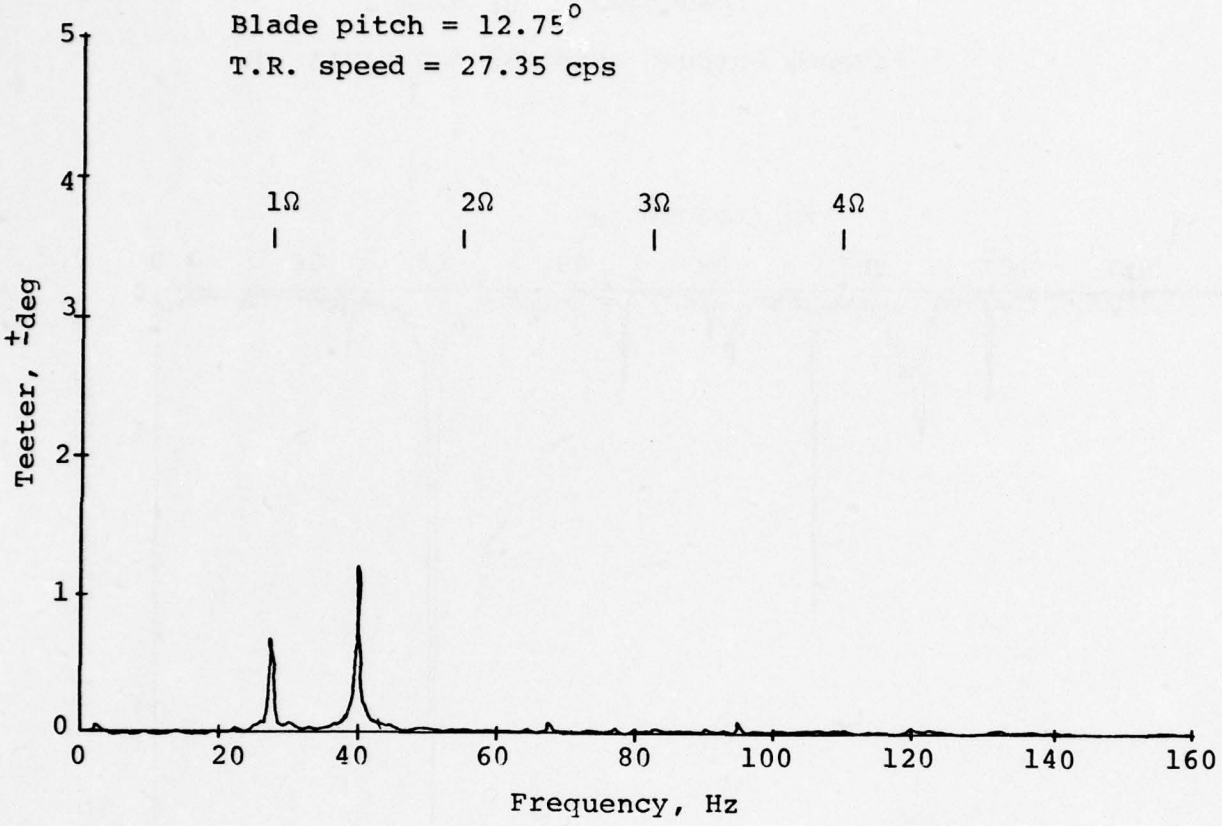

Figure 40. Teeter frequency response during self-excited vibration.

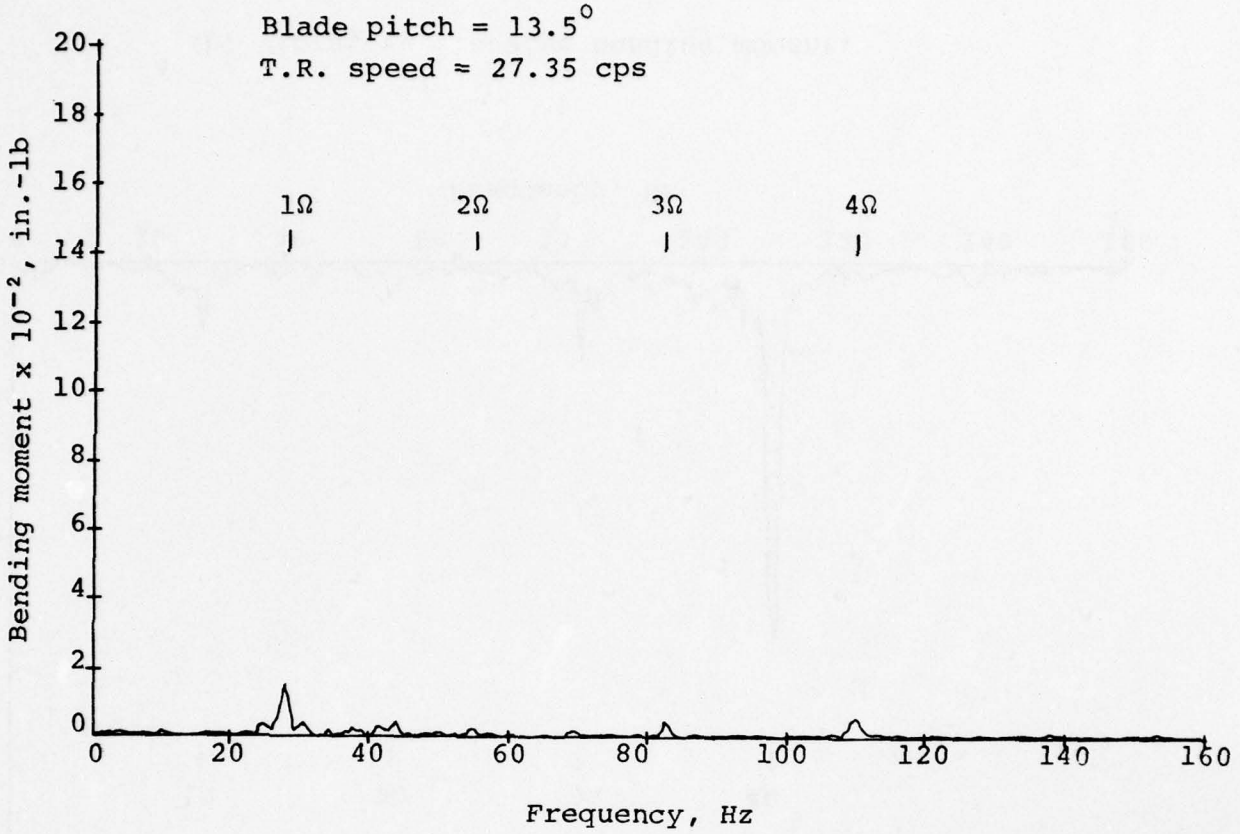

(a) Vibratory edgewise bending moment.

Figure 41. Frequency response at station 18 with teeter locked out.

AD-A035 175 KAMAN AEROSPACE CORP BLOOMFIELD CONN F/G 1/3
ELASTIC PITCH BEAM TAIL ROTOR.(U)
DEC 76 P F MALONEY, J D PORTERFIELD DAAJ02-72-C-0006
UNCLASSIFIED R-1399 USAAMRDL-TR-76-35 NL

2 OF 3
AD A035175

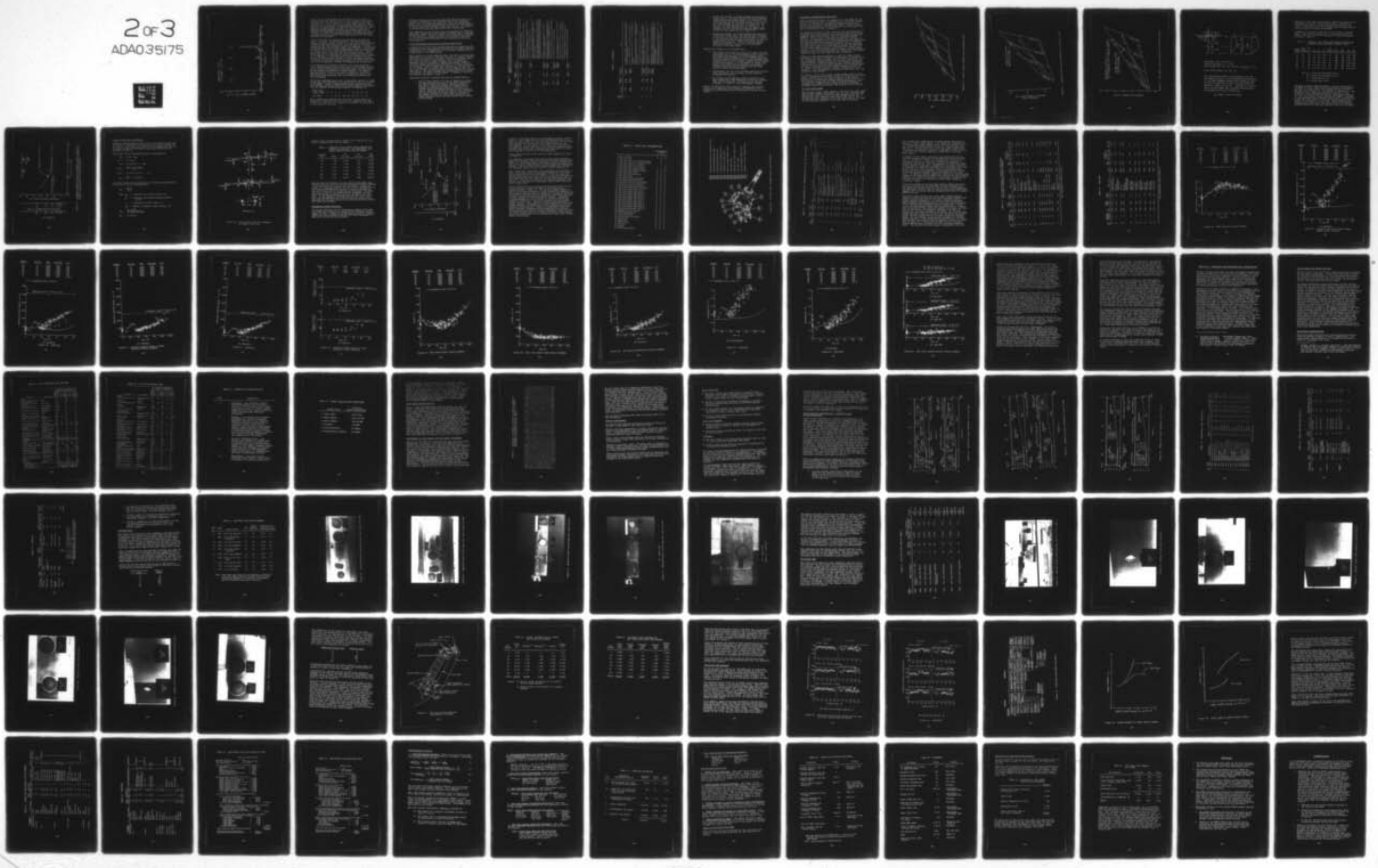

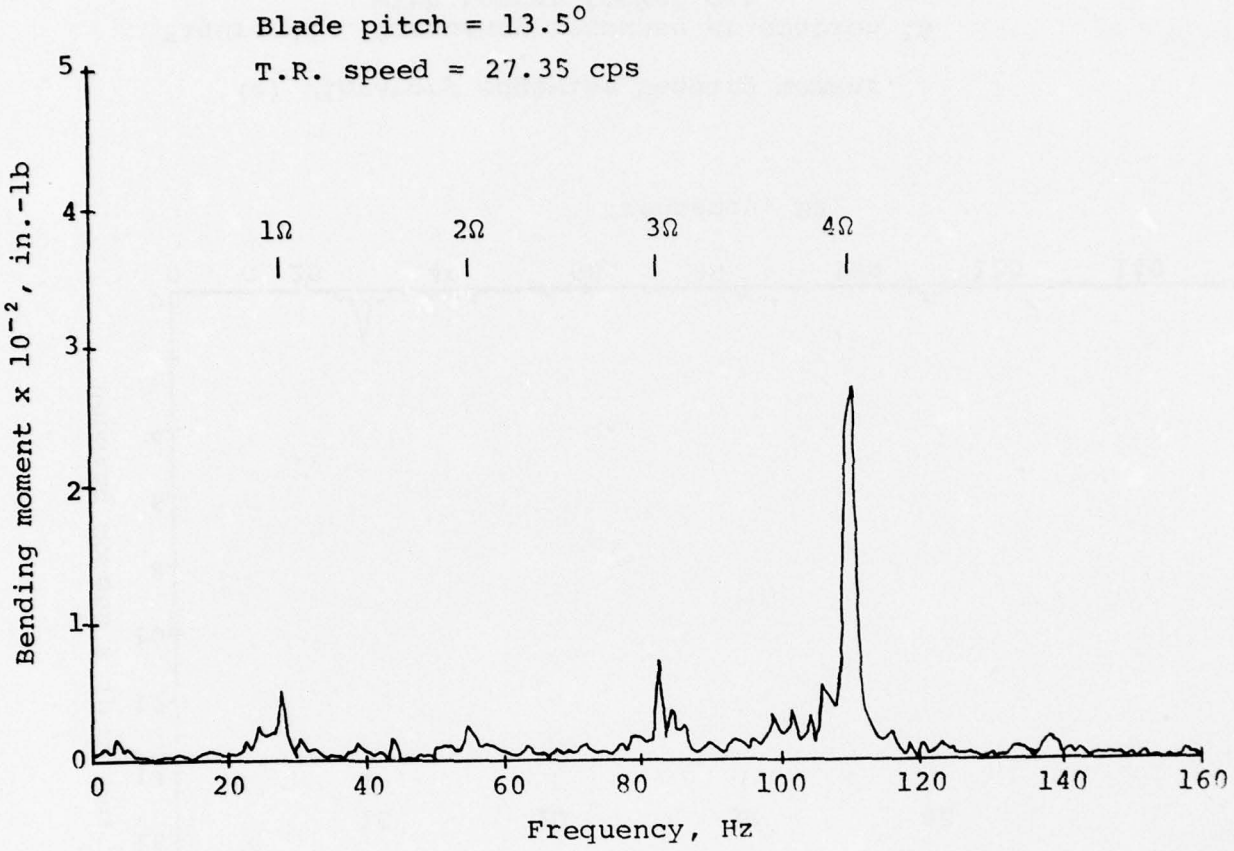

(b) Vibratory flatwise bending moment.

Figure 41. Continued.

Early in the test program with the rotor free to teeter, a review of records obtained after a test run with pitch angles varying from -2 to 19 degrees at a rotor speed of 1650 rpm, revealed that a self-limiting instability had occurred. While running at a pitch angle of approximately 18 degrees with wind gusts up to approximately 20 mph, the vibratory flatwise and edgewise bending moments increased to several times their steady-state magnitudes and the frequency changed from 1/rev to 1.27/rev. As only the instrumentation on one blade was being recorded during this period, full definition of the vibration mode was not available.

Efforts were made to reproduce this phenomenon so that its cause, or causes, could be identified. The instrumentation hook-up for Phase II was changed to permit monitoring parameters on both blades simultaneously so that the mode of vibration associated with the condition could be determined. In addition, torsional moment strain gage bridges were mounted on both blades at Station 26.5 and a linear potentiometer, used for measuring the teeter angle, was installed near the teeter axis. Subsequent test runs at 1650 rpm with pitch angles varying from -6 to 22 degrees, at 19 degrees of pitch with varying rotor speeds up to 1650 rpm, at wind conditions varying between calm and 20 mph, and with various methods of slip ring support employed to reduce the external loading imposed on the rotor system, were made in an unsuccessful attempt to reproduce the instability.

As discussed in the Dynamics Section, this instability was later isolated during the tie-down test with the EPBTR mounted on the UH-1H helicopter, and the principal mode involved teeter motion coupled with symmetric inplane bending. The decision was then made to lock-out the teeter freedom of the EPBTR. Additional runs in the "no teeter" configuration made on the UH-1H helicopter indicated that the instability problem had been eliminated.

The 50-hour endurance whirl test of the EPBTR, having its teeter locked out, was conducted as a prerequisite to the first flight of the EPBTR. Phase II instrumentation was used during this test program and the following pitch angle schedule, representative of a typical UH-1H utility mission, was adhered to:

Blade Pitch Angle (Deg)	-6	-3	0	3	5	7	10	13	16	19
Time (Min)	1	5	10	30	585	90	12	2.5	.5	.25

This schedule was repeated four times for a total time of 49 hours and 5 minutes and was run at a rotor speed of 1650 rpm. In addition, the rotor was oversped for a period of one hour at a rotor speed of 1750 rpm.

Torsional spring rates of each blade were monitored during the program to determine if any deterioration of the torsional spring rate of the EPB was occurring. This was accomplished during rotor shut-down by measuring the pitch link load required to rotate each blade through a given pitch angle. No evidence of EPB deterioration was noted during the test program.

Upon completion of the 50-hour whirl test program the EPBTR was thoroughly inspected and no evidence of damage, wear, or delamination was found. The rotor used for this program was retained for use during the damage resistance and ballistic tolerance whirl test program as described in the following section and in Reference 3.

Damage Resistance and Ballistic Tolerance Whirl Test

A summary of the whirl test program designed to investigate the damage resistance and ballistic tolerance of the EPBTR, reported in Reference 3, is presented herein to further demonstrate the capabilities of the EPBTR design.

Maple dowels of various diameters from 1/4 inch to 5/8 inch were injected into the path of the whirling rotor to simulate contact with brush and light tree branches. Gravel and crushed stones were also injected into the whirling rotor to assess the susceptibility of the EPBTR to damage from foreign objects. Ballistic damage tolerance was evaluated by firing a total of six rounds of 7.62mm AP ammunition through the outboard portion of the blades; four of which were fired through the skin and core, one through the leading edge, and one through the trailing edge spline. The rotor assembly was subsequently whirl tested to determine the effects of the damage. A summary of the whirl test results are shown in Table 7.

Additional ballistic tolerance testing was accomplished by:

1. Firing three rounds of 7.62 mm AP ammunition through the more critical portions of the blade assemblies: One round through the ballast retention block at Station 51, one round through the forward channel flanges and leading-edge section at Station 37.5, and one round that entered through the aft skin/core region, continued through the elastic pitch beam spar, and exited through the leading edge at Station 27. The damage inflicted by these three rounds and the damage locations were such that further whirl testing was precluded.

TABLE 7. SEQUENCE OF FOREIGN OBJECT AND BALLISTIC DAMAGE IMPOSED DURING WHIRL PROGRAM

Whirl Run No.	Duration	Cumulative Time	Test Description	Notes
1	12 min	12 min	3.35 lb gravel	Gravel hits from Station 30.5 to Station 41 with predominant impacts between Stations 32.5 and 36.5.
				A-Blade exhibits numerous cuts and gouges in urethane erosion strips.
				B-Blade, same as A-Blade, plus 3 localized blisters approx 1/4-3/8 in. dia containing grit and sand.
2	8 min	20 min	2.75 lb gravel	Noise level changed; run aborted after 8 min.
				A-Blade - Urethane boot damage was more prevalent compared to Run 1 plus 3 localized blisters. Boot repaired after completion of run.
				B-Blade - Boot torn open from Stations 32 to 37, revealing small impact indentations to .050 in. aluminum L.E. Evidence of occasional hits along entire L.E. to the outboard tip, Station 51 was noted. Boot replaced after completion of run.
3	10 min	30 min	Two 1/4 in. dowels	Both dowels hit B-Blade, one at Station 49, other at Station 50.5. No damage evident.
4	10 min	40 min	Two 3/8 in. dowels	One dowel hit both blades; on A-Blade, contact made on outboard face of outboard rib in an apparent glancing blow; and on B-Blade at Station 50. No damage evident.
				Second dowel hit A-Blade at Station 50. No damage evident.
5	5 min	45 min	One 1/2 in. dowel	Hit B-Blade, Station 50. No damage evident.
6	1 hr 20 min	2 hr 5 min	Ballistic damage	Tail rotor removed from rig for two 7.62mm shots through skin to core bonds prior to Run 6.
				A-Blade hit at Station 30, clean hole, no delamination.
				B-Blade hit at Station 44.5, clean hole, no delamination.
				No propagation of damage after completion of Run 6.
7	5 min	2 hr 10 min	One 1/2 in. dowel	Hit A-Blade, Station 49. No damage evident.

TABLE 7 - CONTINUED

Whirl Run No.	Duration	Cumulative Time	Test Description	Notes
8	5 min	2 hr 15 min	One 5/8 in. dowel	Hit A-Blade, Station 50.5. Approx 1/8 in. dent on L.E. and L.E. deformed to open .015 in. gap with ballast block on one side of airfoil. No other damage.
9	3 hr 40 min	5 hr 55 min	Ballistic damage	Tail rotor removed from rig for four additional 7.6mm shots. A-Blade hit through L.E. at Station 45, and through skin/core at Station 42. B-Blade hit through spline at Station 48. Localized skin delamination on exit side approx 7/8 in. dia. T.E. delamination *5/8 in. long.* No propagation of damage after completion of Run 9.
10	8 min	6 hr 3 min	Crushed Stone 300 gm injected	Numerous cuts in boot evident, 1/4 in. max length, exposing aluminum L.E. Several stones imbedded in boot removed. One stone trapped under the boot in B-Blade.
11	2 min	6 hr 5 min	Crushed Stone 62 gm injected	Boots tore open on both A- and B-Blade. Loose edges of boot cut away for next run. Numerous dents and cuts in .050 in. aluminum L.E.
12	20 min	6 hr 25 min	Gravel 130 gm injected	Hopper lowered 6 in. Blades ran for approx 20 min prior to discharge of gravel. Gravel hits primarily between Station 37 and Station 43. Boot tore open on both blades at Stations 37 to 40. Boot failure occurred within 1 min after discharge. Run immediately terminated. A-Blade disclosed additional boot delamination on L.E. to Station 43 with gravel trapped under boot at Station 43. Figures 49 through 54 of Reference 3 show damage from Runs 10, 11 and 12.

2. Firing four rounds of 12.7mm AP ammunition through a blade section: One round through the forward-channel flanges and leading-edge section, at Station 46, one round through the trailing-edge spline at Station 42, one round through the skin/core at Station 44, and one round through the skin/core at Station 46. In general, the bond delamination was confined to the immediate vicinity of the hit with the damage being similar to that caused by the 7.62mm hits.

3. Firing four rounds of 12.7mm AP ammunition through an elastic pitch beam spar: One round through the spar at Station 5.5, one round through the spar at Station 7, one round through the spar at Station 9.5, and one round through the spar between the forward and aft channels at Station 15. In all cases, the damage inflicted would have resulted in a catastrophic failure of a whirling rotor.

Conclusions reached in this program were:

1. The elastic pitch beam tail rotor will sever seasoned maple dowels up to 1/2-inch-diameter without incurring any damage and will sever 5/8-inch-diameter dowels with only minor deformations to the leading edge that would not prevent further flight. Since seasoned maple represents one of the stronger hardwoods and is stronger than green maple, it is reasonable to assume that larger live brush and tree branches, particularly softwood varieties, may be contacted by the rotor without causing disabling damage.

2. Polyurethane erosion guard provides protection against stone and gravel hits in excess of that normally encountered in service.

3. The elastic pitch beam will survive ballistic hits from 7.62mm and 12.7mm ammunition in both the leading edge and aft structure. A direct hit on the spar structure is likely to cause catastrophic damage.

Results of additional whirl testing of damaged and repaired elastic pitch beam tail rotor blades are presented in the Reliability and Maintainability Investigation section of this report.

STRUCTURAL SUBSTANTIATION FOR FLIGHT

Prior to the first flight, an evaluation of the EPBTR and the UH-1 helicopter was made to determine their structural capabilities for withstanding the applied loads associated with locking out the teeter freedom of the EPBTR. Critical components investigated were the standard UH-1 tail rotor shaft and the root end of the EPB at Station 3.

The principal change in loads resulting from the conversion of the EPBTR into a nonteetering rotor was the addition of blade flapping induced hub moments that are transferred through the EPBTR hub into the tail rotor shaft as vibratory bending moments. The aeroelastic computer program (6F), Reference 5, was used in conjunction with a blade bending moment program and an experimentally obtained flapping spring rate to determine the magnitude of the hub moment applied at various airspeeds. Airloads calculated by the aeroelastic program (6F) were used in the bending moment program to determine the steady state harmonic rotor blade bending moments, slopes, and deflections. Inplane and out-of-plane responses were calculated and harmonic resultant shears at the blade root were integrated.

Results of data points selected to cover the normal flight envelope of the UH-1 helicopter are presented in Figures 42 to 44. Figures 42 and 43 present the tail rotor thrust and the 1/rev resultant flapping angles for various pitch angles and forward speeds. Figure 44 presents the vibratory hub moment derived by using the calculated vibratory 1/rev flapping angle of Figure 43 multiplied by the flapping spring rate of 1795 in.-lb/deg obtained by static testing a nonteetering rotor assembly. Also superimposed on Figures 43 and 44 are the trim points for level flight.

An estimate of the level flight airspeed that could be flown without exceeding the endurance limits of either the tail rotor shaft or the elastic pitch beam at Station 3 was made by determining the loads and bending moments acting at the critical sections, converting the loads and bending moments into stresses, and comparing the stresses with the S-N curves developed during the structural test portion of this program.

UH-1 Tail Rotor Shaft

The principal cyclic loads applied to the UH-1 tail rotor shaft (Bell Drawing Number 204-040-402) are the 1/rev vibratory hub moments (M_H) resulting from the blade flapping angle (β) and the inphase 1/rev vibratory shaft moment (M_V) due to the inplane hub shear component (V) of the thrust vector (T) shown in the following schematic of the UH-1 tail rotor shaft.

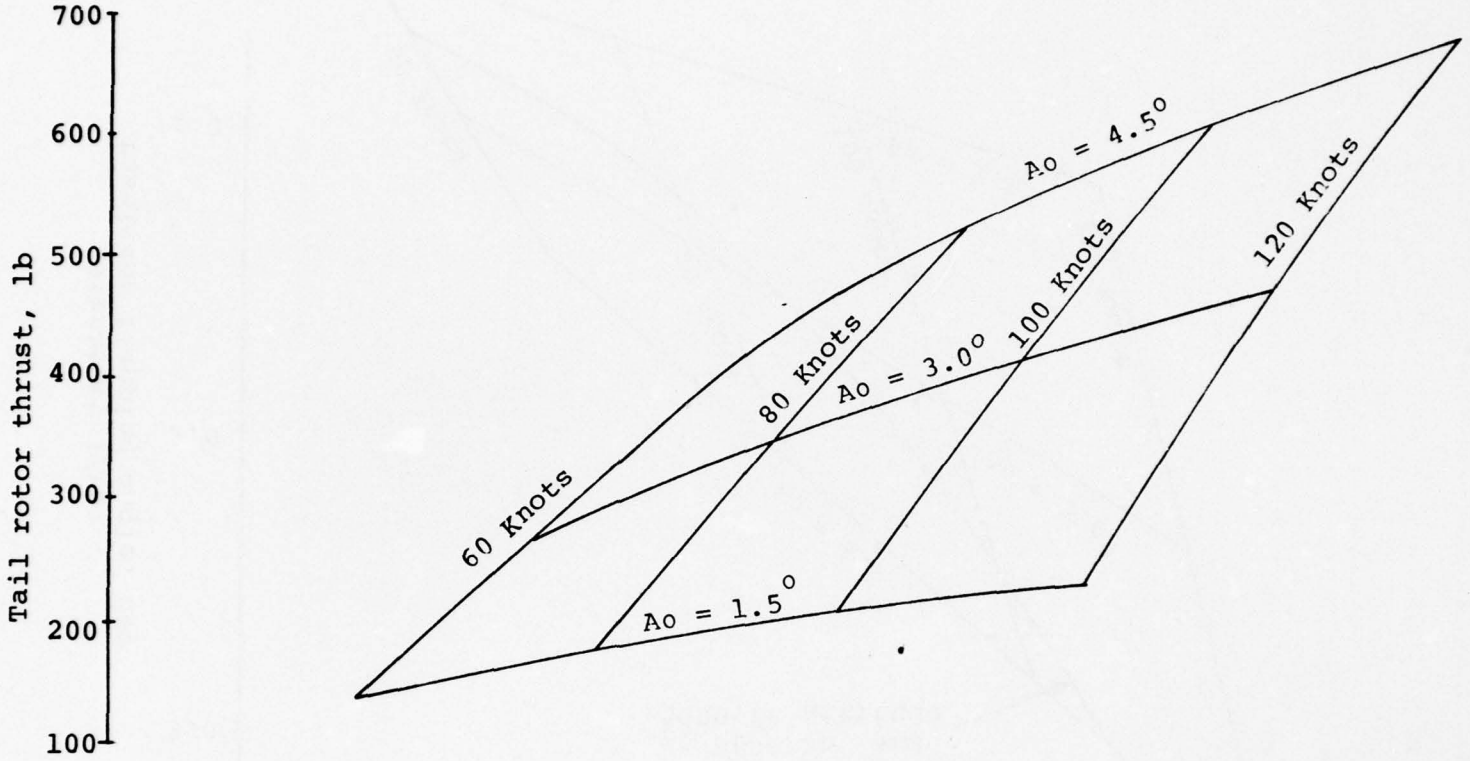

Figure 42. Thrust versus airspeed and collective pitch.

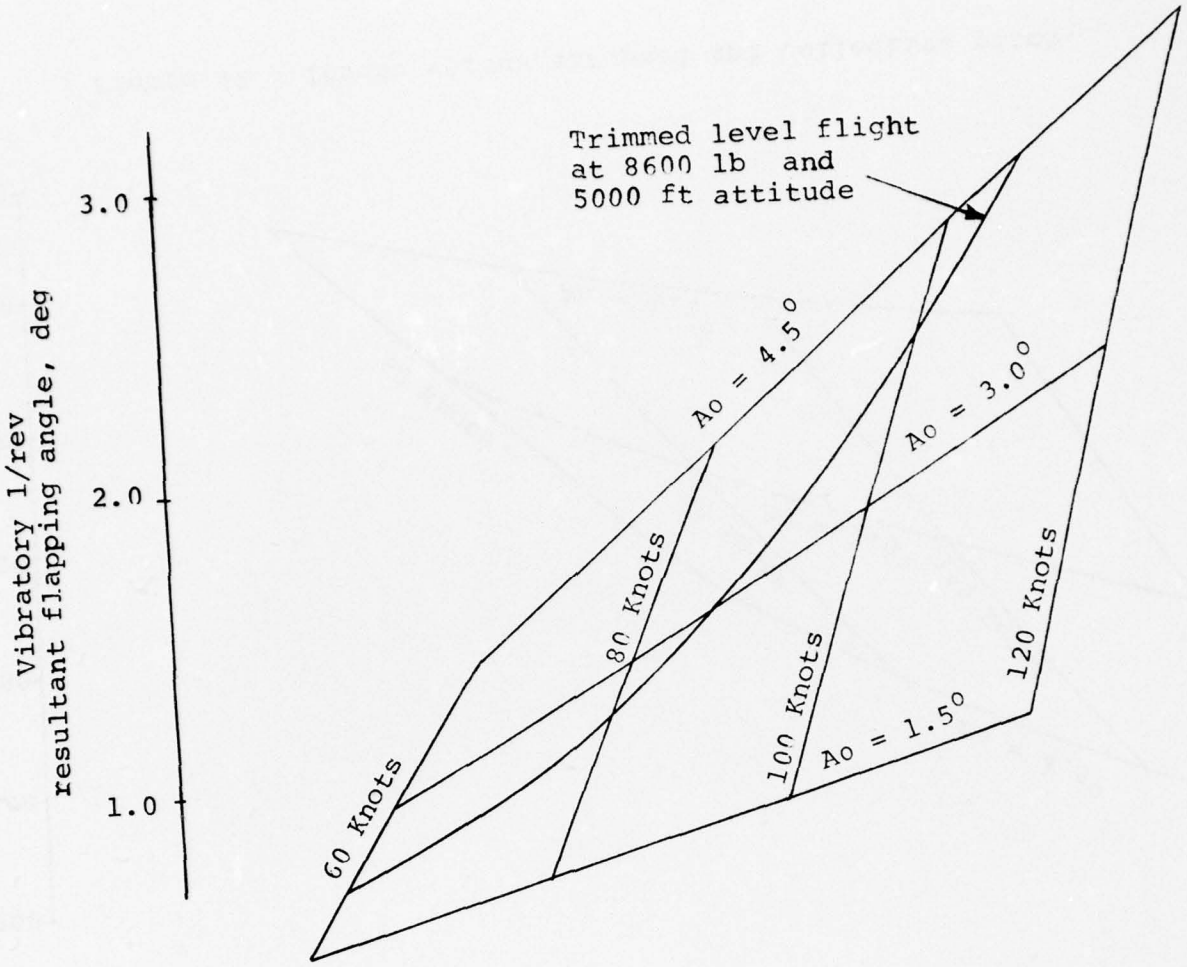

Figure 43. Flapping angle versus airspeed and collective pitch.

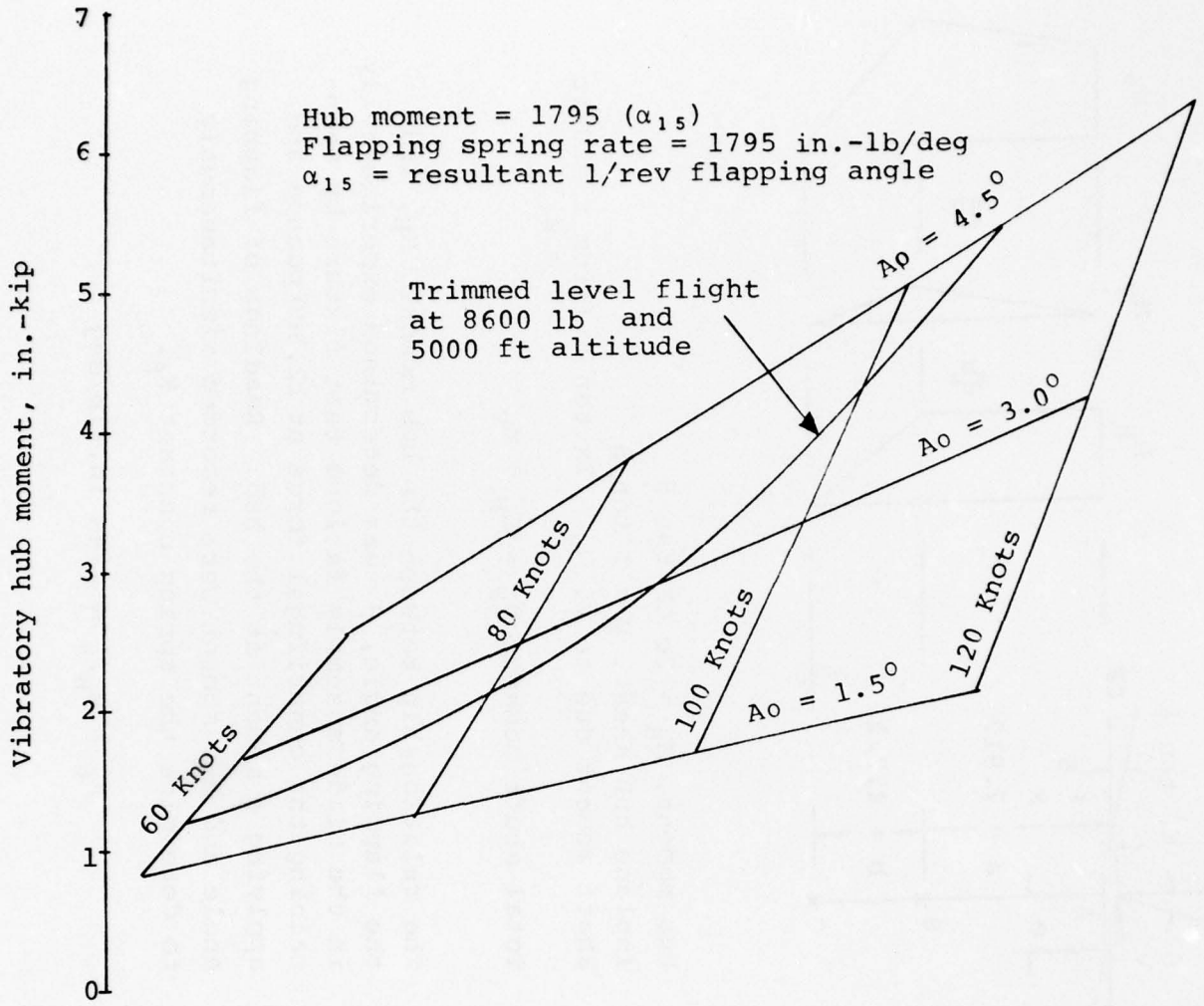

Figure 44. Hub moment versus airspeed and collective pitch.

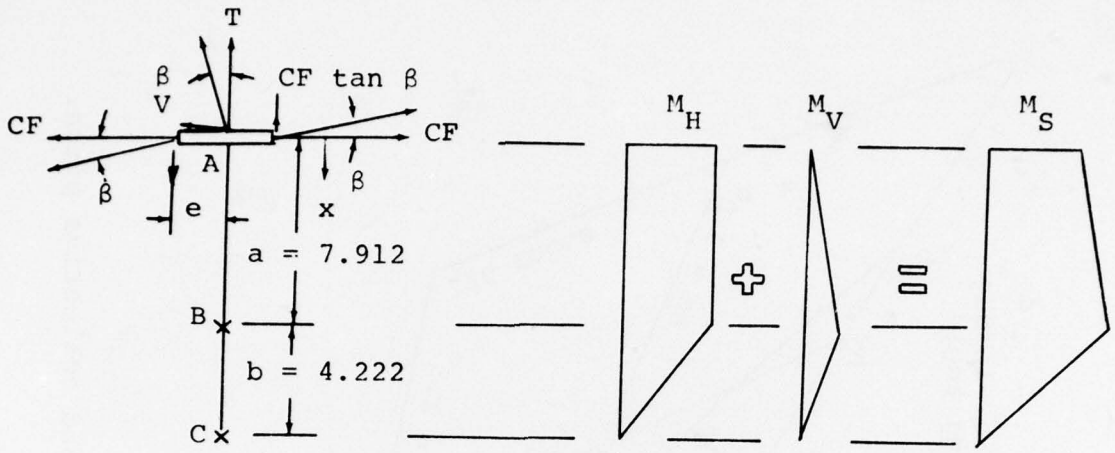

Hub moment, $M_H = 2e\ CF \tan \beta$

Inplane hub shear, $V = T \tan \beta$

Shaft moment due to V, $M_V = Tx \tan \beta$ (from $x = 0$ to $x = a$)

Total shaft moment, $M_S = M_H + M_V$

The relationship between the hub moment, M_H, and the flapping angle, β, was determined experimentally in the blade assembly fatigue test fixture by maintaining the centrifugal force at 12,500 pounds and applying a moment at the hub. Readings of flapping angle and hub moment were recorded simultaneously to determine the spring constant K_β.

$$K_\beta = M_H/\beta = 1795 \text{ in.-lb/deg}$$

Analysis of the stress concentration factors and applied bending moment at Point A (spline fillet radius) and Point B (thread fillet radius at outboard bearing) indicated that Point A would be critical for vibratory shaft bending moments resulting from the nonteetering EPBTR.

A summary of the blade pitch angle, rotor thrust, flapping angle, inplane shear, moment due to the inplane shear, hub moment, and shaft moment and stresses for various airspeeds is shown in Table 8.

TABLE 8. VIBRATORY TAIL ROTOR SHAFT BENDING MOMENTS AND STRESSES VERSUS AIRSPEED AT POINTS A AND B

Airspeed (Knots)	Pitch Angle Ao (Deg)	Thrust T (Lb)	β (Deg)	V (Lb)	a (In.)	M_V at Pt B (In.-Lb)	M_{S_A} (In.-Lb)	M_{S_B} (In.-Lb)	f_a (psi)	f_b (psi)
60	2.1	190	.68	2.26	7.912	18	1200	1218	8670	3993
70	2.4	260	.96	4.37	7.912	35	1700	1735	12,283	5688
80	2.6	315	1.22	6.71	7.912	53	2150	2203	15,535	7223
90	3.2	420	1.75	12.83	7.912	102	3150	3252	22,760	10,667
100	3.9	545	2.47	23.51	7.912	186	4400	4586	31,792	15,069
110	5.0	725	3.52	44.60	7.912	353	6350	6703	45,881	21,977

NOTE: M_{S_A} = Vibratory Shaft Bending Moment at Point A.

M_{S_B} = Vibratory Shaft Bending Moment at Point B.

f_a = Vibratory Stress at Point A.

f_b = Vibratory Stress at Point B.

Vibratory stresses, bending moments, and the corresponding airspeeds at which these stresses and moments are sensed by the UH-1 tail rotor shaft, are compared to the S-N curve developed for the UH-1 tail rotor shaft in Reference 4. The results of this comparison are shown in Figure 45. Also included in Figure 45 are the fatigue test results obtained for tail rotor shafts having nonteetering EPBTR's installed. It was concluded that no fatigue damage would be accumulated by the tail rotor shaft if the level flight airspeed was limited to 90 knots, as at 90 knots, the vibratory bending stress acting on the tail rotor shaft would be 22,760 psi - slightly below the 22,900 psi endurance limit for the shaft.

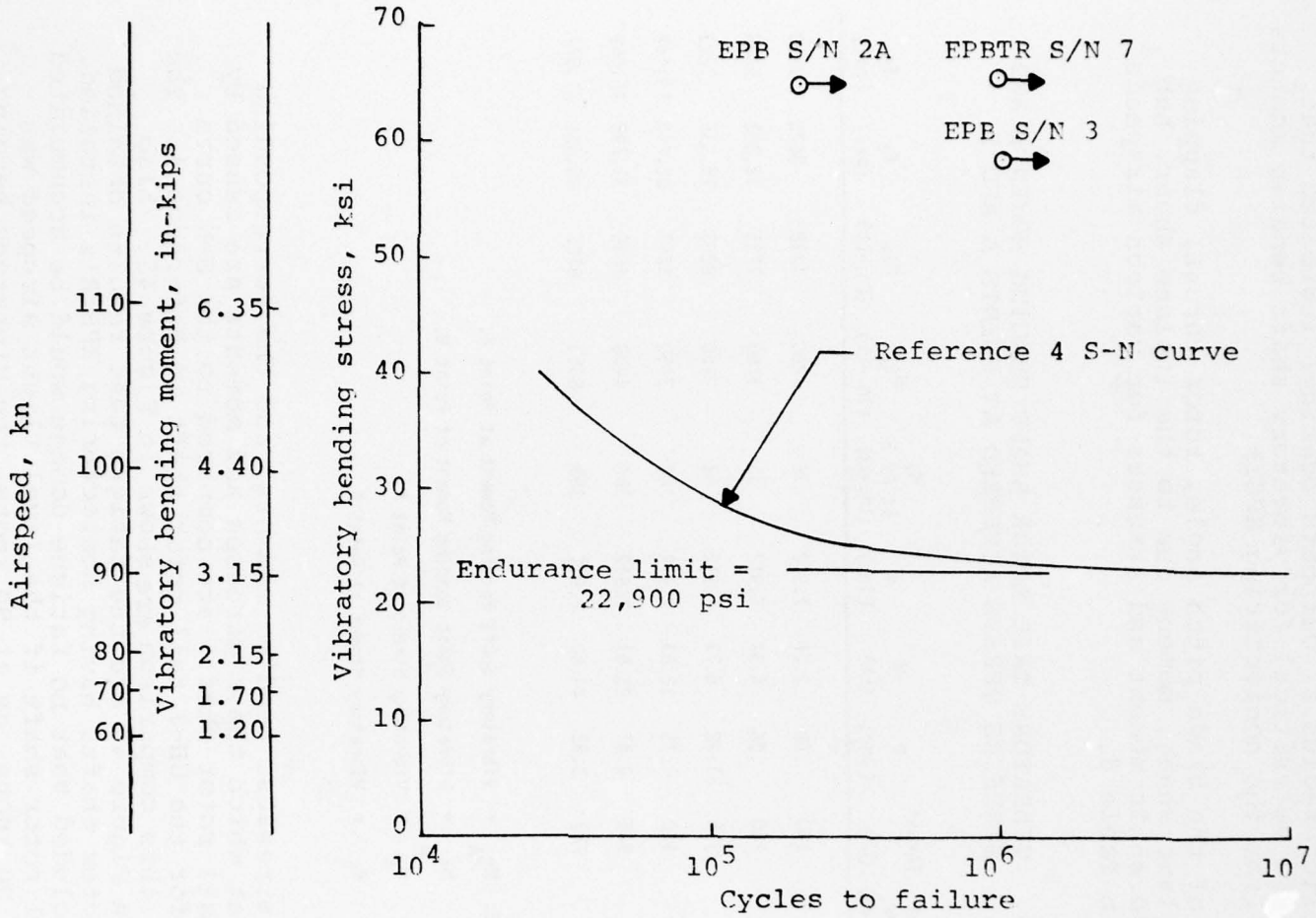

Figure 45. Airspeed, bending moment and stress versus cycles to failure for UH-1 tail rotor shafts having nonteetering elastic pitch beam tail rotors installed.

Elastic Pitch Beam at Station 3

Vibratory bending moments (M_x) acting on the elastic pitch beam at Station 3 resulting from locking out the teeter freedom of the elastic pitch beam tail rotor may be estimated with the aid of Figure 46 and the hub moments previously determined and reported in Table 8.

From Figure 46 the hub moment M_H can be expressed as:

$$M_H = 2\,Ve + 2M_x$$

$$\text{as } V = CF \text{ Tan } \beta$$

$$M_H = 2e\,CF \text{ Tan } \beta + 2M_x$$

$$\text{or } M_x = \frac{M_H - 2e\,CF \text{ Tan } \beta}{2}$$

$$\text{as } CF = 12{,}500 \text{ lb and } e = 3.0$$

$$M_x = \frac{M_H}{2} - 37{,}500 \text{ Tan } \beta$$

Also from Figure 46, the vibratory out-of-plane stresses acting at Station 3 can be determined from

$$f_{bx} = \frac{M_x\, c_y}{I_{xx}}$$

where f_{bx} = vibratory out-of-plane stress, psi

M_x = vibratory out-of-plane bending moments, in.-lb

c_y = y-distance to outer fiber, in.

I_{xx} = moment of intertia, about x-axis, $in.^4$

$$f_{bx} = \frac{M_x\,(.300)}{2(.380)(.600)^3/12}$$

$$f_{bx} = 21.930\, M_x$$

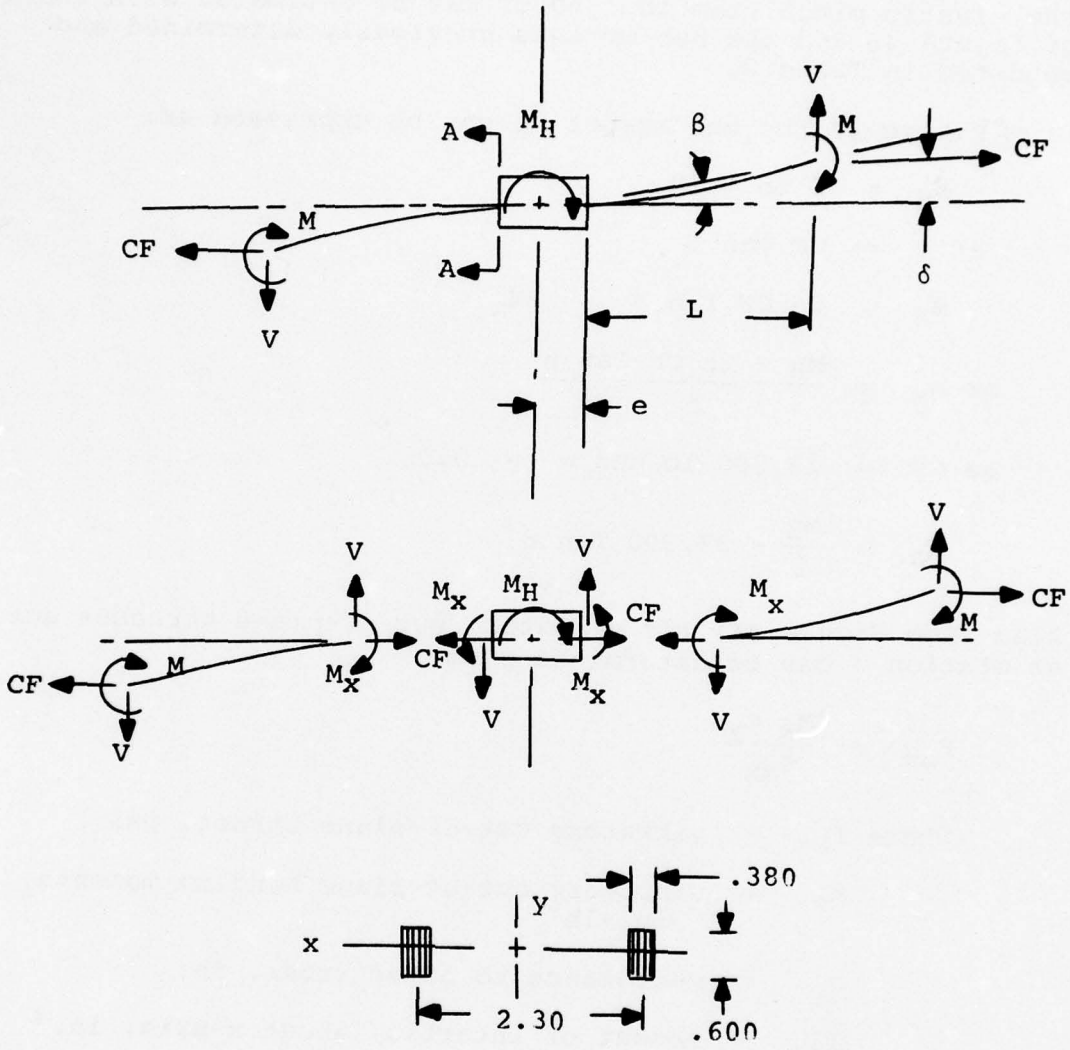

Section A-A

Figure 46. Out-of-plane loads and reactions on elastic pitch beam.

Values of f_{bx} are presented in Table 9 as a function of airspeed, flapping angle, and hub moment.

TABLE 9. VIBRATORY OUT-OF-PLANE BENDING MOMENTS AND STRESSES AT STATION 3 AS A FUNCTION OF AIRSPEED, FLAPPING ANGLE, AND HUB MOMENT

Airspeed (kn)	β (deg)	M_H (in.-lb)	M_x (in.-lb)	f_{bx} (psi)
60	.68	1,200	155	3,399
70	.96	1,700	222	4,868
80	1.22	2,150	276	6,053
90	1.75	3,150	430	9,430
100	2.47	4,400	582	12,763
110	3.52	6,350	868	19,035

The S/N curve for Station 3 of the elastic pitch beam, established from the results of fatigue testing previously reported in the structural test portion of this report, is shown in Figure 47. Stresses acting on the EPB at this location due to the nonteetering EPBTR are plotted in terms of airspeed so that the criticality of the EPB may be determined. As shown, the stress levels at all forward flight airspeeds are well below the estimated endurance limit of the EPB at this location. It was therefore concluded that the UH-1 tail rotor shaft was considerably more critical than the elastic pitch beam and that the shaft should be monitored continually during the flight test program.

ENGINEERING FLIGHT EVALUATION

The flight evaluation of the nonteetering elastic pitch beam tail rotor was conducted on an Army UH-1H helicopter, serial number 68-16401. Airborne instrumentation, having a telemetry capability, was provided to monitor and record parameters in both the rotating and fixed systems.

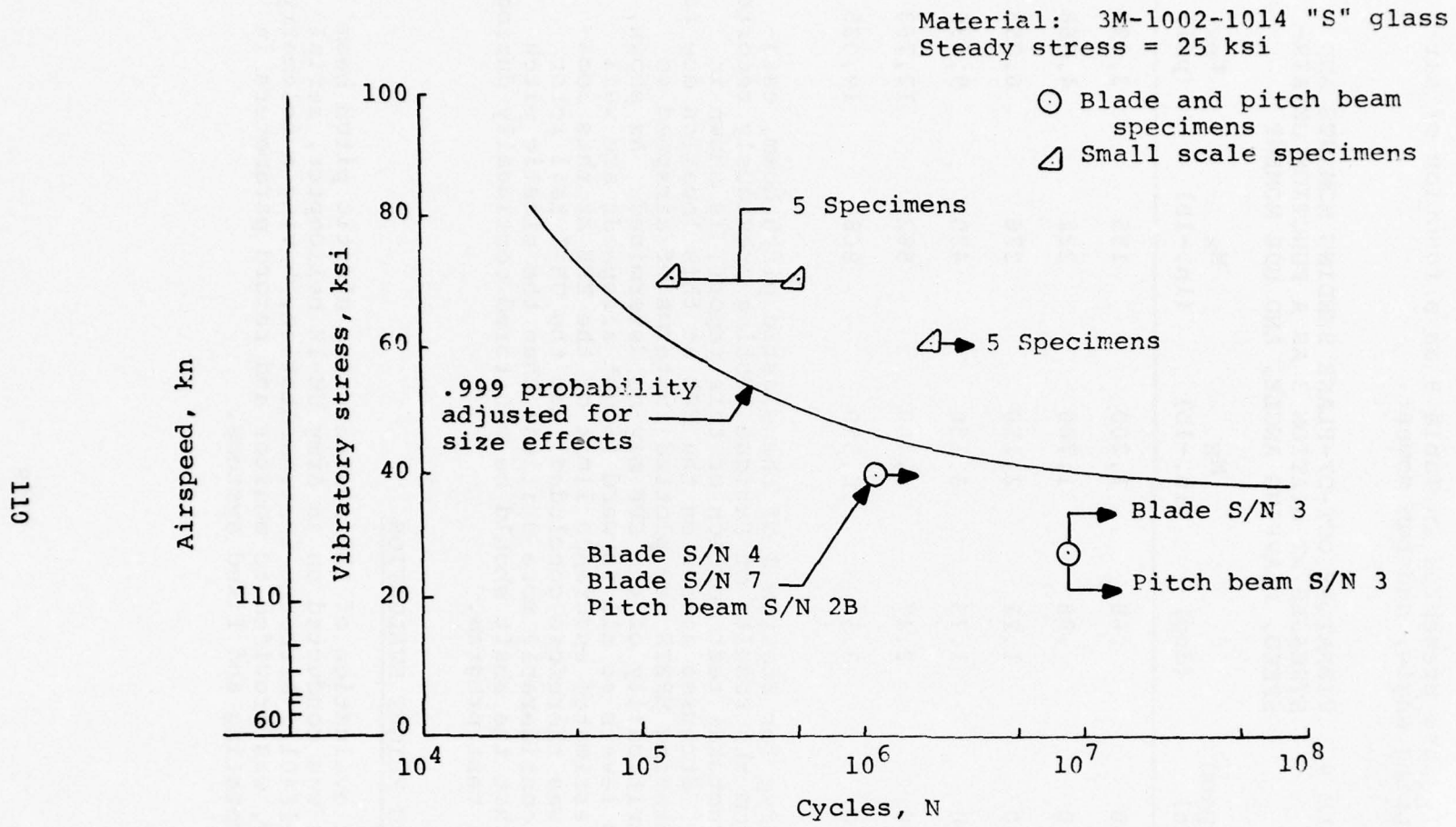

Figure 47. S-N curve for root end of UH-1 elastic pitch beam, station 3.0.

Parameters monitored during this development program, shown in Table 10, were common for both the standard and elastic pitch beam tail rotor configurations with the exception of tail rotor blade bending for the standard UH-1H blade, which was not instrumented. As the number of available slip ring channels for measuring strain gage data on the rotating components were limited, three different instrumentation hook-ups (A, B and C) were required to record all of the parameters.

Strain gage locations on the 90° tail rotor gearbox are shown in Figure 48.

All parameters discussed above were wired to B&F Instruments Model 24-200 balance boxes using Trygon PS312-900F bridge power supplies. The balance boxes, utilized as signal conditioning units, had their outputs wired to a PCM (Pulse Code Modulation) encoder. PCM data signal was transmitted from the aircraft to the telemetry ground station via an "L" band telemetry link.

Test conditions flown during this evaluation are presented in Table 11 and were within the envelope contained in the operator's manual for the UH-1H helicopter. Prior to flying the elastic pitch beam tail rotor, base line data was obtained with the standard UH-1H tail rotor for all the conditions shown in Table 11. This data was used for the detailed planning, monitoring, and evaluation and subsequent elastic pitch beam tail rotor flight tests.

Flight testing with the elastic pitch beam tail rotor configuration involved a gradual buildup to the airspeeds and maneuvers shown in Table 11. The initial phases examined in detail the ground and hovering flight regimes with emphasis on the response characteristics, correlation of measured loads and strains with previous data and predicted tests where applicable to assure adequate directional control margins. Subsequent flights expanded the test envelope to include sideward and rearward flights of 10, 20, and 30 knots as well as forward flight up to 70 knots. These were followed by examination of climbs, descents, autorotations, further expansion of the level flight envelope, and examination of the remaining prescribed maneuvers and conditions. During the expansion of the level flight envelope, airspeeds briefly approached the 120-knot UH-1H airspeed restriction to better define the flight envelope for future flights with the nonteetering EPBTR, and to verify analytical predictions of the airspeed/tail rotor shaft bending moment relationship.

TABLE 10. FLIGHT TEST INSTRUMENTATION

	Instrumentation Hook-Up		
	A	B	C
1. Main rotor RPM	X	X	X
2. Tail rotor RPM		X	X
3. Tail rotor blade sta 18 edgewise bending		X	
4. Tail rotor blade sta 18 flatwise bending		X	
5. Tail rotor blade sta 23 edgewise			X
6. Tail rotor blade sta 23 flatwise			X
7. Tail rotor shaft spanwise bending	X	X	X
8. Tail rotor shaft chordwise bending	X	X	X
9. Tail rotor shaft torque	X	X	X
10. Tail rotor blade pitch angle	X	X	X
11. Tail rotor thrust	X	X	X
12. Tail pylon vertical acceleration	X	X	X
13. Tail pylon lateral acceleration	X	X	X
14. Tail pylon longitudinal acceleration	X	X	X
15. Pilots area vertical acceleration	X	X	X
16. Pilots area lateral acceleration	X	X	X
17. Pilots area longitudinal acceleration	X	X	X
18. Tail rotor gearbox (90°) Strain 1	X	X	X
19. Tail rotor gearbox (90°) Strain 2	X	X	X
20. Tail rotor gearbox (90°) Strain 3	X	X	X
21. Tail rotor gearbox (90°) Strain 4	X	X	X
22. Tail rotor gearbox (90°) Strain 5	X	X	X
23. Tail rotor gearbox (90°) Strain 6	X	X	X
24. Tail rotor gearbox (90°) Strain 7	X	X	X
25. Tail rotor gearbox (90°) Strain 8	X	X	X
26. Tail rotor gearbox (90°) Strain 9	X	X	X
27. Tail rotor gearbox (90°) Strain 10	X	X	X
28. Tail rotor gearbox (90°) Strain 11	X	X	X
29. Longitudinal cyclic position	X	X	X
30. Lateral cyclic position	X	X	X
31. Collective position	X	X	X
32. Directional control position	X	X	X
33. Yaw rate gyro	X	X	X
34. Heading gyro	X	X	X
35. Sideslip angle	X	X	X
36. Bank angle	X	X	X
37. Airspeed	X	X	X
38. Engine torque pressure	X	X	X

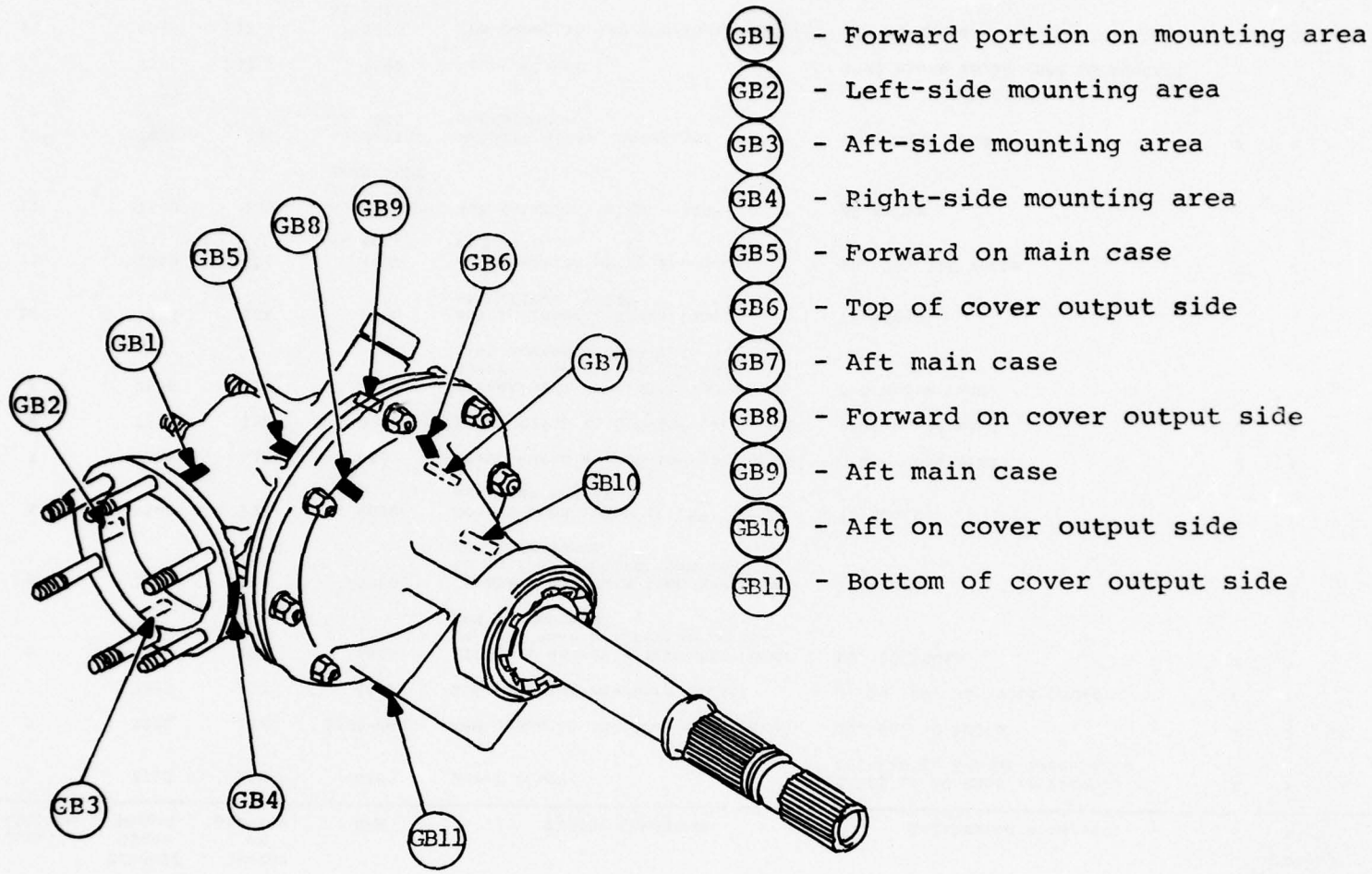

Figure 48. 90° tail rotor gearbox strain gage locations.

TABLE 11. TEST CONDITIONS FOR CONVENTIONAL UH-1H AND EPB TAIL ROTOR

Test Condition	Takeoff Gross Weight	Center of Gravity	RPM	Flight Condition	Calibrated Airspeed	Instrumentation Hook-Up A	B	C
1	7500	138	6600	Level flight	0-100 in 10 knot increments 100-120 in 5 knot increments	X	X	X
2	7500	138	6000-6600	RPM sweep in 100 RPM increments	30, 80, 90 knots	X	X	X
3	7500	138	6600	Sideward and rearward flight	0, 10, 20, 30 knots paced	X	X	
4	7500	138	6600	Climbs & descents from mas power to full down collective in 500 FPM increments	60, 70 knots	X	X	
5	7500	138	6000	Climbs & descents from max power to full down collective in 500 FPM increments	70 knots	X	X	
6	7500	138	6600	Coordinated turns at 15°, 30°, 40° bank angles	70 knots	X	X	
7	7500	138	6600	Hover turns at 30°-40° per second	0-10 knots wind	X	X	
8	7500	138	6000	Hover turns at 30°-40° per second	0-10 knots wind	X	X	
9	7500	138	6600	Directional control response in hover - rapid one-inch step displacements from trim	0-5 knots wind			
10	7500	138	6600	Static lateral directional stability: ± 30°	70 knots			
11	7500	138	6600 at entry	Autorotation entry and power recovery	60, 90, 110 knots	X	X	
12	7500	138	As set approx 310 rotor RPM	Autorotation turns - 360°	60 knots			
13	7400 & 8600	138	6000, 6300 & 6600	Nondimensional hovering performance	0-5 knots wind	X	X	X
14	8550	132.4	6600	Level Flight	0-90 knots in 10 knot increments		X	X
15	8550	132.4	6600 at entry	RPM sweep in 100 RPM increments	30, 80 knots		X	X

Most flights were conducted at one gross weight and center of gravity at varied rotor speeds. One flight was conducted with a slightly lower gross weight and aft center of gravity when the aircraft was flown without a copilot. Three flights were made with a forward center of gravity and higher gross weight to evaluate the apparent reduction in parameter levels at these conditions and to obtain additional hover data at a higher gross weight.

A summary of all flights including the pertinent details for both the standard and elastic pitch beam tail rotor configurations is presented in Table 12. Selected test results for parameters that are of particular concern are presented in Figures 49 through 56. With the exception of tail rotor blade bending moments, flight data recorded with the EPBTR installed is compared to flight data recorded with the standard UH-1 tail rotor installed. The principal cause of differences noted between these two rotor systems is associated with the degree of freedom permitted between the rotor blades and the rotor shaft. In general, bending moments and strains are significantly higher for the nonteetering EPBTR than they are for the teetering standard tail rotor, particularly at the higher airspeeds, and indicate the need for a redesign to reduce these levels to acceptable values.

Figure 49 presents the relationship between rudder pedal position and airspeed for both the EPBTR and the standard rotor. The difference between these two sets of data is attributed to the difference in pitch control sensitivity, with the EPBTR being somewhat more sensitive than the standard rotor due to a longer EPBTR pitch arm.

Figure 50 shows vibratory tail rotor shaft bending moments obtained in both the spanwise and chordwise planes during level flight airspeed sweeps up to 117 knots. Maximum vibratory bending moments recorded at 117 knots with the nonteetering EPBTR installed were approximately ±3500 and ±1500 inch-pounds for the spanwise and chordwise planes, respectively. These values are considerably higher than those obtained at a comparable airspeed with the teetering standard tail rotor installed and are the result of hub moments induced on the shaft by locking out the teeter freedom of the EPBTR. As the 3150 inch-pounds endurance limit for the shaft was exceeded, some fatigue damage had been accumulated by the shaft during the airspeed sweep. For the purpose of determining the amount of fatigue damage incurred, it was conservatively assumed that the vibratory spanwise and chordwise bending moments acting on the shaft were in phase and a cycle-count was made for all resultant bending moments that exceeded the 3150 inch-pounds endurance limit. The cumulative fatigue damage accumulated by the tail

TABLE 12. UH-1H S/N 68-16401 - ELASTIC PITCH BEAM TAIL ROTOR DEVELOPMENT FLIGHT SUMMARY

Flt No.	Instrumentation* Hook-Up	T.O. G.W.	T.O. Longitudinal C.G.	T.O. Lateral C.G.	Type of Flt	Config	Deck Temp	Pressure Altitude on Deck (29:92 In. H_G)	Flt Time
01	A	7500	138.6	-0.3	Instrumentation/ Check Flt	Std	--	--	1.3 hr
02	A	7569	138.6	-0.3	Data A/S and RPM	Std	+8°C	-200	1.1 hr
03	A	7569	138.6	-0.3	A/S and RPM Climb/Descent	Std	+8°C	+430	1.2 hr
04	A	7569	138.6	-0.3	Coord Turns Autorotation	Std	+5°C	+430	0.7 hr
05	A	7569	138.6	-.03	Side Flt Hover Turns Static Lat/Dir Stab	Std	+1°C	+40	1.2 hr
06	A	7569	138.6	-0.3	Side/Rear Flt A/S and RPM Hov Perf	Std	--	--	1.6 hr
07	A	8569	132.4	-0.27	Hov Perf	Std	--	--	0.3 hr
08	B	7569	138.6	-0.3	Gnd Run	EPBTR	--	--	1.7 hr
09	B	7569	138.6	-.03	Gnd Run, Hover	EPBTR	--	--	0.4 hr
10	B	7569	138.6	+0.3	Gnd Run, Hover Turns	EPBTR	--	--	0.8 hr
11	B	7389	140.88	+0.22	Gnd Run, Hover Turns	EPBTR	-1°C	+50	1.3 hr
12	B	7569	138.6	-0.3	Hover Side Flt Rear Flt	EPBTR	-1°C	+930	0.3 hr
13	B	7569	138.6	-0.3	Paced Side and Rearward Flt	EPBTR	-3°C	-100	1.5 hr

*See Instrumentation Hook-Up in Table 10.

TABLE 12 - CONTINUED

Flt No.	Instrumentation* Hook-Up	T.O. G.W.	T.O. Longitudinal C.G.	T.O. Lateral C.G.	Type of Flt	Config	Deck Temp	Pressure Altitude on Deck (29:92 In. H_G)	Flt Time
14	B	7569	138.6	-013	Paced Side Flt Abort due to Wind	EPBTR	0°C	-100	0.6 hr
15	B	7569	138.6	-0.3	Fwd Flt Climbs/Descents Autorotation	EPBTR	+4°C	-200	1.0 hr
16	B	7569	138.6	-0.3	Fwd Flt	EPBTR	+10°C	-320	1.0 hr
17	B	7569	138.6	-0.3	Fwd Flt RPM Sweeps Static Lat Stab Climbs/Descents	EPBTR	+10°C	+40	1.0 hr
18	B	7569	138.6	-0.3	Autoro Turns Hover Turns Step Inputs	EPBTR	+5°C	+140	1.3
19	B	7569	138.6	-0.3	A/S Sweep Autorotation	EPBTR	+12°C	+60	0.8
20	B	7569	138.6	-0.3	Autorotation Pedal Inputs Hover Perf	EPBTR	+12°C	+100	0.6
21	B	8569	132.4	-0.27	Check Flt Hover Perf A/S and RPM	EPBTR	+17°C	-250	1.3
22	C	8569	132.4	-0.27	Hover Perf A/S and RPM	EPBTR	+14°C	+165	0.8
23	C	7569	138.6	-0.3	A/S and RPM	EPBTR	+15°C	+175	0.5

*See Instrumentation Hook-Up in Table 10.

SYMBOL	FLT No.	RPM	G.W.(lb)	C.G.
○	13	6600	7040	138
□	15	6600	7420	138
◇	16	6600	7450	138
△	17	6600	7450	138
⬡	18	6600	6980	138
⬠	19	6600	7415	138
○	22	6600	8345	132.4

——— Standard rotor, Flts 2-9

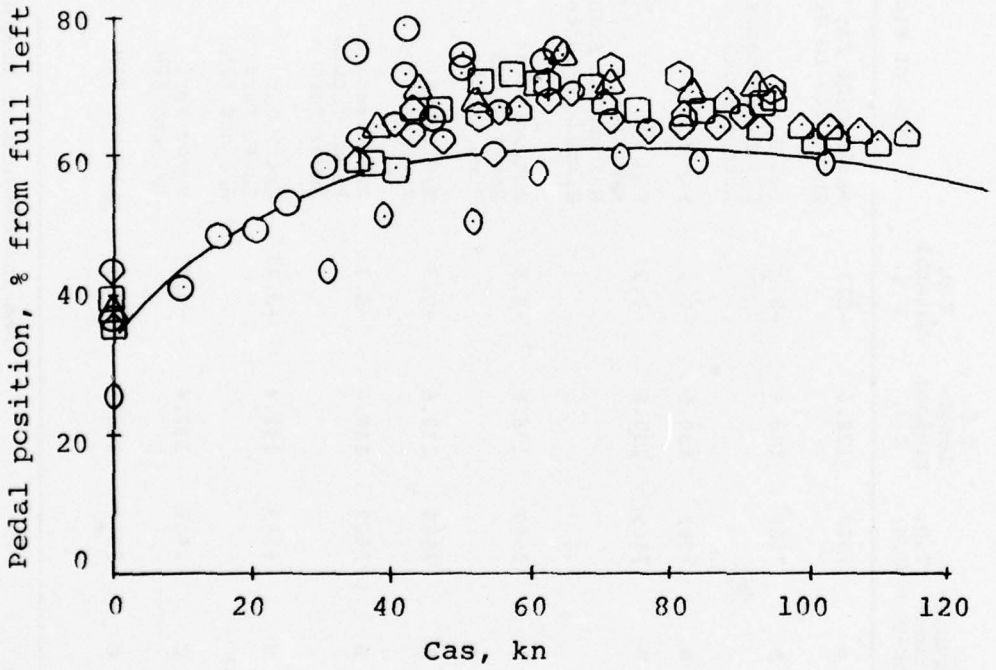

Figure 49. Pedal position versus airspeed.

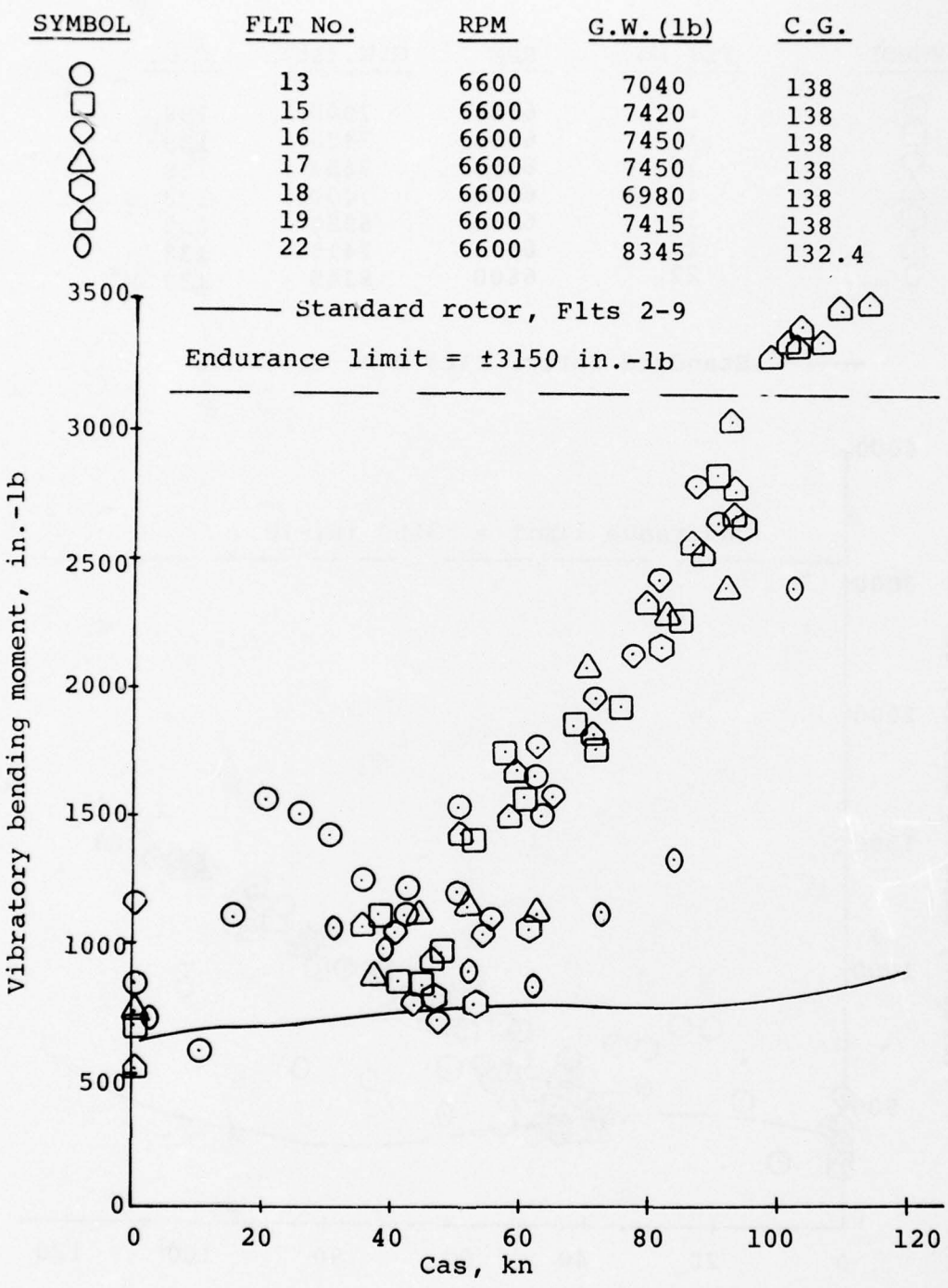

(a) Spanwise.

Figure 50. Vibratory tail rotor shaft bending moment versus airspeed.

SYMBOL	FLT No.	RPM	G.W.(lb)	C.G.
○	13	6600	7040	138
□	15	6600	7420	138
◇	16	6600	7450	138
△	17	6600	7450	138
⬡	18	6600	6980	138
⬠	19	6600	7415	138
○	22	6600	8345	132.4

——— Standard rotor, Flts 2-9

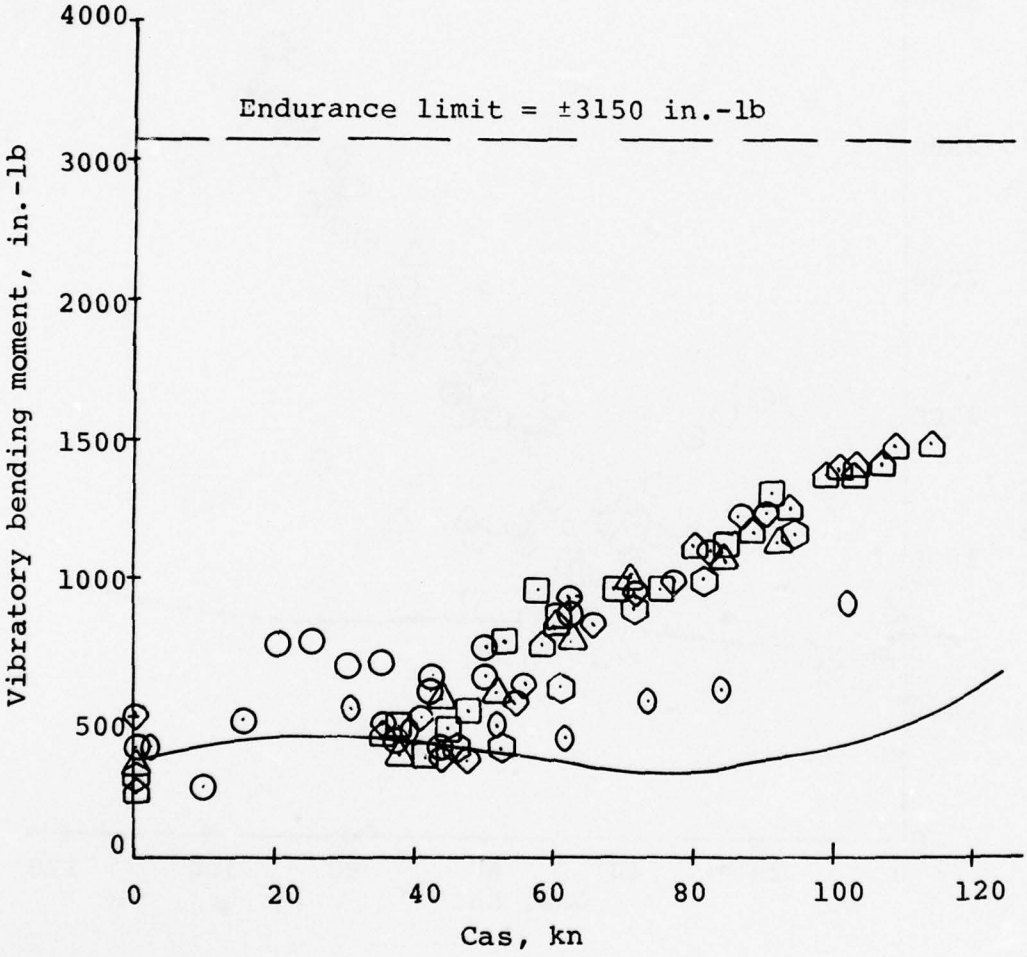

(b) Chordwise.

Figure 50. Continued.

SYMBOL	FLT No.	RPM	G.W. (lb)	C.G.
○	13	6600	7040	138
□	15	6600	7420	138
◇	16	6600	7450	138
△	17	6600	7450	138
⬡	18	6600	6980	138
⬠	19	6600	7415	138

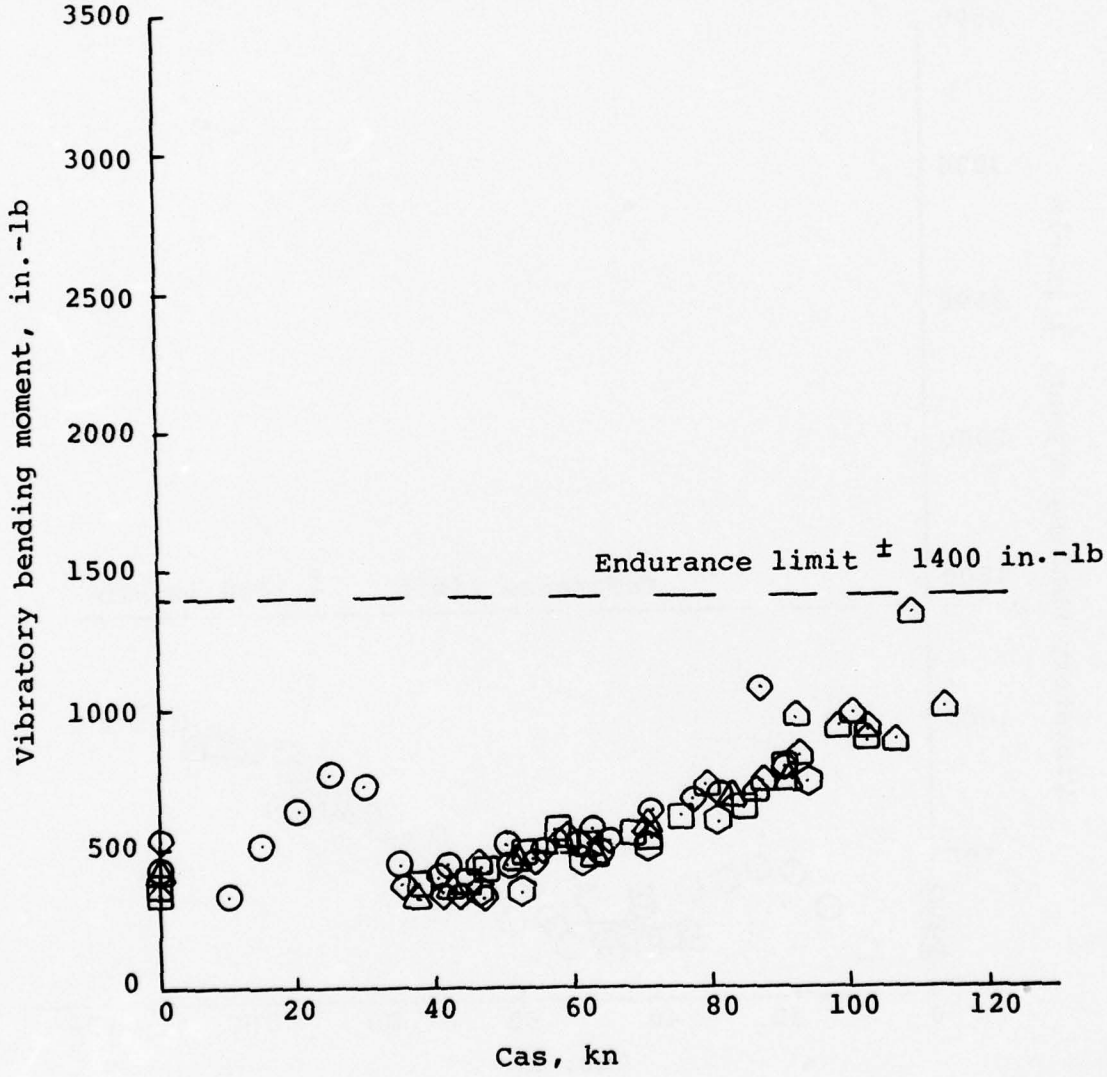

(a) Flatwise.

Figure 51. Vibratory bending moment at blade station 18 versus airspeed.

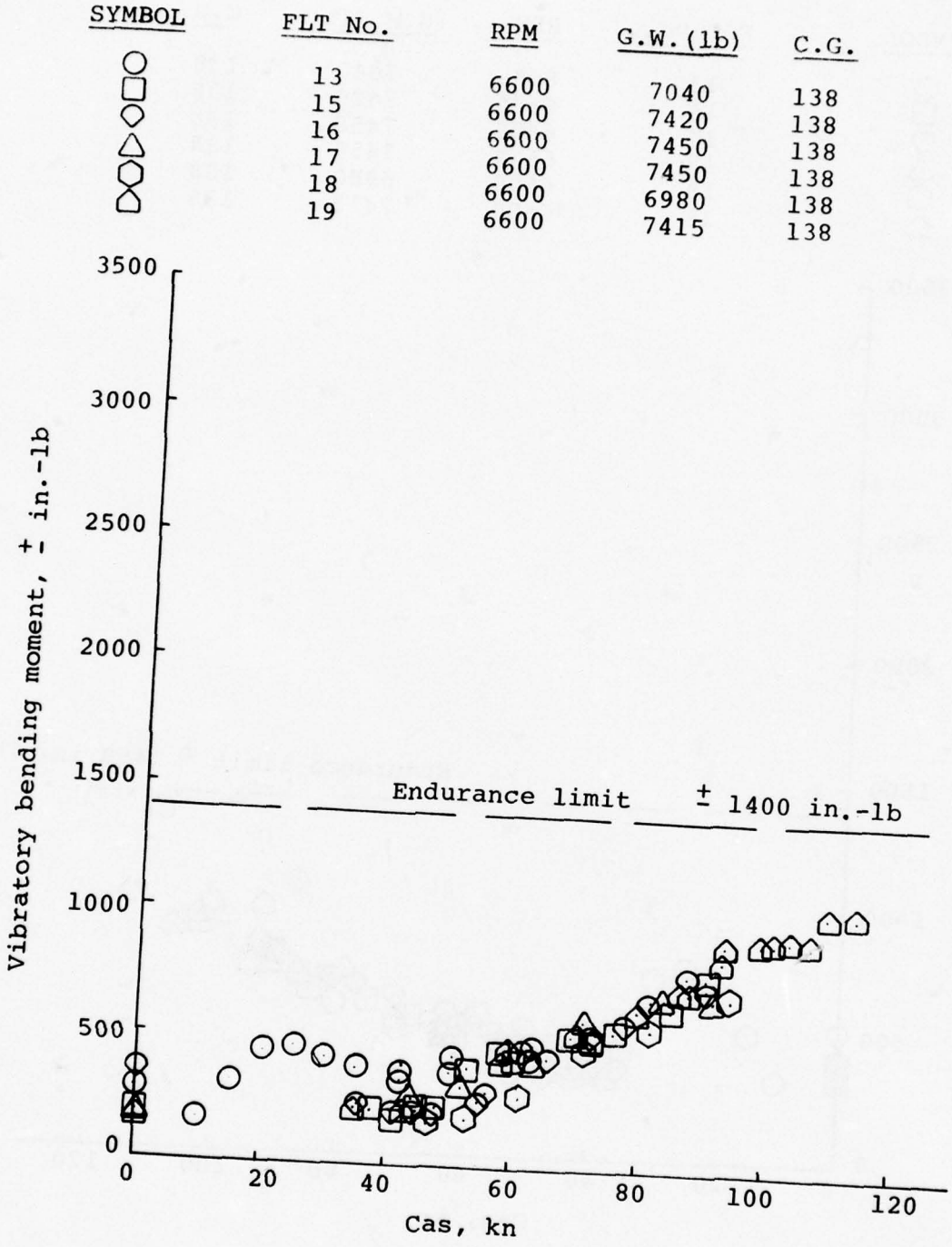

(b) Edgewise.

Figure 51. Continued.

SYMBOL	FLT No.	RPM	G.W.(lb)	C.G.
○	22	6600	8345	132.9
◇	23	6600	7560	138

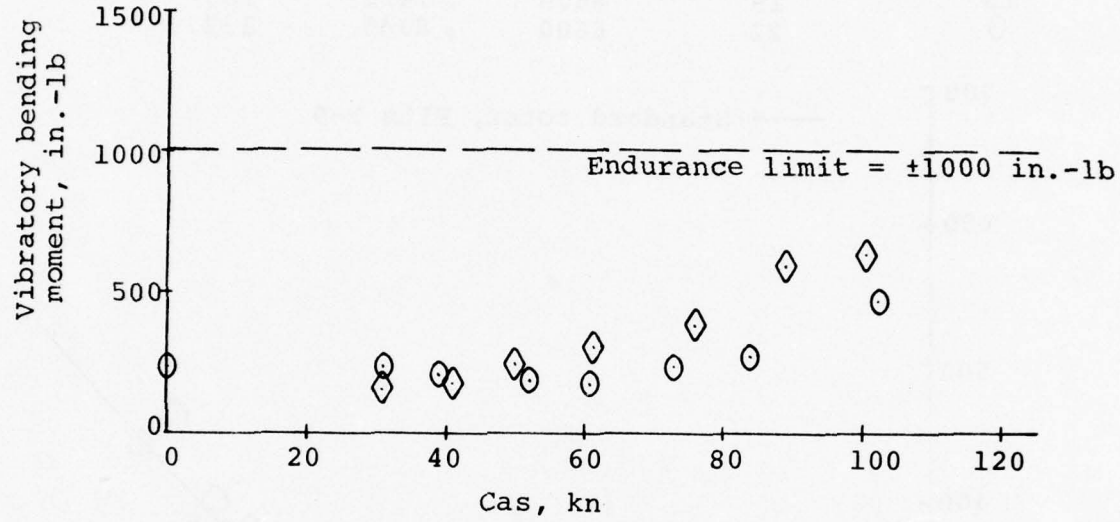

(a) Edgewise

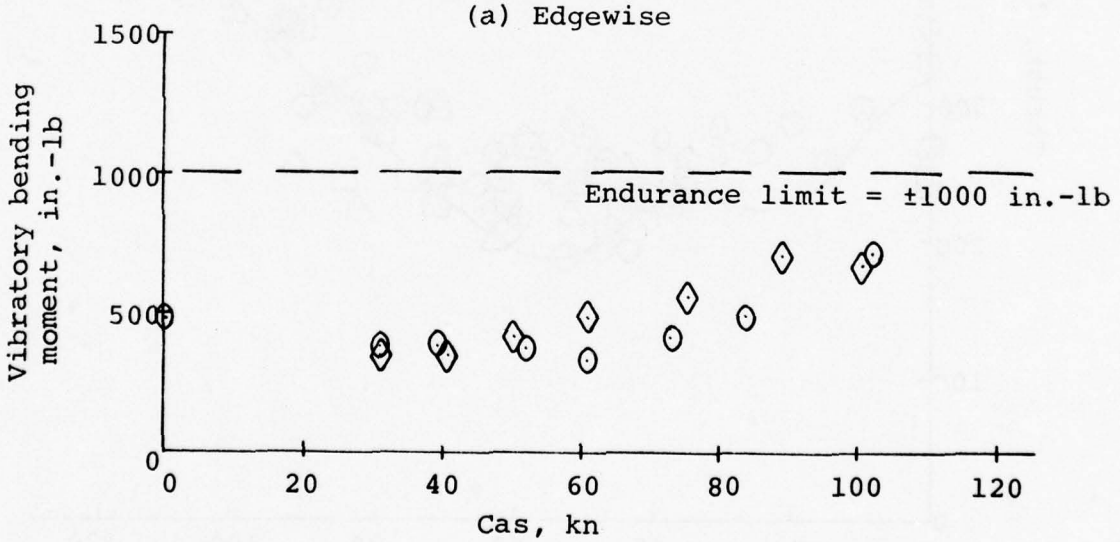

(b) Flatwise

Figure 52. Vibratory bending moment at blade station 23 versus airspeed.

SYMBOL	FLT No.	RPM	G.W. (lb)	C.G.
○	13	6600	7040	138
□	15	6600	7420	138
◇	16	6600	7450	138
△	17	6600	7450	138
⬡	18	6600	6980	138
⬠	19	6600	7415	138
◇	22	6600	8345	132.4

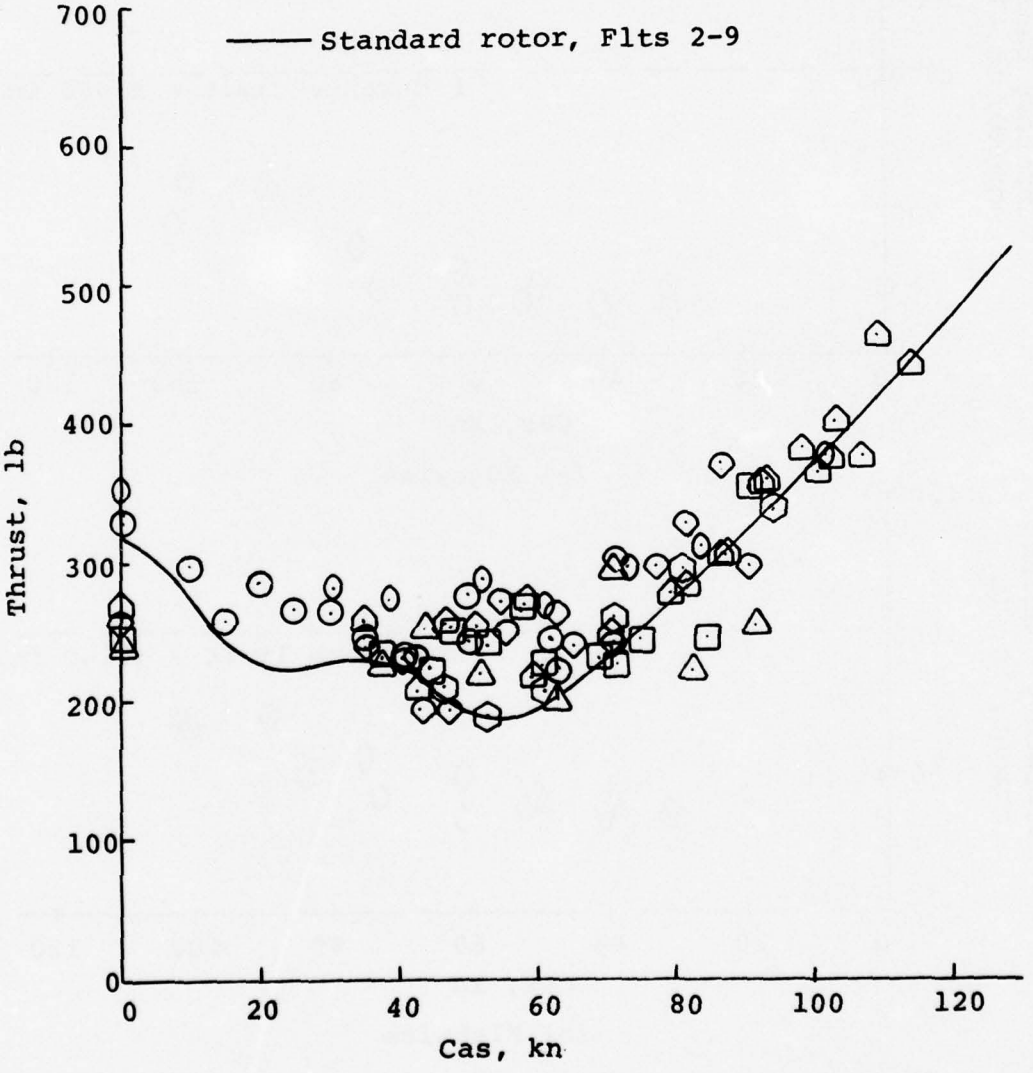

Figure 53. Tail rotor thrust versus airspeed.

SYMBOL	FLT No.	RPM	G.W. (lb)	C.G.
○	13	6600	7040	138
□	15	6600	7420	138
◇	16	6600	7450	138
△	17	6600	7450	138
⬡	18	6600	6980	138
⬠	19	6600	7415	138
○	22	6600	8345	132.4

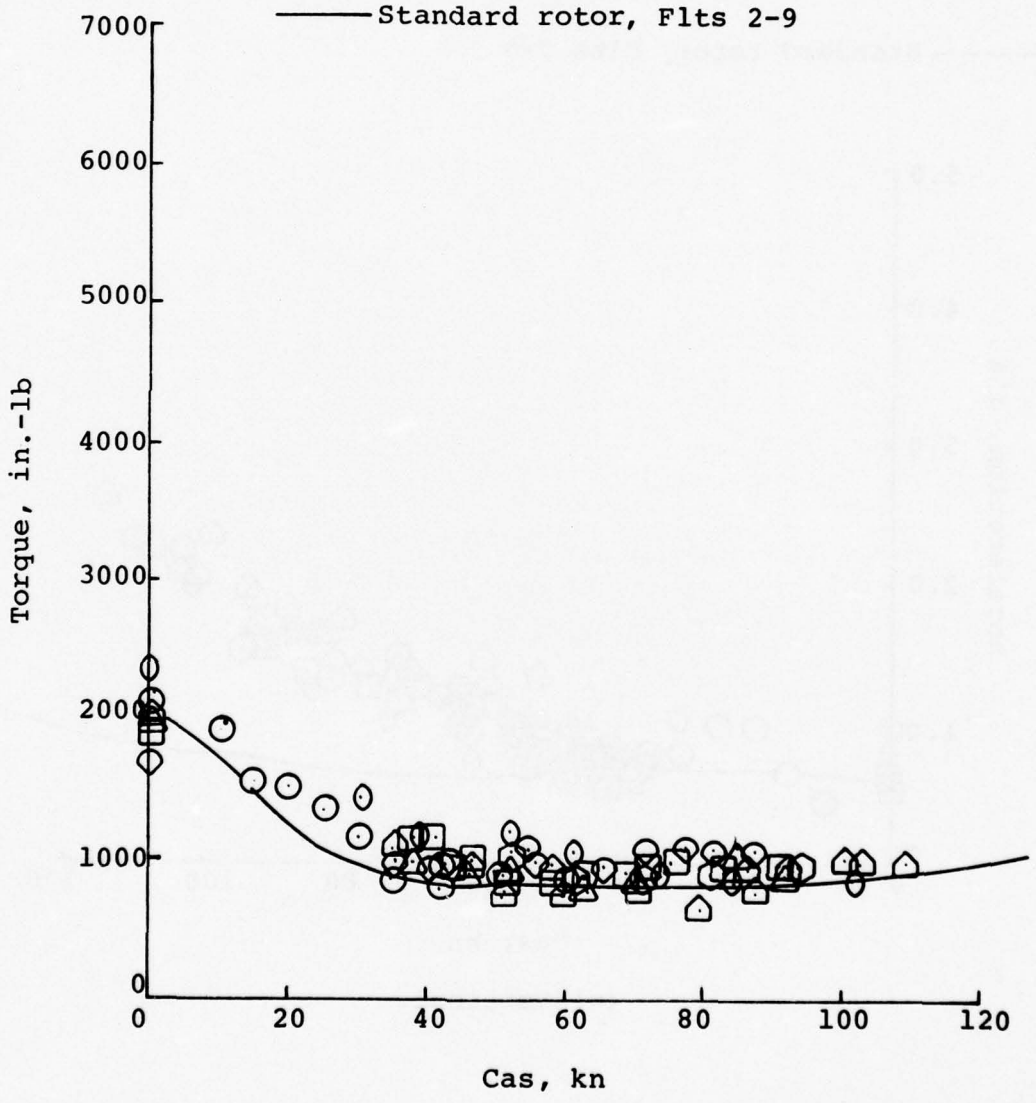

Figure 54. Tail rotor shaft torque versus airspeed.

SYMBOL	FLT No.	RPM	G.W.(lb)	C.G.
○	13	6600	7040	138
□	15	6600	7420	138
◇	16	6600	7450	138
△	17	6600	7450	138
⬡	18	6600	6980	138
▷	19	6600	7415	138
⬭	22	6600	8345	132.4

——— Standard rotor, Flts 2-9

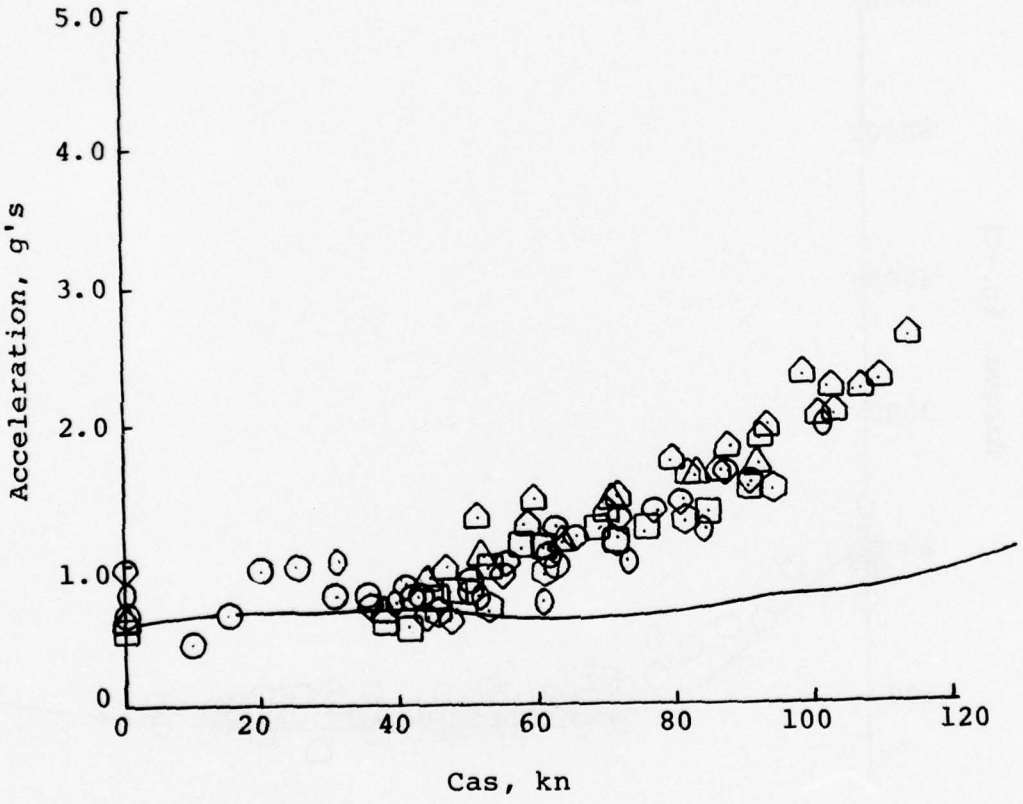

(a) Vertical.

Figure 55. Tail pylon accelerations versus airspeed.

SYMBOL	FLT No.	RPM	G.W. (lb)	C.G.
	13	6600	7040	138
	15	6600	7420	138
	16	6600	7450	138
	17	6600	7450	138
	18	6600	6980	138
	19	6600	7415	138
	22	6600	8345	132.4

——— Standard rotor, Flts 2-9

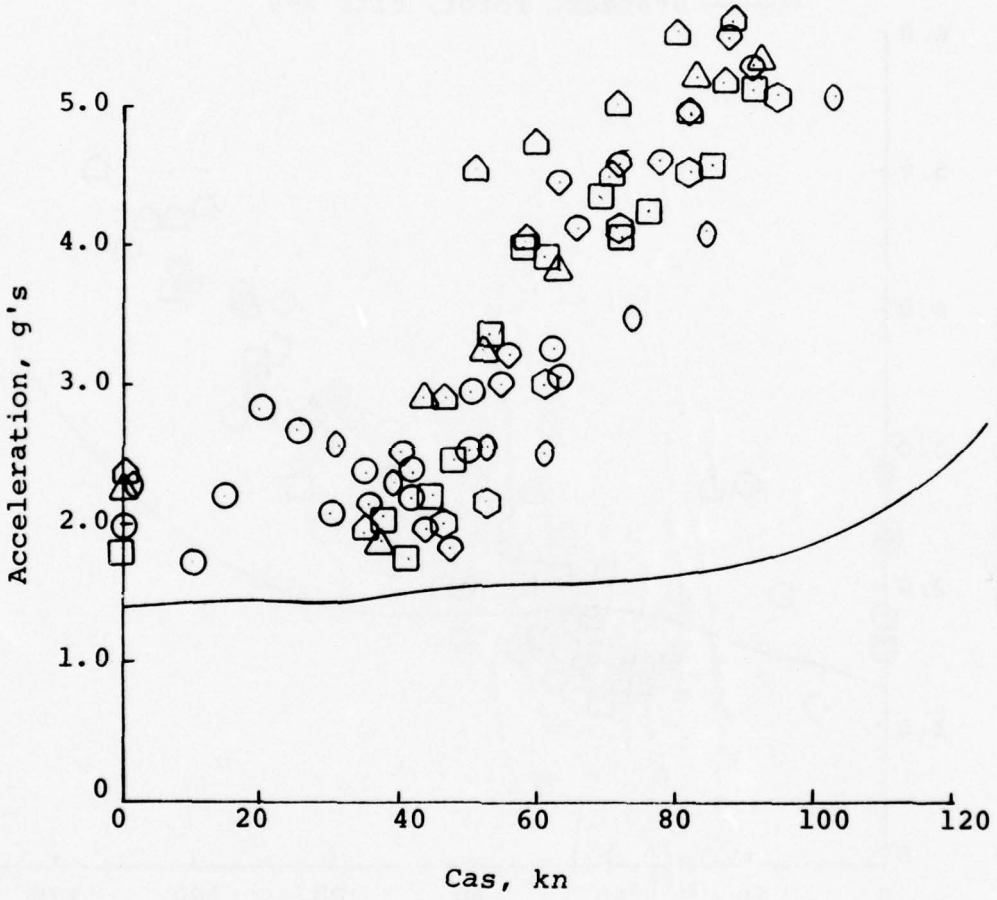

(b) Longitudinal.

Figure 55. Continued.

SYMBOL	FLT No.	RPM	G.W. (lb)	C.G.
○	13	6600	7040	138
□	15	6600	7420	138
◇	16	6600	7450	138
△	17	6600	7450	138
⬠	18	6600	6980	138
⬡	19	6600	7415	138
○	22	6600	8345	132.4

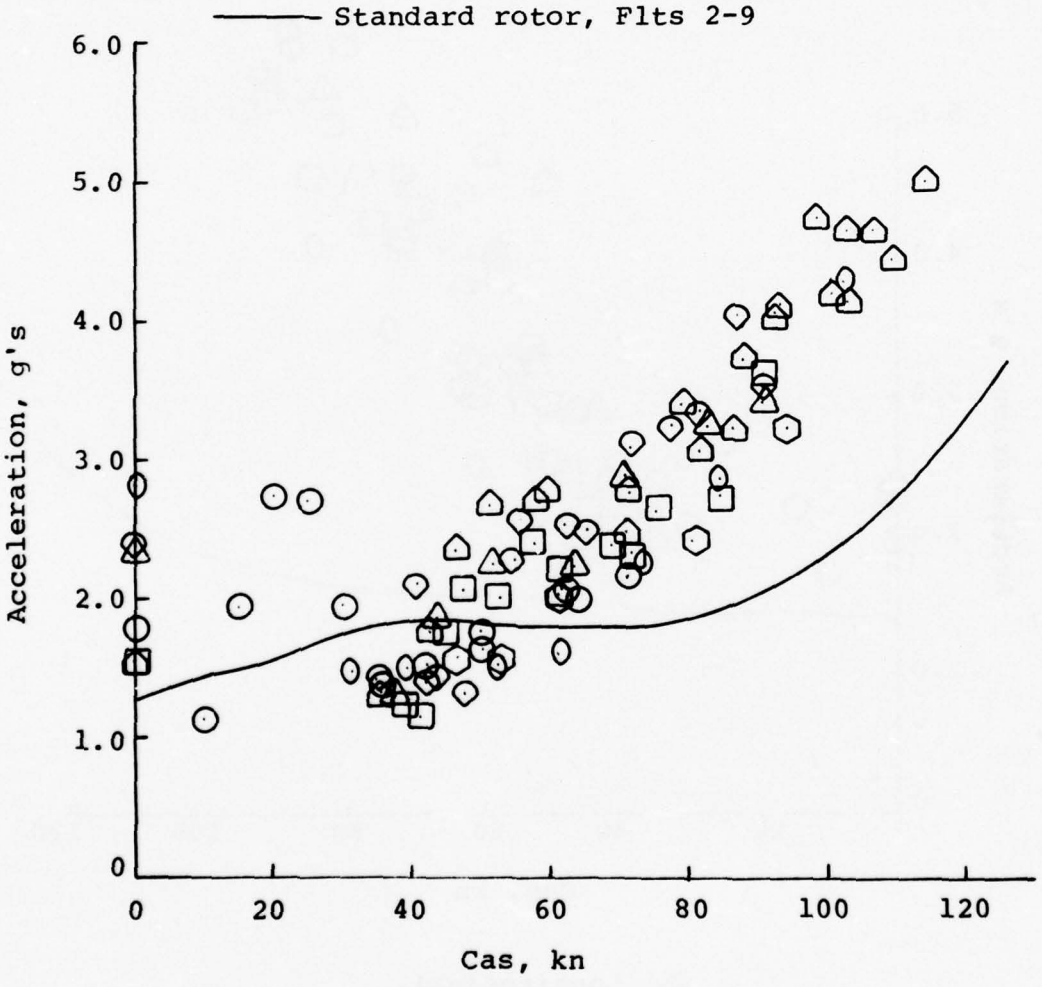

(c) Lateral.

Figure 55. Continued.

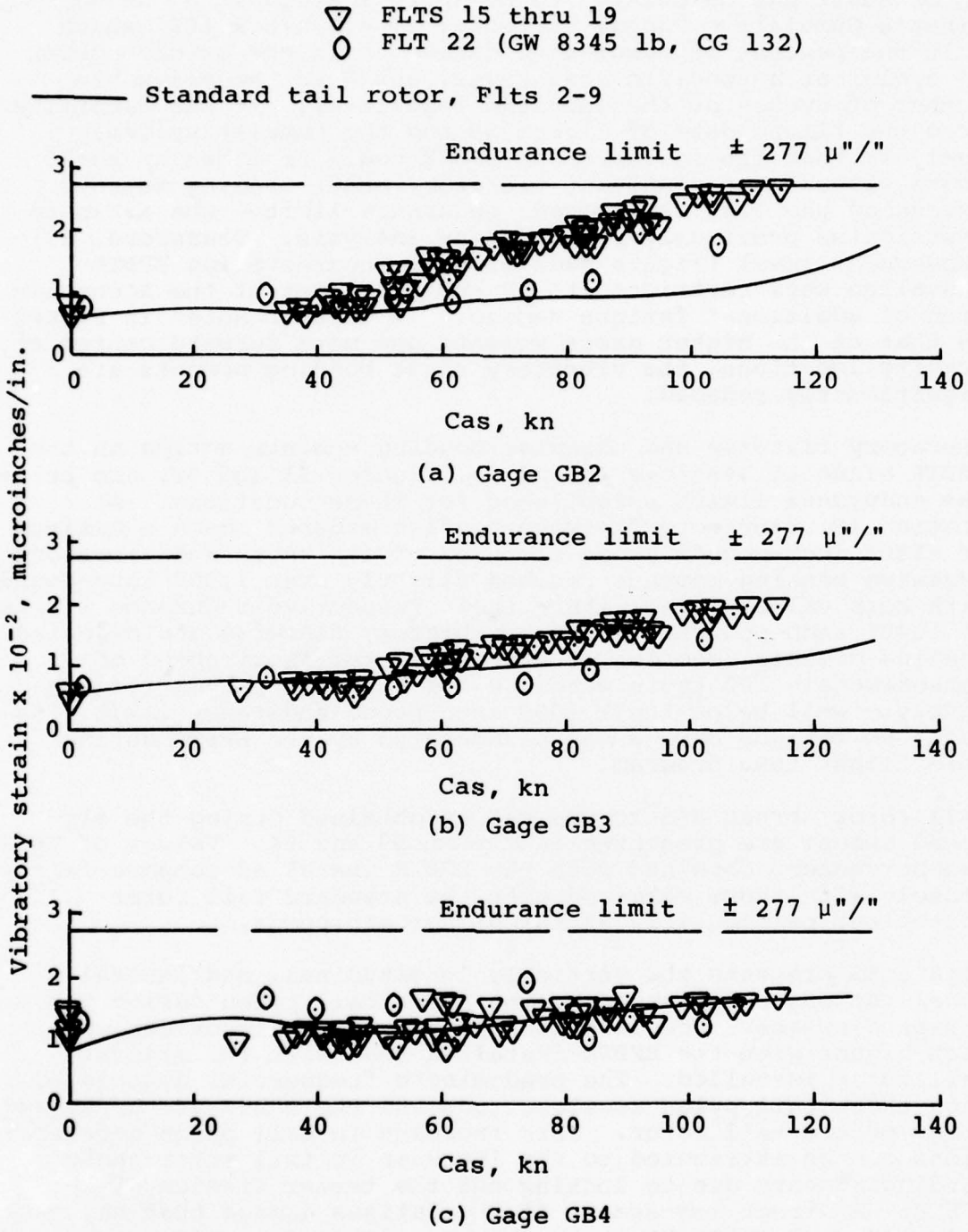

Figure 56. Tail rotor gearbox strains versus airspeed.

rotor shaft was calculated to be approximately 4% by using Miner's Cumulative Damage Criteria: $D = \Sigma\ n/N \times 100$, where D is the percent of cumulative damage, n is the actual number of cycles at a specific load level, and N is the allowable number of cycles at the specific load level. It was determined from the flight data of Figure 50 and the cumulative damage analysis that the nonteetering EPBTR could be flown up to 90 knots without the resultant vibratory shaft bending moments exceeding the 3150 inch-pound endurance limit — the airspeed restriction previously predicted by analysis. Therefore, all subsequent level flights made with the nonteetering EPBTR installed were restricted to 90 knots to prevent the accumulation of additional fatigue damage. It is also noted in Figure 50 that at the higher gross weights and more forward center of gravity locations, the vibratory shaft bending moments are significantly reduced.

Vibratory flatwise and edgewise bending moments acting on the EPBTR blade at Stations 18 and 23, Figures 51 and 52, are below the endurance limits established for these locations. At Station 18, vibratory flatwise bending moments reach a maximum of ±1300 inch-pounds at an airspeed of 110 knots and vibratory edgewise bending moments reached slightly over ±1000 inch-pounds with both values being within their respective endurance limits of ±1400 inch-pounds. Maximum vibratory flatwise and edgewise bending moments recorded at Station 23 for an airspeed of approximately 100 knots were 700 and 650 inch-pounds respectively — well below their 1000 inch-pound endurance limit. As such, no fatigue damage was accumulated by the EPBTR during this flight test program.

Tail rotor thrust and torque values obtained during the airspeed sweeps are presented in Figures 53 and 54. Values of these two parameters obtained with the EPBTR installed compare fairly closely with those obtained with the standard tail rotor installed, particularly at the higher airspeeds.

Figure 55 presents the vertical, longitudinal, and lateral accelerations experienced by the upper tail pylon during the airspeed sweeps. Accelerations in all three directions were much higher with the EPBTR installed than with the standard tail rotor installed. The predominate frequencies associated with these tail pylon accelerations and the EPBTR are 2/rev and 4/rev of the tail rotor. This increase in tail pylon accelerations can be attributed to the increase in tail rotor shaft bending moments due to locking out the teeter freedom of the EPBTR. A direct assessment of the fatigue damage that may have occurred during flight at the higher airspeeds could not be made as tail pylon strain gages were not installed during the

Engineering-Flight Test Program. An estimate of the possible amount of damage that could have occurred can be obtained by noting that the relative relationship of the maximum strains to their respective endurance limits for the tail rotor gearbox and tail pylon, obtained during subsequent R&M flights, were approximately the same, and that during the Engineering Flight Test Program, the tail rotor shaft was found to be more critical than the tail rotor gearbox. It can then be concluded that the fatigue damage incurred by the tail pylon could be no greater than 4%.

Figure 56 shows the variation of the tail rotor 90° gearbox vibratory strain levels with airspeed for both the EPBTR and the standard tail rotor installation. The three locations shown here are the areas that produce the highest strain levels. Strains on the left side mounting area (GB2 Figure 48) with the EPBTR installed were the highest recorded closely approaching the endurance limit of ±277 micro inches/inch. This condition occurred during the high-speed level-flight condition and also during a 40-degree left banked turn at 70 knots. The strain levels are higher than those measured with the standard tail rotor installed due to the increase in shaft bending moments associated with the nonteetering EPBTR. Gage locations GB2 and GB3 are the only areas that showed differences in strain levels between the two tail rotor configurations. No fatigue damage was accumulated by the tail rotor gearbox during these flights, as the resulting strains did not exceed their endurance limit.

The results obtained from the flight test program indicated that subsequent flights could be conducted without accumulating fatigue damage provided the tail rotor vibratory shaft bending moments were monitored to insure that they did not exceed the 3150 inch-pound endurance limit. If this condition was met, stresses in the EPBTR, the tail rotor gearbox and the tail pylon would not exceed their respective endurance limits. No indications of changes in dynamic response were noted during the flight program, and no evidence of structural degradation was found upon completion of the flight program.

Performance and controllability of the EPBTR is at least as good as the standard tail rotor with some improvement noted in stability (damping). The defects noted on the standard tail rotor, primarily pedal reversals in sideward flight and abrupt reductions in controllability at certain wind azimuths in hover were also present in EPBTR.

A distinct increase in tail rotor vibration occurs at about 70 knots and increases proportionately with airspeed. This "pilot feel" correlates well with tail rotor shaft bending data and thus establishes a valuable cue to excessive bending loads.

SECTION II - RELIABILITY AND MAINTAINABILITY INVESTIGATION

The UH-1 elastic pitch beam tail rotor development program was intended to exploit the full potential of composite tail rotor construction by using the elastic pitch beam concept to eliminate failure-prone pitch bearings. Another rotor that the contractor was simultaneously developing (Field Repairable/ Expandable Main Rotor Blade (FREB) for the UH-1 helicopter, Reference 6) showed the feasibility and potential for life-cycle cost reduction of repairing composite blade afterbodies by using plug patches and quick-cure adhesive.

Because the UH-1 EPBTR employed a composite afterbody, it was reasonable to assume that the life-cycle cost advantages of the UH-1 EPBTR would be further enhanced by the development of field repair techniques. In order to develop and evaluate field repair techniques for the EPBTR, a complete Failure Modes and Effect Analysis (FMEA) was produced based on FMEA data for the present UH-1 tail rotor. This was performed in order to determine what types of repairs were required most frequently and would thus have the greatest impact on life-cycle cost. As afterbody damage was a significant contributor to the failure rate, development of repair kits and techniques was initiated. After completion of the FMEA, it was possible to quantify certain parameters that could be used in the contractor's life-cycle cost model. This allowed a prediction of the relative life-cycle cost change available with the field repairable EPBTR. The development of the repair kits consisted of evaluating areas where the blade could be repaired, and choosing a suitable surface preparation technique. In addition, a tool was developed for applying heat and pressure to the repaired area. The repairs were then demonstrated during a simulated field repair demonstration. Subsequently, some severely damaged and repaired blades were whirl tested and flight tested and a life-cycle cost analysis was made using the results of the above studies.

---

6. Frengley, Michael C., DEVELOPMENT PROGRAM FOR FIELD-REPAIRABLE/EXPENDABLE MAIN ROTOR BLADES, PHASE I - PRELIMINARY DESIGN, Kaman Aerospace Corporation, Bloomfield, Connecticut; USAAMRDL Technical Report TR-73-102, U.S. Army Air Mobility Research and Development Laboratory, Fort Eustis, Virginia, April 1974, AD 783444.

FAILURE MODES AND EFFECTS ANALYSIS

Tables 13 and 14 give the failure modes analysis for the blade/hub and control subsystems. These tables are based on Tables CXI and CXIII from Reference 7, and allow comparison between the failure rates and modes from the reliability and maintainability data on the existing UH-1 tail rotor, and predicted failure rates and modes for the UH-1 EPBTR.

The design considered for the maintenance and cost analysis represents the original EPBTR design with modification made to reflex the results of testing recently completed on this rotor system. These modifications were the elimination of teeter freedom to simplify the design and manufacture of the hub region, and the increase in thickness of the aluminum leading edge to improve damage resistance. Deletion of the teeter freedom would eliminate the outer hub, two teeter bearings, and the bearing trunnions of the inner hub, thus reducing the total number of components, simplifying the design of the inner hub, and eliminating teeter bearing failures with an associated increase in reliability, a reduction in maintenance, and a reduction in cost being realized. The elimination of the teeter freedom will require a decrease in the out-of-plane stiffness and an increase in the inplane stiffness of the EPB, reduce flapping restraint at the EPB/hub attachment, and possibly, a reduction in the flapping restraint at the hub/tail rotor shaft attachment to reduce the hub moments being transferred from the rotor system to the tail rotor shaft, tail rotor gearbox, and tail pylon. An increase in leading-edge thickness would not only decrease damage susceptibility, but would possibly eliminate the need for leading-edge abrasion protection. The increased thickness would result in an increase in weight of the airfoil section, which would be more than offset by the weight reduction realized by eliminating the teeter axis components.

ARMY MISHAP CLASSIFICATIONS

The Failure Mode Classifications and Army Mishap Classifications are defined in Tables 15 and 16, respectively. The Failure Mode classifications for the EPBTR are the same as those for the present tail rotor.

---

7. Knudsen, George E., and Carr, Patricia V., R&M DATA ANALYSIS OF THE UH-1/AH-1 TAIL ROTOR SYSTEM, Bell Helicopter Company, Fort Worth, Texas; USAAMRDL Technical Report TR-74-11, U.S. Army Air Mobility Research and Development Laboratory, Fort Eustis, Virginia, April 1974, AD 782858.

TABLE 13. TAIL ROTOR BLADE AND HUB FMEA

Failure Mode	Failure Cause	Class of Failure Mode	Failure Rates Per Million Flt Hr: UH-1D/H Primary: Inherent	UH-1D/H Primary: Induced	UH-1D/H Primary: Combat Damage	EPBTR-UH-1D/H: Inherent	EPBTR-UH-1D/H: Induced	EPBTR-UH-1D/H: Combat Damage	Army Mishap Class
T/R Hub									
Safety Wire From Hub Retaining Nut to Static Stop Broken	Unknown	I	13	-	-	13	-	-	4
Data Plate Missing from T/R Hub/ Bond Failed	Bonding Failure	I	13	-	-	-	-	-	
T/R Hub Components Corroded	Insufficient Plating	I	65	-	-	-	-	-	
T/R Hub Trunnion Bearings Rough/ Worn	Normal Wear/Sandy Environment	II	39	-	-	-	-	-	
T/R Grip Bearings Worn/Loose/Rough	Normal Wear/Lack of Lubrication	II	130	-	-	-	-	-	
T/R Hub Spindle Fretting/Damaged/ Cracked	Fatigue	IV	-	-	-	-	-	-	
T/R Hub Grease Fitting Missing/Loose	Unknown	I	-	-	-	-	-	-	
T/R Grip Nut/Bearing Retainer Nut Loose	Maintenance Under-torqued	III	-	26					
T/R Grip Pitch Change Bushing Worn	Securing Bolt has Low Torque	II	-	-	-	-	-	-	
T/R Hub Removed-Engine Overspeed	Engine Overspeed	N/A	-	65	-	-	65	-	4,6
T/R Hub Removed-Sudden Stoppage	Pilot Error, Tree Strike	N/A	-	143	-	-	143	-	4,6
T/R Hub Bearings will not take Lubrication	Thrust Unit Installed Backwards	I	-	-	-	-	-	-	
T/R Hub Damaged by P/C Link	T/R P/C Link Improperly Installed	I	-	-	-	-	-	-	
T/R Hub Damaged by Armament Debris	Spent Brass Strike	II	-	13	-	-	13	-	4
T/R Hub and Blade Lost in Flight	T/R Yoke Crack/Unknown	IV	-	-	-	-	-	-	
T/R Hub Removed-Wrong Part Number	Maintenance Error	N/A	-	13	-	-	-	-	
T/R Vibration	Out of Track/Balance	II	13	-	-	-	-	-	
HUB SUBTOTAL			273	260	0	13	221	0	
T/R Blade									
T/R Blade has Strike Damage	Contact Tree, Wire, Etc.	III	-	337	-	-	337	-	4
T/R Blade has Leading-Edge Erosion	Wear, Sandy Environment	II	-	169	-	-	169	-	4
T/R Blade Damaged by Armament Debris	Spent Brass Strike	III	-	-	169	-	-	92	4
T/R Blade has Combat Damage	Enemy Combat Fire	III	-	-	32	-	-	32	4,6
T/R Blade has Bonding Void	Bonding Failure	II	20	-	-	20	-	-	4,6
T/R Blade Removed-Overspeed	Overspeed-Pilot Error	N/A	-	65	-	-	65	-	4,6
T/R Blade Removed-Sudden Stoppage	Hard Landing-Engine Failure	N/A	-	39	-	-	39	-	4
T/R Blade has Foreign Object Damage	Foreign Object Damage	III	-	-	-	-	-	-	
T/R Blade Leading-Edge Hole Patch Loose	Bonding Failure	II	-	-	-	-	-	-	
T/R Vibration	Blades Out of Track	II	32	-	-	32	-	-	4,5
Lost in Flight	Unknown	IV	-	-	-	-	-	-	
SUBTOTAL, ONE BLADE			52	610	201	52	506	124	
TOTAL, TWO BLADES AND ONE HUB			377	1480	402	117	1233	248	
TOTAL, ONE ROTOR				2259			1598		

TABLE 14. TAIL ROTOR CONTROLS FMEA

Failure Mode	Failure Cause	Class of Failure Mode	Failure Rates Per Million Flt Hr: UH-1D/H Primary: Inherent	UH-1D/H Primary: Induced	UH-1D/H Primary: Combat Damage	EPBTR-UH-1D/H Primary: Inherent	EPBTR-UH-1D/H Primary: Induced	EPBTR-UH-1D/H Primary: Combat Damage	Army Mishap Class
T/R Boot									
T/R Installation Boot Torn or Cut	Rough Handling, Maintenance Error	II	-	298	-	-	298	-	4
T/R Boot Loose	Unknown	II	-	-	-	-	-	-	
T/R Boot Removed-Sudden Stoppage	T/R Strike		-	26	-	-	26	-	4
T/R Slider									
T/R Slider Worn	Normal Wear, Sandy Environment	II	363	-	-	363	-	-	4
Slide Removed-Sudden Stoppage	T/R Strike			26	-	-	26	-	4
Crosshead Bearing Set									
Bearing Set Worn/Separating	Sandy Environment, Lack of Lube	II	207	-	-	207	-	-	4
Bearing Set Loose	Improper Installation	II	-	52	-	-	52	-	4,6
Bearing Set Removed	T/R Strike	N/A	-	26	-	-	26	-	4
T/R Crosshead									
T/R Crosshead and Attaching Bolt Corroded	Insufficient Plating	II	13	-	-	13	-	-	4
T/R Crosshead Assembly Scored by P/C Link Bearing	Improper Alignment	II	-	117	-	-	177	-	4
Loss of Torque on Crosshead Retaining Nuts	Undertorqued, Maintenance	II	-	13	-	-	13	-	4,6
T/R Crosshead Assembly Removed-Sudden Stoppage	Tree Strike (T/R)	III	-	13	-	-	13	-	4
Crosshead Improperly Shimmed	Maintenance Error	II	-	91	-	-	91	-	4
T/R Crosshead Loose - High Frequence Vibration	Bushing Worn, Misaligned	II	13	-	-	13	-	-	4,6
T/R Pitch Change Link									
T/R P/C Link Bearing Worn	Sandy Environment, Lack of Lube	II	765	-	-	765	-	-	4
T/R P/C Link Bearings Frozen	Sandy Environment	II	13	-	-	13	-	-	4
Teflon Liner Separation in T/R P/C Link Bearing	Bond Failure	II	39	-	-	39	-	-	4
T/R P/C Link Bearing Outer Race Corroding	Unknown	II	7	-	-	7	-	-	4
T/R P/C Link Assy Out of Alignment	Maintenance Error	II	-	39	-	-	39	-	4,6
T/R P/C Link Replaced, Nut Frozen	Bolt Corrosion	II	13	-	-	13	-	-	4
T/R P/C Link Rivet Sheared	Maintenance Error	II	-	-	-	-	-	-	
T/R P/C Link Stack-Up Improper	Maintenance Error	II	-	-	-	-	-	-	
T/R P/C Link Rod Bent/Threads Stripped	Unknown-Suspect Overload	III	-	-	-	-	-	-	
T/R P/C Link Bearing Chafes T/R Crosshead	Bearing Worn	II	-	-	-	-	-	-	
T/R P/C Link Bearing Inner Race Cracked	Unknown	II	-	-	-	-	-	-	
T/R P/C Link Damaged/Hard Landing	Pilot Error	III	-	39	-	-	39	-	4
T/R P/C Link Jam Nut Loose	Maintenance Error	II	-	-	-	-	-	-	
			1433	740	0	1433	740	0	

TABLE 15. FAILURE MODE CLASSIFICATIONS

Class	Description
I	Negligible - Any "nuisance" failure not serious enough to be classified Class II, III or IV and will not result in personnel injury or aircraft system damage but which will require corrective action during routine preventive maintenance.
II	Marginal - Any failure which degrades performance or results in degraded operation (such as loss of automatic function) and can be counteracted or controlled without injury to personnel or major aircraft system damage. Requires special operation techniques or alternative mode of operation which could be tolerated throughout a mission, but should be corrected immediately upon completion of the mission.
III	Critical - Mandatory Abort - Any failure which results in complete loss of function and will cause personnel injury/hazard or major aircraft system damage, or will require immediate corrective action for personnel or aircraft system survival. A time-dependent repair action which, if uncompensated, can cause a catastrophic failure.
IV	Catastrophic - Any single failure which will cause death or severe injury to personnel or aircraft system loss.

TABLE 16. MISHAP CLASSIFICATION DEFINITIONS

Mishap Class	UH-1C/D/H Repair Requirements
1 (Total Loss)	Total Loss
2 (Major Damage)	Over 500 MMH
3 (Minor Damage)	100-500 MMH
4 (Incident)	1-99 MMH
5 (Forced Landings)	No Damage
6 (Precautionary Landing)	No Damage

The Army Mishap Classifications are interpreted to give a relative expense incurred to repair the aircraft if it sustains damage as a consequence of tail rotor subsystem failures. As can be seen from Tables 13 and 14, little if any damage is expected to be incurred by the aircraft as a result of tail rotor blade/hub or control system damages. In some cases, such as bond void failure, a vibration would occur which would lead the prudent pilot to effect a safe landing and check out the system before continuing flight. These precautionary landings were indicated by a second mishap classification number in the tables.

SCRAP VERSUS REPAIR ANALYSIS

Table 17 gives the FMEA broken down by failure type and component. This table is needed to determine repair dispositions, make scrap/repair decisions, and assess which types of repairs could be developed economically, based on predicted usage frequency. The FMEA given in Reference 6 has sufficient detail on failure types and components to be used in this analysis, but it was necessary to make adjustments to this data because of the difference between the FREB and the EPBTR. Adjustments to this data were made based on blade size and complexity, component vulnerability, and swept area ratio (rotor disk area/rotor speed). It was expected that although the above method would not give an accurate overall failure rate, it would give accurate relationships between the various failure rates. The relationship between the various failure rates thus developed were used in conjunction with the field-developed failure rates in Tables 13 and 14 to produce the blade-and-hub-related failure rates of Table 17.

DEVELOPMENT OF FIELD REPAIR KITS AND REPAIR PROCEDURES

Analysis of the FMEA data indicated the types of blade damage anticipated in service. A decision was then made as to whether each such damage was cause for scrap at organizational level or was a structurally acceptable and practical candidate for repair and at what level of maintenance support. The frequency of occurrence, the degree of skill required and the complexity of technique were considered,and a list of candidate repairs was then selected. Then the blade construction and materials utilized in the repairable areas were reviewed to determine what the features of each repair should be. The degree of commonality between the construction of the EPBTR and the Field Repairable/Expendable Main Rotor Blade, Reference 6, indicated that the repair techniques should be very similar. The glass cloth skin and honeycomb core of the two blades are almost identical with respect to repairability.

TABLE 17. FREQUENCY OF DAMAGE BY ELEMENT, TYPE AND CAUSE AS PROJECTED BY FAILURE MODE AND EFFECTS ANALYSIS (FAILURES PER MILLION FLIGHT HOURS)

ROTOR ASSEMBLY MAJOR ELEMENTS AND COMBINATIONS	CRACKED			BENT/ DISTORTED			PUNCTURED TORN			DENTED			NICKED/ SCRATCHED			DELAMINATION			OVERSPEED SUDDEN STOPPAGE			BOND FAILURE			WORN OVERSIZE			LOOSE MISSING			ERODED			SUB-TOTAL
	C	I	E	C	I	E	C	I	E	C	I	E	C	I	E	C	I	E	C	I	E	C	I	E	C	I	E	C	I	E	C	I	E	
SPAR				9.6					69.8	7.2		108.2	8.2		20.5																	9.6	233.1
SPAR/SKIN	1.8	1.3					3.5		25.0	1.3		32.0	3.7		3.7	2.4	0.7	0.4				4.6	1.9										0.2	82.5
SPAR/CHANNEL																							1.3	84.1										85.4
SPAR/STRAP							6.8																											6.8
SKIN	9.2	6.9					18.4		132.5	6.9		170.6	19.6		19.6	12.6	3.4	2.3															1.1	403.1
SKIN/CORE	11.0						21.9		93.1	8.2		115.0										12.1	5.2											266.5
SKIN/SPAR/CORE										1.0												12.1	5.2											18.3
SKIN/T.E. SPLINE		2.7		4.1			16.5		28.8	11.0			4.1					2.7				28.8	4.1									1.3	104.7
CHANNEL/STRAP ASSY																							0.8	28.0										28.8
CHANNEL/SPAR/STRAP																								46.0										46.0
STRAP ASSY		14.3																					0.7	65.0										80.0
TIP CLOSURE												2.7																					1.3	4.0
TIP WGT RETENTION																																	5.5	5.5
INBOARD BOOT																																	5.5	5.5
PITCH FITTING																																	1.3	1.3
CTR WGTS & ARMS																																	1.3	1.3
HUB										3.8									61.8	135.7					18.0			5.7						225.0
	22.0	25.2		13.7			67.1		349.2	39.4		428.5	35.6		43.8	15.0	4.1	5.4		61.8	135.7	57.6	19.1	223.1		18.0			5.7			27.1	1597.2

Note: C = Combat Damage, I = Inherent Damage, and E = External Damage

The tail rotor spar is a composite fiberglass, resin and formed aluminum sheet build-up, whereas the main blade spar is an aluminum extrusion; however, both are critical elements and eligible for only limited repair - even at depot level. Organizational repair of the rotor would consist of blending out, filling and refinishing of shallow nicks, scratches and gouges, removal of damaged skin and core and applying patches and patch/plugs and would be comparable for either configuration. The trailing-edge spline of the tail rotor is made of fiberglass and is covered with fiberglass skin, whereas the FREB main blade has an aft edge spline of aluminum, which is exposed (not completely covered by skin). Repairs to either configuration would, at organizational and intermediate level, be restricted to blending out surface damage, patching and refinishing.

The following guidelines were used to develop repair kits and procedures:

SCOPE OF MAINTENANCE

All repairs and scheduled maintenance should be safely and reliably accomplished at the using unit level.

Repairs requiring replacement of primary structural material shall not be permissible, and such damage shall be cause for scrap. Delamination of adhesive bonds involving primary structure shall be cause for scrap.

Dents, nicks, and scratches shall be repaired by blending and/or filling, except when structural or contour degradation is significant.

Repairs to punctures, tears, and cracks shall be designed to minimize stress concentrations, and shall be permissible only in those areas and materials where stress concentrations will not cause subsequent secondary failures.

Rotor balance shall be corrected using easily accessible and adjustable weights installed at the blade tips and pitch arm. The amount of weight change shall be simply defined and related to each individual repair.

Repair Materials

- Punctures, tears, and cracks shall be cleaned up and repaired using standard prepackaged repair kits. Several different kits shall be provided, each related to a particular type of repair to be accomplished.
- Patches or patch/plug assemblies contained in the kits shall be prefabricated and shall be protected against contamination.
- The kits shall contain all consumable materials necessary to accomplish repair except those which are hazardous substances or have a limited shelf life.
- Two-part epoxy adhesives shall be provided in two-part premeasured packages.

Tools and Equipment

- Special support equipment needed to effect repairs shall be minimized and shall be suitable for deployment at company level.
- Electrical power requirements shall be limited to 110 volt AC or 28 volt DC.

Personnel

- The skill level of the maintenance personnel shall be that of a UH-1 helicopter repairman, MOS 67N20.
- No more than two men shall be required to accomplish any individual maintenance action.

The repair kits developed under the above guidelines consisted of the items listed in Table A-2 of Appendix A. In general, each kit contains one patch per damaged surface and sufficient materials to clean the surfaces and bond the patch. The kits contain all throw-away items (with the exception of the patches) and are completely consumed after the repair is complete.

The nonconsumable items used for the repairs consist of readily available items (workstands, power supply, router, vacuum pump, etc.) and a heat and vacuum pack. The damage to the blade is cleaned out using a carbide bit in a router. Templates (supplied with the repair kits) are used to insure that the cleaned out hole matches the patch size. The heat and vacuum pack (shown in Figure A-7) is vee-shaped and will

cover both sides of the blade afterbody. This allows two-surface repairs as well as trailing-edge repairs to be bonded in one cure cycle. The tool also has vacuum bags under the heating elements to provide uniform pressure during the cure cycle. The heating elements are powered by a 110-volt supply, while vacuum is supplied by a portable vacuum pump. A complete description of repair kits, their application and the use of the tools is given in Appendix A.

After the repair has been made, a chart is consulted that tells the mechanic how to change the balance weights in the blade tip to maintain rotor balance after repair.

MAINTAINABILITY DEMONSTRATION - SIMULATED FIELD SERVICE EVALUATION

Based on their frequency of occurrence as projected by the FMEA, sixteen characteristic failure or damage events were selected for demonstration during the simulated field service evaluation. Figures 57 through 59, along with Table 18, define the type and extent of damage to be repaired, the location of the damage, the type of maintenance action required, and the repair procedure defined in Appendix A to be used to accomplish the repair. After the repair kits and procedures had been developed, repair times predicted, and repair specimens destructively tested, a demonstration was held under simulated field conditions. The purpose of this demonstration was to give interested Government and industry personnel an opportunity to witness the repair procedures, to provide repaired rotors for subsequent whirl and flight test, and to set up a controlled atmosphere in which previously predicted maintenance times could be verified. Table 19 lists predicted maintenance times as well as the actual measured maintenance time. As noted, the predicted and the measured time required for these repairs agreed quite favorably. As Army personnel were unavailable for the simulated field service evaluation, one of the contractor's technicians, having a skill level close to that of a MOS 67N20 helicopter repairman, performed the repairs.

After the demonstration was completed, an informal contractor critique was held to suggest improvements to the repair kits, tools, and procedures. In general, the basic techniques, tools, and materials supplied in the kits were satisfactory and, with only slight modifications, could be used for field repairs. Recommended modifications included:

1. For plug patches, more accurate measurement of the depth of plug required should be made to insure proper fit-up of the patch with respect to the airfoil section skins to minimize air entrapment in the bond line.

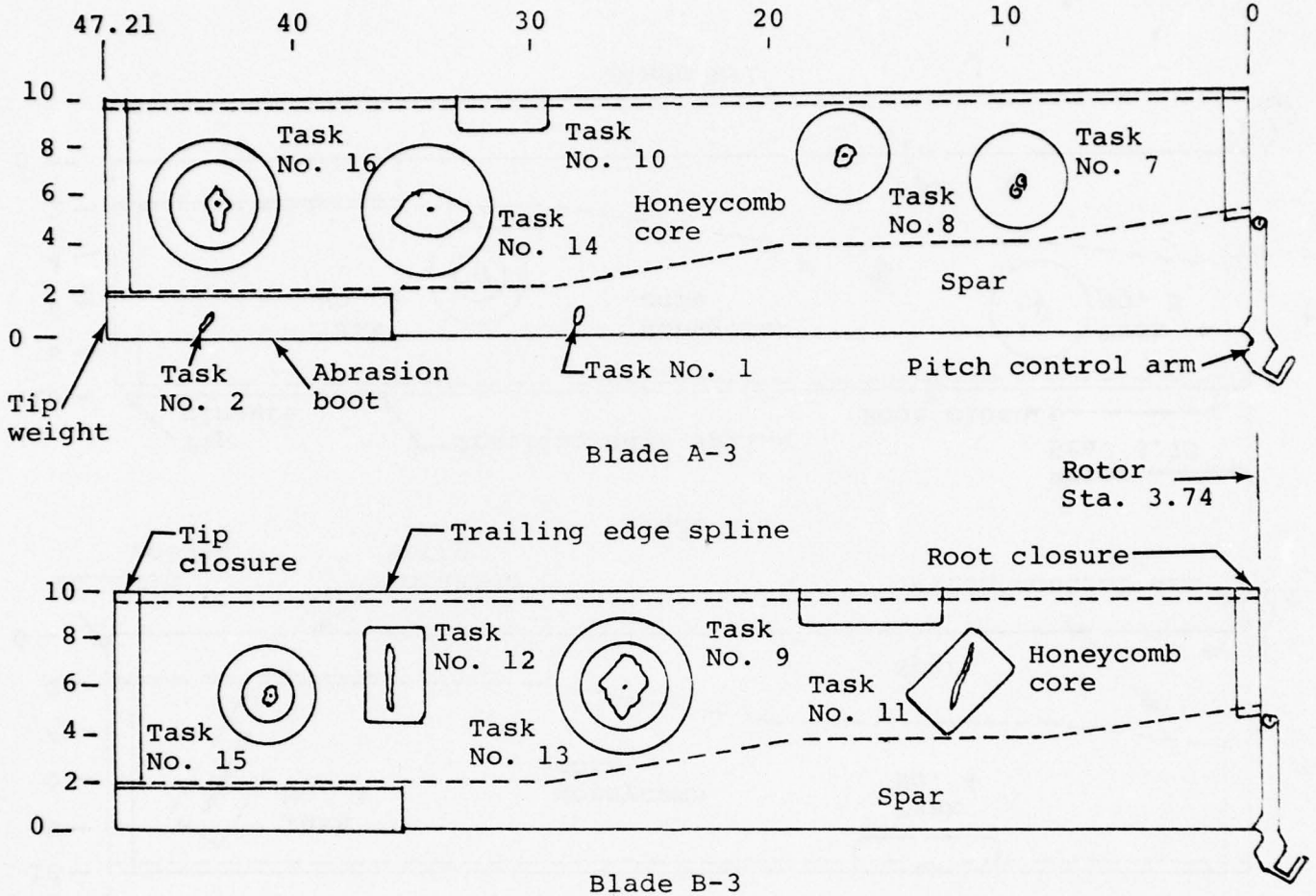

Figure 57. Damage and repair schematic, rotor S/N 008.

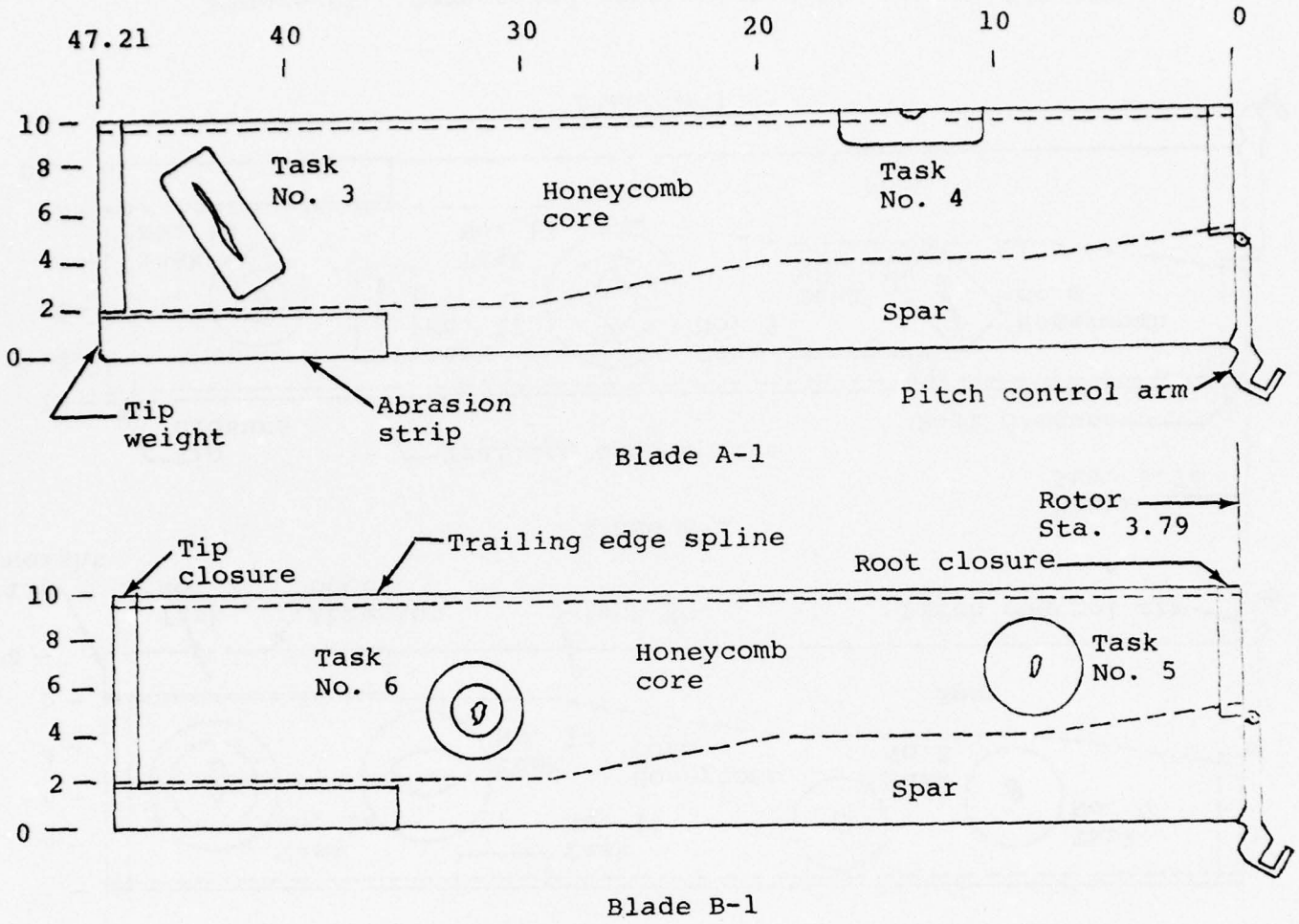

Figure 58. Damage and repair schematic, rotor S/N 009.

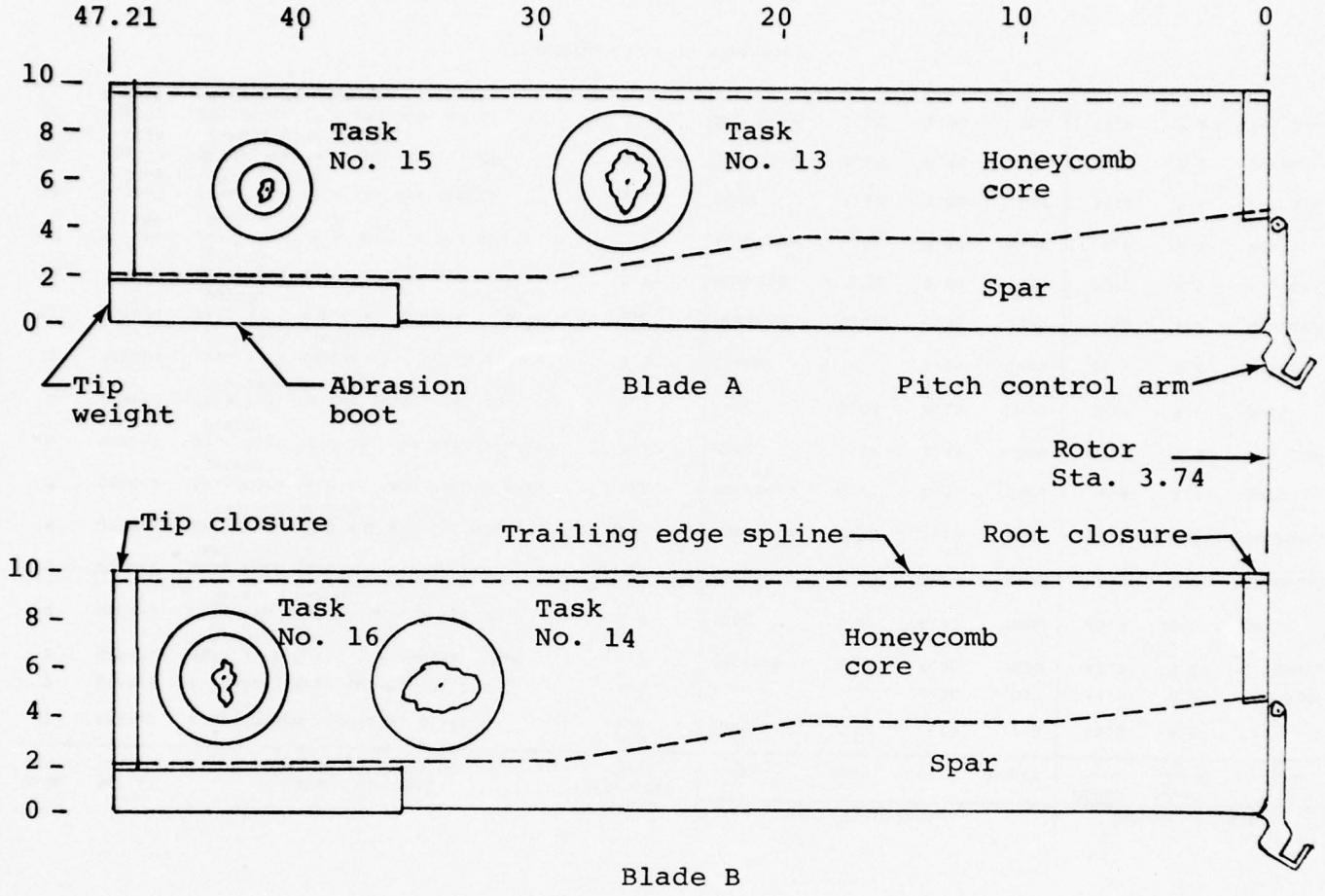

Figure 59. Damage and repair schematic, rotor S/N 012.

TABLE 18. MAINTENANCE TASK DESCRIPTION

Task No.	Blade Serial No.	Blade Element/ Maintenance Action	Repair Procedure No.*	Damage Description				Damage Location		
				Type	Span	Chord	Depth	Blade Span	Blade Chord	Blade Side
1	008A-3	Spar (blend, alodine, fill)	2.3	Dent	0.30	0.80	.050	28.3	0.6	Fin Side
2	008A-3	Abrasion Strip (blend, fill)	2.4	Tear	0.20	0.56	.015	44.0	0.3	Fin Side
3	009A-1	Skin (2.5 x 6.0 in. single, skin patch)	2.1	Scratch	0.40	4.30	.020	42.9	5.7	Outboard
4	009A-1	Skin/T.E. Spline (6.0 x 1.5 in. vee skin patch)	2.1	Tear	1.12	0.32	Thru	13.7	10.0	Both
5	009B-1	Skin/Core (4.0 in. dia single skin patch)	2.1	Puncture	0.40	2.00	.090	8.9	6.8	Outboard
6	009B-1	Skin/Core (4.0 and 2.0 in. dia single plug patch)	2.1	Puncture	0.75	1.10	.500	32.5	5.0	Outboard
7	008A-3	Skin/Core (4.0 in. dia double skin patch)	2.1	Puncture	0.48	0.56	Thru	9.6	6.3	Both
8	008A-3	Skin/Core (4.0 in. dia single skin patch)	2.1	Dent	1.80	2.10	.090	16.9	7.3	Fin Side
9	008B-3	Skin/T.E. Spline (6.0 x 1.5 in. vee skin patch)	2.1	Tear	3.00	0.10	Thru	16.4	9.9	Both
10	008A-3	Skin/T.E. Spline (4.0 x 1.5 in. vee skin patch)	2.1	Crack	-	1.00	Thru	31.4	9.8	Both
11	008B-3	Skin (2.5 x 4.0 in. single skin patch)	2.1	Scratch	0.01	1.52	.120	12.5	6.2	Outboard
12	008B-3	Skin (2.5 x 4.0 in. single skin patch)	2.1	Scratch	0.20	2.90	.015	36.4	6.5	Fin Side
13	008B-3 & 012A	Skin/Core (5.5 and 3.5 in. dia double plug patch)	2.1	Puncture	1.92	2.82	Thru	26.5	5.5	Both
14	008A-3 & 012B	Skin/Core (5.5 in. dia single skin patch)	2.1	Dent	3.40	2.00	.098	34.1	5.6	Fin Side
15	008B-3 & 012A	Skin/Core (4.0 and 2.0 in. dia single plug patch)	2.1	Puncture	0.65	0.80	.450	41.6	4.3	Outboard
16	008A-3 & 012B	Skin/Core (5.5 and 3.5 in. dia single plug patch)	2.1	Puncture	1.20	2.00	.250	43.0	5.2	Fin Side

*Paragraph Number, Appendix A

TABLE 19. REPAIR TASK MAN-HOUR ANALYSIS

Blade Element	Task Number	Failure or Damage Description	Events Per 10^6 Flt Hours	Maintenance Action	Repair Time in Man-Hours		Total Man-Hours Per Event
					Predicted	Demonstrated	
Spar	N.D.	Dented, eroded, nicked, scratched	77	Blend, alodine	0.30	N.D.	23.10
	1	Dented, nicked, scratched	62	Blend, alodine, fill	1.05	1.86	115.32
Skin	3,11,12	Cracked, punctured, torn, delaminated, dented, nicked and scratched	227	Single skin patch	1.25	1.18	267.86
Skin/core	5,8,14	Cracked, punctured, torn, dented	321	Single skin patch	1.25	1.16	372.36
	7	Punctured, torn	7	Double skin patch	1.55	1.37	9.59
	6,15,16	Punctured, torn, dented	66	Single plug patch	1.75	1.45	95.70
	13	Punctured, torn	20	Double plug patch	2.25	1.80	36.00
Skin/T.E. spline	9	Punctured, torn	78	Blend, vee skin patch	1.25	1.23	95.94
	4,10	Bent, distorted, cracked, dented, nicked, scratched, delaminated, bond failure, eroded	34	Vee skin patch	1.05	1.22	41.48
	N.D.	Dented, nicked, scratched	12	Blend	0.25	N.D.	3.00

TABLE 19 - CONTINUED

Blade Element	Task Number	Failure or Damage Description	Events Per 10^6 Flt Hours	Maintenance Action	Repair Time in Man-Hours		Total Man-Hours Per Event
					Predicted	Demonstrated	
Tip Weight	N.D.	Eroded	3	Blend, alodine	0.25	N.D.	.75
Abrasion strip	2	Punctured, torn, eroded	7	Fill	0.50	1.71	11.97
Root closure	N.D.	Dented	2	Closure skin patch	1.25	N.D.	2.50
Skin, root closure	N.D.	Dented	2	Closure skin patch	1.25	N.D.	2.50
Pitch fitting	N.D.	Eroded	3	Blend, alodine	.40	N.D.	1.20
Totals			921				1079.27

$1079.27 \div 10^6 = .00108$ m-hr/blade hour/10^6 hr.

$.00108 \times 2 = .00216$ m-hr/rotor hour/10^6 hr.

$1079.27 \div 921 = 1.17$ m-hr MTTR

NOTE: Total man-hours per event = number of man-hours per event demonstrated x frequency of events (N.D. = Not Demonstrated, therefore predicted value used for calculation of MTTR)

2. An increase in the width of the vacuum/heat pack, used for curing the patches, would make the placement of the pack less critical, particularly when used with the largest (5½-inch diameter) patch.

3. Provide a means for locking or permanently presetting the vacuum/heat pack thermostat control to avoid accidental changes in the cure temperature.

4. Provide a tapped hole or other provisions on or near the trailing edge of the tip cap to aid in its removal to provide an easy access to the inner balance washers.

R&M WHIRL TEST

Two elastic pitch beam tail rotor assemblies (S/N 008 and 013) were used for the reliability and maintainability whirl test to determine the adequacy of the repair kits and the repair procedures. Each rotor assembly was subjected to two levels of damage and repair, with the first level being more severe than the second. After the completion of the repairs at each level, the rotor assemblies were balanced and whirl tested for 30 hours. Thus, first-level repairs were whirl tested for 60 hours and second-level repairs were whirl tested for 30 hours.

Table 20 summarizes the test specimens involved, the types and locations of the various repairs, and the accumulated whirl test endurance hours. The indicated task numbers are for the damage-repair combinations defined in Figures 57 through 59 and are based on the typical damage scenario for the tail rotor installation. Figures 60 through 63 show the repairs made on EPBTR assemblies S/N 008 and S/N 013 as indicated in Table 20.

Each of the 30-hour whirl tests was run in two blocks of 15 hours each at the normal rotor speed of 1650 rpm in accordance with the following schedule:

Blade Pitch Angle (Deg)	Duration (Min)
-3	6
0	10
3	60
5	660
7	150
10	11
13	3

TABLE 20. R&M WHIRL TEST REPAIR SUMMARY

Task No.	Blade S/N	Type of Repair	Fig No.	Total Endurance Time (hr)	Repair Location	
					Station	Chordwise
16	008A	3½-in.-dia plug/patch	60	60	46.79	5.2
13	008B	3½-in.-dia through plug/patch	61	60	30.29	5.1
14	008A	5-in.-dia skin patch	60	30	37.89	5.5
15	008B	2-in.-dia plug/patch	61	30	45.41	4.6
13	013A	3½-in.-dia through plug/patch	62	60	30.29	5.1
16	013B	3½-in.-dia plug/patch	63	60	46.79	5.2
3	013A	2½-in. x 6-in. skin patch	62	30	46.69	5.7
4	013A	6-in.-long Vee patch	62	30	17.49	10.0
6	013B	2-in.-dia plug/patch	63	30	38.29	5.0
5	013B	4-in. skin patch	63	30	14.69	6.8

NOTE: Other repair tasks shown, but not identified, in Figures 60 and 61 for blades S/N 008A and S/N 008B respectively were accomplished subsequent to the R&M whirl test program as part of the simulated field service evaluation.

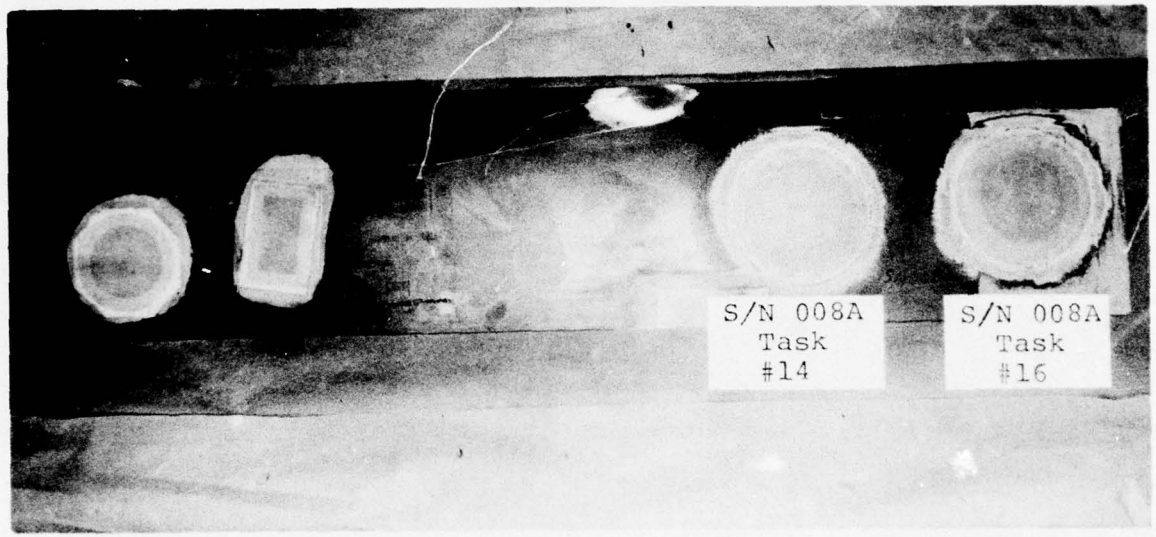

Figure 60. Repaired elastic pitch beam tail rotor blade S/N 008A.

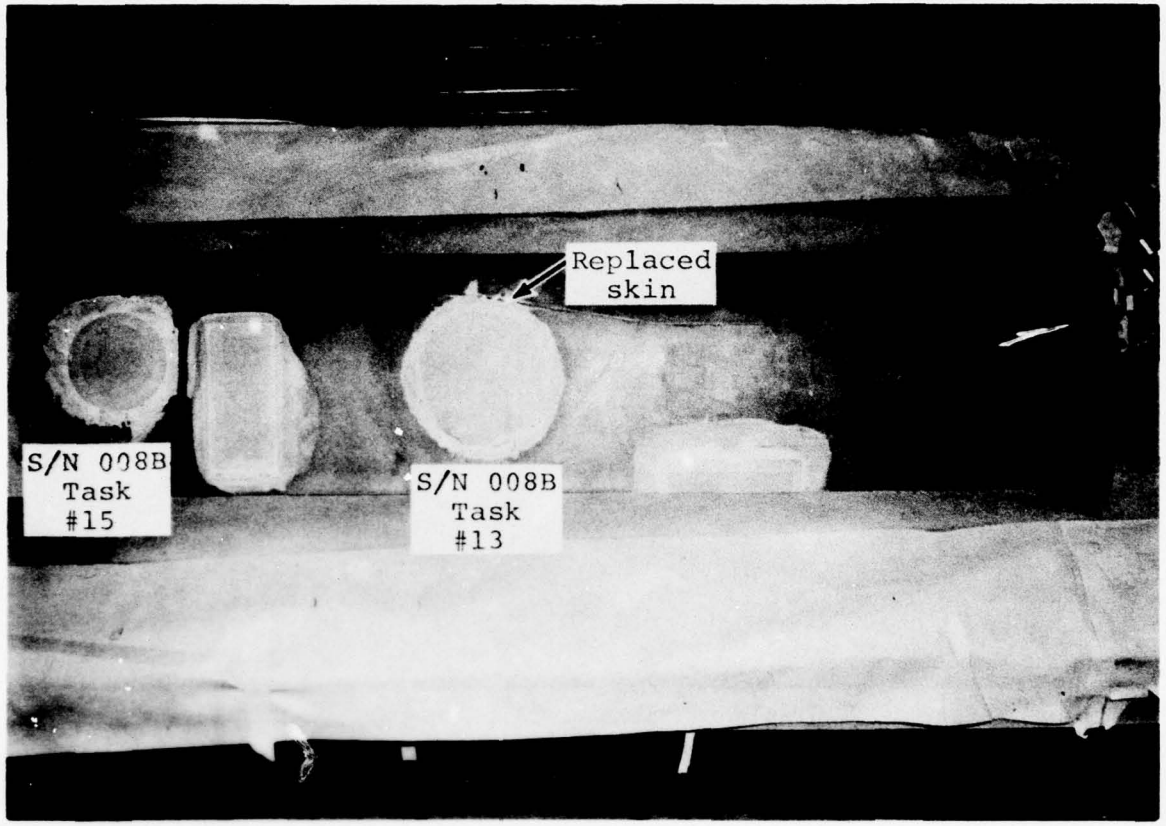

Figure 61. Repaired elastic pitch beam tail rotor blade S/N 008B.

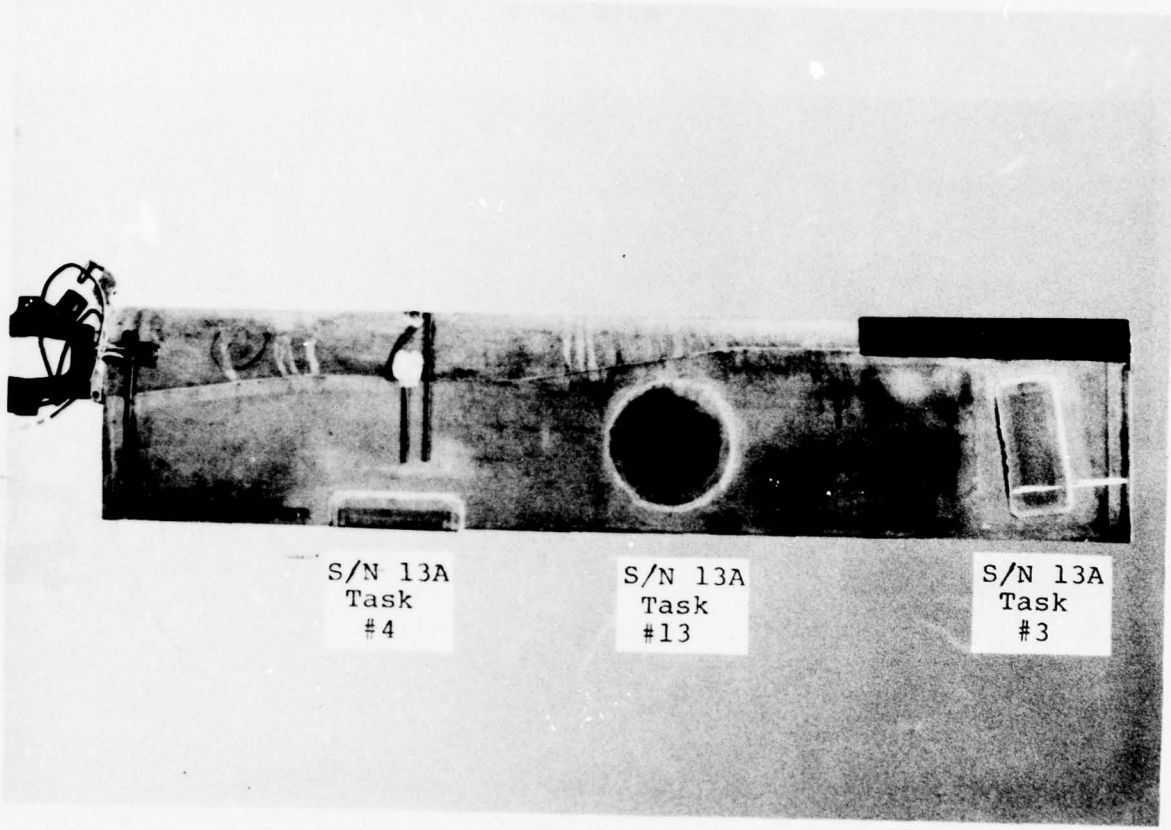

Figure 62. Repaired elastic pitch beam tail rotor S/N 13A.

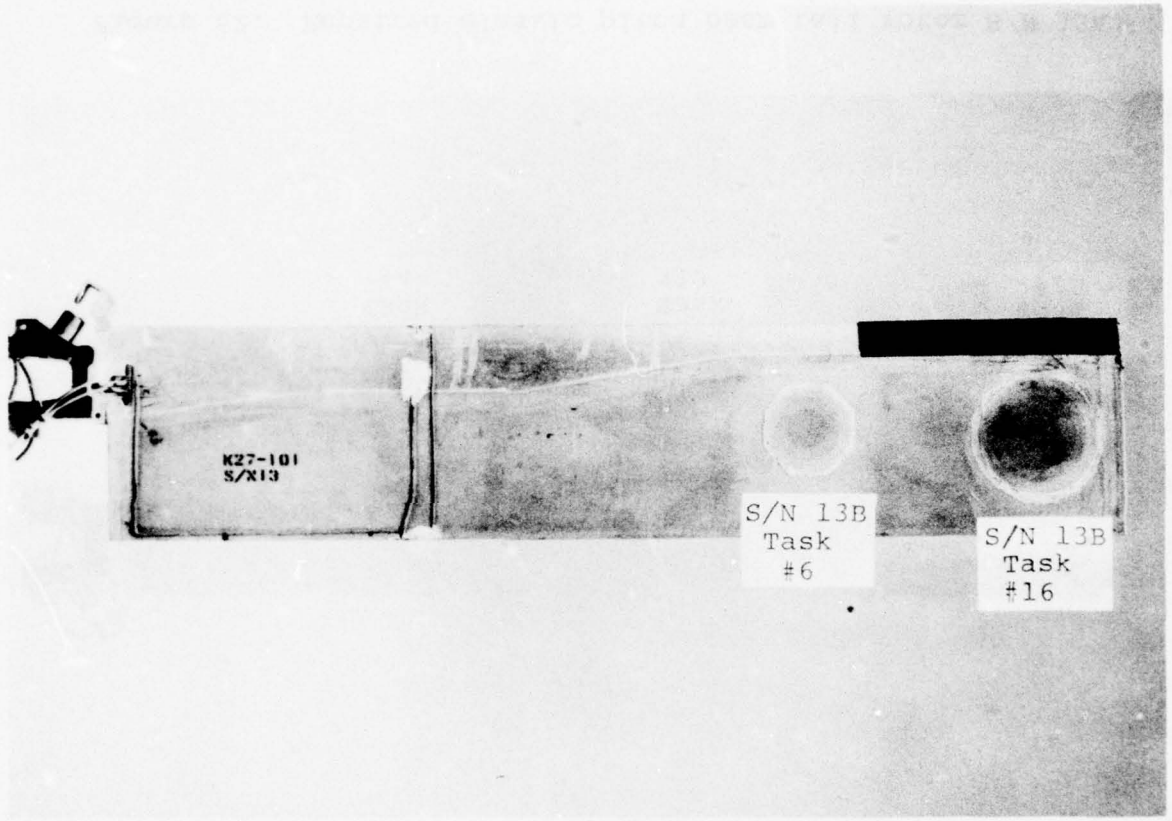

(a) Outer side

Figure 63. Repaired elastic pitch beam tail rotor S/N 13B.

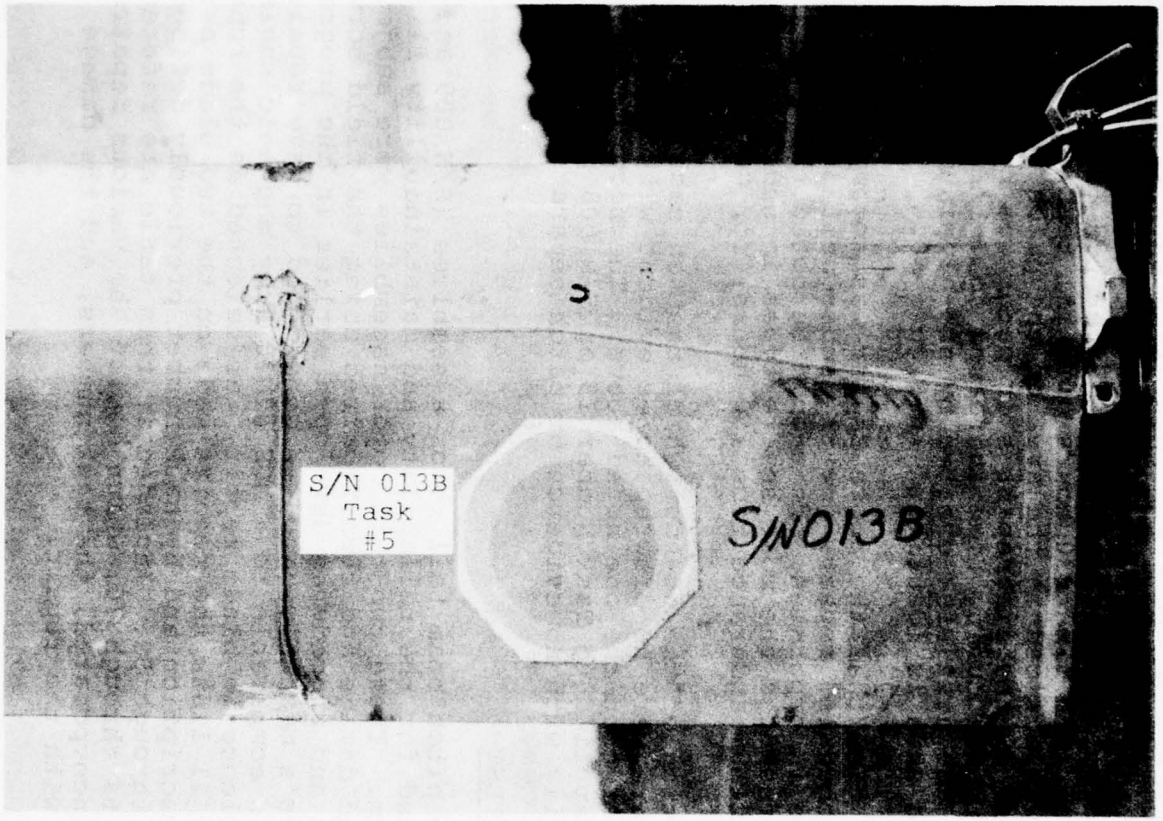

(b) Pylon side

Figure 63. Continued.

The damage and repair defined by Task Number 13 made to EPBTR S/N 008 was inadvertently located too close to the spar for the size of the skin patch used. This resulted in the patch overlapping the channel portion of the spar by about .25 inch. During the curing process, the spar acted as a heat sink interfering with the proper cure cycle for the adhesive. A heat gun was employed to compensate for the difference in temperature; however, after the first 30 hours of whirl testing, a slight separation was noticed in the area of the patch over the spar. The top layer of the discrepant skin patch was removed and replaced with the curing time increased to 1-1/2 hours to compensate for the heat sink created by the aluminum channel. The replaced skin is identified in Figure 60.

At the same time that the above repair was accomplished, the remaining scheduled repairs for the subsequent 30 hours of testing were incorporated. It should be noted that the initial repairs represented the most severe types in order to accumulate the maximum endurance time (60 hours) for conservatism.

Upon completion of the 60-hour whirl test on each tail rotor assembly there were no discrepancies evident with any of the repairs other than the one noted above. The second repair and cure cycle applied to Task Number 13 on S/N 008 performed satisfactorily with no evidence of patch separation.

R&M FLIGHT TEST

Two elastic pitch beam tail rotor assemblies (S/N 009 and 012) were selected for the reliability and maintainability flight test program. These two tail rotor assemblies were subjected to simulated damage and then repaired using the field service repair kits and procedures developed earlier in the program. A Contractor's mechanic, who was considered to have repair skill levels comparable to a MOS 67N20 Army mechanic having no prior experience in blade repair, was selected as the repairman. Table 21 lists the repairs made on the two blade assemblies by description and by task number previously defined in Figures 57 through 59. Included in this table are references to Figures 64 through 70, which depict the various repairs that were incorporated, the task numbers, and the damage associated with the repair.

TABLE 21. R&M FLIGHT TEST REPAIR SUMMARY

Blade S/N	Type of Repair	Task No.	Hours Tested	Repair Location		Figure
				Station	Chordwise	
009A	2-1/2-in. x 6-in. Skin Patch	3	20	46.69	5.7	64 repaired
009A	6-in. Long Vee Patch	4	20	17.49	10.0	64 repaired
009B	4-in.-dia Skin Patch	5	20	12.69	6.8	64 repaired
009B	2-in.-dia Plug/Patch	6	20	36.29	5.0	64 repaired
012A	3-1/2-in.-dia Through Plug/Patch	13	20	30.29	5.1	65 damaged 66 repaired
012A	2-in.-dia Plug/Patch	15	20	45.29	4.6	67 damaged 68 repaired
012B	5-in.-dia Skin Patch	14	20	37.89	5.5	69 damaged 70 repaired
012B	3-1/2-in.-dia Plug/Patch	16	20	46.79	5.2	69 damaged 70 repaired

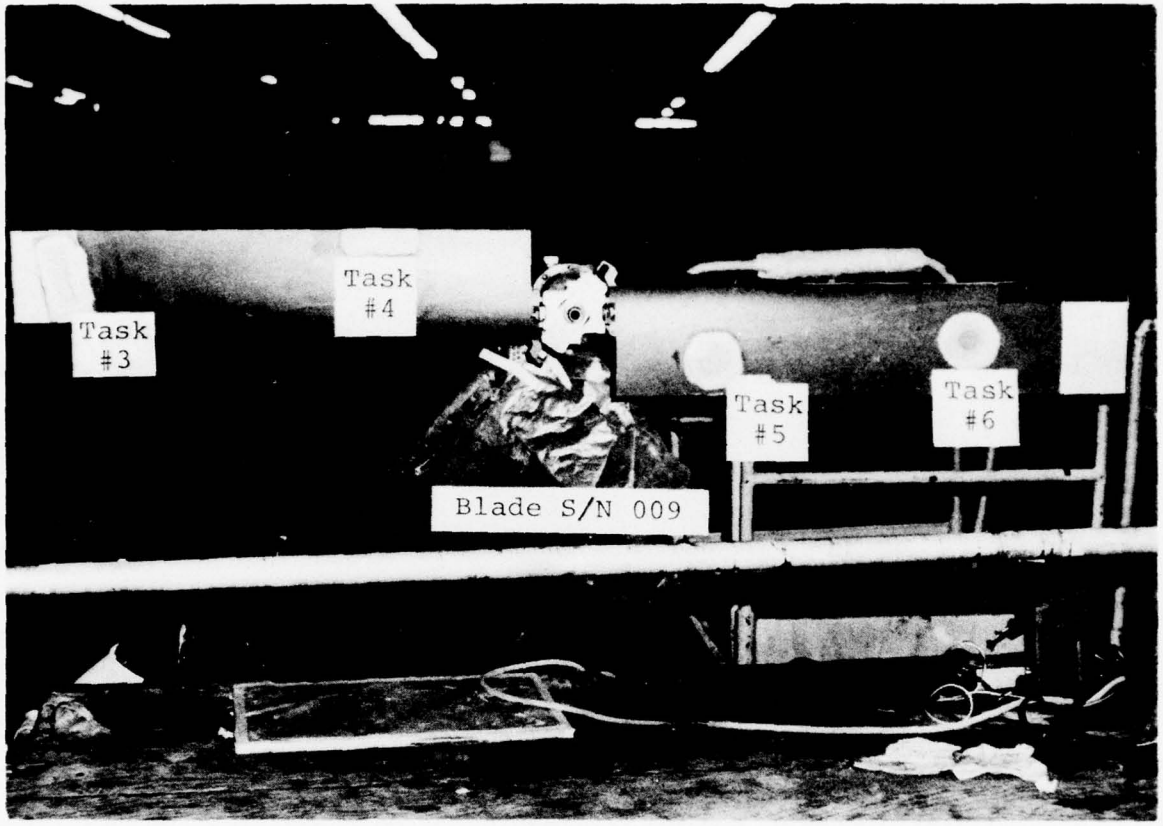

Figure 64. Repaired flight blade specimen (prior to 5 hr whirl).

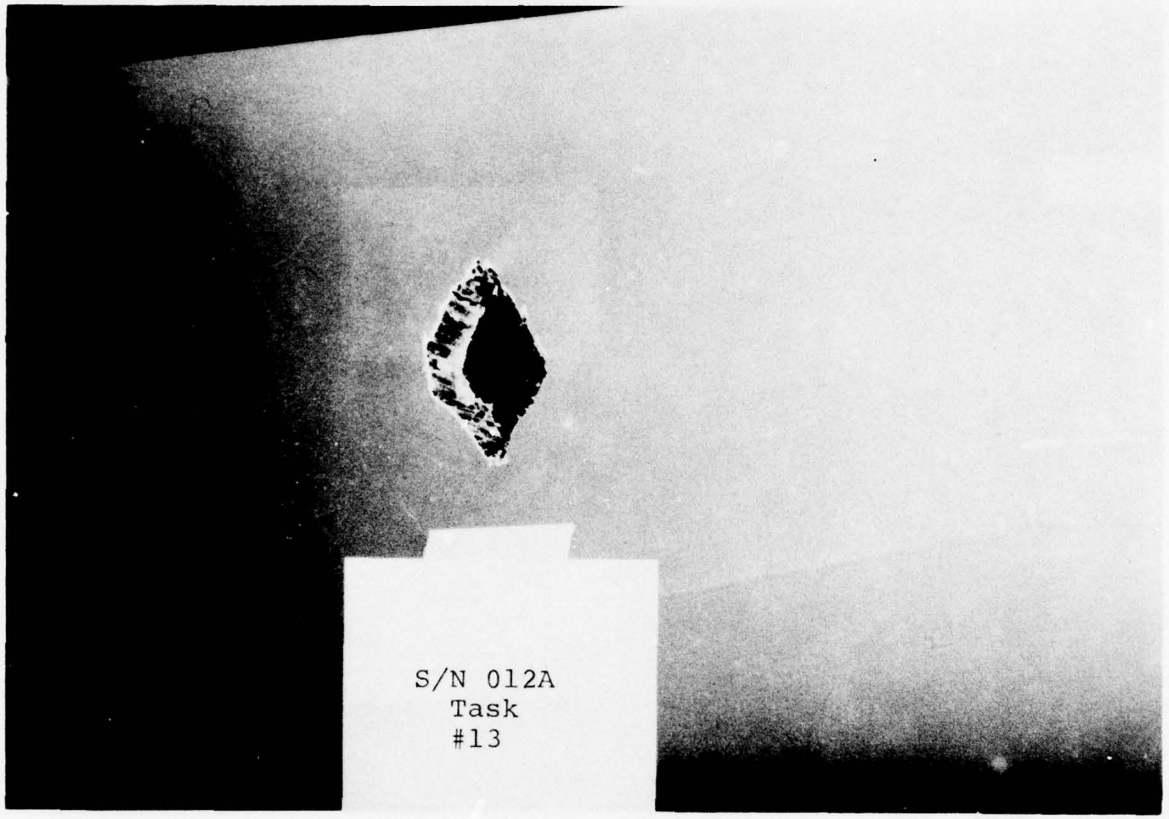

Figure 65. Damaged flight blade specimen.

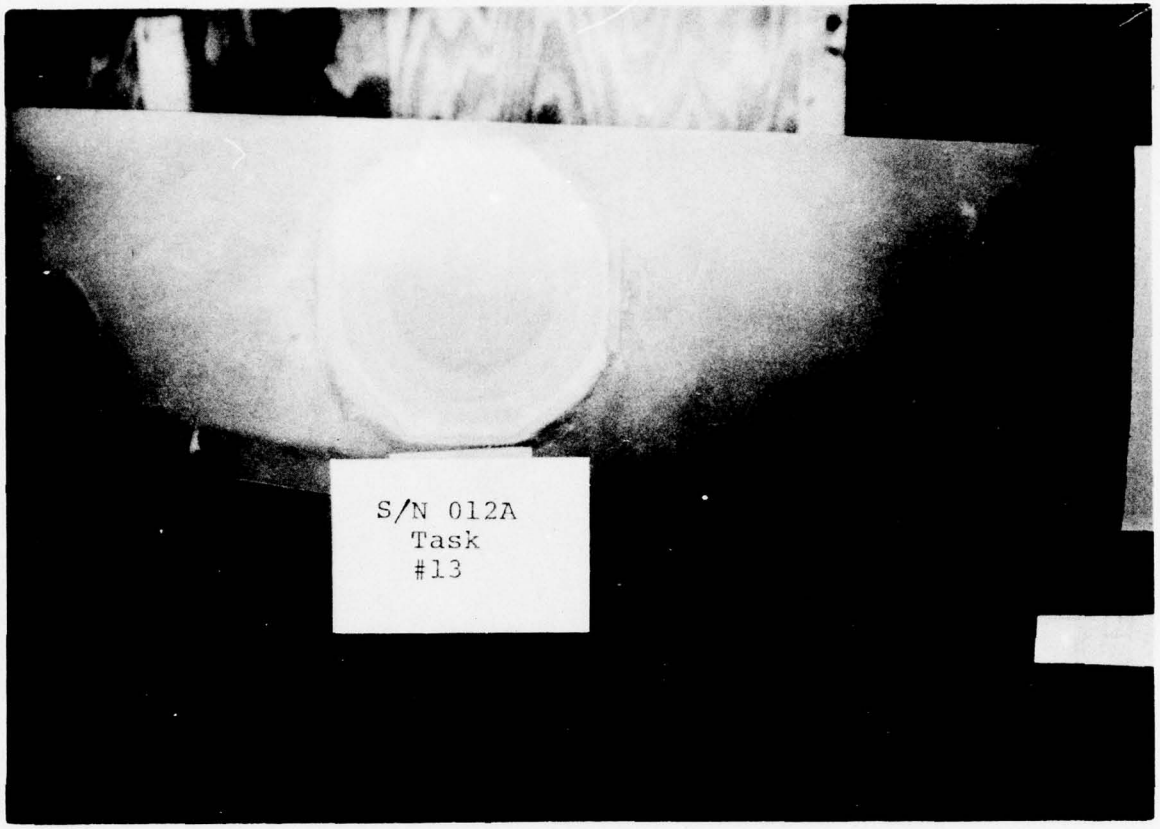

Figure 66. Repaired flight blade specimen.

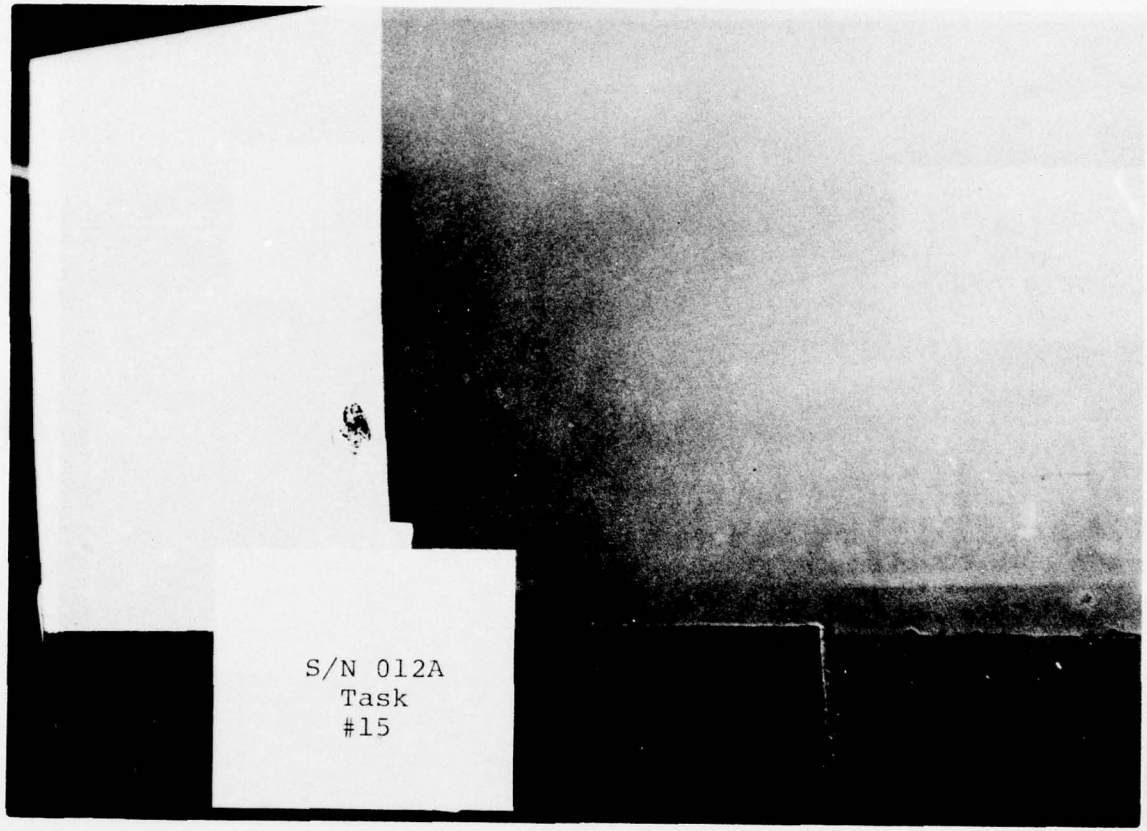

Figure 67. Damaged flight blade specimen, blade punctured.

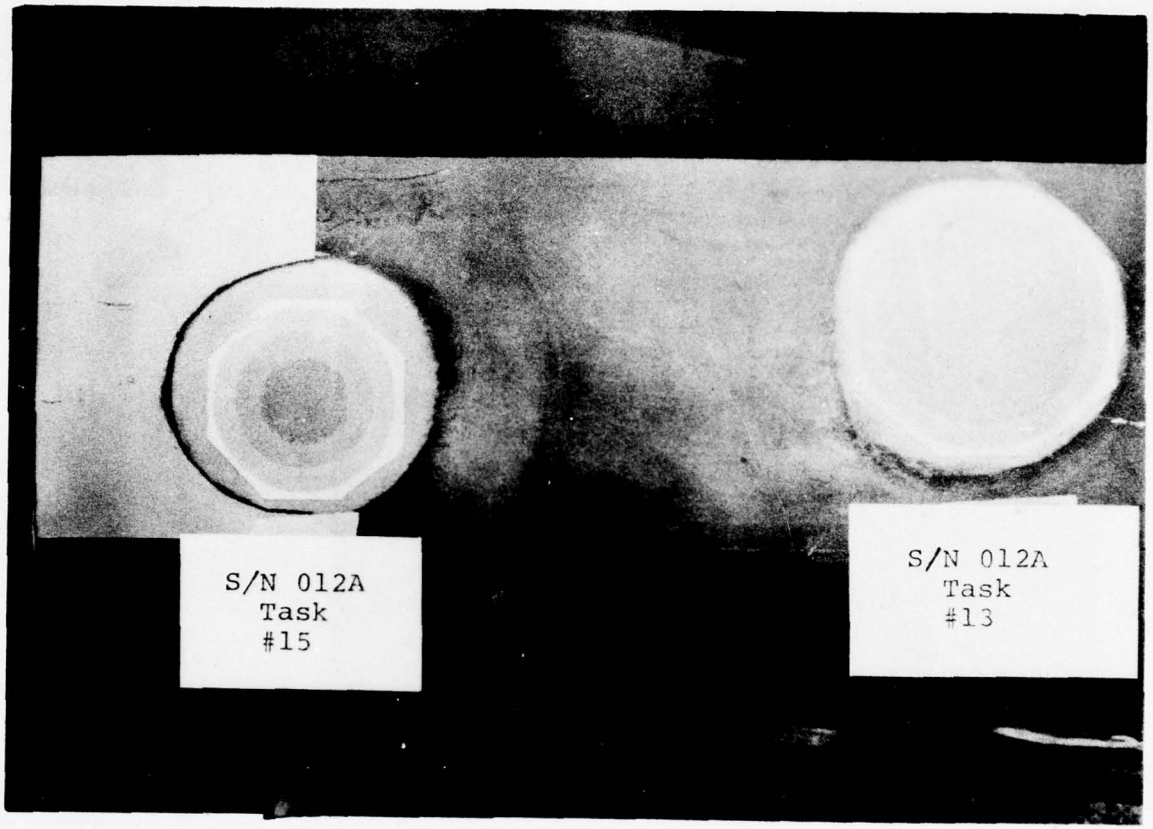

Figure 68. Repaired flight blade specimen.

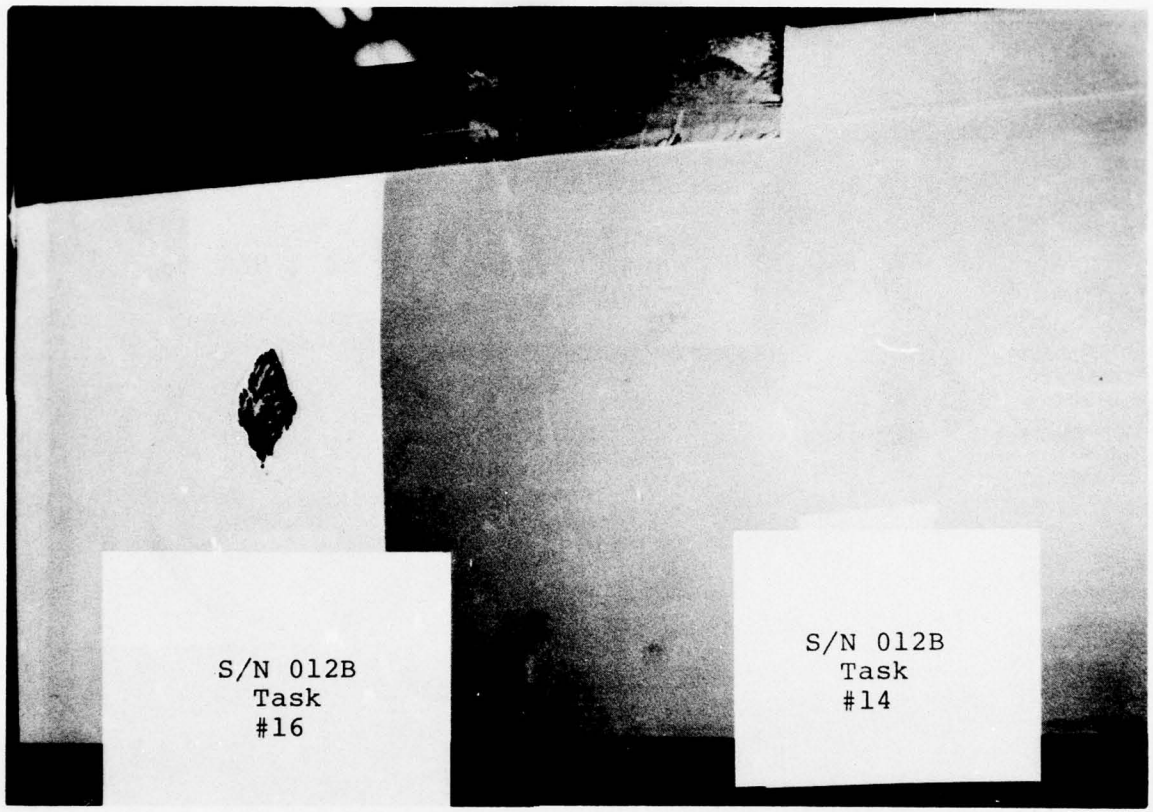

Figure 69. Damaged flight blade specimen, blade punctured and dented.

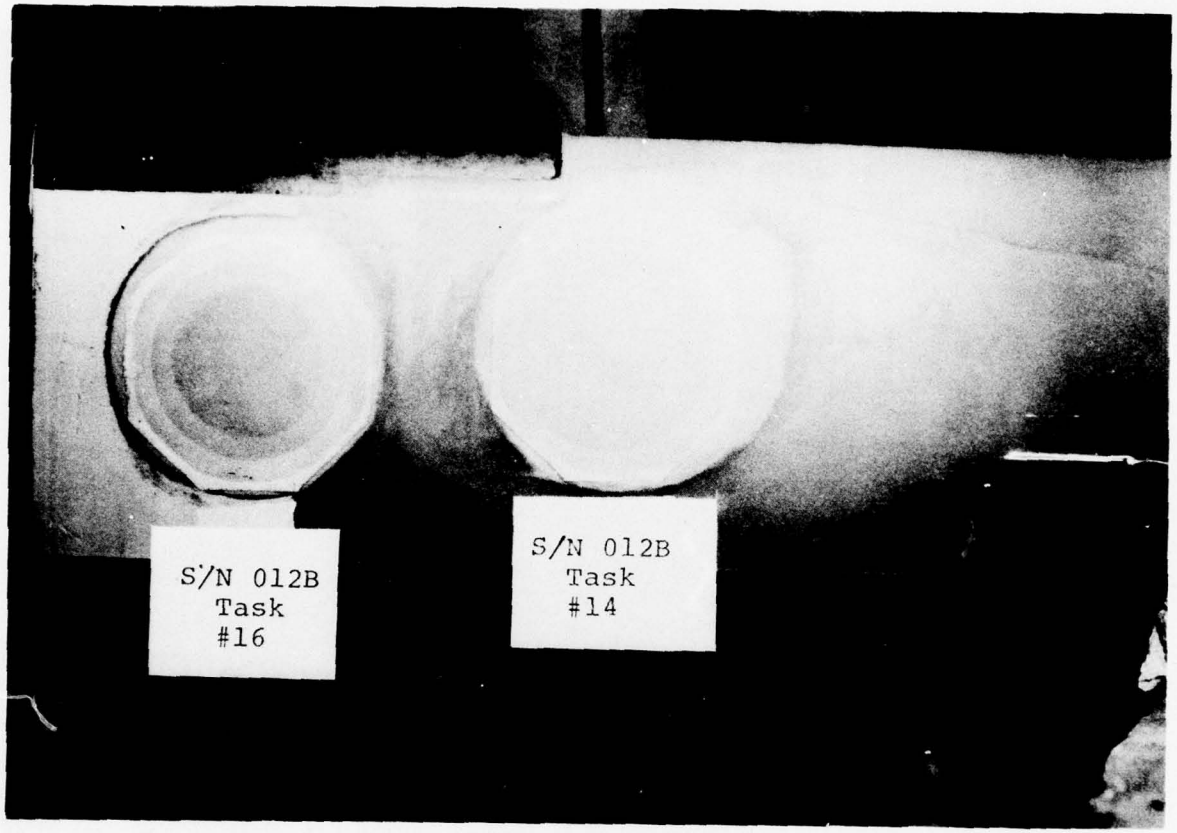

Figure 70. Repaired flight blade specimen.

Upon completion of the repairs to the blades, both rotor assemblies were balanced and then subjected to a 5-hour proof whirl test prior to installation on the aircraft. No blade instrumentation was used during this whirl testing, but whirl rig gearbox vibration levels were monitored so that possible impending problems could be detected. Periodic inspections were made to insure the adequacy of the blade repairs. The pitch angle schedule used during the proof whirl test run at the normal rotor speed was as follows:

Blade Pitch Angle (Deg)	Duration (Min)
-3	2
0	3
3	20
5	220
7	50
10	4
13	1

Inspections performed on the blade assemblies upon completion of the proof whirl tests did not reveal any abnormalities or defects in either of the rotor assemblies.

Instrumentation available during the R&M flight endurance program was the same as provided during the development flight program, shown in Table 10, with additional strain gages being provided to measure stresses at critical locations on the tail pylon as shown in Figure 71.

Using the test results obtained during the development flight program, a flight envelope or flight spectrum was established to insure that the endurance limits of the critical components would not be exceeded. The components considered to be most critical were the tail rotor shaft, the tail rotor gearbox, and the upper portion of the tail pylon in the vicinity of the tail rotor gearbox attachment. Table 22 presents the selected flight spectrum in terms of the percentage of time spent in each flight condition, and Table 23 presents the flight spectrum in terms of the time in minutes spent in each flight condition for a 30-minute flight. Each flight was limited to 30 minutes, and each flight was flown to the flight spectrum shown in Table 23. Inspections were performed after each flight to determine the adequacies of the repairs. The 30-minute flight-inspection cycle was repeated until 20 hours of flight time was accumulated on each rotor assembly.

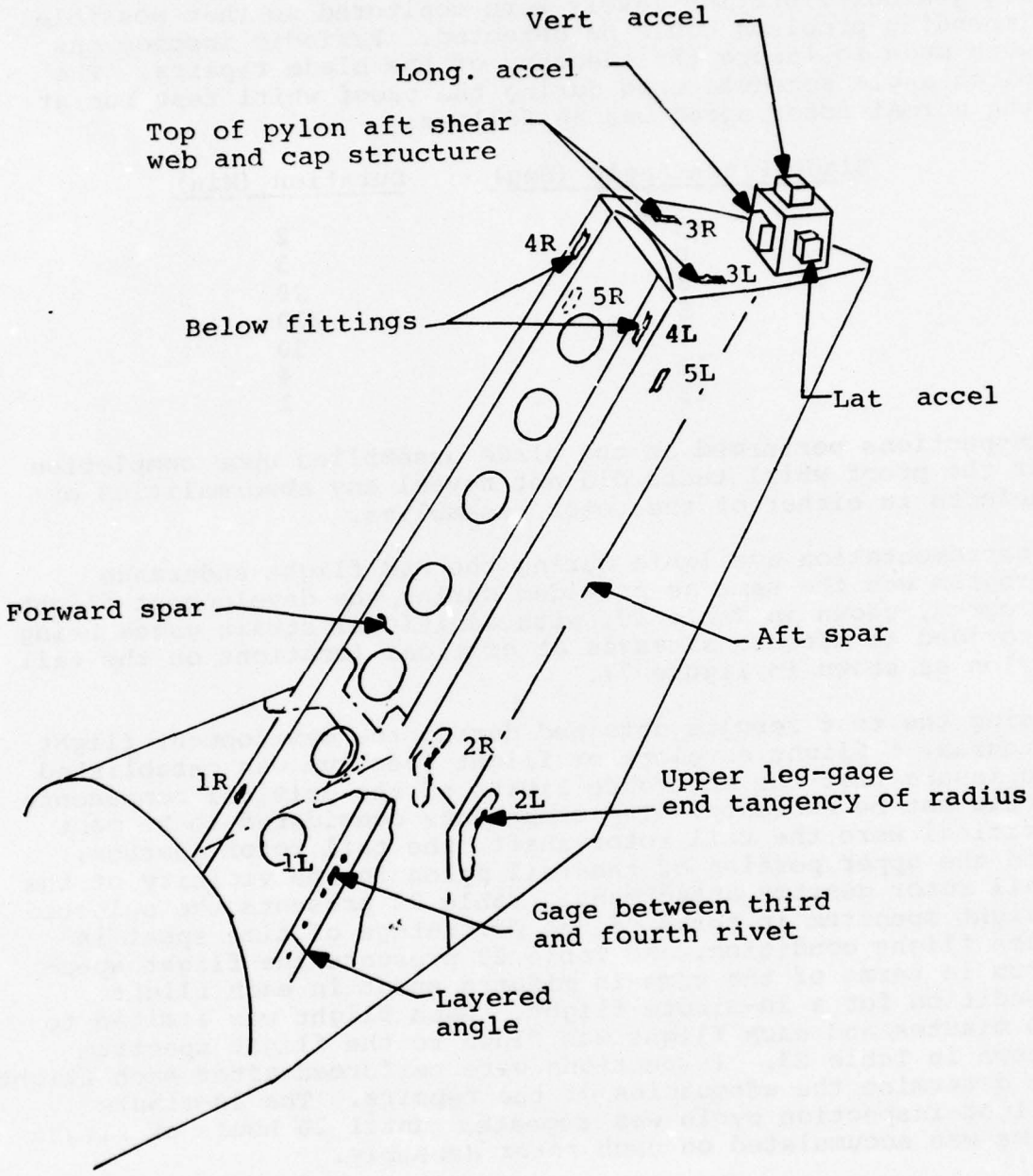

Figure 71. Tail pylon strain gage and accelerometer locations.

TABLE 22. FLIGHT SPECTRUM FOR UH-1 EPBTR R&M FLIGHT TEST PROGRAM

A/S (Knots)	Total Time %	Ascents (1) %	Maneuver (2) %	Descent %	Steady State %
0	6.67	---	---	---	6.67
20	3.33	.832	.166	.832	1.500
40	6.00	1.500	.300	1.500	2.700
60	32.00	8.000	1.600	8.000	14.400
70	21.00	5.250	1.050	5.250	9.450
80	24.00	6.000	1.200	6.000	10.800
85	7.00	---	---	---	7.00
OTALS	100.00	21.582	4.316	21.582	52.520

Notes: (1) Rate of climb and descent to be limited to 500 ft/min maximum.

(2) Angle of bank to be limited to 15 degrees maximum.

TABLE 23. 30-MINUTE FLIGHT SPECTRUM FOR UH-1 EPBTR R&M FLIGHT TEST PROGRAM

A/S (Knots)	Total Time (min)	Ascent Time (min)	Maneuver Time (min)	Descent Time (min)	Steady State Time (min)
0	2.000	---	---	---	2.000
20	1.000	.250	.050	.250	.450
40	1.800	.450	.090	.450	.810
60	9.600	2.400	.480	2.400	4.320
70	6.300	1.575	.315	1.575	2.835
80	7.200	1.800	.360	1.800	3.240
85	2.100	---	---	---	2.100
TOTALS	30.000	6.475	1.295	6.475	15.755

Data recorded during these flights indicated that the resultant vibratory bending moments acting on the tail rotor shaft were below the 3150 inch-pound endurance limit previously established for this component. The highest strains recorded on the tail rotor gearbox were at strain gage Number GB2, Figure 48, and the highest strains recorded on the tail pylon were at strain gage Number 5L, Figure 71.

Figure 72 presents the results of data obtained during the R&M endurance flight program for the two critical strain gage locations and the corresponding test condition during which the strains were recorded. The 277 microinch/inch strain endurance limit for the tail rotor gearbox and the 288 microinch/inch strain endurance limit for the tail pylon are also shown for comparison. As noted, the endurance strain limits were approached but not exceeded during this test program.

Final inspection of the repairs made on the two tail rotor assemblies did not reveal any discrepancies after the completion of this test program.

LIFE-CYCLE COST ANALYSIS

The maintainability indices for the EPBTR will be calculated by the methods discussed below. These methods are used in the contractor's "LCOST" computer program which predicts a subsystem's cost over the duration of the entire system's life cycle. The program uses the flowchart given in Figure 73 to compute life-cycle costs based on statistical analysis of rotor reliability data.

The predicted failure rate for the EPBTR results from comparing this advanced design to the existing tail rotor. Wherever the EPBTR does not employ failure-prone hardware that has a reported failure rate on the present tail rotor, the EPBTR failure rate was considered to be zero. As an example, the present tail rotor's hub trunnion bearings had a failure rate of 39 per million flight hours. Since the EPBTR has no trunnion bearings, this rate becomes zero for the EPBTR. In other cases, the relative damage susceptibility of the two designs was used to adjust failure rates.

As an example, impact tests were performed on representative rotor blade afterbodies, one made of aluminum and the other of fiberglass/nomex. These tests showed that the fiberglass/nomex afterbody had a wider and shallower "crater" than the aluminum afterbody at the same impact kinetic energy. A "damage susceptibility ratio" of .546, based on the curves given in Figures 74 and 75 was applied which decreased the armament

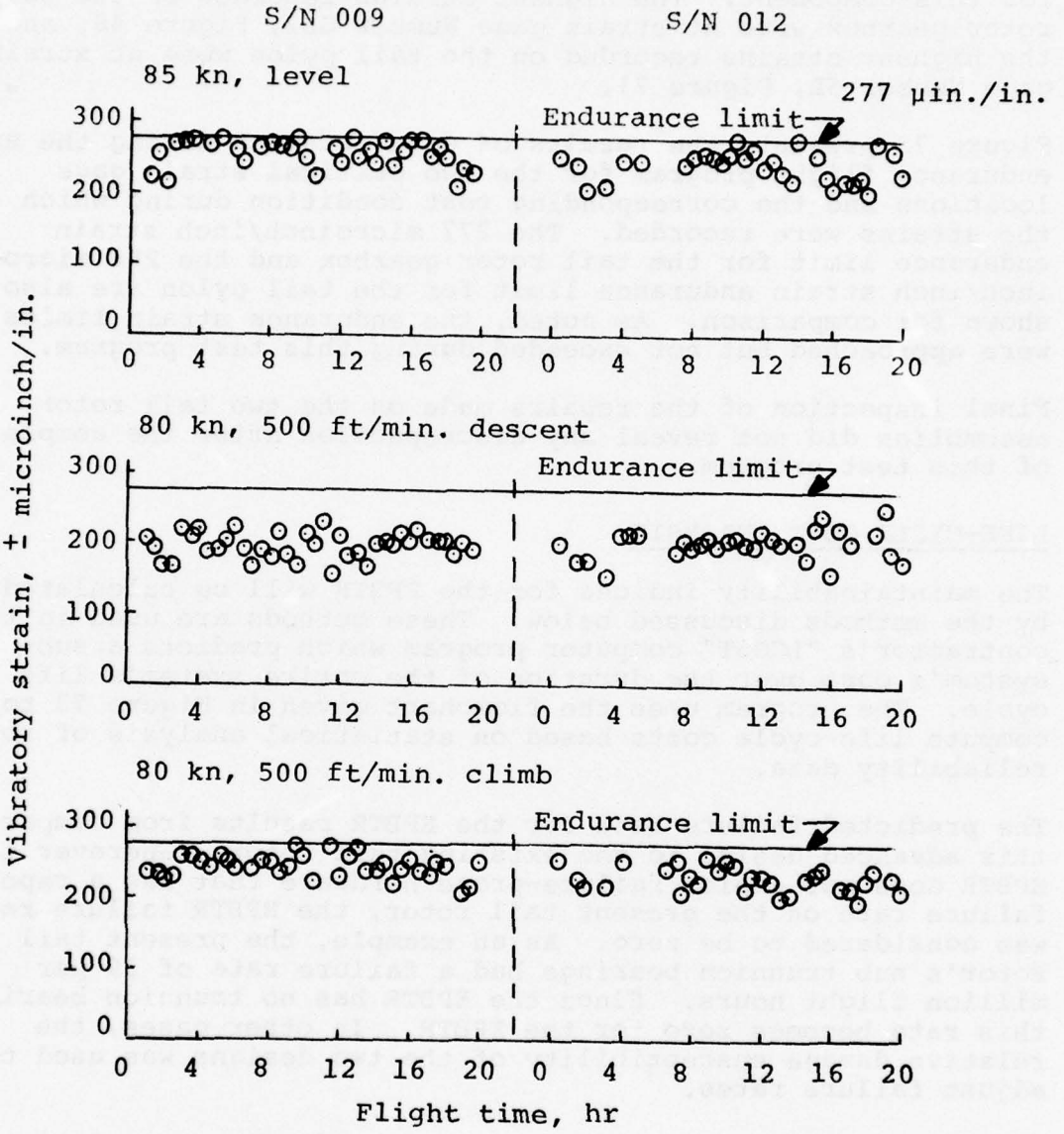

(a) Tail rotor gearbox gage No. 2.

Figure 72. Vibratory strain versus flight time for the tail rotor gearbox and tail pylon.

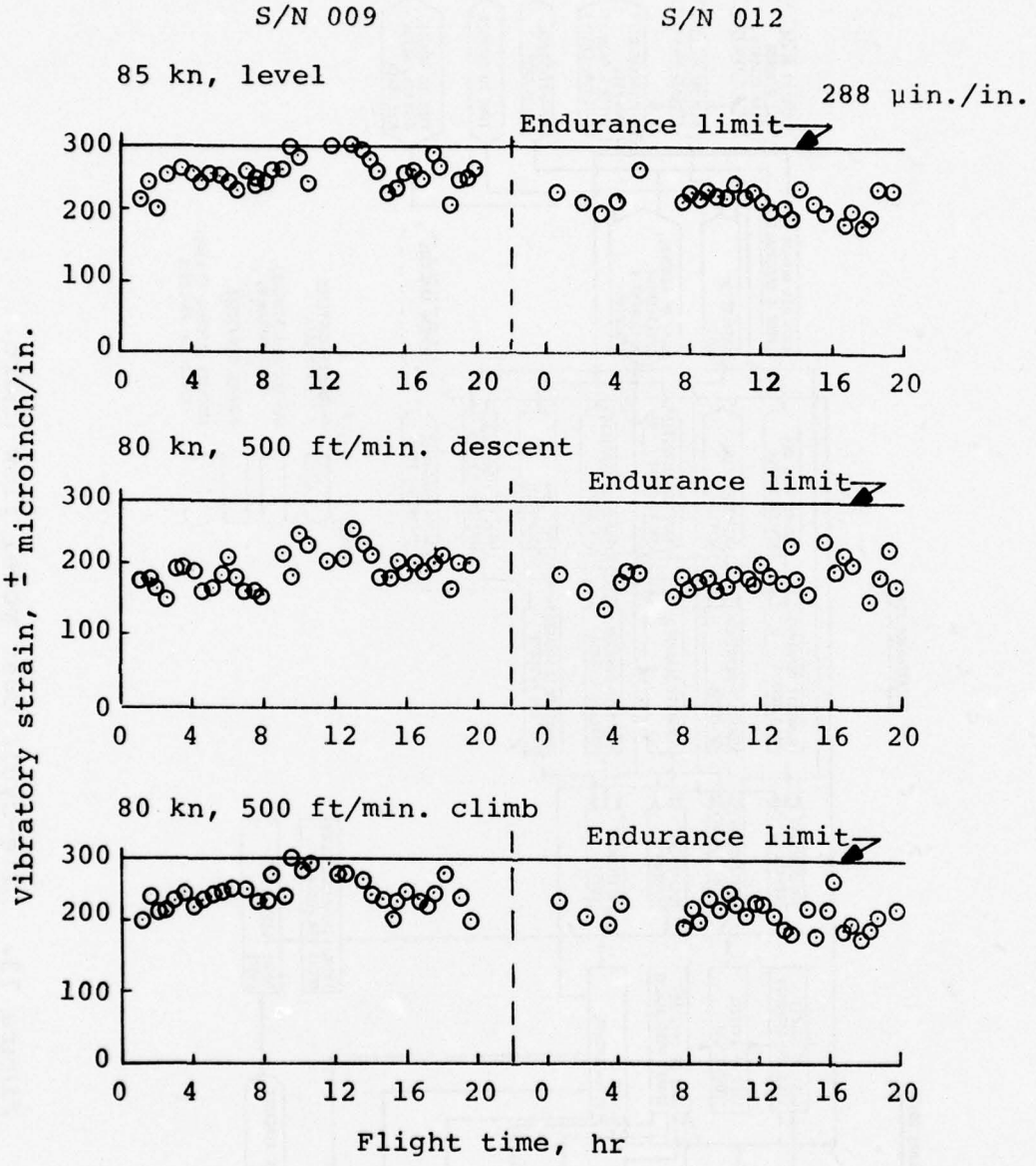

(b) Tail pylon gage No. 5L.

Figure 72. Continued.

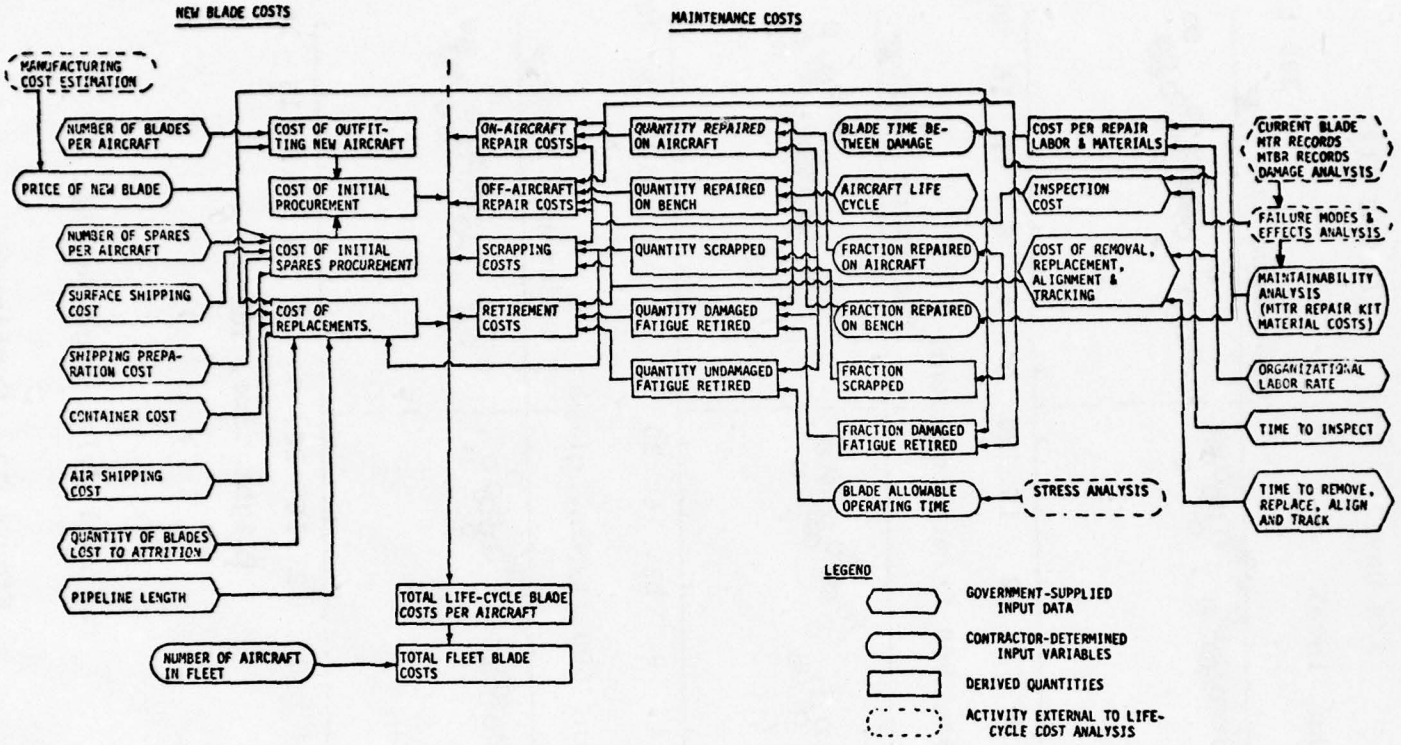

Figure 73. Life-cycle cost model flow chart.

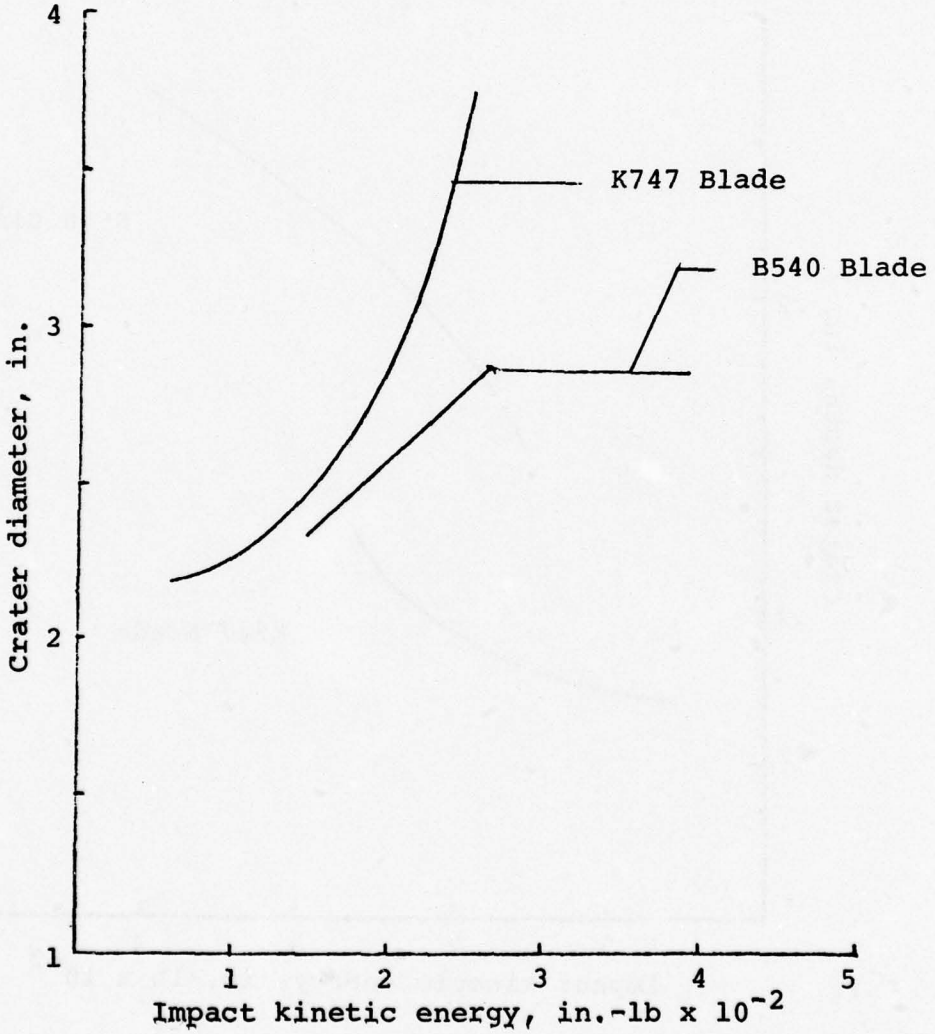

Figure 74. Crater diameter vs impact kinetic energy.

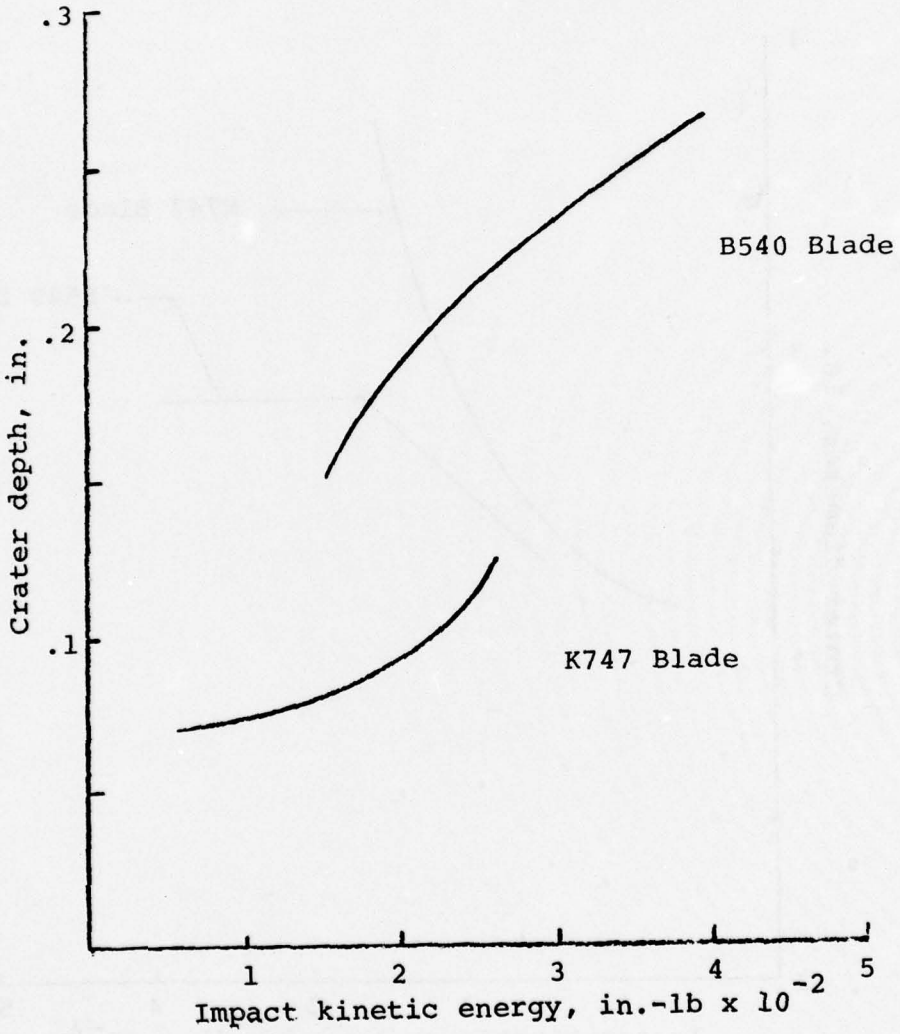

Figure 75. Crater depth vs impact kinetic energy.

debris damage rate from 169 incidents per million flight hours for the existing UH-1 tail rotor to a predicted rate of 92 incidents per million flight hours for the EPBTR. This ratio is the damage diameter on the fiberglass/nomex blade at a representative energy level divided by the damage diameter on the aluminum blade.

The adjustments described above allowed the prediction of the failure rate for the EPBTR blades and hub given in Table 13. Table 14 gave the failure rates for the control hardware. The EPBTR uses the same control hardware as the present rotor with the exception of the crosshead assembly. The EPBTR crosshead is larger than that on the present rotor to move the pitch link attachment farther out from the axis of rotation.

The increased damage susceptibility due to the larger target area is offset by the increased damage resistance due to a part with heavier sections. The predicted failure rate for the EPBTR control subsystem is therefore assumed to be identical to that of the present tail rotor's control subsystem.

Reference 7, Page 98, states that "in the analysis of M&R data (for the existing tail rotor) the secondary failure rates were negligible, accounting for less than 1% of the total primary and secondary failure rates". The EPBTR should not have any design deficiencies which would change its predicted secondary failure rate from that of the present tail rotor. The only secondary failure rate quoted for the present tail rotor is that of 13 failures per million flight hours from frozen pitch link nuts due to bolt corrosion. Considering both the low failure rate and the nature of the failure, it is not unreasonable to relabel this as a primary failure.

Rotor reliability data and repair dispositions are taken from Tables 13, 14 and 24. Table 24 gives the same information as Table 17, but adds repair dispositions.

Costs data quoted in Tables 25 and 26 for the nonteetering EPBTR are based on engineering estimates of production costs for quantity lots.

TABLE 24. DAMAGE AND MAINTENANCE ACTION SUMMARY

Rotor Elements Damaged	Type of Damage	Total No. of Events	Disposition		Type of Repair	Quantity	Work Level
			Repair	Scrap			
Tip Weight Retention	Eroded	5.5	5.5	0	Blend aluminum, refinish	5.5	Organizational
Tip Closure	Dented	2.7	2.7	0	Replace closure	2.7	Depot
	Eroded	1.3	1.3	0	Replace closure	1.3	Depot
Skin	Cracked	16.1	16.1	0	Skin patch, single	16.1	Organizational
	Punctured/Torn	150.9	150.9	0	Skin patch, single	150.9	
	Delaminated	18.3	18.3	0	Skin patch, single	18.3	
	Dented	177.5	177.5	0	Skin patch, single	177.5	
	Eroded	1.1	1.1	0	Skin patch, single	1.1	
	Nicked/Scratched	39.2	39.2	0	Skin patch, single	39.2	
Skin/Core	Cracked	11.0	11.0	0	Skin patch, single	11.0	
	Punctured/Torn	115.0	115.0	0	Skin patch, single Double skin patch Single plug patch Double plug patch	79.0 5.0 18.0 13.0	
	Dented	123.2	123.2	0	Single plug patch Single skin patch	23.2 100.0	
	Bond Failure	17.3	10.0	7.3	Single skin patch	10.0	
Skin/T.E. Spline	Bent, Distorted, Cracked	6.8	5.0	1.8	Vee skin patch	5.0	
	Punctured/Torn	45.3	45.3	0	Blend and Vee skin patch	45.3	
	Dented	11.0	1.0	0	Vee skin patch Blend	6.0 5.0	
	Nicked/Scratched	4.1	4.1	0	Vee skin patch Blend	1.1 3.0	
	Bond Failure	35.6	6.0	29.6	Vee skin patch	6.0	
	Eroded	1.3	1.3	0	Vee skin patch	1.3	Organizational
Skin/Spar/Core	Dented	1.0	0	1.0	---	0	---
	Bond Failure	17.3	0	17.3	---	0	---
Span/Channel	Bond Failure	85.4	0	85.4	---	0	---

TABLE 24 - CONTINUED

Rotor Elements Damaged	Type of Damage	Total No. of Events	Disposition		Type of Repair and Quantity		Work Level
			Repair	Scrap			
Spar/Strap/Channel	Bond Failure	46.0	0	46.00	---	0	---
Spar	Bent/Distorted	9.6	0	9.6	---	0	---
	Punctured/Torn	69.8	0	69.8	---	0	---
	Dented	115.4	70.0	45.4	Blend and alodine Blend, fill and refinish	37.0 33.0	Organizational
	Eroded	9.6	4.8	4.8	Blend and refinish	4.8	
	Nicked/Scratched	28.7	19.0	9.7	Blend and refinish Blend, fill and refinish	10.6 8.4	
Spar/Skin	Eroded	0.2	0.2	0	Blend, alodine	0.2	Organizational
	Bond Failure	10.0	0	10.0	---	0	---
	Punctured/Torn	28.5	0	28.5	---	0	---
	Dented	33.3	16.0	17.3	Blend, skin patch	16.0	Depot
	Nicked/Scratched	7.4	4.0	3.4	Blend, skin patch	4.0	Depot
	Cracked	3.1	0	3.1	---	0	---
Spar/Strap	Punctured/Torn	6.8	0	6.8	---	0	---
Channels/Strap	Bond Failure	28.8	0	28.8	---	0	---
Strap Assembly	Cracked	14.3	0	14.3	---	0	---
	Bond Failure	65.7	0	65.7	---	0	---
Inboard Boot	Eroded	5.5	5.5	0	Replace boot	5.5	Organizational
Pitch Fitting	Eroded	1.3	1.3	0	Refinish	1.3	
Weights and Arms	Eroded	1.3	1.3	0	Refinish	1.3	
Hub	Dented	3.8	3.8	0	Blend, refinish	3.8	Organizational
	Overspeed	197.5	0	197.5	---	0	---
	Worn Oversize	18.0	0	18.0	---	0	---
	Loose/Missing	5.7	5.7	0		5.7	Organizational
		1597.2	876.1	721.1		876.1	

TABLE 25. HELICOPTER LIFE-CYCLE BLADE SET COSTS

EPBTR-UH-1 EPBTR BLADE SET

New Blade Set Price	= $ 1931		
Mean Time Between Failures	= 612	Blade Set Hours	
Field Repairability	= 62.6	Percent	
Main Time Between Maintenance Actions (Blade Set Hours):			
Replacements	= 1486.4		
Removals for Repair or Replacement	= 1448.0		
Repairs	= 960.9		
Damage Replacements	= 1685.6		
Unscheduled Maintenance	= 612		
Scheduled Maintenance (Retirement)	= 12580.6		
All Maintenance Actions	= 583.6		
Blade Sets Events Per Aircraft Life Cycle:			
Number Lost to Attrition	= 0.0000		
Number Fatigue Retired Undamaged	= 0.3974		
Number Repaired on Aircraft	= 5.1411		
Number Repaired off Aircraft in Field	= 0.0000		
Number Scrapped in Field	= 2.9412		
Number Damaged and Retired in Field	= 0.0000		
Number Repaired at Depot	= 0.0892		
Number Scrapped at Depot	= 0.0000		
Number Damaged and Retired at Depot	= 0.0252		
Total Number Damaged and not Repaired	= 2.9664		
Total Number all Replacements	= 3.3638		
Tail Rotor Blade Set Costs Per Aircraft Life Cycle:			
Cost of Initial Procurement:			
New Aircraft Outfitting Cost	= $ 1931.00		
Spares Cost, with Containers	= 619.80		
Spare Repair Materials	= 28.10		
Repair Support Equipment	= 125.00		
Total Initial Procurement Cost	=		$ 2703.90
Cost of Replacement Blade Sets for Those Lost and Unserviceable (Including Shipping and Container Shipping Costs):			
Blade Sets Lost to Attrition	= $ 0.00		
Damaged Blade Sets not Repaired	= 5609.9		
Time-Expired Undamaged Blade Sets	= 785.3		
Total Replacement Cost	=		$ 6395.3
Cost of Maintenance Actions (Labor and Material to Inspect, Remove, Repair, Replace, Align, and Track):			
Field Repair on Aircraft	= $ 547.00		
Field Repair off Aircraft	= 0.00		
Field Scrap	= 21.80		
Field Retirement	= 2.00		
Depot Repair	= 46.20		
Depot Scrap	= 0.00		
Depot Retirement	= 2.40		
Total Maintenance Cost	=		$ 620.00
Total Life-Cycle Blade Set Cost per Aircraft			$ 9719.20
Maintenance Man-Hours/Flight Hour	= .0031		
Blade Set-Related Aircraft Downtime	= 13	Hours	

TABLE 26. HELICOPTER LIFE-CYCLE HUB COSTS

EPBTR-UH-1 HUB

New Hub Price	= $ 469		
Mean Time Between Failures	= 3497 Hub Hours		
Field Repairability	= 34.2 Percent		
Main Time Between Maintenance Actions (Hub Hours):			
Replacements	= 2575.3		
Removals for Repair or Replacement	= 2574.4		
Repairs	= 10239.5		
Damage Replacements	= 5310.7		
Unschedule Maintenance	= 3497.0		
Scheduled Maintenance (Retirement)	= 5000.0		
All Maintenance Actions	= 2057.8		
Hub Events Per Aircraft Life Cycle:			
Number Lost to Attrition	= 0.0000		
Number Fatigue Retired Undamaged	= 1.0000		
Number Repaired on Aircraft	= 0.4876		
Number Repaired off Aircraft in Field	= 0.0007		
Number scrapped in Field	= 0.9395		
Number Damaged and Retired in Field	= 0.0020		
Total Number Damaged and not Repaired	= 0.9415		
Total number all Replacements	= 1.9415		
Tail Rotor Hub Costs Per Aircraft Life Cycle:			
Cost of Initial Procurement:			
New Aircraft Outfitting Cost	= $ 469.00		
Spares Cost, with Containers	= 147.60		
Spare Repair Materials	= 0.00		
Repair Support Equipment	= 0.00		
Total Initial Procurement Cost	=		$ 616.60
Cost of Replacement Hubs for those Lost and Unserviceable (Including Hub Shipping and Container Shipping Costs):			
Hubs Lost to Attrition	= $ 0.00		
Damaged Hubs not Repaired	= 353.00		
Time-Expired Undamaged Hubs	= 478.00		
Total Replacement Cost	=		$ 831.00
Cost of Maintenance Actions (Labor and Material to Inspect, Remove, Repair, Replace, Align, and Track):			
Field Repair on Aircraft	= $ 1.90		
Field Repair off Aircraft	= 0.00		
Field Scrap	= 5.40		
Field Retirement	= 5.00		
Total Maintenance Cost	=		$ 12.30
Total Life-Cycle Hub Cost Per Aircraft			$ 1460.00
Maintenance Man-Hours/Flight Hour	= .0006		
Hub-Related Aircraft Downtime	= 2 Hours		

Maintainability Indices

1. Mean Time Between Removals. Tables 25 and 26 use the mean time between removal for any reasons on the EPBTR. The method of calculation is as follows:

$$\frac{1}{MTBR_{TOTAL}} = \frac{1}{MTBR_1} + \frac{1}{MTBR_2} +++ \frac{1}{MTBR_N} \quad (1)$$

$$\text{where } MTBR_N = \frac{\text{Total Service Hours}}{\text{Total Removals Due to Cause N}} = \frac{T}{R_N} \quad (2)$$

$$\text{thus } \frac{1}{MTBR_{TOTAL}} = \frac{R_1}{T} + \frac{R_2}{T} +++ \frac{R_N}{T} = \frac{\Sigma R_N\text{'S}}{T} \quad (3)$$

$$\text{and } MTBR_{TOTAL} = \frac{\text{Total Service Hours}}{\Sigma \text{ Removals for all Causes}} \quad (4)$$

The life-cycle cost model employs equation (4) to calculate overall mean time between removals. The components of the mean times between various actions are as follows:

Mean time between removals ($MTBR_{rem}$): given in Tables 25 and 26 as "Mean Time Between Removals for repair or replacement".

Mean time between scheduled maintenances ($MTBM_s$): a field repair requiring removal with replacement after repair. Minor repair of the EPBTR can be accomplished on the aircraft while major repairs are performed at depot level. This $MTBM_s$ is not applicable to this rotor.

Mean time between replacements ($MTBR_{repl}$) consists of:

(a) MTB removal for scheduled retirement as given in Tables 25 and 26.

(b) MTB removal due to unscheduled retirement given as replacements in Tables 25 and 26.

(c) MTB overhaul which, because the EPBTR has no required overhauls, does not apply to this rotor.

2. Maintenance Man-Hours per Flight Hour (MMH/FH). The MMH/FH unscheduled are calculated by summing all the various required maintenance actions and multiplying them by their respective times to accomplish according to the following equation:

MMH/FH, Schedule, = $18.175 \div 10^6 = .018$ where 18,176 is the total man-hours allocated to scheduled maintenance as derived in Table 27. The MMH/FH, Unscheduled, is calculated by the cost model as shown in Tables 25 and 26.

3. Mean Time Between Replacements: Mean time between replacements will be calculated according to the formula:

$$MTBR_{repl} = \frac{\text{Total Rotor Hours per A/C Life Cycle}}{\text{Number of blades fatigue retired per life cycle} + \text{Number of damaged blades replaced per life cycle}}$$

4. Mean Time Between Repairs: Mean time between repairs will be calculated according to the formula:

$$MTBR_{REP} = \frac{\text{Total Rotor Hours per A/C Life Cycle}}{\text{Qty repaired on A/C per life cycle} + \text{Qty repaired off A/C in field per life cycle} + \text{Qty repaired at Depot per life cycle}}$$

5. Mean Time Between Unscheduled Maintenance: Mean time between unscheduled maintenance will be calculated according to the formula:

$$MTBM_u = \frac{\text{Total Rotor Hours per A/C Life Cycle}}{\text{Quantity repaired on A/C per life cycle} + \text{Quantity repaired off A/C in field per life cycle} + \text{Quantity repaired at depot per life cycle} + \text{Quantity damaged blades replaced per life cycle}}$$

6. Mean Time Between Scheduled Retirement: Mean time between scheduled retirement will be calculated according to the formula:

$$MTBM = \frac{\text{Total Rotor Hours Per A/C Life Cycle}}{\text{Total number fatigue retired per A/C life cycle (number of blades replaced without damage - number of blades that are retired with the aircraft)}}$$

TABLE 27. SCHEDULED MAINTENANCE

Item	Scheduled Maintenance Action	Frequency 10^6 Hr	M-Hr/ Action	Total M-Hr
S_1	500 hr spring rate check of spar/strap subassembly	2,000	0.7	1,400
S_2	Inspection of spline and cone set each scheduled rotor change	278	0.2	56
R	Scheduled retirement and replacement of rotor	278	1.25	356
D	Daily inspection	633,354	0.022	13,234
I	Intermediate (25 hours)	40,000	0.022	880
P	Periodic (100 hours)	10,000	0.225	2,250
	Totals	685,910		18,176

7. Mean Time Between All Maintenance Actions.

$$MTBM \doteq \frac{\text{Total Rotor Hours per A/C Life Cycle}}{\begin{array}{l}\text{Number of unscheduled repairs per A/C life cycle} \\ + \\ \text{Number of fatigue ret'd per A/C life cycle}\end{array}}$$

Cost Analysis Definitions

1. Number Lost to Attrition. This value is an input to the program which reflects field experience. Table 13 is based on R & M field data and indicates that an unknown number of damaged rotors result in flight loss. Zero will therefore be used in the analysis for number of rotors lost to attrition per aircraft life cycle.

2. Number Fatigue Retired Undamaged. The number fatigue retired undamaged is obtained by determining the fraction of all replaced rotors that are retired undamaged. This quantity, when multiplied by the rotor time between damage replacements, gives a prediction of the time between replacements of undamaged rotors. When divided into total aircraft life, this gives the number of rotors replaced for fatigue retirement per aircraft. Subtracting the number of rotors retired with the aircraft gives the total number of rotors predicted to be fatigue retired undamaged.

3. Numbers Scrapped in Field, Scrapped at Depot and Repaired on Aircraft. These numbers are all calculated by multiplying the fractional repair/scrap dispositions from Table 17 by the total number of damages during the aircraft life cycle.

4. Number Damaged and Retired in Field and at Depot. This number is calculated by assuming a trade-off decision is made which compares the dollar value of the rotor's remaining fatigue life to the dollar cost to repair the damaged rotor.

5. Number Repaired at Depot. The number repaired at depot is calculated by determining the fraction of damage incidents that result in the blade being sent to the depot, but neither scrapped nor fatigue retired.

Inputs to Life-Cycle Cost Model

Table 28 gives the inputs required for the life-cycle cost analysis of the elastic pitch beam for the UH-1D/H helicopter.

TABLE 28. INPUTS TO LIFE-CYCLE COST MODEL

Parameter	Value	Source
Average material cost per on-A/C repair	9.63	Contractor cost estimate
Average material cost per off A/C in field repair	*	
Average material cost per depot repair	15.00	
Cost of repair support equipment	241.25	Cost of router, kit, heat pack, vacuum pump; one complete set for 4 A/C
Fraction damaged and sent to depot	.015	Table 25
Fraction damaged and repaired on A/C	.534	Table 25
Fraction damaged and scrapped at depot	.004	Table 25
Fraction damaged and scrapped in field	.451	Table 25
Allowable rotor life	3600 hr	Estimated
On A/C MTTR, Man-hours	1.21	Calculated from MD** data
Off A/C MTTR, Man-hours	*	
Mean elapsed time for on-A/C repair	1.21	Calculated from MD** data

*Not applicable to the EPBTR UH-1. A value of zero removes the quantity from consideration in the cost model.

**MD = Maintainability Demonstration.

TABLE 28 - CONTINUED

Parameter	Value	Source
Air shipping cost (field to depot/factory)	65	UH-2 data
Container cost	292	UH-2 data
Shipping preparation cost	12	Estimate
Surface shipping cost	65	UH-2 data
Container shipping cost	65	UH-2 data
Depot processing cost	12	Estimate
A/C life cycle	5000 hr	Government-furnished data
Blades per A/C	2	Government-furnished data
Spare blades per A/C	.3	Estimate
Quantity of blades lost to attrition per A/C	0	Estimate
Field labor rate	11.60	Government-furnished data
Depot labor rate	13.50	Government-furnished data
Man-hours to inspect in field	.167	Estimate
Depot MMT repair	4.65 hr	Estimate, see Table 24
Time to remove, replace, realign and track	1.25 hr	Estimate
New blade price	2400	KAC Cost Est
MTBF	626 hr	Table 17
Spares delivery time, months	6	Estimate

Generation of Life-Cycle Cost Analysis

The data from Table 23 was used to generate the life-cycle cost analysis shown in Table 25, for the blade, and Table 26 for the hub.

Table 29, the life-cycle cost estimate for the existing UH-1D/H tail rotor, was developed from Table LX of Reference 7, which is an R & M analysis of the UH-1D/H tail rotor system. Table LX allowed computation of the life-cycle cost of the entire tail rotor system, including the right angle gearbox, control quill, etc.

TABLE 29. EXISTING UH-1 TAIL ROTOR LIFE-CYCLE COST ESTIMATE

	Amount
Cost of tail rotor subsystem delivered on A/C	1,605
Spares cost	14,486
Spares transportation costs	296
Maintenance costs	3,780
Total life-cycle cost of tail rotor subsystem	20,167

The data given in Table 29 of this report has been adjusted to provide an estimate of the life-cycle costs for just the blades and hub of the existing UH-1 tail rotor to allow a direct comparison with the EPBTR cost model output shown in Table 30, Life-Cycle Cost Summary, UH-1 EPBTR.

TABLE 30. LIFE-CYCLE COST SUMMARY, UH-1 EPBTR

Cost Element	Blade Set	Hub	Total
New Item Cost	1,931	469	2,400
Total Initial Procurement Cost (Incl. Spares, Supp. Eq.)	2,865	619	3,484
Spares Cost	7,880	995	8,875
Maintenance Cost	190	32	222
TOTAL COST PER A/C LIFE-CYCLE	10,934	1,645	12,579
ITEM-RELATED A/C DOWNTIME, HR	9	1	10
MMH/FH	.0023	.0005	.0028

Comparison of Tables 29 and 30 shows that, due to increased MTBF and simplicity of repair, the EPBTR's maintenance costs are a small fraction of the present tail rotor's maintenance cost. The increased repairability is also evident in the reduced spares cost. When all of these factors are taken into account, it is obvious that the higher acquisition cost and the necessity to scrap the complete EPBTR blade assembly rather than a blade or a hub, in the event of nonrepairable damage, are more than offset by the improved fatigue life, MTBF and repairability. Comparing the total life-cycle cost of the existing UH-1 tail rotor (Table 29) with that obtained for the EPBTR (Table 30) it can be predicted that the savings in overall life-cycle cost for the EPBTR over the present rotor is $7588 or 38%.

CONCLUSIONS

1. The Elastic Pitch Beam tail rotor for the UH-1 helicopter has been demonstrated as feasible and practical through a series of bench tests, whirl tests and flight tests.

2. The reliability and maintainability of the EPBTR was successfully demonstrated during the R&M portion of this program wherein several intentionally damaged EPBTR blades were whirl tested as damaged, field repaired and subsequently whirl tested and flight tested.

3. The increased hub moments related to rigid connection of the EPBTR hub to the shaft limited the flight envelope of the UH-1 helicopter somewhat due to increased stresses imposed on the tail rotor shaft, tail rotor gearbox, and tail pylon. Redesign of the rotor and installation would eliminate these limitations.

4. The EPBTR, designed specifically as a nonteetering tail rotor system with emphasis placed on restricting the magnitude of the hub moments being transferred to the tail rotor shaft, tail rotor gearbox, and tail pylon, can be cost effective when compared to the standard UH-1H tail rotor. Improvements in reliability and maintainability coupled with the elimination of the teeter axis components are the prime factors influencing this conclusion.

5. Applicable results from the related EPBTR program reported in Reference 3 are:

   a. The damage resistance and ballistic tolerance of the EPBTR was demonstrated by injection of maple dowels, gravel and crushed stone into the path of the whirling rotor and by the whirl testing of ballistic damaged rotor assemblies without failure.

   b. Results of the EPBTR leading edge erosion testing indicated that polyurethane material provided the maximum cost effectiveness on the basis of maximum sand abrasion resistance, lowest weight, field repairability, and low cost.

RECOMMENDATIONS

It is recommended that a production design of the elastic pitch beam tail rotor for a service helicopter be pursued to incorporate design improvements indicated by the present program so that a fully operational elastic pitch beam tail rotor system may be realized. Among the recommended improvements are:

1. Redesign the teetering EPBTR, specifically as a nonteetering rotor system to obtain design simplification through the elimination of teeter axis components. Improvements in cost, reliability and maintainability may thus be realized by a reduction in the number of components to be retained in the Government's inventory and by eliminating the troublesome teeter bearings. A concentrated effort must be made to minimize the increase in hub moments, associated with blade flapping, that are applied to the tail rotor shaft, tail rotor gearbox and tail pylon as a result of the teeter axis elimination so that flight envelope restrictions, imposed during the present program with the teeter freedom locked out, will not be required. Methods that may be used to limit the effects of these hub moments to, or below, the respective endurance limits of the tail rotor shaft, tail rotor gearbox, and tail pylon include:

    a. Reducing the out-of-plane bending stiffness of the elastic pitch beam.

    b. Reducing the effective out-of-plane hinge offset of the EPB by decreasing the spanwise length of the hub and by decreasing the out-of-plane bending restraint of the EPB at its attachment to the hub.

    c. If need be, providing additional out-of-plane flexibility between the hub and shaft.

2. Reduce or eliminate the delta-three axis, reduce the out-of-plane bending natural frequency to 1.10/rev or lower, and increase the inplane bending natural frequency to approximately 1.7/rev to improve the dynamic response of the EPBTR by minimizing the possible occurrence of instability problems associated with a coupling of teeter motion and symmetric inplane bending, or with a coalescence of inplane and out-of-plane natural frequencies and bending modes. A

AD-A035 175 KAMAN AEROSPACE CORP BLOOMFIELD CONN F/G 1/3
ELASTIC PITCH BEAM TAIL ROTOR.(U)
DEC 76 P F MALONEY, J D PORTERFIELD DAAJ02-72-C-0006
UNCLASSIFIED R-1399 USAAMRDL-TR-76-35 NL

3 OF 3
ADA035175

END
DATE FILMED
3-77

decrease in the out-of-plane natural frequency and an increase in the inplane natural frequency may be obtained by a redesign of the EPB. Cross-sectional dimensions of the individual EPB straps, planform shape of the EPB, and/or the combination of composite materials selected for use in the layup of the EPB are factors that may be varied to obtain the desired natural frequencies.

3. Investigate the improvement in overall cost effectiveness of the EPBTR system resulting from a redesign of the airfoil section attachment to the elastic pitch beam to provide a method for readily replacing individual airfoil sections.

REFERENCES

1. Maloney, Paul F., Clark, Frank B., McIntyre, Hugh H., APPLICATION OF DIRECTED GLASS FIBER REINFORCED PLASTIC TO HELICOPTER TAIL ROTOR ASSEMBLY, Kaman Aerospace Corporation, Bloomfield, Connecticut; USAAVLABS Technical Report TR 68-29, U.S. Army Aviation Materiel Laboratories, Fort Eustis, Virginia, June 1968, AD 674252.

2. Maloney, Paul F., Clark, Frank B., and McIntyre, Hugh H., STUDY AND EVALUATION OF DIRECTED GLASS FIBER REINFORCED PLASTIC HELICOPTER TAIL ROTOR ASSEMBLY, Kaman Aerospace Corporation, Bloomfield, Connecticut; USAAVLABS Technical Report TR 69-43, U.S. Army Aviation Materiel Laboratories, Fort Eustis, Virginia, October 1969, AD 863062.

3. Falcone, A.S., Clark, F.B., and Maloney, P.F., ELASTIC PITCH BEAM TAIL ROTOR OPERATIONAL SUITABILITY INVESTIGATION, Kaman Aerospace Corporation, Bloomfield, Connecticut; USAAMRDL Technical Report TR-74-60, U.S. Army Air Mobility Research and Development Laboratory, Fort Eustis, Virginia, July 1974, AD 784595.

4. J. Childs, FATIGUE LIFE SUBSTANTIATION OF DYNAMIC COMPONENTS OF UH-1B & UH-1E HELICOPTERS INCORPORATING THE MODEL 540 DOOR-HINGE ROTOR, Bell Report Number 204-099-297, Bell Helicopter Company, Fort Worth, Texas, June 1, 1966.

5. Lemnios, A.Z. and Smith, A.F., AN ANALYTICAL EVALUATION OF THE CONTROLLABLE TWIST ROTOR PERFORMANCE AND DYNAMIC BEHAVIOR, Kaman Aerospace Corporation, Bloomfield, Connecticut; USAAMRDL Technical Report 72-16, U.S. Army Air Mobility Research and Development Laboratory, Eustis Directorate, Fort Eustis, Virginia, May 1972, AD 747808.

6. Frengley, Michael C., DEVELOPMENT PROGRAM FOR FIELD-REPAIRABLE/EXPENDABLE MAIN ROTOR BLADES, PHASE I - PRELIMINARY DESIGN, Kaman Aerospace Corporation, Bloomfield, Connecticut; USAAMRDL Technical Report TR-73-102, U.S. Army Air Mobility Research and Development Laboratory, Fort Eustis, Virginia, April 1974, AD 783444.

7. Knudsen, George E., and Carr, Patricia V., R&M DATA ANALYSIS OF THE UH-1/AH-1 TAIL ROTOR SYSTEM, Bell Helicopter Company, Fort Worth, Texas; USAAMRDL Technical Report TR-74-11, U.S. Army Air Mobility Research and Development Laboratory, Fort Eustis, Virginia, April 1974, AD 782858.

APPENDIX A

REPAIR PROCEDURES FOR THE

UH-1 ELASTIC PITCH BEAM TAIL ROTOR BLADE

This appendix establishes the repair limits and the detailed repair procedures used to effect field level repairs on the UH-1 EPBTR blade. Table A-1 presents the configurations of the fiberglass patches and Nomex honeycomb core plugs to be used for repairing damaged blades. Table A-2 presents a list of items included in each individual repair kit and Table A-3 presents the consumable materials used during the repair process. Tools and equipment required to make a specific repair are listed in Table A-4. As the repair made to a blade involves adding weight to it, a balance adjustment must be made to insure the proper operation of the repaired system. Table A-5 indicates the number of trim weight washers, Figure A-1, that must be removed at the outboard blade tip to compensate for the added weight of the repair and also the location of the repair.

1 REPAIR LIMITS (Reference Figure A-2)

1.1 Elastic Pitch Beam Assembly (Fiberglass)

1.1.1 Nicks, dents, cracks and delaminations regardless of size and location are cause for blade scrappage.

1.2 Leading-Edge C-Section Spar (Aluminum)

1.2.1 Bent, distorted, punctured, torn or a bond failure requires the blade to be scrapped.

1.2.2 Smooth dents not over .100 inch deep, .25 inch wide and .75 inch long are acceptable as is. Dents which are .050-.100 inch deep and over .25 inch wide and .75 inch long must be filled in accordance with the Repair Procedures. Dents exceeding .100 inch deep or causing fracture will require blade scrappage.

1.2.3 Erosion in excess of a depth of .020 inch is cause to scrap the blade.

1.2.4 Corrosion may be reworked by smooth blending up to .020 inch deep from Sta. 40 to tip and to .010 inch deep from Sta. 40 inboard to the root end fitting. Corrosion extending into the bond area of the skin and spar is cause for blade scrappage.

TABLE A-1. BLADE REPAIR KITS

Kit No.	Description	Reference Number
1	4-Inch-Diameter Skin Patch and Related Consumable Materials	K27-120-1
2	5-1/2-Inch-Diameter Skin Patch and Related Consumable Materials	K27-120-3
3	2-1/2- x 4-Inch Rectangle Skin Patch and Related Consumable Materials	K27-120-5
4	2-1/2- x 6-Inch Rectangle Skin Patch and Related Consumable Materials	K27-120-7
5	2-1/2-Inch x 4-Inch-Long Vee Shape Skin Patch	K27-120-9
6	2-1/2-Inch x 6-Inch-Long Vee Shape Skin Patch	K27-120-101
7	2-Inch-Diameter x 1/4-Inch-Deep Plug/4-Inch-Diameter Patch and Related Consumable Materials	K27-120-103
8	2-Inch-Diameter x 1/2-Inch-Deep Plug/4-Inch-Diameter Patch and Related Consumable Materials	K27-120-105
9	3-1/2-Inch-Diameter x 1/4-Inch-Deep Plug/5-1/2-Inch-Diameter Patch and Related Consumable Materials	K27-120-107
10	3-1/2-Inch-Diameter x 1/2-Inch-Deep Plug/5-1/2-Inch-Diameter Patch and Related Consumable Materials	K27-120-109
11	3-1/2-Inch-Diameter x 1-3/4-Inch-Deep Plug/5-1/2-Inch-Diameter Patch and Related Consumable Materials	K27-120-201

TABLE A-2. ITEMS CONTAINED IN REPAIR KITS

QTY	UNIT	ITEM	DESCRIPTION	SPEC	K27-120 Repair Kit Dash Number										
					1	3	5	7	9	101	103	105	107	109	201
1	ea	Skin Patch	4-In.-Dia		X										
1	ea	Skin Patch	5-1/2-In.-Dia			X									
1	ea	Skin Patch	2-1/2- x 4-In. Rectangle				X								
1	ea	Skin Patch	2-1/2- x 6-In. Rectangle					X							
1	ea	Vee Skin Patch	2-1/2- x 4-In. Segment						X						
1	ea	Vee Skin Patch	2-1/2- x 6-In. Segment							X					
1	ea	Plug/Patch	2-In. Plug x 1/4-In. Deep/4-In. Patch								X				
1	ea	Plug/Patch	2-In. Plug x 1/2-In. Deep/4-In. Patch									X			
1	ea	Plug/Patch	3-1/2-In. Plug x 1/4-In. Deep/5-1/2 In. Patch										X		
1	ea	Plug/Patch	3-1/2-In. Plug x 1/2-In. Deep/5-1/2 In. Patch											X	
1	ea	Plug/Patch	3-1/2-In. Plug x 1-3/4-In. Deep/5-1/2-In. Patch												X
1	ea	Wafer*	2-In.-Dia								X	X			
1	ea	Wafer*	3-1/2-In.-Dia										X	X	
1	ea	Template	For 2-In. I.D./4-In. O.D. Patch		X						X	X			
1	ea	Template	For 3-1/2-In. I.D./5-1/2-In. O.D.			X							X	X	X
1	ea	Template	For 2-1/2- x 4-In. Rectangular Patch				X								
1	ea	Template	For 2-1/2- x 6-In. Rectangular Patch					X							
1	ea	Template	For 2-1/2- x 4-In. Vee Skin Patch						X						
1	ea	Template	For 2-1/2- x 6-In. Vee Skin Patch							X					
1	ea	Plastic Gloves	Light Weight, Medium		X	X	X	X	X	X	X	X	X	X	X
1	ea	Cotton Gloves	Light Weight, Medium		X	X	X	X	X	X	X	X	X	X	X
1	ea	Paint Brush	1-In. Wide		X	X	X	X	X	X	X	X	X	X	X
1	ea	Masking Tape	1-In. Wide x 10-Ft Long		X	X	X	X	X	X	X	X	X	X	X
3	sq yd	Cheesecloth		CCC-C-440	X	X	X	X	X	X	X	X	X	X	X
1	ea	Wooden Spatula	Tongue Depressor	LLL-S-007.20	X	X	X	X	X	X	X	X	X	X	X
3	ea	Abrasive Paper	180 Grit, 9 x 11	P-P-121 & P-P-101	X	X	X	X	X	X	X	X	X	X	X
3	ea	Abrasive Paper	240 Grit, 9 x 11	P-P-121 & P-P-101	X	X	X	X	X	X	X	X	X	X	X
2	ea	Peel Ply	Segment		X	X	X	X	X	X	X	X	X	X	X
2	ea	Tab Washer	K27-115-11		X	X	X	X	X	X	X	X	X	X	X
2	ft	Pliable Sealant	Roll		X	X	X	X	X	X	X	X	X	X	X
1	ea	Teflon	Film	Dupont #50R	X	X	X	X	X	X	X	X	X	X	X
1	ea	Adhesive	Two-Part Arline Systems Thixotropic Paste	Airline Sys AS-401-1	X	X	X	X	X	X	X	X	X	X	X

*Fiberglass Fabric Disk, .010-In.-Thick Impregnated with Epoxy Resin

TABLE A-3. LIST OF CONSUMABLE MATERIALS

Item No.	Nomenclature	Color No.	Specification
	PAINTS, PRIMERS, THINNERS AND MARKING COMPOUNDS		
	NOTE: All color numbers to be in accordance with Fed Std 595.		
100	Primer Coating, Epoxy-Polyamide, Chemical and Solvent Resistant		MIL-P-23377
101	Lacquer, Acrylic, Olive Drab (Camaflage)	34087	MIL-L-81352
102	Lacquer, Acrylic, Insigna White (Gloss)	17875	MIL-L-81352
103	Lacquer, Acrylic, Orange Yellow (Gloss)	13538	MIL-L-81352
104	Methyl-Isobutyl-Ketone		TT-M-268
105	Toluol		TT-T-548
	ADHESIVES, CEMENTS AND SEALING COMPOUNDS		
200	Adhesive, Two Part Thixotropic Paste Airline System's Number AS-401-1		MIL-S-8802 Class B
201	Sealer		Kaman Material Data Sheet A0367
202	Adhesive Paste Epoxy (two part), Pittsburgh Plate Glass Co. Bondmaster M777		8615A/BX
203	Uralane Filler (Two-Part)		

TABLE A-3 - CONTINUED

Item No.	Nomenclature	Specification
	CHEMICALS, COATINGS AND CLEANING COMPOUNDS	
300	Methyl-Ethyl-Ketone	TT-M-261
301	Corrosion Preventive Compound, Hot Application, Petrolatum	MIL-C-11796 Class 3
302	Alodine Solution	
303	Thinner, Dope and Lacquer Nitrate	TT-T-266
304	Soap, Toilet, White, Floating	P-S-620
305	Tongue Depressor	LLL-S-007-20
	ABRASIVES, PAPER, PLASTICS AND MISCELLANEOUS	
500	Tape, Masking	UU-T-106
501	Cloth Crocus	P-C-458
502	Abrasive Paper, No. 0000, 000, 180, 220, 240, 320, 360, 400, and 420 Grit, Wet or Dry Type, Commercial Grade	P-P-121 and P-P-101
503	Cloth, Cheesecloth Type 2 Class B	CCC-C-440

TABLE A-4. TOOLS AND EQUIPMENT REQUIRED FOR REPAIRS

ITEM	REPAIR REQUIRED								
	Skin Patches	Plug/Skin Patches (One Side Only)	Plug/Skin Patches (Both Sides)	Blending Nicks and Scratches	Alodine on Aluminum	Spar Dent Filling	Abrasion Strip Hole Filling	Paint Touch-Up	Blade Balancing
Vacuum/Heat Pack	X	X	X						
Vacuum Air Source, 28 In. Hg Min	X	X	X						
Electrical Source, 110 Volt AC	X	X	X						
Electrical Extension Cord, 16-3	X	X	X						
Safety Goggles	X	X	X	X	X	X	X	X	
Router		X	X						
Router Base		X	X						
Router Pads			X						
Router Bit, Carbide, 1/4-In. Dia, 1-1/2-In. Lg		X	X						
Vacuum Cleaner		X	X						
Coarse Hacksaw Blade Segment		X	X						
Depth Micrometer, Depth Gage, or Dial Indicator				X				X	
Hand File				X					
Abrasive Wheel, (Optional)				X					
Compressed Air					X			X	
Paint Sprayer								X	
Heat Lamp						X	X		
Wrench, 5/16-In. Hex Deep Socket									X
Torque Wrench, 0-300 In.-Lb									X

TABLE A-5. BLADE BALANCE CHART

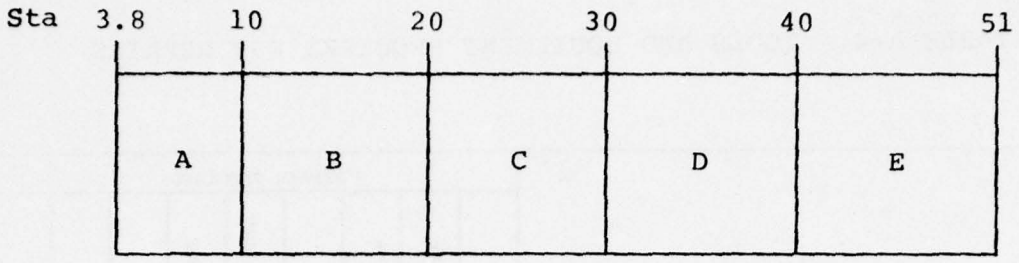

Patch	Number of AN 960-416 Washers to be Removed From the Tuning Stud to Adjust Blade Balance				
	Zone A	Zone B	Zone C	Zone D	Zone E
2.5 x 4 (Skin)	1	1	2	4	5
4 Dia (Skin)	1	2	4	5	7
5.5 Dia (Skin)	2	5	7	11	13
2.5 x 6 (Skin) 2 Dia (Plug)	1	3	5	6	8
2.5 x 4 (Vee Skin)	2	2	4	8	10
2.5 x 6 (Vee Skin)	2	6	10	12	16
3.5 Dia (Plug)	3	7	11	16	20
3.5 Dia (Through Plug) and 5.5 Dia Skin Combination	5	12	18	24	33

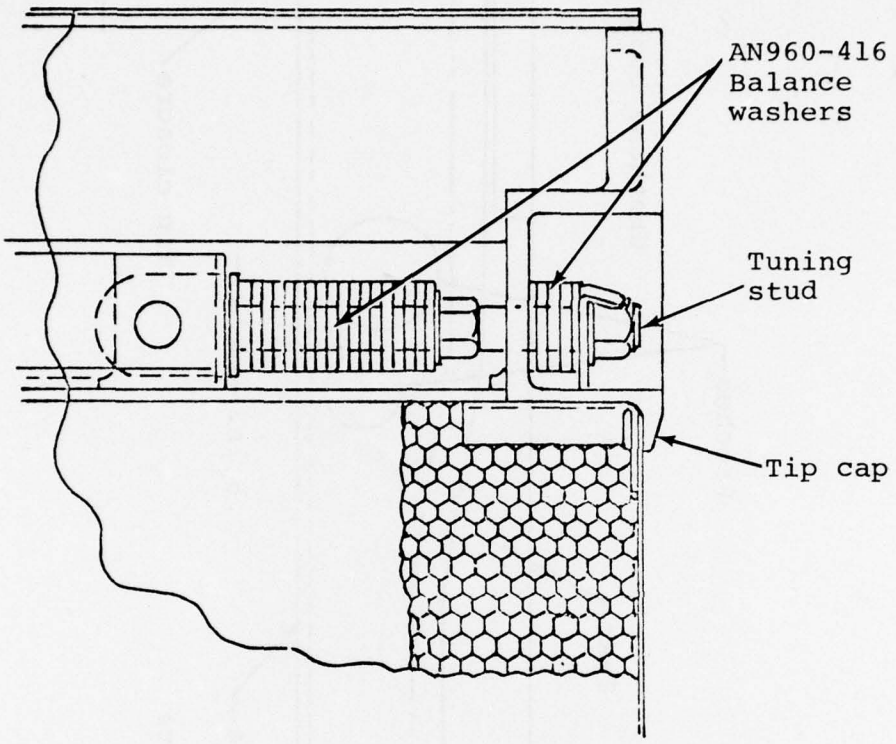

Figure A-1. Balance weight arrangement.

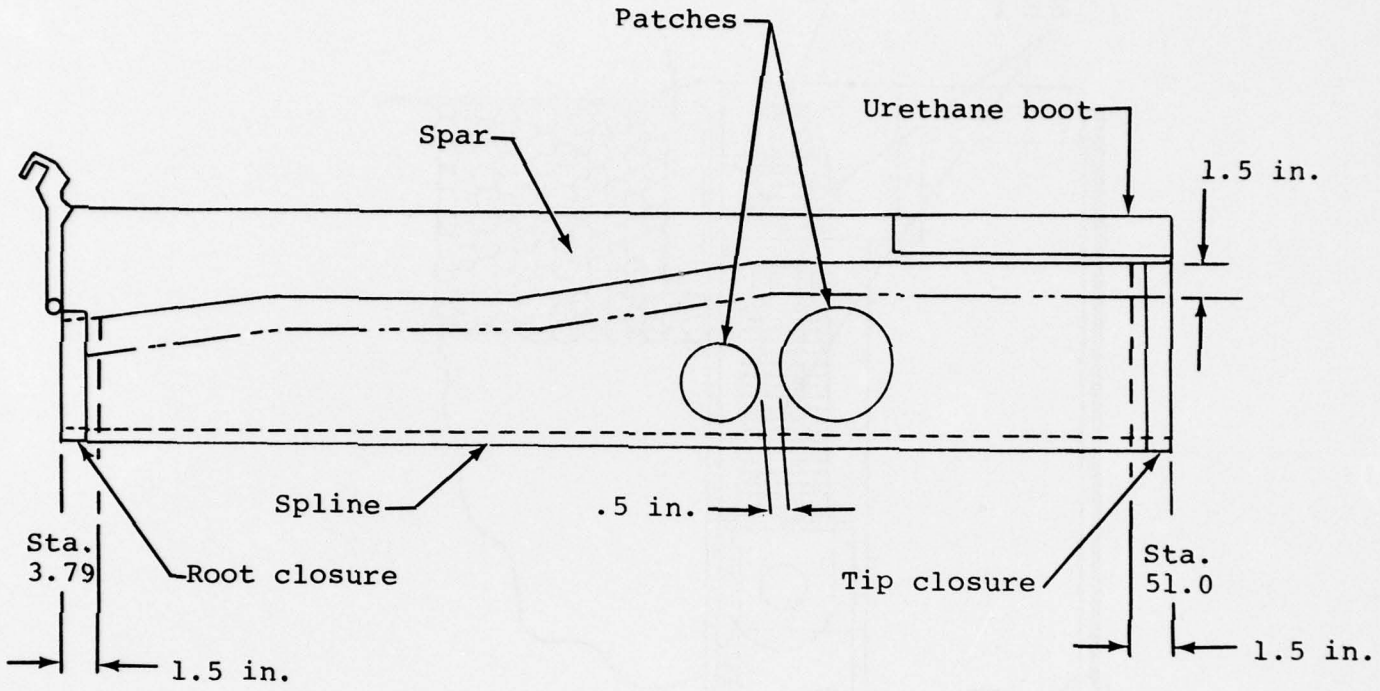

Figure A-2. Limits of repairable damage.

1.2.5 Nicks and scratches should be removed by smooth blending not to exceed the depth specified in 1.2.2 above.

1.3 Channel, Forward and Aft (Aluminum)

1.3.1 A bond separation is cause for scrappage.

1.4 Abrasion Strip (Urethane)

1.4.1 Loss of bond to the spar, loss of a rubber segment(s) larger than .50 square inch area, and excessive erosion are causes for replacement of the abrasion strip. Holes or missing rubber segment(s) under .50 square inch may be repaired according to instructions.

1.5 Skin and Core (Fiberglass and Nomex Honeycomb)

1.5.1 Skin cracks and tears with minor core damage may be repaired with a skin patch provided the patch will overlap the damage by a minimum of 1.0 inch.

1.5.2 Punctures and delaminated areas may be repaired with a plug/patch provided the damage is not greater than 3.5 inches in diameter and the periphery of the damage is no closer than 1.5 inches to the spar, tip closure or root closure and that .5 inch minimum clearance is maintained with the edge of any previously installed patch on the same side of the blade.

1.5.3 A through puncture may be repaired by a skin patch on each side of the blade provided the core damage falls within a 1.0-inch diameter.

1.5.4 Nicks and scratches in the skin up to .004 inch deep are acceptable as is. Nicks and scratches greater than .004 inch deep should be repaired if within limits allowed for repair of cracks described in steps 1.5.1 and 1.5.2 above.

1.5.5 Smooth dents up to .030 inch deep not having broken skin, core or delamination, are acceptable as is. Dents greater than .030 inch deep will be treated as a puncture and should be repaired if within the limits allowed in steps 1.5.1 and 1.5.2 above.

1.5.6 Should damage occur within a previously repaired area that cannot be cleaned out and covered by the next larger patch, the blade must be scrapped.

1.6 Trailing-Edge Spline (Fiberglass)

1.6.1 Nicks and gouges up to .030 inch deep are acceptable as is. Nicks and gouges greater than .030 inch deep and not over 4.0 inches long may be reworked by smooth blending to a maximum chordwise depth of .200 inch and an application of a vee skin patch. Blades with cracks extending chordwise deeper than .200 inch shall be shipped to depot for repair.

1.7 Tip Closure (Fiberglass) and Root Closure (Fiberglass)

1.7.1 Cracks, punctures and tears within the closure require that the blade be shipped to depot for repair.

1.7.2 Dents are acceptable as is, provided the surface is not broken and delamination of the closure from adjacent structure has not occurred.

1.7.3 Nicks and scratches are acceptable as is, provided the damage has not penetrated through the closure skin.

1.7.4 Failure of the bond between the pitch arm fitting and the blade skin and/or core requires blade scrappage.

1.7.5 Any damage extending into adjacent structure and/or accompanied by delamination of root closure requires that the blade be shipped to depot for repair.

1.8 Tip Cap (Aluminum)

1.8.1 Corrosion, nicks and scratches greater than .005 inch deep, but less than .030 inch deep, shall be smooth blended. Damage exceeding these limits requires tip cap fitting replacement.

1.9 Outboard Boot (Urethane)

1.9.1 Punctures less than .75 inch square may be repaired.

1.9.2 Tears up to 3.0 inch long that do not extend through the edge of the boot may be repaired.

1.9.3 Boot replacements shall be accomplished at depot.

1.10 Pitch Arm Fitting (Aluminum)

1.10.1 In the clevis area, dents must be smooth or reworked by blending to a maximum of .030 inch deep. Damage greater than .030 inch deep shall require scrapping the blade.

1.10.2 In all other areas, smooth dents up to .030 inch deep are acceptable as is. Irregular dents up to .045 inch deep must be reworked to blend out sharp corners.

1.11 Crosshead Assembly (Steel)

1.11.1 Corrosion, nicks and scratches in excess of .010 inch deep must be reworked by blending smooth. Damage may be reworked to a maximum of .050 inch deep.

1.12 Pitch Link Assembly (Aluminum Tube)

1.12.1 Corrosion, nicks and scratches up to .010 inch deep shall be reworked by blending smooth. Pitch link assemblies damaged in excess of .010 inch deep must be replaced.

1.12.2 Dents up to .060 inch deep are acceptable as is, provided no sharp corners exist. Pitch link assemblies with sharp corners must be replaced.

1.13 Inner Hub Assembly (Steel)

1.13.1 Corrosion, nicks and scratches in excess of .010 inch deep must be reworked by smooth blending. Damage may be reworked to a maximum depth of .030 inch.

1.14 Outer Hub Assembly (Steel)

1.14.1 Corrosion, nicks and scratches in excess of .010 inch deep must be reworked by blending sharp corners. Damage may be reworked to a maximum depth of .030 inch.

1.14.2 Fretting debris in the spline must be washed clean and a film of grease applied prior to installation on the aircraft.

1.15 Cover Plate (Steel)

1.15.1 Corrosion, nicks and scratches in excess of .010 inch deep must be reworked by smooth blending. Damage may be reworked to a maximum depth of .040 inch.

1.16 Tee Fitting (Aluminum)

1.16.1 Corrosion, nicks and scratches in excess of .010 inch deep must be reworked by blending sharp corners. Damage may be reworked to a maximum depth of .040 inch.

1.17 Control System Boot (Rubber)

1.17.1 Punctured or torn sliding boots must be replaced.

1.18 Safety Wires (Steel)

1.18.1 Safety wires are to be replaced as required.

1.19 Data Plates (Aluminum)

1.19.1 Data plates must be replaced when pertinent information is no longer clearly visible.

2 REPAIR PROCEDURES

2.1 Skin and Core Patches. The general procedure for making field repairs to the skins, and/or honeycomb core of the aft structure of the EPBTR airfoil section is as follows:

2.1.1 Determine if the damage is acceptable as is, repairable, or if it is cause for scrapping the EPBTR by referring to the repair limits presented in the previous section.

2.1.2 If the damage is repairable, select a skin patch or plug/patch from the repair kits listed in Table A-1. For skin patches, the size of the patch should be selected to insure that there is a minimum of a 1.0-inch overlap all around the damaged area after clean-up. Plug/patches should be selected large enough to replace the damaged core area.

2.1.3 Determine, from Table A-5, the number of balance washers that must be removed to rebalance the blade after a given patch or plug/patch has been used at a given spanwise location. Check the balance washers installed in the spar tip to insure that a sufficient quantity of washers is available for removal.

2.1.4 Clean-up damage area and bond area by first removing the paint with Methyl-Ethyl-Ketone (Item 300 - Table A-3).

2.1.5 If damaged core must be removed, a router is used to cut a circle around the damaged area to the required depth as shown in Figure A-3. If the damaged core does not extend through the full thickness of the blade, the skin within the routed circle is first removed, as shown in Figure A-4, and the remaining core within the circle is then routed to the prescribed depth of the blind hole. For those cases where the damage extends through the blade, the damage area is completely removed in one step by adjusting the depth of cut of the router so that the bit extends beyond the blade thickness.

2.1.6 Using 180 grit abrasive paper (kit item) uniformly abrade the surface of the blade skin to which the skin patch and/or plug patch are to be bonded.

2.1.7 Remove all debris (cuttings, sanding, dust, etc.) from the repair area of the blade. In those cases where the core has been routed, clean the area with a vacuum cleaner.

2.1.8 Clean skin area to be bonded using Methyl-Ethyl-Ketone until the area is free from grease, oil, wax, and other foreign matter.

2.1.9 For those cases requiring a full-depth plug with skin patches on both sides of the blade, the core plug must be routed to the blade contour to insure a proper fit-up when the repair is completed. This is accomplished by placing the proper plug/patch in the routed hole and letting the core excess extend beyond the skin surface on the opposite side of the blade. Pads are attached to the router base, the router bit is set flush with the outer skin contour, and the excess core is removed by the router as shown in Figure A-5.

2.1.10 Mix the two-part paste adhesive, supplied with the repair kit (Item 200 - Table A-3), and apply to the following designated surfaces:

2.1.10.1 Skin patches and vee-shaped trailing-edge patches. Apply a thin coat of the adheisve to the area of the blade skin to be bonded and to the inner surface of the patch.

2.1.10.2 Plug/patches (one side of blade only). Apply adhesive to both sides of the fiberglass disk-shape wafer (Table A-2) and insert it into the blind hole

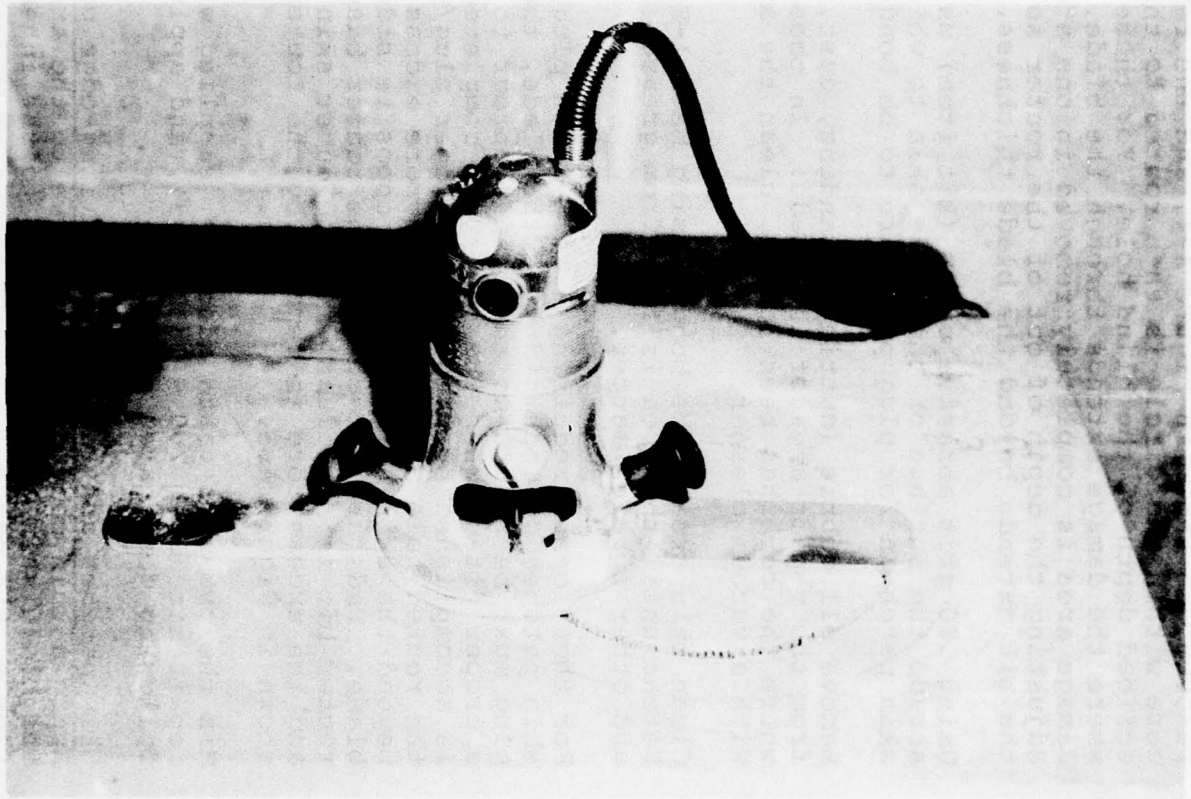

Figure A-3. Routing skin.

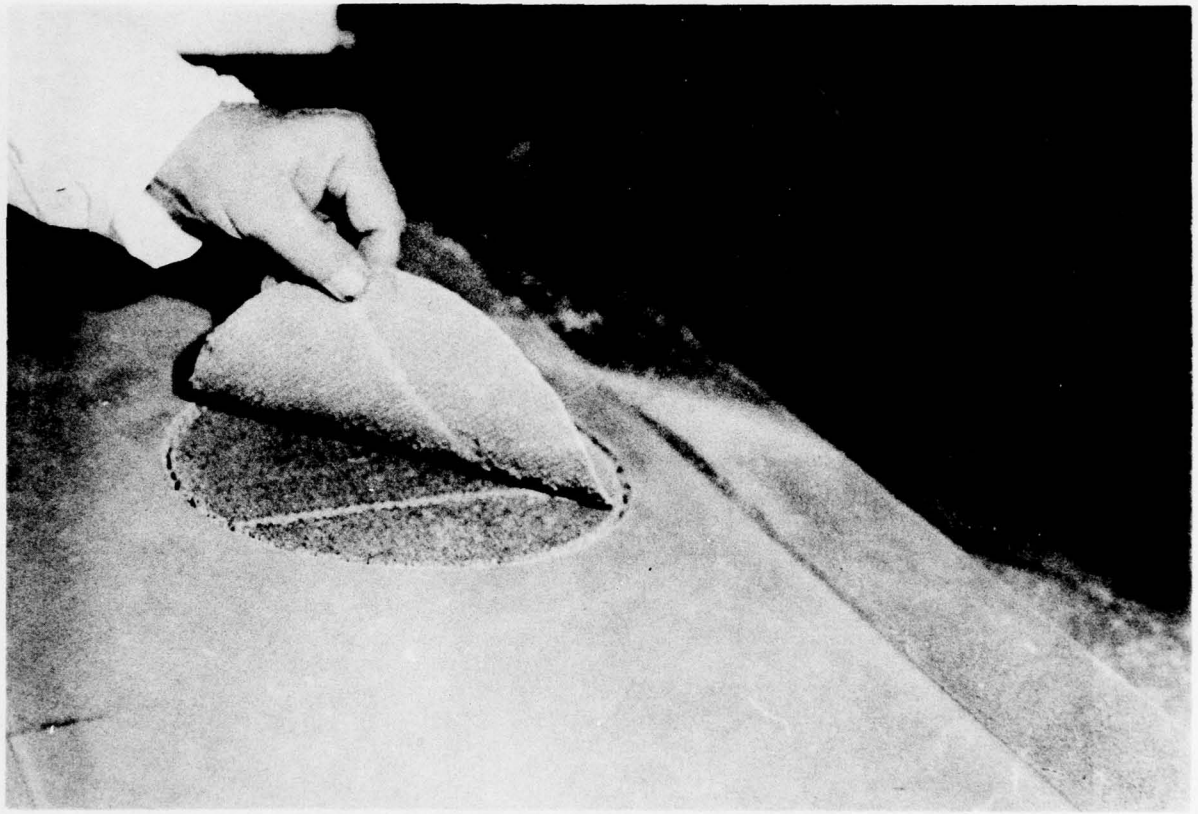

Figure A-4. Peeling off routed skin.

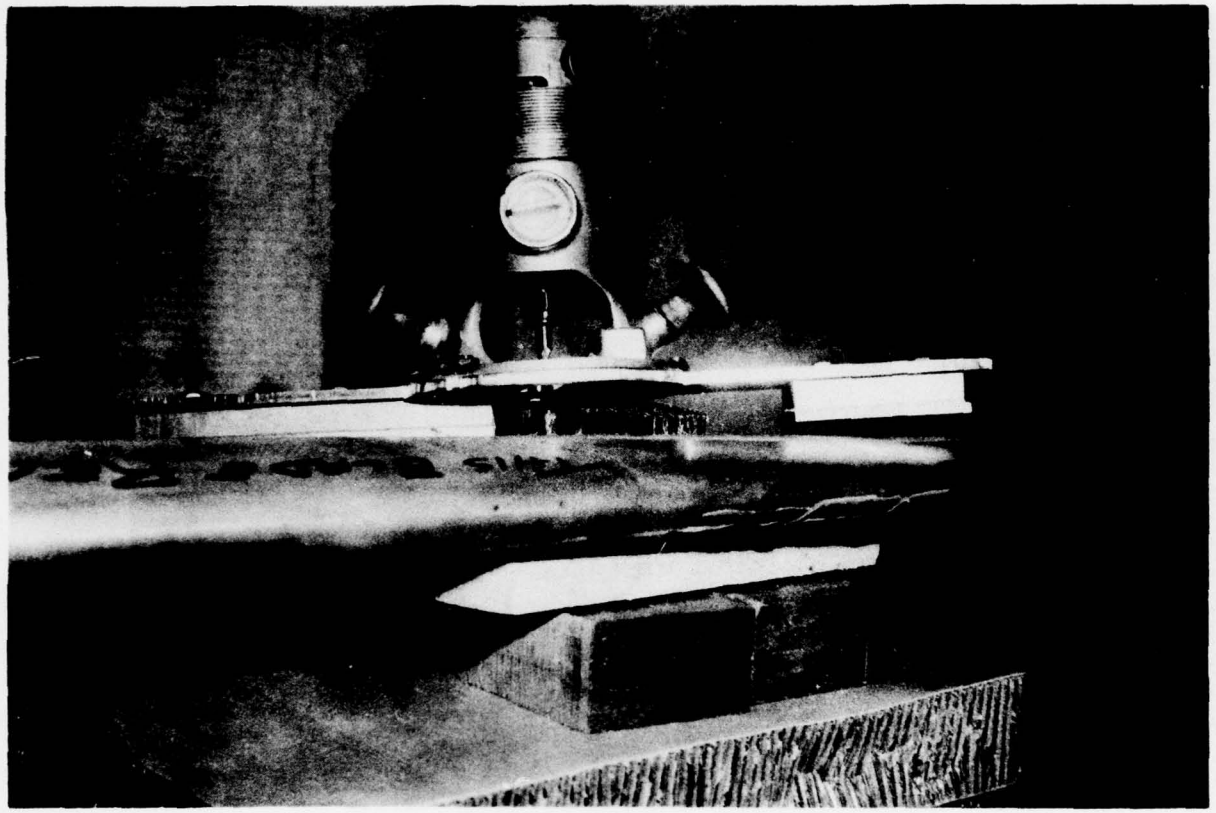

Figure A-5. Routing plug flush with skin.

routed into the core. Coat the remaining surface of the hole, blade skin, outer surfaces of the honeycomb plug, and the inner patch surface with the adhesive.

2.1.10.3 Through plug/patch and skin patch combination. Apply adhesive to the wall of the hole, the blade surface around the hole on both sides of the blade, exposed surfaces of the honeycomb plug, and the inner surfaces of the skin patches. Figure A-6 shows the plug/patch and skin patch ready for assembly.

2.1.11 Place skin patch, plug/patch, and/or through plug/patch and skin pitch combination in their proper position and tape to prevent movement during cure.

2.1.12 Tape on the nylon cloth (kit item) over the patch area to absorb excess adhesive, position the Teflon sheet (kit item), and tape to blade.

2.1.13 Place the vacuum/heat pack, Figure A-7, on the blade so that the rubber vacuum pad will come in contact with the repair and secure the vacuum/heat pack to the blade after using a pliable heat resistant sealant as required to obtain a vacuum of 28 inches of mercury.

2.1.14 Set the temperature control thermostat to maintain a curing temperature of 185°F at the skin bond line. Cure the adhesive for 25 minutes maintaining the proper temperature and vacuum.

2.1.15 Remove the vacuum/heat pack, the Teflon sheet, the absorbant cloth, and the outer peel ply (shown in Figure A-8).

2.1.16 Refinish the repaired area using 180-grit abrasive paper, abrade lightly with 360-grit abrasive paper and clean area with Methyl-Ethyl-Ketone.

2.1.17 Spray on a light coat of epoxy primer (Item 100, Table A-3) followed by a light coat of acrylic lacquer (Item 101, 102 and/or 103, Table A-3), matching the original color of the repaired area.

2.1.18 Rebalance the blade by removing the number of balance washers specified in Table A-5, install tip cap, install new tab washer (kit item), and secure with the tip cap retention nut. Seal between the tip cap and the spar with sealant (Item 201, Table A-3).

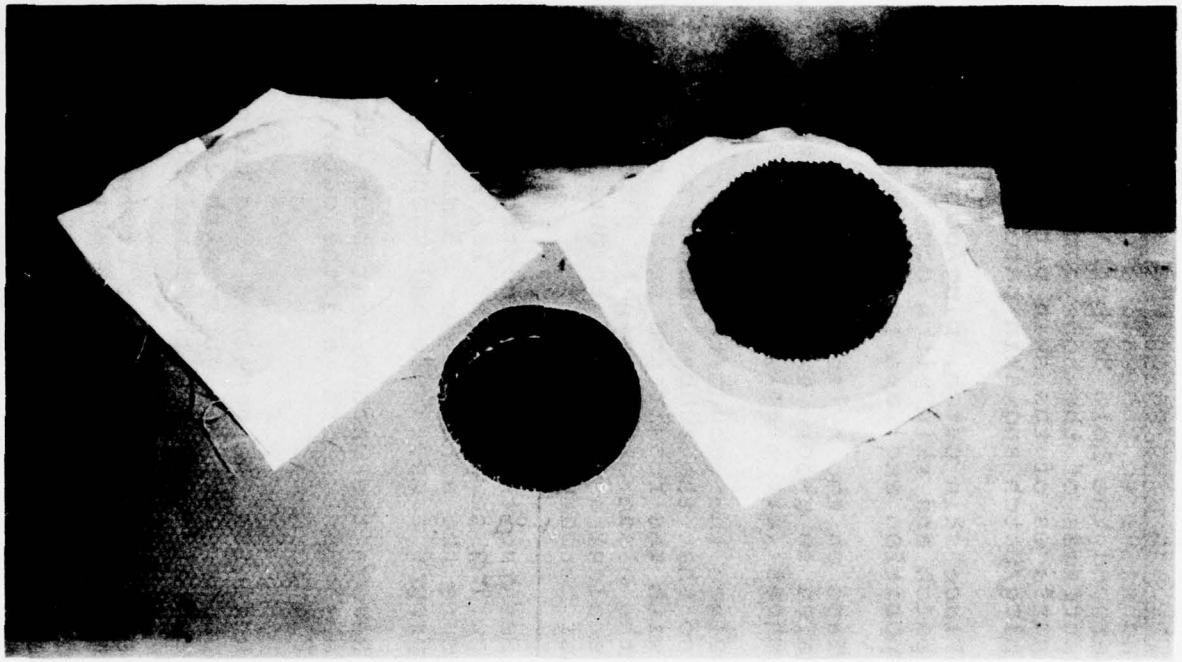

Figure A-6. Plug/patch and skin patch combination ready for assembly.

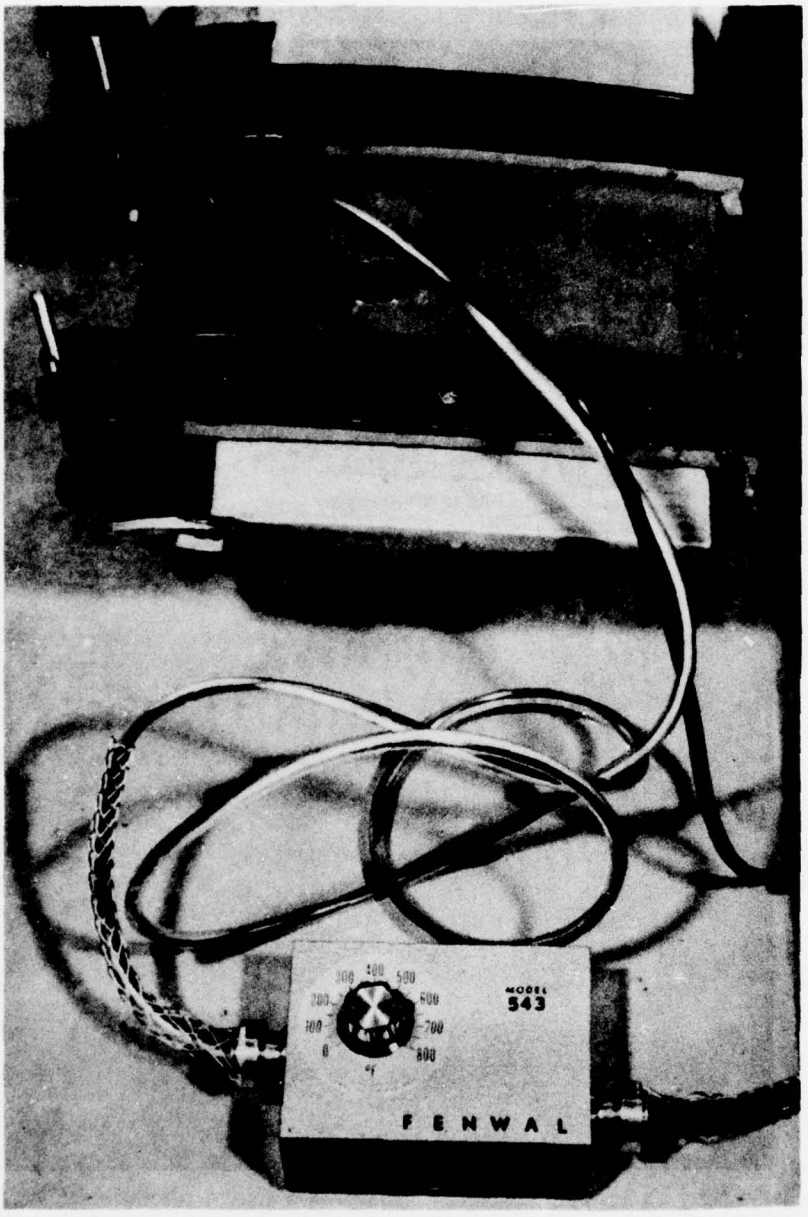

Figure A-7. Vacuum/heat pack secured to blade.

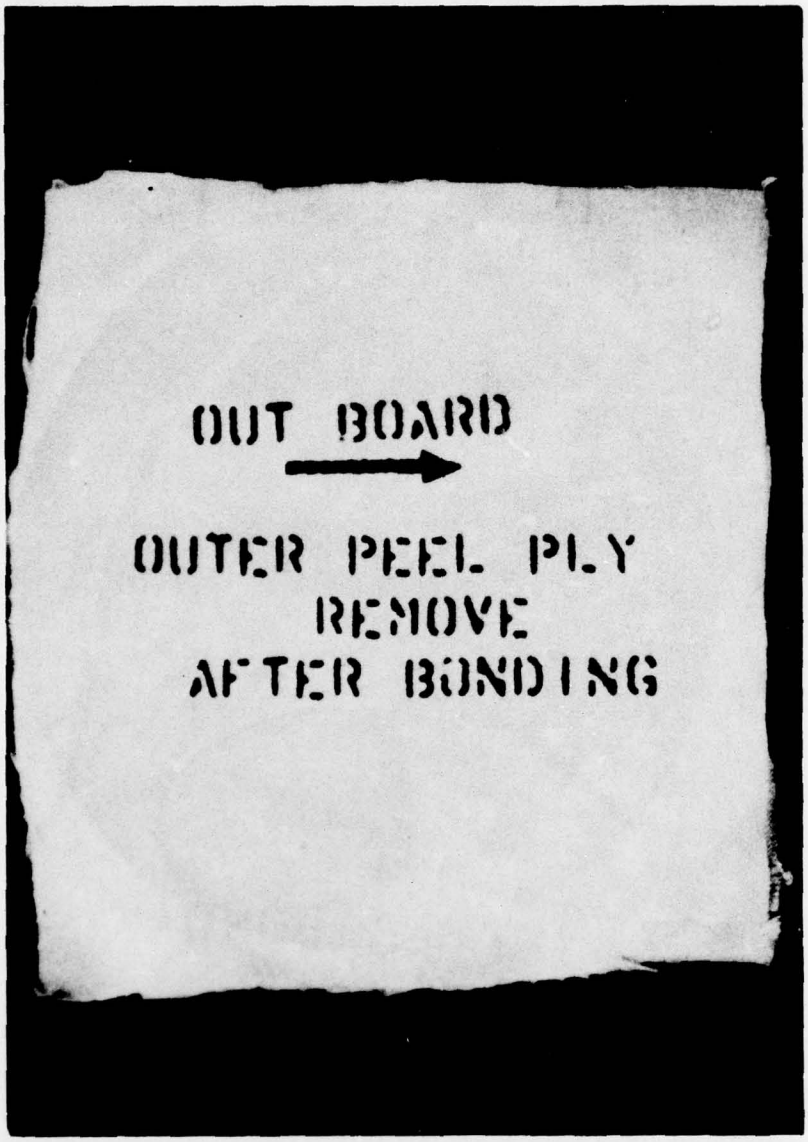

Figure A-8. Patch outer marking.

2.2 Blending Out Nicks and Scratches

2.2.1 Determine if the damage is within the reworkable limits established in the applicable section of paragraph 1.

2.2.2 Remove the paint and clean the immediate area surrounding the damage using Methyl-Ethyl-Ketone.

2.2.3 Using a hand file, abrasive paper, or abrasive wheel, blend out the scratch, nick, pitting, etc. Remove filing marks, sanding scratches, etc., by polishing with crocus cloth.

2.2.4 Alodine aluminum surfaces and repaint as per paragraph 2.1.17.

2.2.5 Apply a light film of corrosion preventative compound (Item 301, Table A-3) to reworked steel areas.

2.3 Filling Spar Dents

2.3.1 Determine if the dents are within the acceptable limits established in the applicable section of paragraph 1.

2.3.2 Remove paint from damaged area using Methyl-Ethyl-Ketone (Item 300, Table A-3).

2.3.3 Remove yellow primer with 180-grit abrasive paper and then roughen area using 240-grit abrasive paper.

2.3.4 Clean area with Methyl-Ethyl-Ketone until it is free of grease, oil, wax, and other foreign matter.

2.3.5 Fill in dents with Bondmaster 777 adhesive paste epoxy (Item 202, Table A-3) and cure with a heat lamp for 1½ hours at 150°F.

2.3.6 Sand repair area using 240-grit abrasive paper, alodine sanded area of spar, and repaint as necessary.

2.4 Abrasion Strip Repair

2.4.1 Determine if damage is within the acceptable repair limits established in the applicable section of paragraph 1.

2.4.2 Clean hole or tear area using Methyl-Ethyl-Ketone.

2.4.3 Apply Uralane (two-part system), Item 203, Table A-3, and smooth to contour.

2.4.4 Use a sheet of teflon over the repair area and tape it to the blade to retain the proper contour during cure.

2.4.5 Cure the Uralane for 1½ hours at 150°F using a heat lamp.

2.4.6 Blend to contour with wet 240-grit abrasive paper.